BASHIR, Abdulaadem A. 2000. *An experimental investigation of some capillary pressure-relative permeability correlations for sandstone reservoir rocks*. Robert Gordon University, PhD thesis. Hosted on OpenAIR [online]. Available from: https://doi.org/10.48526/rgu-wt-2807295

An experimental investigation of some capillary pressure-relative permeability correlations for sandstone reservoir rocks.

BASHIR, A.A.

2000

THE ROBERT GORDON UNIVERSITY
SCHOOL OF MECHANICAL AND OFFSHORE ENGINEERING

AN EXPERIMENTAL INVESTIGATION OF SOME CAPILLARY PRESSURE-RELATIVE PERMEABILITY CORRELATIONS FOR SANDSTONE RESERVOIR ROCKS

Abdulaadem A Bashir
BSc, DIC, MSc

A thesis submitted in partial fulfilment
of the Robert Gordon University
for the degree of Doctor of Philosophy

FEBRUARY, 2000

Form RDDecl

THE
ROBERT GORDON
UNIVERSITY
ABERDEEN

RESEARCH DEGREES COMMITTEE

Candidate's Declaration Form

NAME:

DEGREE FOR WHICH THESIS IS SUBMITTED:

1 Material Submitted for Award

(a) I declare that the work has been composed by myself.

(b) I declare that all verbatim extracts contained in the thesis have been distinguished by quotation marks and the sources of information specifically acknowledged.

(c) *either* *I declare that no material contained in the thesis has been used in any other submission for an academic award.

or *I declare that the following material contained in the thesis formed part of a submission for the award

of.. *(state the award and awarding body and list the material below):*

2 Concurrent registration for two or more academic awards

either *I declare that while registered as a candidate for the University's research degree, I have not been a registered candidate or enrolled student for another award of the University or other academic or professional institution.

or *I declare that while registered for the University's research degree, I was, with the University's specific permission, a *registered candidate/*enrolled student for the following award:

Signature of candidate .... Date ....

*Delete as appropriate

ABSTRACT

The water-oil relative permeability of the reservoir rock is one of the essential properties in petroleum engineering studies, and the use of this data is critical in the evaluation and management of oil fields, particularly in water flooding predictions and oil recovery calculations. The experimental measurement of these quantities can not be carried out without resorting to complicated and expensive coring. Furthermore, it is very time consuming, laborious and has great difficulties associated with it. Some mathematical models have been developed to predict these important parameters from capillary pressure measurements. This study has evaluated these models, and suggests now selecting and/or modifying the most appropriate one. A new model is verified including an error analysis against representative samples.

A group of homogeneous sandstone rock samples were selected based on x-ray computed tomography (CT) imaging. Adopting a medical scanner for core analysis led to poor quantitative results. It has been found that to obtain reliable images, the scanner must be recalibrated using a reference point which falls within the geological region of interest. The technique has been extended to measure non-destructively the porosity (using dual-scan method) for small sub-volumes within the tested sample. Measuring porosity variations within the rock samples with CT scanning is a very powerful tool which allows the assessment of the degree of heterogeneity quantitatively and assists in sample selection. Porosity measured using the CT scanning technique showed excellent agreement with the conventional helium and liquid porosities.

A new CT single-scan method was developed for porosity measurement based on using average x-ray attenuation coefficient measurements. The newly developed CT single-scan porosity measurement technique has formed the basis of the use of CT as a means for logging porosity of the whole core. CT porosity logs were performed for 24 and 27 foot sections on sandstone whole cores in fiber glass sleeving. Subsequently, 26 and 30 plugs were removed from the scanned positions. CT porosity showed good agreement with helium porosity for core plugs which were removed from the scanned zones.

Since most of the existing models rely on the wetting and the non-wetting phase determination, the wettability of the selected samples has been restored, then measured using the Amott/USBM method. As a result, water and oil have been defined as the wetting and non wetting phase respectively. Using random samples with no wettability assessment will lead to misuse of the existing models especially in intermediate and oil wet rock samples.

To evaluate the existing mathematical models, capillary pressure curves have been generated using the porous plate diaphragm, centrifuge and mercury injection for all selected samples. Relative permeability curves have been generated using the proposed mathematical models respectively. It was intended to use either CT or the 1-D x-ray technique in the experimental relative permeability measurements, however, it was discovered early on that using these techniques in unsteady state experiments definitely leads to significant errors. The limitations of the existing facilities and the required technical modifications to eliminate errors are presented as part of the thesis. Therefore, an unsteady state relative permeability rig was constructed. Results obtained showed that, apart from the difficulty in interpreting the unsteady state floods, it is impossible to produce a complete relative permeability curve. In order to obtain full and reliable experimental relative permeability curves, essential for comparison with the mathematically generated relative permeability data, a steady state

relative permeability rig was constructed. Steady state water and oil relative permeabilities were measured for all selected samples. Although the technique is laborious and very time consuming, it successfully generated the most reliable and complete data set. Accordingly, the experimentally measured steady state relative permeability data was selected for comparison with data derived by the proposed mathematical models.

Comparison results show that the use of existing mathematical models for deriving relative permeability data from capillary pressure curves for water wet rock samples leads to significant errors. However, Burdine's model exhibited a "numerically" reasonable agreement with the laboratory experimental data, yet, using this model in its existing form certainly produced serious errors. The model incorrectly continues generating oil relative permeability values below the residual oil saturation, (water saturation $\geq 1.0 - S_{or}$). Using these false relative permeabilities in classical reservoir engineering calculations will incorrectly predict that the reservoir will produce far more oil than is physically possible. Burdine's model (like others) also ignores the effect of rock wettability type and is assumed to be valid for any wettability including intermediate wettability. This is considered to be a major shortcoming in the mathematical model.

Burdine's model has been newly modified to suit water wet samples. The new model showed outstanding results; it is representative, efficient, flexible and suits the practical applications for oil reservoirs. Considering the reservoir rock properties such as porosity, wettability and allowing for the residual oil saturation, minimized errors significantly. This gives the new model superiority in predicting the relative permeability data from the capillary pressure curves. Although the new model developed used air-brine capillary pressure data, results obtained show that relative permeability curves can be reliably generated from capillary pressure data obtained by the centrifuge or mercury injection methods. This makes the technique more versatile and widely applicable in practice.

In addition to the work detailed above, the following new approaches are presented:

Since the air-brine capillary pressure data are the most representative measurements, but very time consuming, a new experimental approach has been developed which employs thin, large diameter samples, for measuring the capillary pressure. The time required to obtain a complete capillary pressure curve is remarkably reduced.

A new method for correcting permeability measurement using Darcy's law was presented for discussion. This method allows for the inflow end effect and the depth of mud invasion in formation damage assessment.

ACKNOWLEDGEMENTS

First of all I am most grateful to Allah, without his help this thesis wouldn't brought to completion. Secondly, I would like to express my sincere thanks and appreciation to my supervisor Dr W E Mason for his unlimited support. Special thanks to Professor Daniel Gorman, former Head of School of Mechanical and Offshore Engineering for allocating financial support for the construction of the unsteady and steady state relative permeability rigs. Thanks to all the staff within The Robert Gordon University in general and the School of Mechanical and Offshore Engineering in particular for being helpful in different aspects. Special thanks to Dr Cameron Stewart and Dr Susan Darcy for reading most of the thesis and their valuable comments and constructive criticism. Many thanks to Dr Ian Mackenzie for making available the x-ray computed tomography facilities in the Aberdeen Rock Imaging Centre whenever needed and providing the required training for using them.

I am indebted to Robertson Research International Limited for their help in constructing the relative permeability rigs and allocating working space within their laboratory, and for providing all routine and special core analysis apparatus including materials and training. Their constant help and support were really invaluable. Once again, many thanks to all the staff for their help, support and encouragement, especially Mr Jack Ore, The Unit Head of Special Core Analysis and Craig Baxter, The Special Core Analysis Team Leader. Working with them was a most pleasant and rewarding experience.

I would like to thank Dr X Jing , Lecture in petroleum Engineering and Leader of the Petrophsics Reassert Group (Imperial College, London) and Dr Bashir Al-Ashhab, the Reservoir Engineering Co-ordinator at the Arabian Golf Oil Company (ex PhD student at Imperial college, London) for providing me with many rock samples and their sound advises, and to Dr M P Enwere(ex PhD student at Imperial college, London) for providing me with a lot of valuable references. Thanks to Dr Z Omoregie Reservoir Engineering Manger, Chevron, for his initial guidnace in preparing the proposed plan of this work.

Many thanks to my dear friends, Abdulrazag Ghuma, Ahmed Rabab, S Abusaida, Abderrazak Sebai, Issa Albaroni, S Turky, Dr Abosef, Dr El-Mahtot, Fouad, Dr Azhary Al-Bashir, Abdulmajid, Dr L Korban, Mustafa, Dr Benhusain, Ahmed yousf, Edward Fikri, Dr Baroni, Ian Campbell, Dr Hisham and last but certainly not least Dr Montaser Haj, for their friendship and support.

Thanks to my wife for her constant support and encouragement. Thanks to my children, Redha, Mariam and Riyhan for praying for me and filling my heart with love, joy and delight whenever I look at them. Definitely, with out their company, away from home, life would have been harder.

Finally, I am really grateful to my parents and family back home for their continued support.

TABLE OF CONTENTS

INTRODUCTION

LITERATURE REVIEW

EXPERIMENTAL APPARATUS AND PROCEDURE

CORE SAMPLE EVALUATION USING X-RAY COMPUTED TOMOGRAPHY

CT SCAN RESULTS AND DISCUSSION

RELATIVE PERMEABILITY/CAPILLARY PRESSURE RESULTS AND DISCUSSION

LIST OF FIGURES

NOMENCLATURE

A	cross section area
CT_{Nf}	CT number of the fluid saturating the sample
CT_{Ng}	CT number of the rock grains
Dkro	drainage oil relative permeability
Dkrw	drainage water relative permeability
DUSS	drainage unsteady state
dP/dx	pressure gradient along x
g	acceleration due to gravity
g'	centrifugal acceleration
h	height
I	the beam intensity after traversing
Ikro	imbibition oil relative permeability
Ikrw	imbibition water relative permeability
ISS	*imbibition steady state*
IUSS	imbibition unsteady state
I_0	the initial intensity of x-ray beam
Ikro	imbibition oil relative permeability
Ikrw	imbibition water relative permeability
Ir	relative injectivity $I = U/\Delta p \div (U/\Delta p$ at start of injection)
K_a	absolute permeability
k_e	effective permeability
k_g	gas permeability
k_o	oil permeability
k_{rf}	produced fluid relative permeability
k_{rg}	gas relative permeability
k_{rnwt}	non wetting phase relative permeability
$k_{ro_{,,}}$	oil relative permeability
k_{ro}''	psuedo relative permeability for oil
$k_{rw_{,,}}$	water relative permeability
k_{rw}''	psuedo relative permeability for water
k_{rwt}	wetting phase relative permeability
k_w	water permeability
K_z	the Kozeny constant
L	length
M	mass
OWC	oil-water contact
P_c	capillary pressure
Q	flow rate
q_f	produced fluid rate
r	tube radius

S_{av}	average saturation
S_o	oil saturation
S_{or}	the irreducible (residual)oil saturation
S_w	water saturation
S_w^*	the normalized water saturation.
s_w''	thickness averaged water saturation
S_{wi}	irreducible water saturation
T	time
UDkro	unsteady state drainage oil relative permeability
UDkrw	unsteady state drainage water relative permeability
UIkro	unsteady state imbibition oil relative permeability
UIkrw	unsteady state imbibition water relative permeability
V	macroscopic fluid velocity
V_b	bulk volume
V_g	grain volume
V_p	pore volume
Vs	flow rate per unit area of the porous medium
w	centrifuge speed, rpm
wi	cumulative injection in pore volumes
x	distance in direction of flow and is always positive
Z	vertical coordinate
z	vertical co-ordinate, considered positive downward
ρ	density of the fluid
ϕ	porosity
θ	contact angle
μ	viscosity
μ_f	produced fluid viscosity
μ_g	gas viscosity
μ_o	oil viscosity
μ_w	water viscosity
ρ	density
σ	interfacial tension
σ_{wo}	interfacial tension between water and oil
σ_{sw}	interfacial tension between water and surface
σ_{so}	interfacial tension between oil and surface
λ	the lithology factor
$\Delta\rho$	density difference
χ_i	tortusity factor
η	linear attenuation coefficient
η_g	grain linear attenuation coefficient
η_f	fluid linear attenuation coefficient

CHAPTER 1

INTRODUCTION

1.1 General Background

There are two essential properties for a reservoir rock to produce fluid, water, oil or gas or combinations of these fluids. The first is porosity (ϕ), which is defined as the ratio of void space (pore volume (V_p) which is the bulk volume (V_b) - the grain volume (V_g)) in rock to the bulk volume of that rock multiplied by 100 to express in percent, therefore,

$$\phi = \frac{V_p}{V_b} \times 100 \qquad (1.1)$$

Unless the rock is porous it can contain no water, oil or gas. The porosity is the sole measure of the storage capacity of the underground formation.

Second, the rock must have continuity of pore spaces to permit its contained fluids to flow. This property is called permeability (k), which can be defined as a property of the porous medium which measures its ability to conduct or transmit fluids. This property is influenced to a certain degree by porosity and to a very important degree by texture or pore size distribution. The permeability of a rock is a property of the rock alone, dependent solely on the physical geometry of the pores. It has the same value for a given rock regardless of what kind of fluid is flowing though it, as long as there is only one fluid flowing at a time and provided that this fluid does not interact with the rock, in which case its internal physical structure will not be changed. This rock property is specifically called absolute permeability (K).

In 1856, Darcy investigated the flow of water through sand filters. His conclusions were presented in the form of the so-called Darcy's Law. Later investigators realized that

Darcy's Law could be applied to other fluids. The generalized form of Darcy's Law is presented in API code 27[1] is:

$$V_s = -\frac{K}{\mu}\left(\frac{dP}{dX}\rho g\frac{dZ}{dX}\times 10^9\right) \tag{1.2}$$

Where:

X = distance co-ordinate in direction of flow, m

V_s = flow rate per unit area of the porous medium, m/sec

Z = vertical coordinate, m

ρ = density of fluid, kg/m^3

g = acceleration of gravity, 9.80665m/sec^2

dP/dX = pressure gradient, Pa/m

μ = viscosity of the flowing fluid, Pa.sec

K = permeability of the porous medium, Darcy

When a porous medium simultaneously contains two or more fluids e.g. water and oil, water and gas, or water, oil and gas together, the absolute permeability for the rock does not represent the ability of the rock to conduct or transmit one fluid in the presence of others. Reservoir rocks usually contain two or more fluids, therefore, the concept of effective permeability has been introduced to describe the simultaneous flow of more than one fluid. The effective permeability is a relative measure of the ability of rock to transmit one fluid (e.g. oil) when it is saturated with more than one fluid (e.g. water and oil). By definition, any reservoir rock can have a distinct and measurable conductance (effective permeability) to each phase present in the rock.

So, the relative permeability can be defined as the ratio of the effective permeability of a fluid (k_o, k_w, or k_g i.e. effective permeability to oil, water or gas, respectively) at a certain saturation to the absolute permeability.

saturation value, which makes it predictable from capillary pressure in principle. For any porous and permeable rock, the capillary pressure is constant at each saturation point, which means that for any rock containing more than one fluid, there will be certain values for the capillary pressure and the relative permeability at each saturation point.

Relative permeability and capillary pressure measurements are made as part of special core analysis procedures. Several methods for capillary pressure and relative permeability measurements have been reported in the literature, and many investigators have attempted to develop mathematical models of fluid flow in porous media. One fruitful line of approach began with the work of Kozeny (1927)[2] and its development by Carman (1937)[3]. Their work was restricted to single phase flow but their methods were extended to multi-phase flow. Purcell (1949)[4], Gates and Lietz (1950)[5], Wyllie and Gardner (1958)[6] and others adopted an alternative approach which related the relative permeability to capillary pressure data. The water-oil relative permeability characteristics of the reservoir rock are one of the most important properties in petroleum engineering, and represent a corner- stone in reservoir engineering, particularly, in water flooding predictions and oil recovery calculations.

"If the objective of the study is to design a water flood for a field, proceeding with the study on anything other than the most conceptual basis if no water/oil relative permeability data are available would be foolish" [7]

The experimental measurement of these quantities is time consuming, laborious and associated with great difficulties. This project is intended to evaluate selected mathematical models which attempt to predict the relative permeability curves from capillary pressure data and to compare the results with those obtained by direct experimental measurements.

1.2 Objectives

Direct laboratory measurements for relative permeability data, apart from the amount of work and time are needed. The retrieval of a regular, descent, cylindrical and square core sample is a crucial requirement. This condition will not be fulfilled unless a successful coring operation is accomplished while drilling the payzone. Furthermore, it is impossible to obtain a full range of relative permeability data using the unsteady state method for the complete range of water saturation encountered (from S_{wi} to $(1-S_{or})$) in any oil reservoir. On the other hand, a full range of capillary pressure data can be obtained for any reservoir rock sample, regardless of shape or size. It can be easily measured on any crushed core sample or even drilling cuttings retrieved from the shale shaker screen. Hence, the importance of the mathematical models use to predict the relative permeability data led to the following objectives:-

1. Selection of a soundly based non-destructive method for assessing quantitatively the degree of homogeneity and to assist in core screening and/or selection, based on 3-D porosity measurements for interior small sub-volumes within the rock samples non destructively. X-ray computed tomography is a suitable method well-adapted for this purpose.

2. Utilization of the CT Scan to improve core samples evaluation

3. Evaluation and refinement of the mathematical models for predicting relative permeability data from capillary pressure curves and comparison of the results obtained against high quality experimental data.

4. Investigating of the reliability and limitations of the mathematical models for predicting relative permeability in the following situations frequently encountered:-
    - Lack or non successful coring operation.

- Interpretation of unsteady state measurements, especially at low oil viscosity, where piston like displacement occurs.
- Minimal data due to cost constraints.

1.3 Project Approach and Summary

The work done in this project can be summarized as follows:-

1 A literature search and review has been completed covering relative permeability and its measurement, capillary pressure and its measurement, relative permeability-capillary pressure relationships, the wettability, x-ray computed tomography and the relevant areas of interest such as the use of the routine and special core analysis in reservoir engineering[8-11].

2 In preparation for the special core analysis, the following work has been carried out at each stage:

i) cleaning of rock samples to remove any water, salt and/or oil followed by drying

ii) measurement of helium porosity and gas permeability

iii) measurement of liquid porosity and permeability

3 A group of the most homogeneous sandstone rock samples has been selected using CT Scan. The selected core samples exhibit a wide porosity and permeability range which varies from 7.0 to 30 porosity percent and with permeability from less than 100 to few thousands millidarcy. The work using x-ray computed tomography falls into the following parts:-

a The medical scanner is usually calibrated using two main reference points, air and water which is accurate enough for medical purpose. It has been found that the use of the ordinary calibrated CT scan gives a poor data reproducibility for core analysis, which leads to a significant error in producing quantitative results rather than the qualitative ones. Therefore it is extremely important that the medical scan must be re-calibrated using special sample falling within the geological region of interest before its use in core analysis.

b To validate CT measurements in core analysis after scan re-calibration, porosity has been measured for the selected samples using dual scan method then compared with values obtain by the routine laboratory measurements using helium and liquid.

c A new method to quantify rock heterogeneity has been developed, rather than the common qualitative description. The method was based on the non-destructive porosity measurements for interior sub-volumes, along and across the tested sample. The main advantage of this method is that it can be applied on any rock sample regardless of size or shape and has the ability to take measurement at any interior point while the sample is not damaged. This permits the extension of CT imaging to be used as an new tool to assess the degree of homogeneity quantitatively and to assist in core screening. The new approach has been used to monitor porosity variation within a group of sandstone rock samples from UK which has been believed to be a homogeneous and to compare them with Berea Sandstone which is often used as a standard.

d Development of a new single scan method for porosity measurement using x-ray computed tomography, based on the reasonable consistency of x-ray attenuation of sandstone rock grains. The method saves more than 50% of time and money compared to the multiple scan method.

- **e** The developed relationship between x-ray attenuation coefficients and porosity (single scan method), formed the basis of the use of CT imaging as a means for porosity logging on whole core.

- **f** The new single scan technique was compared against the multiple-scan method by measuring porosity for a group of sandstone samples.

- **g** The CT porosity logging method was used to measure the variation of porosity with depth in poorly consolidated dry sandstone whole cores, and the results were compared with helium porosity data obtained by plugging the whole core .

- **h** It was intended to perform the relative permeability tests using both, CT Scan and the 1-D x-ray monitoring technique which believed to be the latest technology in core analysis. It has been found that a significant error arises in using both techniques for measuring relative permeability by dynamic displacement (unsteady state), specially at high flow rate which is the most desirable in water flooding. The problem was discussed with experts in industry and a remedial solution is introduced in this thesis. This required some technical modifications in both techniques. Therefore, it was decided to measure the relative permeabilities using the conventional methods.

4 Wettability of each selected sample has been restored by aging for 40 days[12,13] under 200^0F (93^0C) and 2000psi (13,790kPa) in crude oil then measured using Amott/USBM method, which is known as the most precise method. These are very time consuming (it takes up to 8 weeks per sample). All selected samples are water-wet, so water and oil can be defined as the wetting phase and non-wetting phase, respectively. For oil wet samples, oil is the wetting phase and water is the non-wetting phase.

5 Capillary pressure measurements were carried out using both the porous plate diaphragm and centrifuge methods, for each selected sample to generate capillary pressure curves from which the relative permeability can be predicted. Although porous plate technique is classified as the best method to produce the capillary pressure curves it is very much time consuming. Full curve may take more than six weeks to determine.

6 An unsteady state and an steady state relative permeability rigs have been constructed. Imbibition and drainage relative permeability experiments have been carried out, and relative permeability curves have been generated using both steady and unsteady state techniques. Nevertheless, while the relative permeability data using the unsteady state technique can be obtained in a few hours, sample preparation requires at least one week. Steady state tests need around three weeks including preparation. Some samples may take longer due to difficulty in attaining stabilization. That is only per one cycle i.e. either drainage or imbibition.

7 Capillary pressure using mercury injection (pore size distribution) was carried out for the selected samples. Because of the nature of this test, the sample is destroyed, so it was carried out as the very last test.

8 Relative permeability curves derived from capillary pressure data using different mathematical models, were generated, then compared with those measured directly (experimentally) in laboratory.

9 Critical comparison between relative permeabilities derived from capillary pressure data and those measured in laboratory was carried out. The comparison included data obtained by the following methods:-

1. Relative permeability.
    a) steady state (Including drainage and imbibition).
    b) unsteady state (Including drainage and imbibition).

2. Capillary pressure.
    a) air-brine porous plate.
    b) centrifuge.
    c) mercury injection.

10 Selection and modification of the appropriate mathematical model to derive the relative permeability from capillary pressure data.

11 Verification of the modified model, including an error analysis when applied to representative rock core samples. This provided a balance between the theoretical and experimental work.

In addition to the previous work, the following studies has been carried out :

- Since the air-brine capillary pressure data is the most representative measurements, but very much time consuming. A new promising approach for sampling to reduce the experimental time was presented.

- A new method for correcting permeability measurement using Darcy law was presented for discussion.

CHAPTER 2

LITERATURE REVIEW

2.1 Relative Permeability

The porous media in water reservoirs contain no more than a single fluid phase, i.e. rocks are 100% saturated with water. The fluid flow in these reservoirs obeys Darcy's Law. Unfortunately, all oil reservoirs contain more than one fluid phase. In reservoir rocks oil is always accompanied by water; the water saturation varies from the irreducible water saturation (S_{wi}) at virgin zones to very high saturations at the transition zones, close to the oil water contact or at water flooded areas. For these reasons, the relative permeability (k_r) concept is introduced[14] to handle multiphase flow in porous media. It can be defined as the ratio of the effective permeability to the fluid (k_e) to absolute permeability (K), since

$$k_r = \frac{k_e}{K} \qquad (2.1.1)$$

Where, k_r can be to oil (k_o) or to gas (k_g) or to water (k_w). The absolute permeability for any rock is constant and the effective permeability of the rock to a particular fluid is a function of its saturation ,therefore, relative permeability is a function of saturation. Thus:

For oil , $k_{ro} = k_o / K$

For gas, $k_{rg} = k_g / K$

For water, $k_{rw} = k_w / K$

Figure 2.1 shows a typical relative permeability relationship over the water saturation range. Data covering the full range of saturations is only obtained in the laboratory. In the oil reservoir, relative permeability values will be restricted to the water saturation range from connate or irreducible water saturation (S_{wi}) to (1 - S_{or}), where S_{or} is the irreducible oil saturation. It is well known that the sum of relative permeabilities for two or three phases is always less than 1.0. It has previously been reported by Hawkins[15] that k_{ro} at S_{wi} could be higher than 1.0. Similar results were obtained in the present work, i.e. the effective permeability at S_{wi} for some samples is higher than the absolute permeability. These results require further explanation.

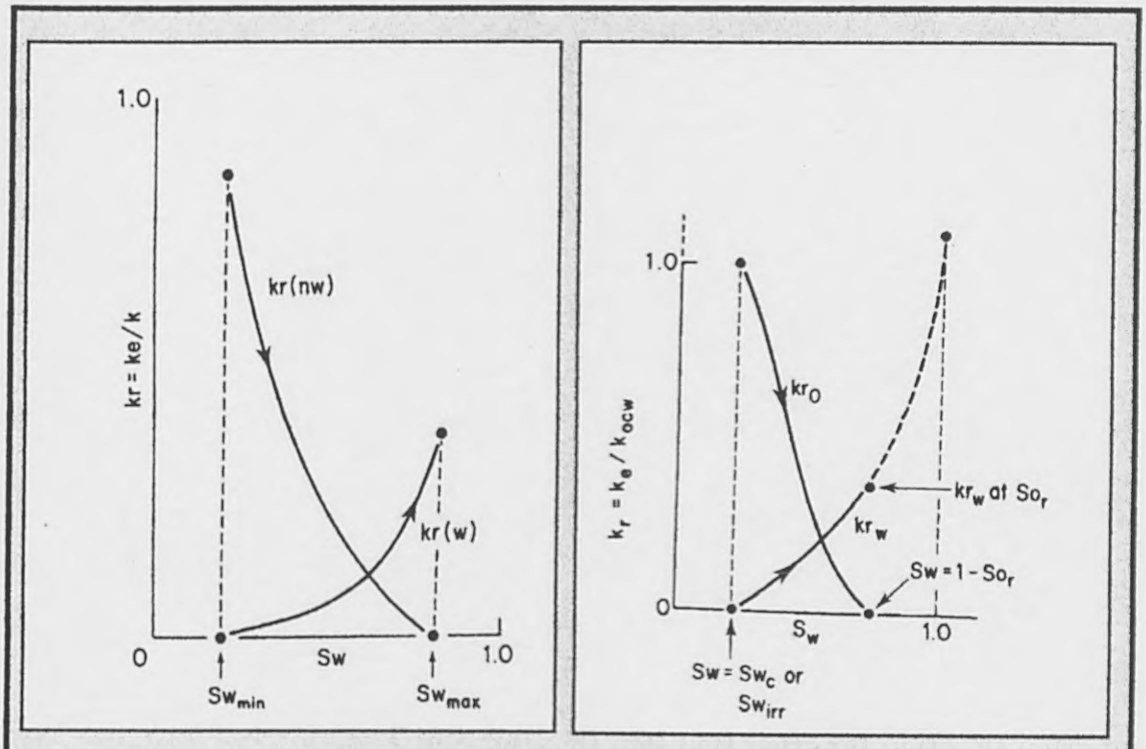

(a)
wetting and non wetting relative permeability (K base =k at 100 % saturation.

(b)
oil-water relative permeability (K base = k_o at S_{wi}.

Figure (2.1) Representation of relative permeability.

2.1.1 Relative Permeability Measurements

2.1.2 Unsteady State Technique

Unsteady state relative permeability measurements[17] can be carried out much more quicker than steady state methods[18] and are more representative of the fluid displacement in oil reservoirs. The interpretations of these measurements are based on the Buckley and Leverett theory[19] as extended by Welge[20]. Johnson, Bossler and Numan[21] extended this theory to permit calculation of individual relative permeabilities (the JBN method). They presented the following equations:

$$k_{ro} = f_o \, d\left(\frac{1}{w_i}\right) / d\left(\frac{1}{w_i I_r}\right) \qquad (2.2.1.1)$$

$$k_{rw} = \frac{1 - f_o}{f_o} \frac{\mu_w}{\mu_0} k_{ro} \qquad (2.2.1.2)$$

Where f_o, the fraction of oil at sample outlet is defined as

$$f_o = \frac{dS_{av}}{dw_i} \qquad (2.2.1.3)$$

and I_r, the relative injectivity is defined as
$I_r = U/\Delta P \div (U/\Delta P$ at start of injection) and,
w_i = cumulative injection in pore volumes
S_{av} = average saturation
μ_w = water viscosity
μ_o = oil viscosity
U = average velocity of approach toward entering

They assume two conditions before this method is applicable, which are that the displacement must occur at a stabilized state and that velocity is constant at all cross-sections of the sample. Although JBN method is the most common in the oil industry, several alternative[22,23] methods for obtaining the relative permeability from the displacements experiments are available in the literature.

2.1.3 Steady State Technique

The relative permeability can be measured using steady state methods. In the steady state method, two fluids are injected simultaneously at a fixed ratio until saturation and pressure equilibria are established. The full relative permeability curve over a wide range of saturations can be obtained easily. Numerous techniques have been successfully employed to obtain uniform saturation. These methods are summarized by Honarpor[24].

Richardson *et al*[25] compared the following steady state methods: Penn state, Single core dynamic, Dispersed feed, Hafford technique, Hassler technique and Gas drive technique. The results show excellent agreement between all these methods except for single core dynamic and gas drive technique. The interpretation of steady state relative permeability measurements is based on a modified Darcy's Law, which can be applied to each phase individually.

2.1.4 Centrifuge Method

The centrifuge method for measuring relative permeabilities requires monitoring the fluid produced from the tested rock sample. Few laboratories have the capability to conduct these tests under confining pressures[8]. The centrifuge is spun at certain speed and the pressure differential induced by the centrifuge will displace the oil. The equation[26-28] for deriving the relative permeability from these measurements is as follows:

$$k_{rf} = \frac{11.09\, Q_f\, \mu_f}{K_a\, A\, \Delta\rho\, g'} \qquad (2.1.4.1)$$

In which

k_{rf} = produced fluid relative permeability, friction

Q_f = produced fluid rate, m^3/sec

μ_f = produced fluid viscosity, Poise

K_a = absolute permeability, Darcy

A = cross section area of core plug, m^2

$\Delta\rho$ = density difference, kg/m^3

g' = centrifugal acceleration

Where:

$g' = 1.117\times10^{-7}\, w^2\, r$ in which:

w = centrifuge speed, rpm

r = radius of centrifuge arm to center of sample, m

Although this method is not common in core laboratories, it offers some advantages such as the ability to create large pressure differentials across the core plug and speed in measuring relative permeability data.

2.2 Averaging Relative Permeability Data

Although the relative permeability curve is known to be a constant for a rock type, it varies significantly in some instances. In these cases it is very convenient to average the data, and then present it as a single curve. There are three common methods for averaging the measured relative permeability data in order to present it in a single group. (Note that the averaged relative permeability must be re-averaged against the reservoir thickness only in one case, when the fluid displacement neither diffuse nor segregated flow i.e. when transition zone is close to the reservoir thickness). This method is direct averaging by plotting the arithmetic means of both water and oil.

2.2.1 Curve Averaging

Relative permeabilities against water saturation (S_w). This method is applicable when the obtained experimental data is very close and consistent specially S_{wi} and S_{or} values, where S_w varies from S_{wi} to $(1-S_{or})$. The S_{wi} and S_{or} are the arithmetic average for the included samples.

2.2.2 Craig's Method

Craig described his method in his book[29]. It can be summarized as follows:
Average water saturations are calculated for chosen values of oil relative permeability k_{ro} to cover average of water saturation from S_{wi} to $(1-S_{or})$. Then average water relative permeability (k_{rw}) values are calculated from $k_{ro}\times(k_w/ko)$ for the average water saturation. Then the average data is displaced in the normal way.

2.2.3 Normalizing of the relative permeability curves

The standard method of normalizing the relative permeability data was presented by Schneider[30] using the following equation:

$$S_w^{*} = \frac{(S_w - S_{wi})}{(1 - S_{wi} - S_{or})} \qquad (2.2.3.1)$$

Where S_w^{*}, is the normalized water saturation. This method will allow the relative permeability data to be compared on an equivalent basis as all the relative permeability values will starts at 0% and ends at normalized saturation. This method is based on the assumption that all samples have similar S_{wi} values and forcing all the curves to end at a normalized saturation of 100%.

Hawkins[16] presented a new equation taking into account varying S_{or} values. The new equation starts all the relative permeability curves at 0% and ends them at the final saturation of $(1-S_{or})$. His equation is as follows:

$$S_w^* = \frac{(S_w - S_{wi})(1 - S_{or})}{(1 - S_{wi} - S_{or})} \tag{2.2.3.2}$$

2.2.4 Thickness averaged relative permeability (pseudo relative permeability)

The relative permeability generated using this method is commonly known as the pseudo relative permeability, and is necessary only if the capillary transition zone is comparable with the reservoir thickness. This means that the saturation distribution is non uniform over the reservoir thickness. The water saturation varies from S_w =100% at the bottom of the reservoir to S_{wi} at the top. Therefore, it is extremely important to present the relative permeability data in its pseudo form. For a homogeneous reservoir, the thickness averaged water saturation (S_w") can be expressed as follows:

$$S_w'' = \frac{\int_0^h S_w(z)\,dz}{h} \tag{2.2.4.1}$$

Similarly:

$$k_{rw}''(S_w'') = \frac{\int_0^h k_{rw}(S_w(z))dz}{h} \tag{2.2.4.2}$$

and

$$k_{ro}''(S_w'') = \frac{\int_0^h k_{ro}(S_w(z))dz}{h} \tag{2.2.4.3}$$

Where, k_{rw}'' and k_{ro}'' are pseudo relative permeability for water and oil respectively. The method was described in details by Dake[15]. Hearn[33] presented another averaging technique for stratified flooding.

2.3 Capillary Pressure in Porous Media

The equilibrium saturation distribution in a virgin petroleum reservoir (before production is started) is governed by pore space characteristics. This happens as a result of hydrocarbons (oil) entering pore spaces initially saturated by water during migration of hydrocarbons from the source rock region to a reservoir trap. A differential pressure is required for oil to displace water. It is equivalent to a minimum threshold capillary pressure.

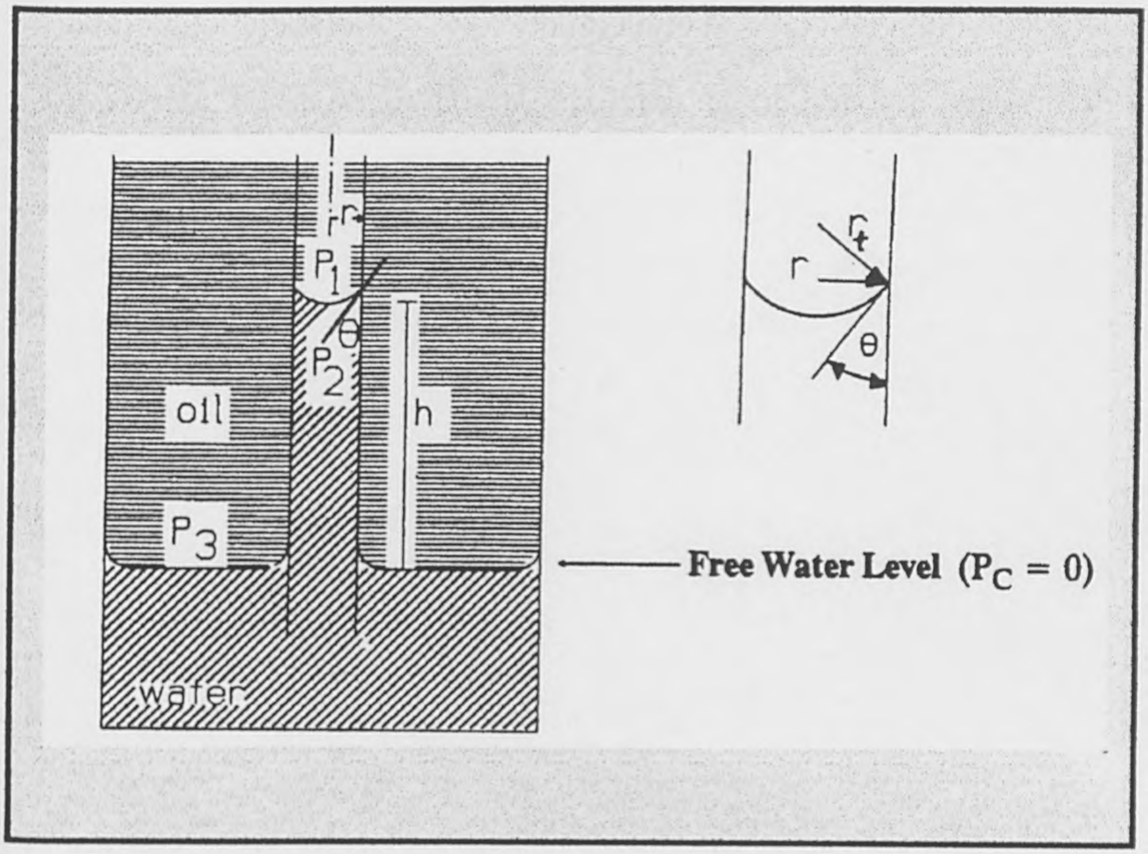

Figure (2.2) Capillary tube with oil/water system[31].

Capillary pressure (P_c) can be defined as the pressure difference across the contact surface between two immiscible fluids. For an immiscible fluid pair confined in a circular cross-section pore of radius r, the capillary pressure can be derived as follows:

If σ is the interfacial tension between the immiscible fluids and θ the contact angle as per Figure 2.2 the pressure differential across the curved interface is:

$$P_1 - P_2 = 2\sigma/r_t \tag{2.4.1}$$

but r_t is related to r by

$$r_t = r/\cos\theta \tag{2.4.2}$$

thus:

$$P_c = P_1 - P_2 = \frac{2\ \sigma \cos\theta}{r} \tag{2.4.3}$$

This relationship defines the capillary pressure in terms of the tube radius. It can also be defined as the pressure difference which causes the rise of a wetting liquid in a capillary tube. If a glass capillary tube is immersed in a water/oil system, the surface tension around the periphery of the contact pulls the water interface upward against gravity till equilibrium is reached i.e. the capillary force balances the effect of the hydrostatic pressure. The pressure equilibrium can be expressed as follows:

surface tension × circumference = area × hydrostatic pressure of water capillary rise.

$$\sigma\cos\theta(\ 2\pi r\ ) = \pi r^2\ h\ (\ \rho_{water} - \rho_{air}\ )\ g \tag{2.4.4}$$

Where:

σ = surface tension, Newton/m

θ = contact angle between water and glass

r = tube radius, m

h = capillary rise, m

ρ = density, kg/m^3

g = acceleration due to gravity (9.80665m/sec^2)

substituting equation (2.4.3) in equation (2.4.4) gives:

$$P_c = h\ (\ \rho_{water} - \rho_{oil}\ )\ g \tag{2.4.5}$$

Where P_c in Newton/m^2

For a large tube, P_c and h will be approach to zero. The water level will be essentially the same, inside and outside. This level is call the free water level, which is defined as the level at which $P_c = 0$. This level in oil reservoir is called the oil-water contact (OWC). The water saturation from and below the OWC is 100%. The capillary pressure, obviously increases with height above OWC as per equation (2.4.5). Figure 2.3 shows a typical capillary pressure curve for a homogeneous oil reservoir at drainage and imbibition displacement.

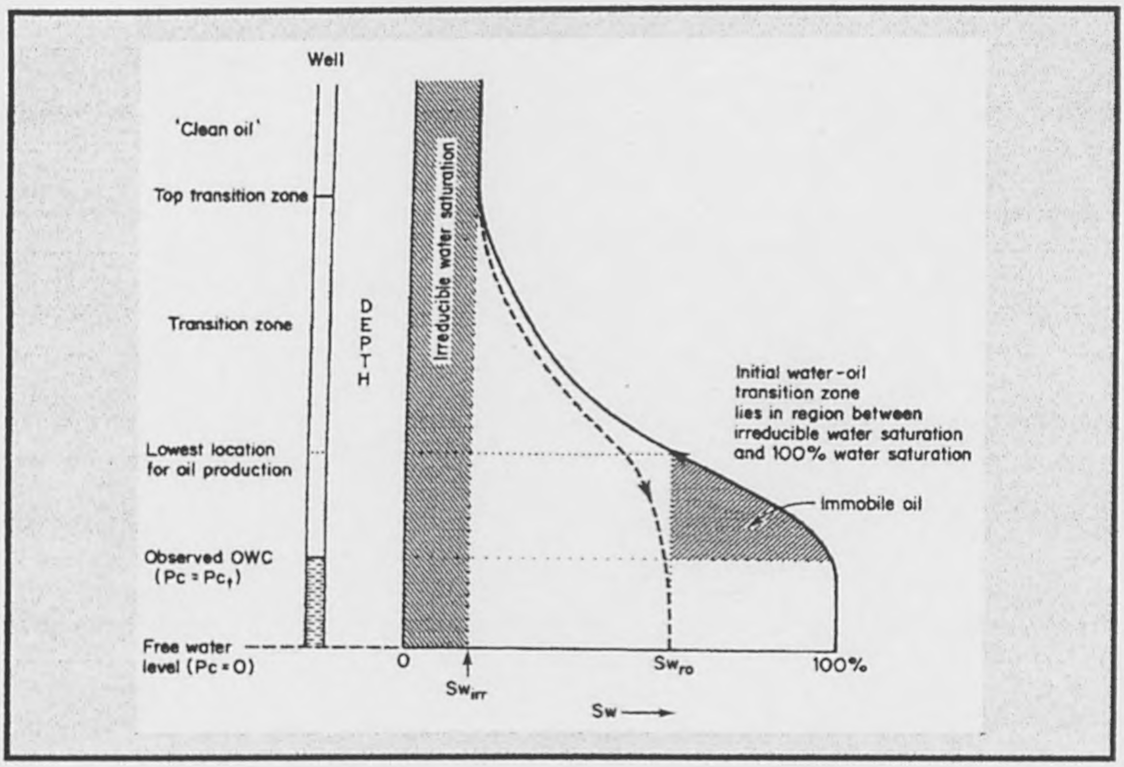

Figure (2.3) Water saturation distribution vs depth from OWC to S_{wi}[32].

Figure 2.3 shows how the capillary pressure curve can be simulated by a bundle of capillary tubes of different sizes. The capillary pressure increases with decreasing tube diameter and vice versa. In reservoir terms, the capillary pressure of a reservoir rock increases as pore size (or more specifically pore throat) diameter decreases.

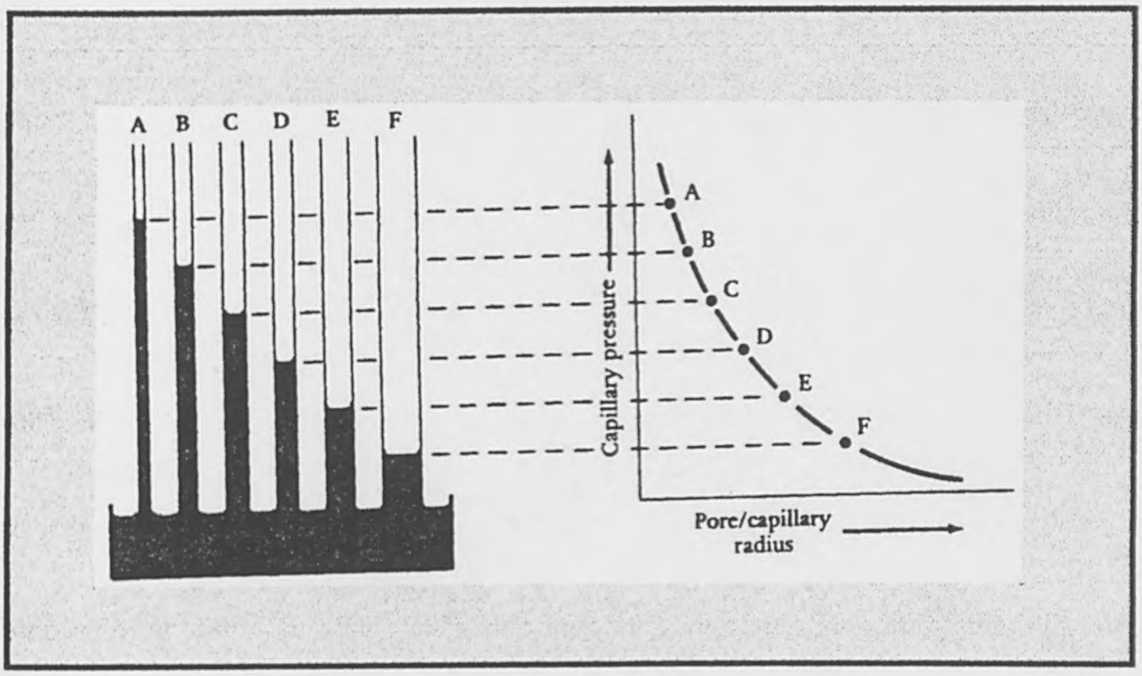

Figure (2.4) Capillary tubes of various diameters showing that the heights of the liquid columns are proportional to the diameters of the tubes[149].

2.3.1 Capillary Pressure Data

Capillary pressure data is used to generate capillary pressure curves which represent the relationship between fluid saturations and capillary pressure. In general these curves can be used to:

1 measure the pore size distribution (more precise data can be obtained using the mercury injection method)
2 estimate absolute permeability of the rock
3 derive relative permeabilities for the rock/fluid system
4 predict the distribution of oil and water saturations above the water-oil contact
5 determine the irreducible water saturation
6 approximate[34] the irreducible oil saturation
7 define the reservoir flow regime, either diffuse (disperse), segregated or in between

2.3.2 Capillary Pressure Measurements

The most common methods for measuring capillary pressure in core laboratories are the following:

1 **Porous Plate Diaphragm**

A complete set of data can be obtained, which is adequate to generate the full capillary pressure curve. However, this is a time consuming method (taking several weeks). It gives the most reliable measurements[35-37] since the capillary displacement in a porous plate diaphragm is more representative[38] of the fluid displacement in a porous media medium.

2 **Centrifuge Method**

In this technique, the saturated core sample is placed in centrifuge and subjected to centrifugal force[39,40]. The sample saturation is measured at each stage, and the capillary pressure is calculated at each centrifuge speed. Using this method the equilibrium is established rapidly, therefore the capillary pressure curve can be generated in one day. On the other hand, the pressure calculation from centrifuge may add additional uncertainties[35].

3 **Mercury Injection Method**

This method[4] is much quicker than the previous methods; a complete curve can be obtained within a few hours and very high pressures can be applied. Therefore, it is the method of choice for determining pore size distribution. The disadvantage of this method is the use of mercury whose wetting properties are completely different from those of the reservoir fluids. Furthermore, this method is destructive for the samples, so the core samples will be spoiled and can no longer be used for further experimental work.

2.4 Pore Size Distribution

The pore size distribution for a porous material has a major influence on saturation distributions[41,42]. It is usually measured by mercury injection. Its main advantages are that high pressures can be applied and the mercury can be forced into the extremely small pores, and the test can be completed within few hours. The pore size distribution function $D_{(r)}$ is determined from the volume of mercury injected over a certain pressure step as shown in Figure 2.5.

$$D_{(r)} = \frac{P_c}{r}\frac{ds}{dP_c} \qquad (2.5.1)$$

Where

$D_{(r)}$ = Distribution function, (cm^2)

ds/dP_c = saturation gradient

P_c = capillary pressure ($dynes/cm^2$)

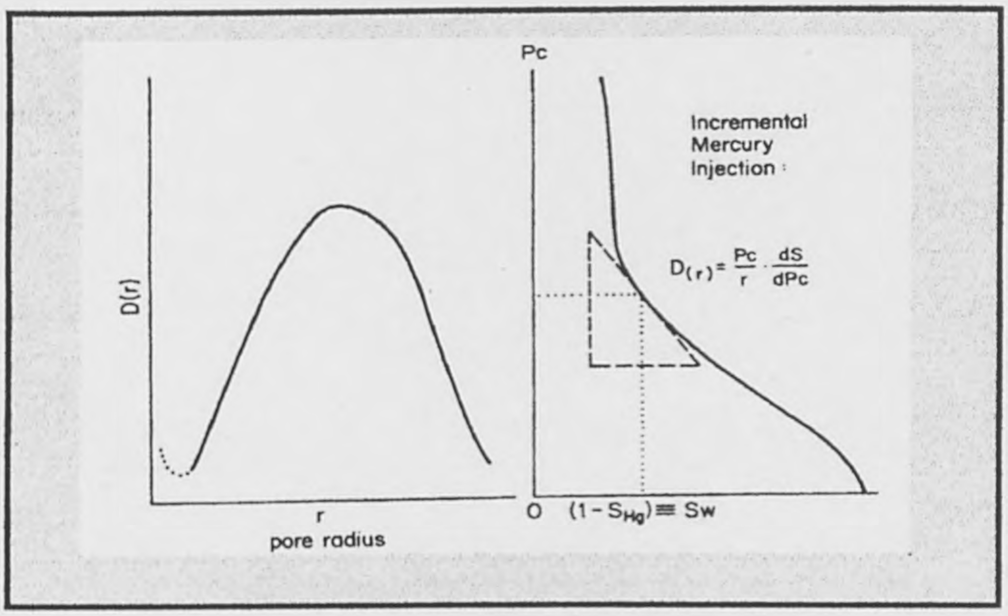

Figure (2.5) Pore size distribution function.

2.5 Wettability

2.5.1 Definition

Wettability can be defined as the relative preference of a solid surface to be covered by one fluid over the other. The fluid which spreads more is called the wetting phase. The angle between the wetting phase and the solid surface is known as the contact angle (θ). It gives a direct indication for surface wettability, and it is influenced by the tendency of one of the fluids in the immiscible pair to spread on the surface. For the oil-brine system, wettability can be described according to the contact angle either on a solid surface as shown in Figure 2.6 or within a confined capillary (Figure 2.7) as the following:

$\theta = 0^{o} - 30^{o}$	is strongly water wet
$\theta = 30^{o} - 90^{o}$	is preferentially water wet
$\theta = 90^{o}$	is neutral wettability
$\theta = 90^{o} - 150^{o}$	is preferentially oil wet
$\theta = 150^{o} - 180^{o}$	is strongly oil wet

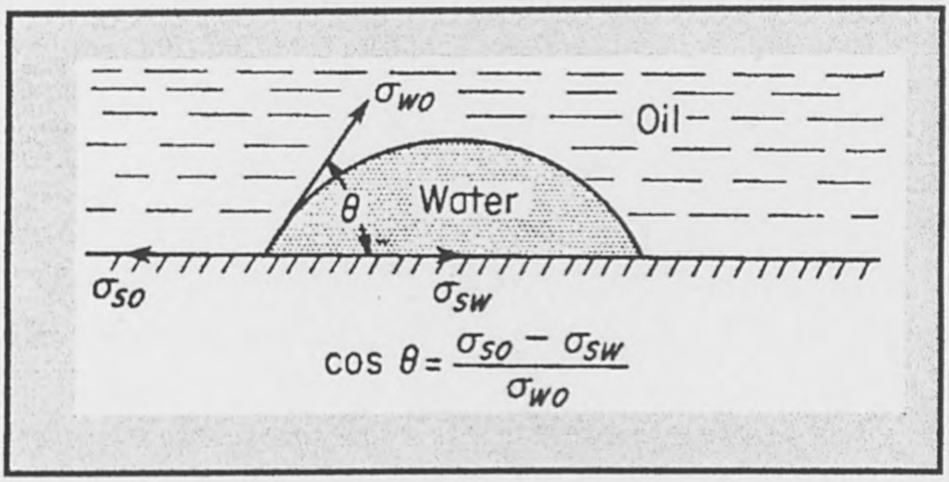

Figure (2.6) The combination of forces governing wettability for water/oil rock system[43].

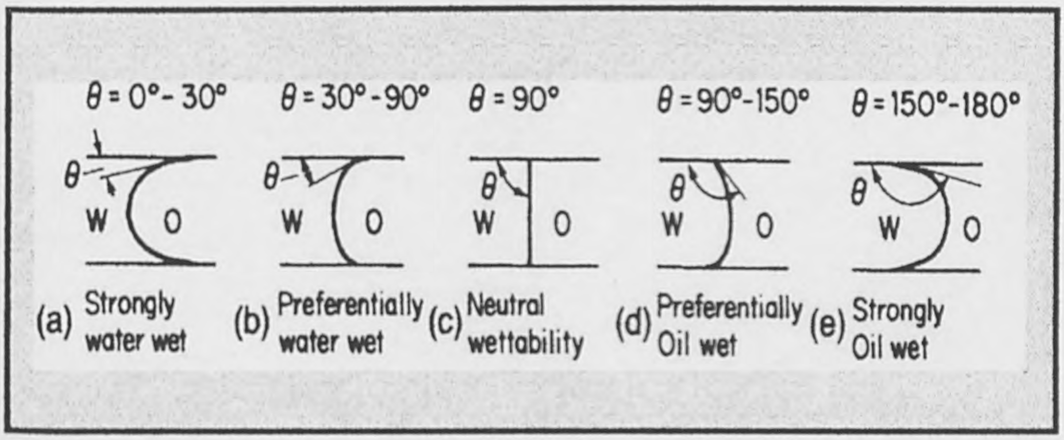

Figure (2.7) Relationship between the wetting contact angles and rock wettability.

When the contact angle is 90^0, both water and oil have equivalent tendencies to occupy the small pores and to cover the rock surface. As the contact angle decreases, the tendency for water to occupy the small pores and to cover the majority of the rock surface increases. Similarly, as the contact angle increases the rock is preferentially in contact with oil. The behavior of the two fluids is then the reverse of that in the water-wet case, and oil occupies the small pores and covers the majority of the rock surface. As a result the wettability has a significant influence on the static and dynamic properties of the porous media[44-52].

2.5.2 Wettability of Reservoir Rocks

Historically, all petroleum reservoirs were believed to be strongly water-wet. In 1934, Nutting[53] found that some reservoirs are strongly oil-wet. Yen[54] suggests that most carbonate reservoirs range from neuterally to oil wet. Brown and Patt[55], Fatt and Klikoff[56], Gimatudinov[57], Holbrook and Bernard[58] and Iwankow[59] discussed the term "fractional" wettability which is also called heterogeneous or spotted wettability. In fractional wettability, a portion of a rock is strong oil-wet, while the rest is strongly water-wet. Salathlie[60] introduced the term "mixed wettability" term which is a special case of fractional wettability in which the oil wet surfaces form continuous paths through the large pores. The smaller pores remain water-wet and contain no oil[61-63].

2.5.3 Methods of Wettability Determination

Numerous methods have been reported in the literature[29,38,64-74]. However, the most commonly used methods in the oil industry are the Amott method[66], Centrifuge technique (USBM), combined Amott/USBM and the Contact Angle method[36,45]. Many other methods have been summarized by Honarpour[24].

2.5.4 Influence of Wettability on Capillary Pressure and Relative Permeability

Many researchers[47,75-78] have studied the effect of wettability on capillary pressure measurements. One of Anderson's[47] final conclusions in his literature survey on this subject is that the capillary pressure/saturation relationship depends on the interaction of wettability, pore structure and saturation history. No simple relationship exists that relates the capillary pressures determined at two different wettabilities. Figure 2.8 demonstrates how capillary pressure curve can be shifted significantly if wettability is changed. Studies on fluid displacement showed that relative permeability also depends on wettability, as discussed in section (2.7).

Knowing that any variation in rock sample wettability can affect the capillary pressure and relative permeability measurements, it becomes programme essential to keep the rock sample wettability constant through all the experimental work by following the same handling procedures.

2.6 Factors Affecting Relative Permeability Measurements

2.6.1 Effect of Flow Rate

The relative permeability of a porous medium to oil and water was known as a rock property which is function of water saturation only and independent of flow rate[76] or any other factors. In core measurements it was found out that the relative permeability is significantly influenced by the rate[17] of flow at which the test is performed. Figure 2.9 show the effect of flow rate on oil recovery and relative permeability, for water wet, oil wet and mixed wettability samples.

Rapoport and Leas[79] introduced the concept of stabilized flow based on the scaling coefficient ($LV\mu_w$). Their finding was, that all floods corresponding to scaling coefficients greater than the critical value i.e. ($LV\mu_w$) ≥ 1.0, become similar to each other, in which

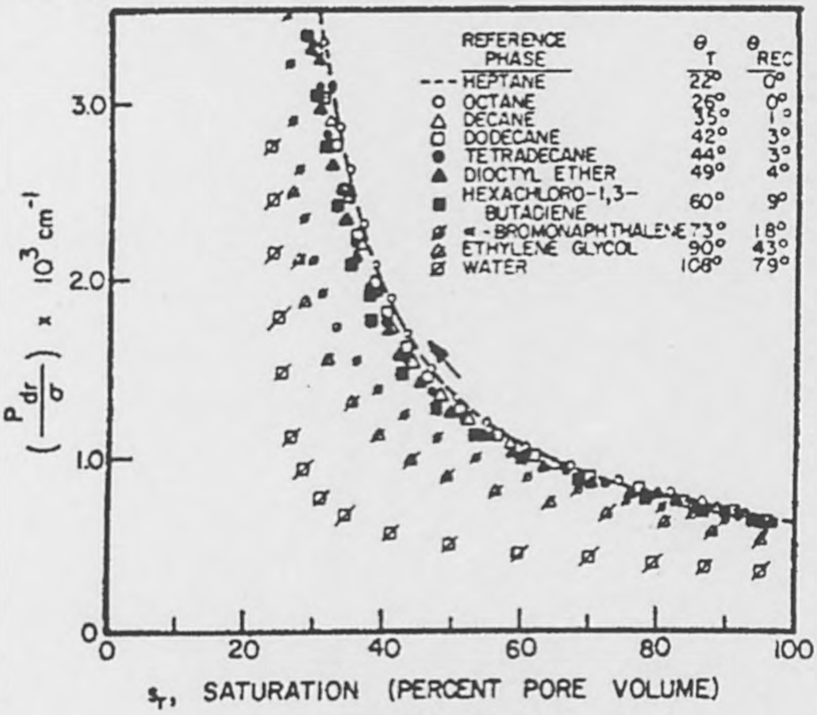

(a) DRAINAGE

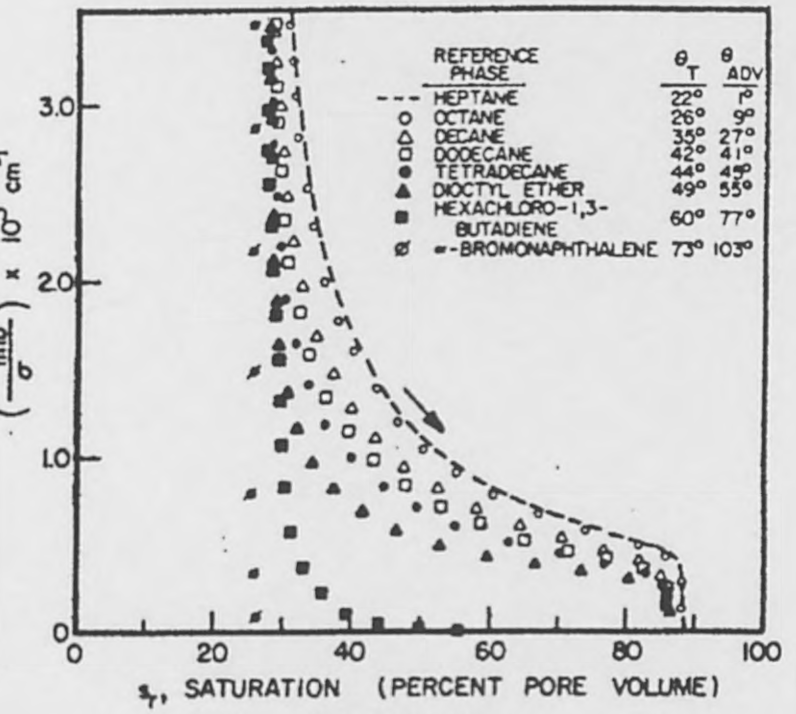

(b) IMBIBITION

Figure (2.8) Effect of contact angle on drainage and imbibition capillary pressures[78].

L = length of core plug, cm

V = Darcy velocity, cm/sec

μ_w = water viscosity, cp

In conclusion, for floods at scaling coefficient values higher than the critical value i.e. at higher flow rates, the capillary discontinuity (end effect) becomes negligible compared to the viscous forces due to the velocity increase, therefore the recovered oil versus injected water will be almost constant after certain flow rate. The oil recovery and the relative permeability is directly affected by the flow rate in tests carried out at scaling coefficient values below the critical value.

2.6.2 Effect of Fluid Viscosity

This is again one of the controversial aspects in relative permeability measurements. Leverett[80] studied the effect of viscosity on relative permeability of oil-water system, using different viscosity ratios μ_o/μ_w from 0.057 to 90. He concluded from data displayed on Figure 2.10 that the relative permeability is independent of fluid viscosities. Although data are obviously scattered, they do not show any regular trend. Similar results obtained by Sandberg *et al* [81] and Richardson[82] presented another elegant example of relative permeabilities being independent of fluid viscosity. The relative permeability curve was displayed as k_{rw}/k_{ro} against water saturation (Figure 2.11) using oil (kerosene) viscosities from 1.8cp to 151cp for both steady state and unsteady state displacement. No effect of viscosity can be observed. Many other authors [83-86] supported the previous point of view.

On the other hand, many researchers[87-90] believe that relative permeability measurement is significantly influenced by viscosity change. Clear variation in the non-wetting phase relative permeability reported by Odeh[91] as shown in Figure 2.12. His conclusion was that the non-wetting phase relative permeability increases with an increase in viscosity ratio and its deviation increases by increasing its saturation. Some researches[92-94] believe that viscosity has very small effect on relative permeability measurements. Downie and Crane[95] found out that viscosity variation has effect on some rock samples only.

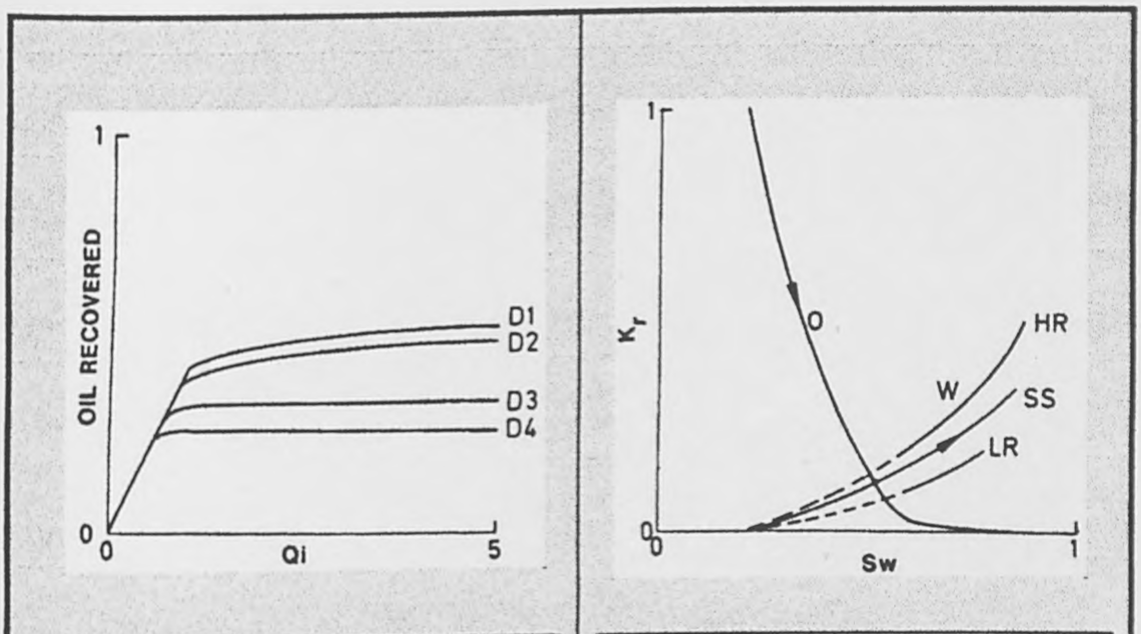

(a) oil recovery vs injected pore volumes at different displacement rate

(b) oil water relative permeability for water wet system

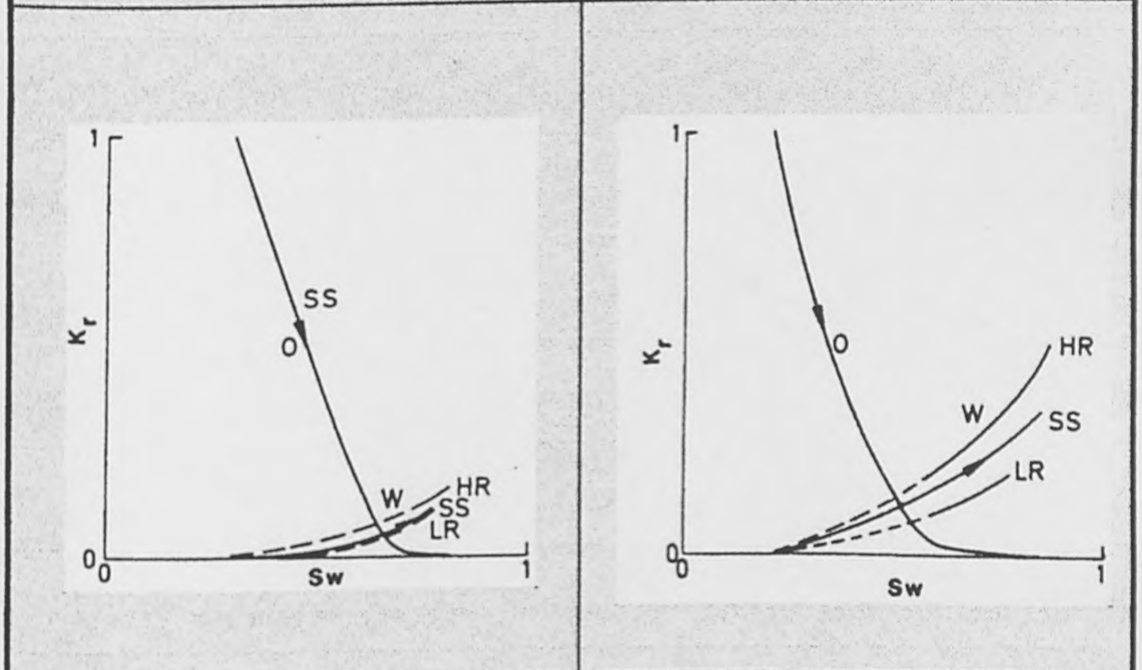

(c) oil water relative permeability for oil wet system

(d) oil water relative permeability for mixed wettability system

Figure (2.9) Effect of flow rate on oil recovery and relative permeability, for water wet, oil wet and mixed wettability sample[17].

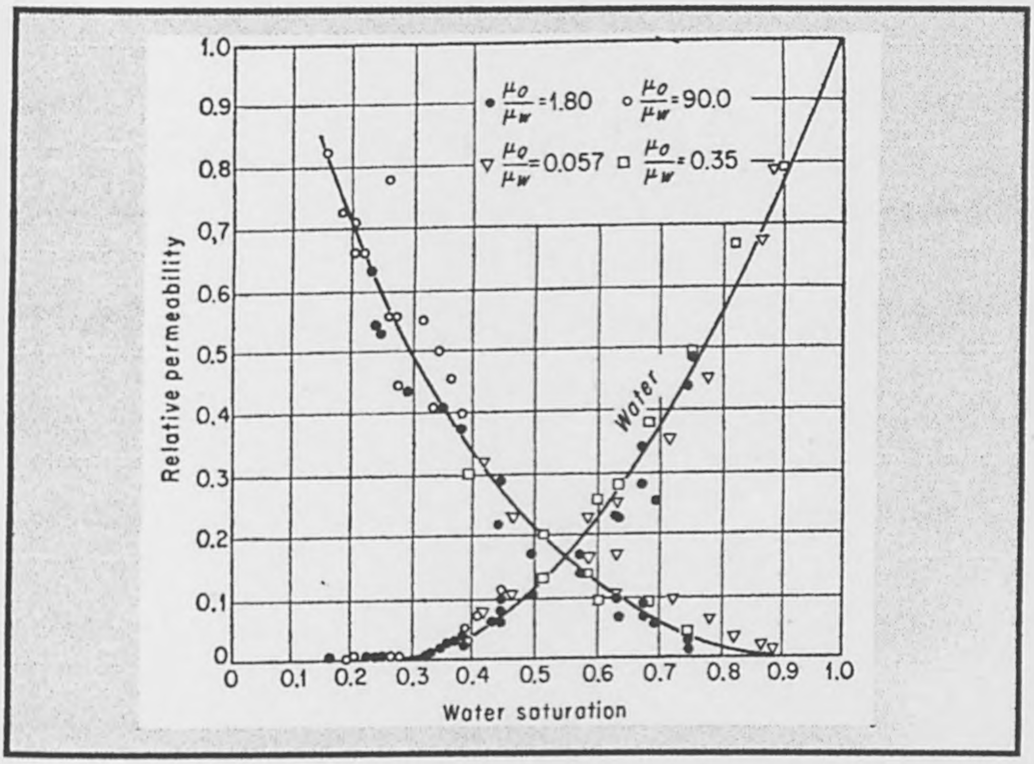

Figure (2.10) The effect of viscosity on relative permeability measurement. No regular trend[103].

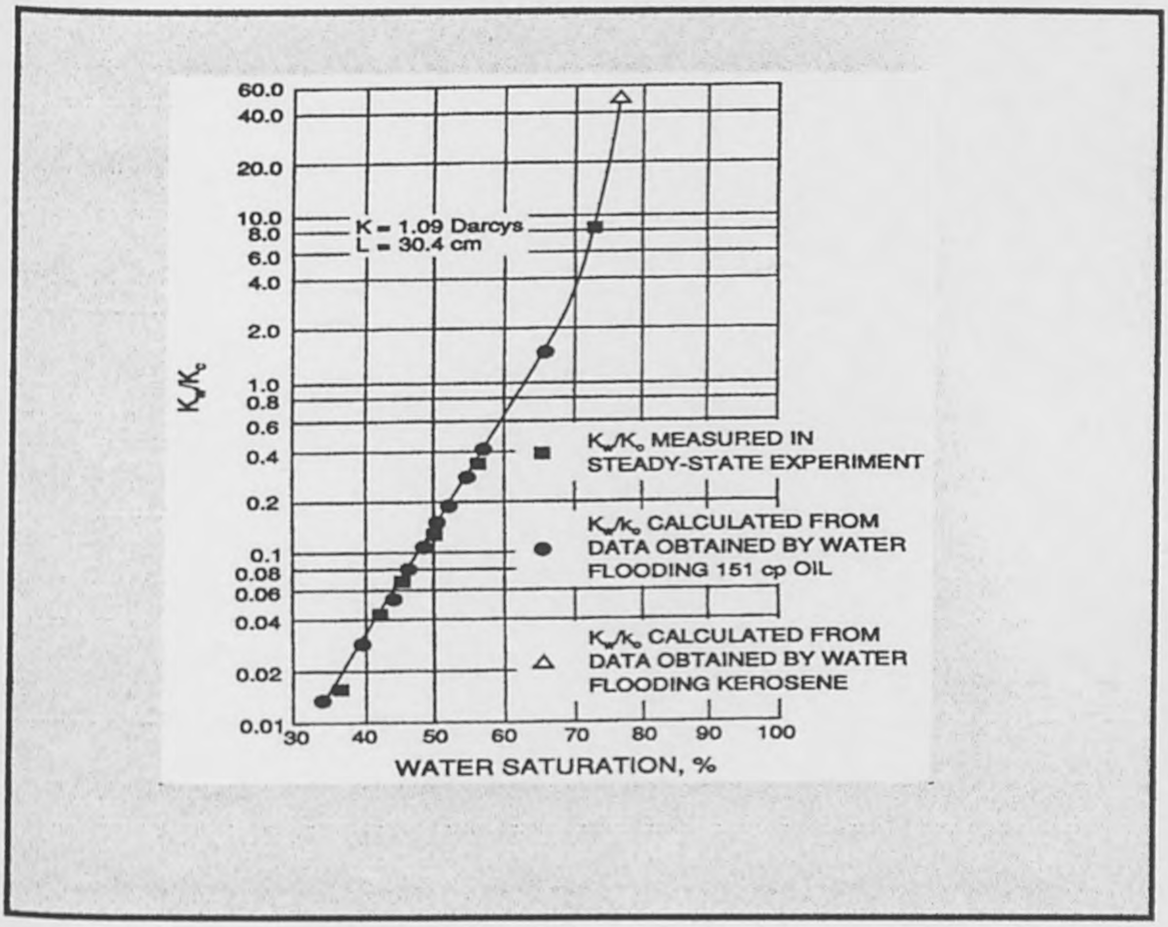

Figure (2.11) Effect of oil/water viscosity ratio on relative permeability as a ratio of k_{rw}/k_{ro}[82].

It is concluded that fluid viscosity changes can effect relative permeability measurements therefore it is strongly recommended that relative permeability tests should be carried out using matched fluid viscosity ratio (identical to the reservoir condition).

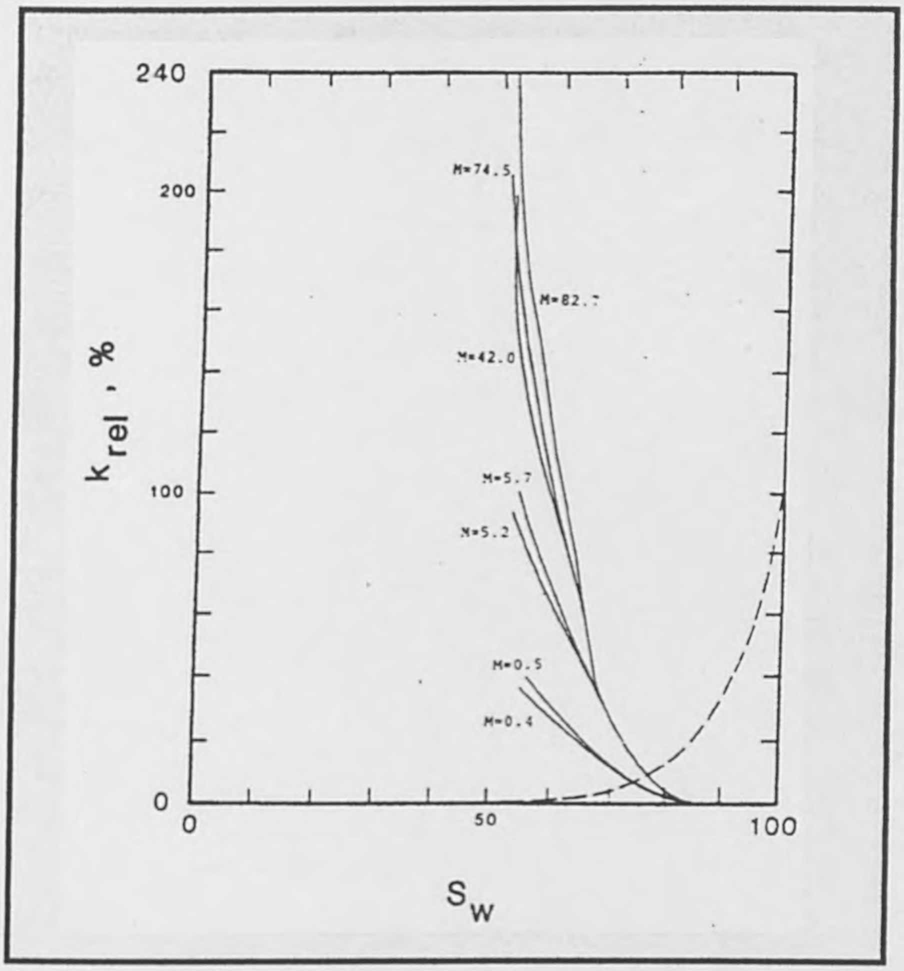

Figure (2.12) Effect of oil/water viscosity ratio(M) on non-wetting phase relative permeability[91].

2.6.3 Effect of Rock Wettability

The water flood behavior in an oil reservoir rock system is very dependent on reservoir rock wettability[18,29,36,97-104]. In a strongly oil wet system the rocks are preferentially in contact with oil and inference in water wet case. The microscopic distribution of fluids in a reservoir rock system is generally influenced by rock wettability as shown in Figure 2.13.

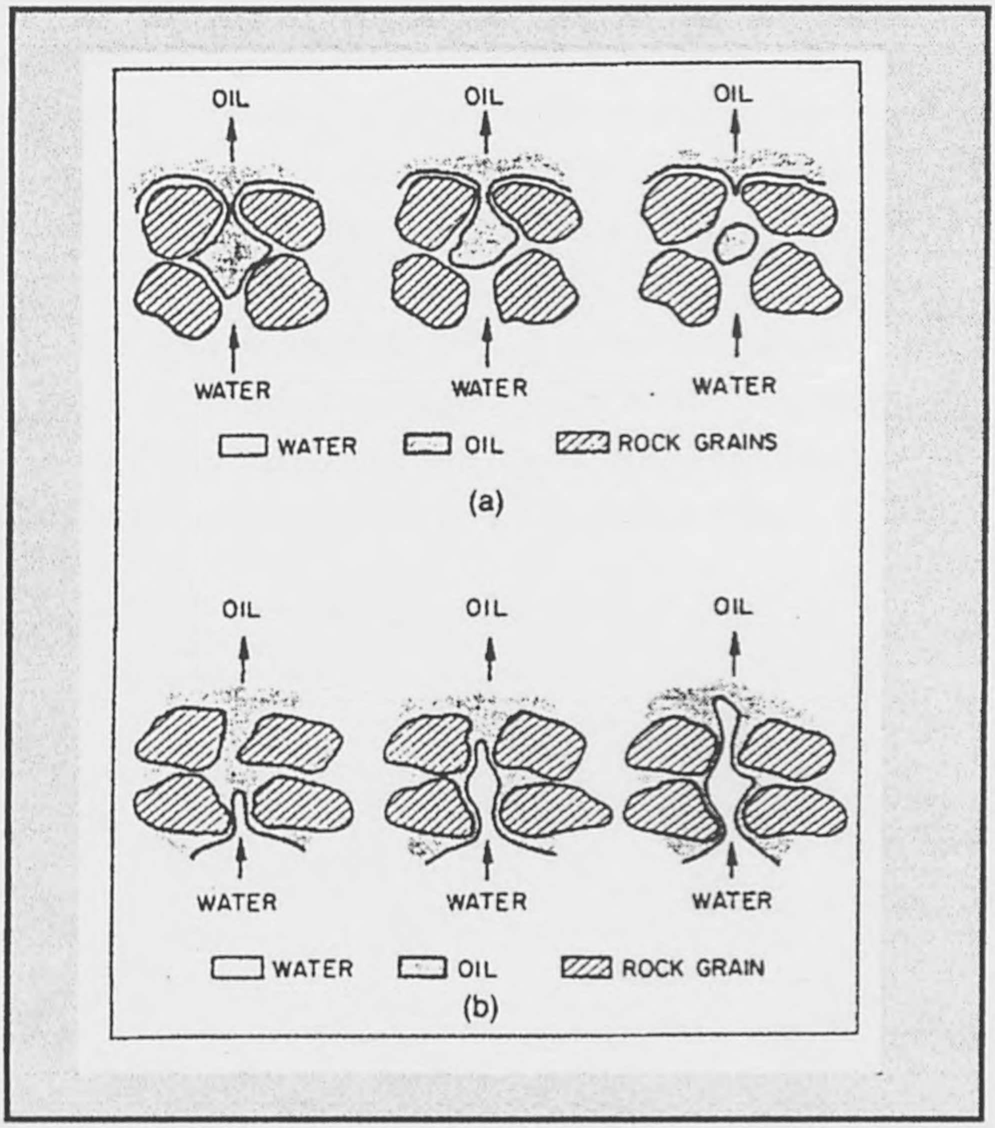

Figure (2.13) Water displacing oil from a pore during water flood :(a) strongly water wet, (b) strongly oil-wet rock[104].

There is no dispute that rock wettability has a great influence on relative permeability[105-114]. Any reservoir rock sample relative permeability curve can be changed by altering its wettability[115,116]. Figure 2.14 demonstrates how a relative permeability curve is shifted dramatically as wettability changes.

Anderson[48] concluded that relative permeability is a function of rock wettability. In uniform wetted core, the effective oil permeability at a given initial water saturation decreases as the wettability varies from water-wet to oil-wet; furthermore the water relative permeability increases and the oil relative permeability decreases as the sample becomes more oil-wet. In a fractional wetted system relative permeability appears to be affected in a manner similar to a uniformly wetted system. The water relative permeability increases and oil relative permeability decreases as the fraction of oil-wetted surfaces increases. In mixed-wettability samples, the continuous oil-wet paths in the large pores change the relative permeability curves compared with uniformly or fractionally wetted system. This usually leads to low residual oil saturation.

Based on the previous discussion, it can be concluded that the most accurate relative permeability measurements are carried on native-state core, which represents the reservoir wettability conditions. Cores which have their wettability altered due to mud invasion or any other contamination must be cleaned and restored.

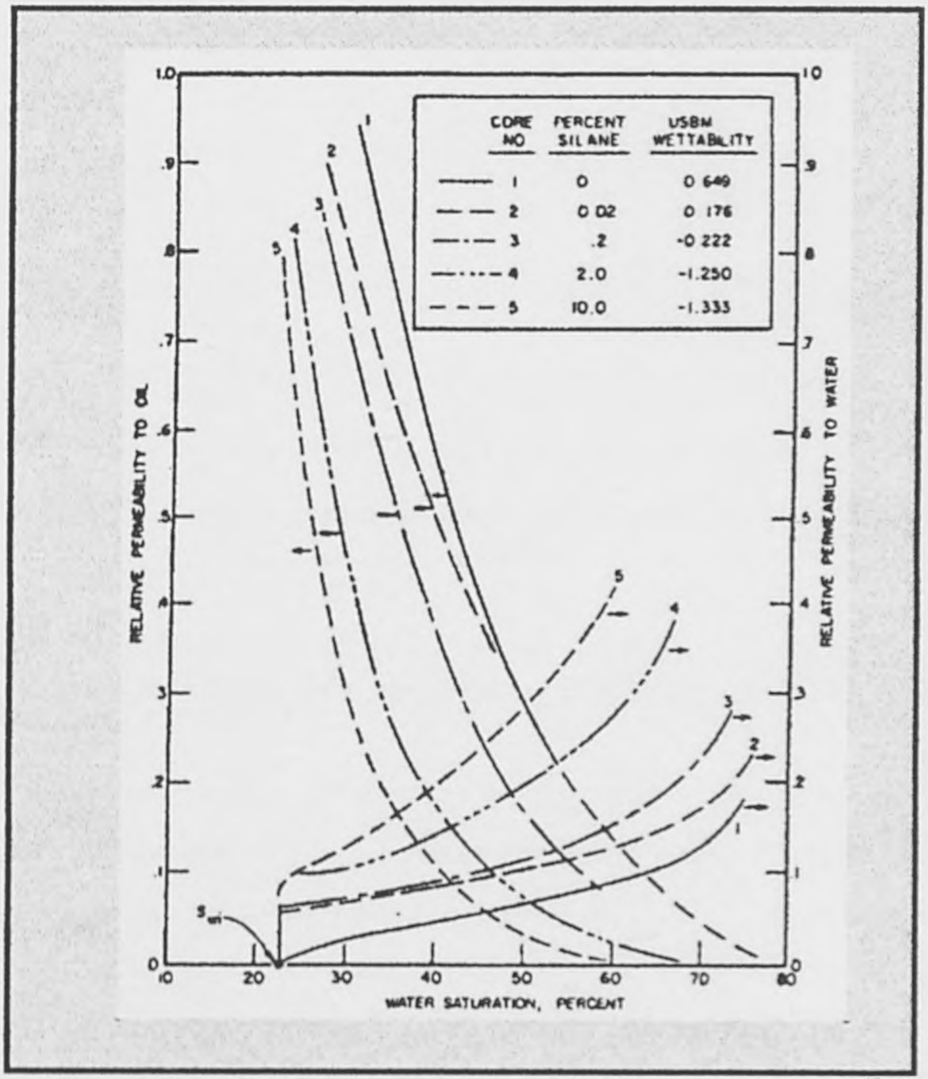

Figure (2.14) Effects of wettability on relative permeability[48].

2.6.4 Other Factors Effecting Relative Permeability

Many researchers[117-133] studied the effect of other different fluid and rock properties on relative permeability curves as summarized in table 2.1.

Fluid / Rock Property	**Effect on Relative Permeability**	**Remarks**
Capillarity[80,89,117-120]	Significant	Only at low flooding rate
Saturation History[16,97,121-123]	Significant	It is cycle dependent
Permeability/Porosity[21,124-126]	Negligible	
Temperature[127-130]	Significant	Handling high temperature in the lab can be difficult
Liquid density[121,124]	Insignificant	It is related to gravity effect
Interfacial Tension[103,112,124,131]	Controversial	Small or has no influence
Overburden Pressure[132-133]	Insignificant	Moderate to no change

Table (2.1) Influences of some fluid and rock properties on relative permeability data.

2.7 Mathematical Models for Relative Permeability Derivations

Laboratory measurements of reservoir rock/fluid relative permeabilities have been used for a long time in the oil industry. These direct measurements require a lot of work and time, involving as careful sample preparation, running of the time consuming experiments and data interpretation. However, empirical methods and mathematical models for determining relative permeability are becoming more widely used, particularly with the advent of reservoir simulators[24]. Since capillary pressure data is one of the essential measurements required in reservoir engineering, it would be a great advantage to be able to use these data for relative permeability calculations. Since Darcy derived his famous equation in 1856, many workers have tried to model fluid flow in porous media. An important work has been done by Kozeny (1927)[2] and the further development of this work in 1937 by Carman[3] led to the so-called Kozeny-Carman equation[6], which was based on Poiseuille's Law and Darcy's Law.

In 1949, Purcell[4] developed an equation to calculate the absolute permeability of a porous medium in terms of porosity and capillary pressure data. He based his model on the assumption that the porous medium can be represented by a bundle of capillary tubes of varying sizes. Several workers adapted the Kozeny-Carman and Purcell equations for relative permeability calculations.

Most of the existing mathematical models of fluid flow in porous media adopted/or adapted the two basic equations, Poiseuille's and Darcy's laws. Similarly, the derived models to predict relative permeability for rock system from capillary pressure data are based on these two laws. For this reason it has been thought that, it is useful to present these laws in some details and to work out their derivations as a good introduction to the basics of the concept.

2.7.1 Poiseuille's Law (1840)

Poiseuille carried out an experimental study for viscous fluid flow behavior in tubes (1840). He found that the functional relationship involved four variables: the flow rate from the tube (Q), the pressure differential (ΔP), the tube length (L), and the tube inside diameter (D). The diameter of his glass tubes ranged from 0.015mm to 0.6mm (Sutera 1993)[134].

Poiseuille expressed his empirical equation as follow:

$$Q = K'' \Delta P D^4 \qquad (2.7.1.1)$$

K" = 2495.224 for distilled water expressed in mixed units (mg/sec) (mmHg) mm^3

The more modern form of the relation is:-

$$Q = \frac{\pi \, \Delta P \, R^4}{8 \, \mu L} \tag{2.7.1.2}$$

Where, R is the tube radius, and μ is the fluid viscosity.

The difference between equation 2.7.1.1 and Poisseuille's equation 2.7.1.2 is simply that the Poisiuille constant K" is replaced by π / 128μ which can be derived as follows:- When fluid is in laminar flow in a tube (Figure 2.15), the velocity varies from a maximum at the center to zero at the tube wall.

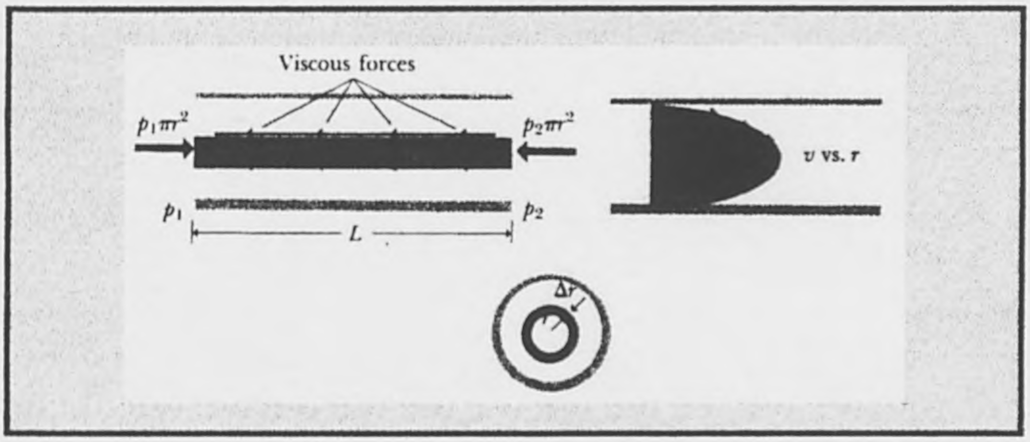

Figure (2.15) Forces and velocity distribution on a cylindrical element for a laminar flow in a tube.

The force on a cylindrical fluid element of length L and radius r is thus,

$$F = (P_1 - P_2) \, \pi \, r^2 \tag{2.7.1.3}$$

This force must be equal to the viscous forces on the element in steady flow

$$\mu = \frac{F/A}{V/L} \quad , \quad F = \mu A \frac{V}{L} \tag{2.7.1.4}$$

but the velocity is non uniform with distance from the center, so V/L is replaced by δV/δr, this viscous forces is :

$$F = \mu 2\pi \, r L \frac{\delta v}{\delta r} \qquad (2.7.1.5)$$

when the pressure force balances the viscous force:

$$\frac{\delta v}{\delta r} = \frac{(P_1 - P_2) r}{2 \mu L} \qquad (2.7.1.6)$$

by integration from (r = 0 to r = R)

$$V = \frac{P_1 - P_2}{4 \mu L} (R^2 - r^2) \qquad (2.7.1.7)$$

So, the change in flow rate of the cylindrical element will be as follows

$$dQ = 2 V \pi r \delta r \qquad (2.7.1.8)$$

$$= \frac{2\pi \, \Delta P \, r}{4 \mu L} (R^2 - r^2) \delta r \qquad (2.7.1.9)$$

by integration (V = 0 to R)

$$Q = \frac{\pi \, \Delta P \, R^4}{8 \mu L}$$ which is Poisseuille's Law

2.7.2 Darcy's Law

Darcy (1856) carried out an experimental investigation of the flow of water through a packed sand bed. The experimental apparatus is shown schematically in Figure 2.16. His observations were represented by the following equation:

$$Q = K A \frac{h_1 - h_2}{L} \equiv \frac{K A \Delta P}{\mu L} \qquad (2.7.2.1)$$

Where Q is the water flow rate down and through the packed sand, A is the cross sectional area of the cylindrical sand body and L its length, h1 and h2 are the up-stream and down-stream hydrostatic heads, respectively, μ is fluid viscosity, ΔP is the pressure drop and K is a constant. Darcy's work was restricted to the single phase flow of water through sand packs at only 100% water saturation.

Other investigations found that Darcy's equation could be extended to other fluids and the proportionality constant K is replaced by the term K/μ, where μ is the viscosity of the flowing fluid and K is a constant representing a property of the porous mediaum which is termed the permeability.

Darcy's law in its commonly used form is as follows:

$$Q = -\frac{KA}{\mu}\left(\frac{dP}{dX} \rho g \frac{dZ}{dX} \times 10^9\right) \qquad (2.7.2.2)$$

Where:

Q = flow rate, m^3/sec

X = distance co-ordinate in direction of flow, m

A = cross section area of porous medium, m^2

Z = vertical coordinate, m

ρ = density of fluid, kg/m^3

g = acceleration of gravity, 9.80665 m/sec^2

dP/dX = pressure gradient, Pa/m

μ = viscosity of the flowing fluid, Pa.sec

K = permeability of the porous medium, Darcy

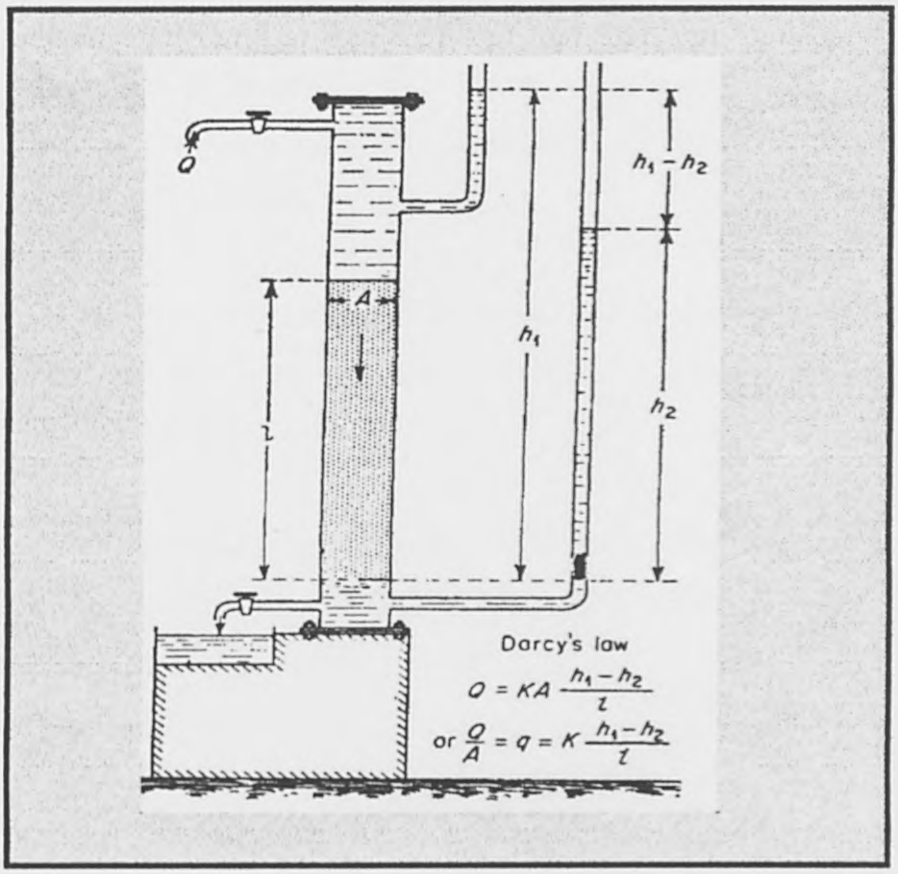

Figure (2.16) Schematic drawing of Darcy's experimental apparatus[43].

The dimensions of permeability according to Darcy's law can be established using the dimensional analysis.

By substitution in the previous equation.

L = length

M = mass

T = time

$Q = L^3 / T$

$\mu = M / LT, P = M / LT^2, S = L, \rho = M / L^3, g = L / T^2, Z = L$

$$\frac{L^3}{T} = \frac{KL^2}{M/LT^2}\left(\frac{M/LT^2}{L} - (M/L^3)(L/T^2)\frac{L}{L}\right)$$

$K = L^2$

It is shown that the permeability has units of length squared, i.e. centimeter square in cgs system or feet square in English system. Both were found to be inconveniently large to measure permeabilities of porous media. Therefore, the common unit in the oil industry to measure permeability is Darcy or millidarcy. If a porous medium with 1.0cm^2 cross sectional area and 1.0cm length will permit a single fluid at 100% saturation with a viscosity of 1.0cp to flow at 1.0cm^3/sec when applied pressure gradient is 1.0atm/cm, the permeability will be 1.0Darcy.

Darcy's law has been extended to a more general form in order to deal with presence of more than a single fluid in an oil reservoir. Each fluid has its own effective permeability which is a function of the fluid saturations.

If the relative permeability is defined as a ratio of effective permeability to absolute permeability, Darcy's Law can be restated for a rock system containing oil, water and gas as follows:

$$Q_o = -\frac{K\,A k_{ro}}{\mu_o}\left(\frac{dP_o}{dX}\ \rho_o g \frac{dZ}{dX} \times 10^9\right) \tag{2.7.2.3}$$

$$Q_w = -\frac{KA\,k_{rw}}{\mu_w}\left(\frac{dP_W}{dX}\ \rho_w g \frac{dZ}{dX} \times 10^9\right) \tag{2.7.2.4}$$

$$Q_g = -\frac{KA\,k_{rg}}{\mu_g}\left(\frac{dP_g}{dX}\ \rho_g g \frac{dZ}{dX} \times 10^9\right) \tag{2.7.2.5}$$

Where the subscripts o, w and g represent oil, water and gas respectively, and K is the absolute permeability and k_{ro}, k_{rw} and k_{rg} are the relative permeabilities of oil, water and gas.

Darcy's law is the basis for almost all the calculations of fluid flow in hydrocarbon reservoirs. To use this law for hydrocarbon reservoirs it is necessary to determine the relative permeability of the reservoir rock to each fluid throughout the range of fluid saturations that will be encountered in the reservoir. Obtaining this relative permeability data in core laboratories is associated with a lot of problems. Many investigators have attempted to predict this data instead from capillary pressure curves. A critical comparison of some correlations is presented in this thesis.

2.7.3 Kozeny-Carman Equation

If the porous media is conceived to be a bundle of capillary tubes, then the permeability can be related to porosity and pore radius (pore size distribution). Consider a medium formed of a bundle of cubical arranged capillaries. The space between the tubes sealed by cementing material. Neglecting the tube thickness leads to the following:

$$\text{Porosity } (\phi) = \frac{\text{Pore Volume}}{\text{Bulk Volume}} = \frac{\pi \ r^2 . r}{(2r)^2 . r} = \pi/4 \tag{2.7.3.1}$$

The number of tubes per area is given by

$$n = \frac{\text{Area} \times \phi}{\text{Tube Area}} \tag{2.7.3.2}$$

So number of tubes per unit area

$$= \frac{\phi}{\text{Tube Area}} = \frac{\pi/4}{\pi \ r^2} = \frac{1}{4r^2} \tag{2.7.3.3}$$

Again the flow rate can be given by:

$$Q = \frac{1}{4r^2} \ \frac{\pi \ r^4 \Delta P}{8 \mu \ L} = \frac{K \, \Delta P}{\mu \ L} \tag{2.7.3.4}$$

$$K = \frac{\pi \ r^2}{32} \tag{2.7.3.5}$$

From equation (2.7.3.1),

$$K = \frac{\phi \, r^2}{8} \qquad (2.7.3.6)$$

The internal surface area for pore volume unit (S_p) can be defined as follows:

$$S_p = \frac{\text{Surface Area}}{\text{Pore Volume}} = \frac{n \, 2\pi \, r \, L}{n \, \pi \, r^2 \, L} = 2/r$$

By substitution in equation (2.7.3.6)

$$K = \frac{\phi}{2 \, S_p^{\,2}} \qquad (2.7.3.7)$$

by substitution the constant 2 by constant K_z gives:

$$K = \frac{\phi}{K_z \, S_p^{\,2}} \qquad (2.7.3.8)$$

Where,

K_z is the Kozeny constant.

Wyllie and Gardner[6] presented the modified Kozeny-Carman equation as follows:

$$K = \frac{\phi^3}{2.5 \, (La / L)^2 \, S^2} \qquad (2.7.3.9)$$

S is the surface area per unit bulk volume of the medium. It is related to the surface per unit volume of pore space S_p as follows:

$$S = \phi \, S_p \qquad (2.7.3.10)$$

Where 2.5 is shape factor it is conventionally assumed it lies in the range 2-3, L is the actual length of bulk porous medium through which the fluid flows and La the apparent length of travel along the actual capillary flow path.

2.7.3.1 Assumption of Kozeny-Carman Equation

The Kozeny-Carman model is essentially an analogue model. The key assumptions are:-

1. The porous medium consists of one straight capillary of complex shape oriented in a direction parallel to that of microscopic flow.
2. The capillary mean hydraulic radius can be defined as porosity (Pore volume/ bulk volume) to internal surface per unit bulk volume S, i.e. ϕ/S.
3. Capillary shape is complex, therefore a shape factor is introduced it lies in the range 2-3, and is assumed to be 2.5.
4. The porous medium is uniform and isotropic, the flow area is ϕ per unit bulk area.
5. The fluid velocity (V_e) is defined by (V/ϕ (La/L), V is the macroscopic fluid velocity.

2.7.3.2 Limitation of Kozeny-Carman Equation

1. It can lead to significant errors if the porous medium possesses pores of identical size.
2. Small variations in La/L will be squared.
3. No counting for sealed or partially sealed pores.
4. The necessity for laminar flow.
5. A uniform pore size distribution is a fundamental requisite such as in un-consolidated system.

For any porous system with highly non very uniform pore sizes the Kozeny-Carman model will not be applicable and must break down seriously.

According to Poiseuille's Law, the fluid flow rate through a capillary is proportional to the fourth power of the capillary radius. As any porous medium contains small pores as well as large pores, the fluid flow will tend to be dominated by the large pores.

The initial surface per unit bulk volume (S) will be reasonably affected by the large surface of the small pores. The use of hydraulic radius concept (ϕ/S) in Kozeny-Carman model ignores or neglect the existing of individual pores by lumping all pores in one hydraulic radius.

In conclusion, the Kozeny-Carman model can be applied with confidence only if the range of pore sizes is small. Therefore it is acceptable to apply the model only to unconsolidated systems. It is also important that the distribution of particle sizes to be within certain limits[6].

In the consolidated reservoir rock, pore sizes vary quite significantly, therefore Kozeny-Carman model cannot be applied. For this reason Wyllie and Gardner[135] introduced the generalized Kozeny-Carman equation in which pore size variation has been allowed for explicitly. Pore size measurement is obtained directly from capillary pressure data.

2.7.3.3 The Generalized Kozeny-Carman Equation for Permeability Calculations

It is necessary to account for pore size distribution in order to modify Kozeny-Carman equation to suit any porous material.

Pore sizes and their distribution[41,42] can be obtained from the capillary pressure curves. This will introduce a solution for one of the major defects in the Kozeny-Carman model. The original assumption that ϕ/S is a convenient measure of a fundamental property of porous medium must be discounted.

Wyllie and Spangler[135] introduced another approach based on experiment and theory presented by Carman[3]. This assumes that :-

$$S = \frac{P_c \phi}{\sigma} \qquad (2.7.3.3.1)$$

by substitution in equation (2.7.3.9)

Where 2.5(La/L)^2 is the Kozeny constant(K_z)

$$K = \frac{\phi \sigma^2}{K_z P_c^2} \qquad (2.7.3.3.2)$$

For pore size measurement using an air-brine capillary pressure curve it is can be assumed with great confidence that the porous medium consist of small ideal pore volumes ($\phi \Delta S_w$), where ΔS_w is a small increment of water saturation over which the capillary pressure can be considered constant (especially at very small ΔS_w), therefore equation (2.7.3.3.2) can be expressed as follows:

$$K = \frac{\phi \ \Delta S_w \ \sigma^2}{K_z P_c^2} \qquad (2.7.3.3.3)$$

Combining equation (2.7.3.3.3) with Darcy's law, the flow rate ΔQ passing through each ideal porous volume is given by

$$\Delta Q = \frac{\phi \ \Delta S_w \ \sigma^2}{K_z P_c^2} \frac{\Delta P}{\mu L} \qquad (2.7.3.3.4)$$

The gross or total flow rate (Q) for the whole porous system is equal to the summation of ΔQ. Thus,

$$Q = \Sigma \Delta Q = \frac{\phi \ \sigma^2}{K_z} \frac{\Delta P}{\mu \ L} \sum \frac{\Delta S_w}{P_c^2} \qquad (2.7.3.3.5)$$

$$K = \frac{\phi \ \sigma^2}{K_z} \sum \frac{\Delta S_w}{P_c^2} \qquad (2.7.3.3.6)$$

Therefore,

$$K = \frac{\phi \ \sigma^2}{K_z} \int_0^1 \frac{dS_w}{P_c^2} \qquad (2.7.3.3.7)$$

This is called the **generalized Kozeny-Carman equation**, which is the foundation of permeability modeling based on the pore size distribution. It is important to observe that the Kozeny-Carman constant K_z is considered to be a constant for all pore sizes. It was excluded from the summation $\Sigma(\Delta S_w / P_c^2)$.

Similar assumptions were adopted by many authors to predict absolute rock's permeability[136-138] and/or relative permeability from capillary pressure data.

2.7.4 Purcell (Gates, Lietz)

Purcell[4] developed an equation for calculating the permeability of porous material from capillary pressure data. His mathematical model was based on the assumption that the porous medium consists of a number of capillary tubes of the same length but different diameters. His derivation was essentially based on combination of the laws of Poiseuille and Darcy with the pressure of displacement equation (PDE) which expresses the capillary pressure for each individual tube,

$$P_c = \frac{2\sigma\cos\theta}{r} \qquad (2.7.4.1)$$

Purcell expressed Poiseuille's equation in slightly different form which as follows:

$$Q = \frac{V R^2 \Delta P}{8\mu L} \qquad (2.7.4.2)$$

Where :

Q is the flow rate of fluid of viscosity μ, through a single cylindrical tube or capillary of length L, internal radius R, volume V ($\pi R^2 L$) and ΔP is the pressure drop across the tube.

Solving equation (2.7.4.1) for R and substituting in equation (2.7.4.2) will yield:

$$Q = \frac{(\sigma \cos\theta)^2 \, V \, \Delta P}{2\mu L^2 (P_c)^2} \qquad (2.7.4.3)$$

The porous system is considered to be composed of a large number (N) of capillary tubes of equal length but randomly varied radii. The total rate of flow Q_t through the entire system is equivalent to the summation of the flow rates contributed by each capillary tube. The total flow rate, therefore, may be represented as follows:

$$Q_t = \frac{(\sigma \cos\theta)^2 \, \Delta P}{2\mu L^2} \sum_{i=1}^{N} \frac{V_i}{(P_c)_i^{\,2}} \qquad (2.7.4.4)$$

By equating the right-hand sides of equation (2.7.4.4) and flow rate of a porous system from The Darcy's law (equation 2.7.2.1), the following is obtained

$$K = \frac{(\sigma \cos\theta)^2}{2AL} \sum_{i=1}^{N} \frac{V_i}{(P_c)i^2} \qquad (2.7.4.5)$$

For simplification the volume of each capillary tube can be expressed as a percentage, %, of the total pore space V_t of the system i.e.

$$\frac{V_i}{V_t} \times 100 = S_i$$

Since AL is the bulk volume of the system, then porosity ϕ is introduced as a percent

$$\phi = \frac{V_t}{AL} \times 100$$

and equation (2.7.4.5) becomes as follows:

$$K = \frac{(\sigma \cos\theta)^2 \, \phi}{2 \times 10^4} \sum_{i=1}^{N} \frac{S_i}{(P_c)_i^{\,2}} \qquad (2.7.4.6)$$

Equation (2.7.4.6) is convenient for a system of parallel capillary tubes of the same length, but different radii i.e. non interconnected pores. It is necessary, therefore to introduce a correction factor which is called the lithology factor (λ). Equation (2.7.4.6) in its general form becomes:

$$K = \frac{(\sigma \cos \theta)^2 \phi \lambda}{2 \times 10^4} \int_{s=0}^{s=1} \frac{dS}{(P_c)_i^2} \qquad (2.7.4.7)$$

For permeability calculations from mercury capillary pressure data a surface tension of 480dynes/cm, and a contact angle of 140° are assumed. Equation (2.7.4.7) then can be reduced to:

$$K = 0.66 \lambda \phi \int_{S=0}^{S=100} \frac{dS}{(P_c)^2} \qquad (2.7.4.8)$$

Where, K is the absolute permeability in millidarcy, ϕ is porosity (%), S is percent of total pore space occupied by the liquid injected, and P_c is the capillary pressure expressed in atmospheres.

Gates and Lietz

Gates and Lietz[5] adapted the model developed by Purcell[4] for permeability calculation to the computation of wetting phase relative permeability.

By definition the relative permeability is the ratio of effective permeability to the absolute permeability.

Purcell's Equation (2.7.4.7) was generalized for the wetting phase permeability (k_{wt})

$$k_{wt} = \frac{(\sigma \cos \theta)^2 \phi \lambda}{2 \times 10^4} \int_{s=0}^{s_{wt}} \frac{dS}{(P_c)^2} \qquad (2.7.4.9)$$

The relative permeability for the wetting phase was obtained by dividing equation (2.7.4.9) by equation (2.7.4.7)

$$k_{rwt} = \frac{k_{wt}}{K} = \frac{\int_{s=0}^{s=s_{Wt}} \frac{dS}{(P_c)^2}}{\int_{s=0}^{s=1} \frac{dS}{(P_c)^2}} \qquad (2.7.4.10)$$

The relative permeability of the non wetting phase (K_{rnwt}) can be derived in the same way.

$$k_{rnwt} = \frac{k_{rnwt}}{K} = \frac{\int_{s=s_{Wt}}^{s=1} dS/(P_c)^2}{\int_{s=0}^{s=1} dS/(P_c)^2} \qquad (2.7.4.11)$$

2.7.5 Burdine Equation

Burdine derived his relative permeability equation[139] based on previous work by himself and co-workers. This equation relates absolute permeability (K) to pore entry radius (R_i) as follows:

The rate of flow of fluid through an assemblage of parallel capillaries each of the same length but having varying radii is according to Poiseuille's equation

$$Q = \frac{\pi \, \Delta P}{8 L \mu} n_i \, \overline{R}_i{}^4{}_{\rightarrow i+x} \qquad (2.7.5.1)$$

Where:

$$\overline{R_i}^4 = \sum_{i}^{i+x} \frac{R_i{}^4{}_{\rightarrow i+x}}{n} \qquad (2.7.5.2)$$

and n_i is the number of pores in the range ΔR ($i \rightarrow i+x$). The porosity (ϕ) can be expressed as follows:

$$\phi = \frac{\pi}{A} \sum n_i \, \overline{R^2}_{i \rightarrow i+x} \qquad (2.7.5.3)$$

Instead of assuming that the capillaries have equal lengths. Burdine and others[2] considered each radii interval has an effective length, Li and apparent length L. So, they introduced the concept of tortusity factor (χ_i) which is defined as follows:

$$\chi_i = \frac{L_i}{L} \tag{2.7.5.4}$$

$$\frac{Q\mu}{\Delta P} = \frac{\pi}{8L} \sum_{i=0}^{n} \left[\frac{n_i}{\chi_i} \sum_{i}^{i+x} \frac{R_i^{\ 4}}{n} \right] \tag{2.7.5.5}$$

similarly,

$$\phi = \frac{\pi}{A} \sum_{i=0}^{n} \left[n_i \left(\chi_i \sum_{i}^{i+x} \frac{R_i^{\ 2}}{n} \right) \right] \tag{2.7.5.6}$$

Writing Darcy's law in the following form

$$\frac{Q\mu}{\Delta P} = \frac{C\,A}{100\,L} K \tag{2.7.5.7}$$

Where C is a conversion factor and K is the permeability in darcy
Combining Equations (2.7.5.5),(2.7.5.6) and (2.7.5.7) gives:

$$K = \frac{100\,\phi}{8C} \frac{\displaystyle\sum_{i=0}^{n} \left[\frac{n_i}{\chi_i} \sum_{i}^{i+x} \frac{R_i^{\ 4}}{n} \right]}{\displaystyle\sum_{i=0}^{n} \left[\frac{n_i}{\chi_i} \sum_{i}^{i+x} \frac{R_i^{\ 2}}{n} \right]} \tag{2.7.5.8}$$

By definition

$$V_i = \pi\ \chi_i\ L \sum_{i}^{i+x} \frac{n_i\, R_i^{\ 2}}{n} \tag{2.7.5.9}$$

Where V_i is fractional of total pore volume in the radii interval R_i to R_{i+x}

$$n_i = \frac{V_i}{\pi \, \chi_i \, L \sum_{i}^{i+x} \frac{R_i^{\,2}}{n}} \qquad (2.7.5.10)$$

Combining equations (2.7.5.10) and (2.7.5.8)

$$K = \frac{100\phi}{8C} \sum_{i=0}^{n} \frac{V_i \, \overline{R_i^{\,4}}}{\chi_i^{\,2} \, \overline{R_i^{\,2}}} \qquad (2.7.5.11)$$

$$K = \text{constant}\, \phi \sum_{i=0}^{n} \frac{V_i \, \overline{R_i^{\,4}}}{\chi_i^{\,2} \, \overline{R_i^{\,2}}} \qquad (2.7.5.12)$$

By similarity in a two phase system, the effective permeability of the wetting phase k_{rwt} is

$$k_{rwt} = \text{constant}\, S_{wt} \, \phi \sum_{0}^{n} \frac{V_{iwt} \, \overline{R_i^{\,4}}}{\chi_{iwt} \, \overline{R_i^{\,2}}} \qquad (2.7.5.13)$$

Where (V_{iwt}) is the incremental pore volume of the wetting phase, $\chi_{iwt} = L_{iwt}/L$ which is tortuosity of the wetting phase and L_{iwt} being the effective length of the flow path for the wetting phase. The tortuosity ratio was expressed as follows:-

$$\chi_{rwt} = \chi_i / \chi_{iwt} \qquad (2.7.5.14)$$

and it is assumed that

$$V_{iwt} = V_i / S_{wt} \qquad (2.7.5.15)$$

By substituting equation (2.7.5.14) and (2.7.5.15) in equation (2.7.5.13):

$$k_{wt} = \text{constant}\,\phi \sum_{0}^{n} \frac{\chi_{rwti}\, V_i\, \overline{R_i^{\,4}}}{\chi_i^{\,2}\, \overline{R_i^{\,2}}} \qquad (2.7.5.16)$$

The equation for the wetting phase relative permeability can be obtained by dividing equation (2.7.5.16) by (2.7.5.12).

$$\frac{k_{wt}}{K} = k_{rwt} = \frac{\displaystyle\sum_{0}^{n} \frac{\chi_{rwti}^{\,2}\, V_i\, \overline{R_i^{\,4}}}{\chi_i^{\,2}\, \overline{R_i^{\,4}}}}{\displaystyle\sum_{0}^{n} \frac{V_i\, \overline{R_i^{\,4}}}{\chi_i^{\,2}\, \overline{R_i^{\,2}}}} \qquad (2.7.5.17)$$

If χ_i and χ_{rwti} are assumed to be a constant for the porous medium and $r = 2\sigma\cos\theta/P_c$, then

$$k_{rwt} = (\chi_{rwt})^2 \frac{\displaystyle\int_{s=0}^{s=S_{wt}} dS/P_c^{\,2}}{\displaystyle\int_{s=0}^{s=1} dS/P_c^{\,2}} \qquad (2.7.5.18)$$

Similarly the non wetting phase relative permeability can be shown to be given by the equation:-

$$k_{rnwt} = (\chi_{rnwt})^2 \frac{\displaystyle\int_{s=S_{wt}}^{s=1} dS/P_c^{\,2}}{\displaystyle\int_{s=0}^{s=1} dS/P_c^{\,2}} \qquad (2.7.5.19)$$

Where :

$$\chi_{rwt} = \frac{S_{wt} - S_{wi}}{1 - S_{wi}}$$

χ_{rnwt} is assumed to have 1 at S_{wi} and value of zero at minimum saturation of the non wetting saturation, therefore χ_{rnwt} can be estimated by ($1-\chi_{rwt}$), thus,

$$\chi_{rnwt} = \frac{1 - S_{wt}}{1 - S_{wi}}$$

2.7.6 Rapoport and Leas

Rapoport and Leas[140] presented two equations for the wetting phase relative permeability. The equations give two values for the wetting phase relative permeability at each saturation point. These values represent the minimum and the maximum expected values. They adopted the Kozeny-Carman Equation to define their relative permeability equations for a liquid/gas system, where the liquid is the wetting phase and the gas is the non-wetting phase.

It was shown that the absolute permeability can be expressed as :

$$K = \frac{\phi^3}{K_z A^2} \qquad (2.7.6.1)$$

Where;

A = the surface area per unit bulk volume ($A \equiv S$ in Equation (2.7.3.9))

The Kozeny - Carman Equation was applied to the liquid phase in the following manner:

1- The total rock porosity, ϕ, can be replaced by the effective porosity, ϕS_L, where S_L is the liquid saturation
2- The total pore surface area A is replaced by A_L, which represents the liquid phase area.

By substitution of the above terms into equation (2.7.6.1) the effective liquid phase permeability k_L is obtained.

$$k_L = \frac{S_L{}^3 \phi^3}{K_z A_L{}^2} \qquad (2.7.6.2)$$

The liquid relative permeability can be obtained by dividing equation (2.7.6.2) by equation (2.7.6.1).

$$\frac{K_L}{K} = K_{rL} = \frac{S_L{}^3}{\left(\frac{A_L}{A}\right)^2} \qquad (2.7.6.3)$$

For more realistic application of equation (2.7.6.3) two further consideration must be taken into account:

a- The total liquid saturation, S_L, is replaced by an effective liquid saturation, S_{LE}, such that

$$S_{LE} = \frac{S_L - S_{wi}}{1 - S_{wi}}$$

Where, S_{wi} is the irreducible water saturation

b- The total area A is replaced by the effective area A_E , which represents the area of the mobile liquid by substitution in equation (2.7.6.3) the relative permeability of the liquid phase can be expressed as follows :

$$K_{rL} = \frac{S_{LE}{}^3}{\left[\frac{A_L}{A_E}\right]^2} = \left[\frac{S_L - S_{Wi}}{1 - S_{Wi}}\right]^3 \left[\frac{A_E}{A_L}\right]^2 \qquad (2.7.6.4)$$

To obtain K_{rL} requires knowledge of the surface areas A_L and A_E. The following expressions were derived from the liquid, gas capillary pressure curve as shown in Figure 2.17.

$$A_G = \sum S = \frac{\phi}{\sigma}\int_1^{S_L} P_c \, dS \qquad (2.7.6.5)$$

$$A_E = \sum S_{Wi} = \frac{\phi}{\sigma}\int_1^{S_{Wi}} P_c \, dS \qquad (2.7.6.6)$$

$$A_L = \sum w + 2I = \frac{\phi}{\sigma}\int_S^{S_{wi}} P_c \, dS + 2I \qquad (2.7.6.7)$$

A_G and A_E are very well defined from the capillary pressure curve. Solution for A_L or I is required. A_L minimum and maximum values are evaluated as follows:

Maximum (A_L) Leads to Minimum Relative Permeability Value

From Figure 2.17 and equation (2.7.6.5) and (2.7.6.7) the following equation can be considered

$$\sum W = A_L - 2I \qquad (2.7.6.8)$$

$$\sum S = R_G + I \qquad (2.7.6.9)$$

From equation (2.7.6.8) A_L has its maximum value when I has its maximum value. From equation (2.7.6.9), the value of I will have it maximum value when $R_G = 0.0$, so,

$$A_{L(\max)} = \Sigma W + 2\Sigma S = \Sigma S_{Wi} + \Sigma S \qquad (2.7.6.10)$$

According to equation (2.7.6.4). The liquid relative permeability has its minimum value when A_L maximum so, then:

$$k_{rL(\min)} = \left(\frac{S_L - S_{wi}}{1 - S_{wi}}\right)^3 \left(\frac{A_E}{A_{L(\max)}}\right)^2 = \left(\frac{S_L - S_{wi}}{1 - S_{wi}}\right)^3 \left(\frac{\Sigma S_{wi}}{\Sigma S_{wi} + \Sigma S}\right)^2 \qquad (2.7.6.11)$$

As the liquid is the wetting phase

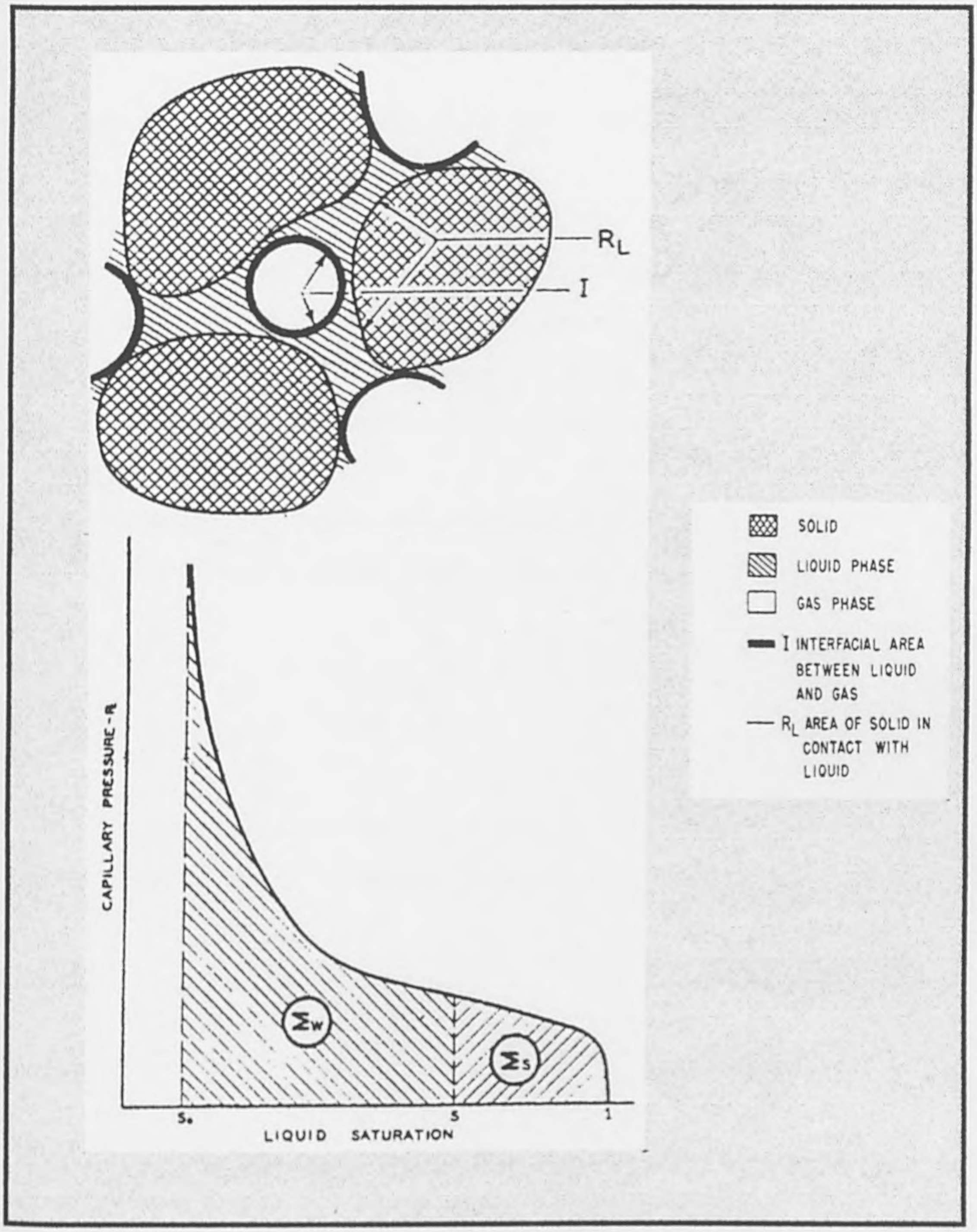

Figure (2.17) Representation of fluid distribution and capillary pressure curve at reservoir rock sample.

$$k_{rwt(min)} = \left(\frac{S_{wt} - S_{wi}}{1 - S_{wi}} \right)^3 \left(\frac{\int_1^{S_{Wi}} P_c \, dS}{\int_1^{S_{Wi}} P_c \, dS + \int_1^{S_{Wi}} P_c \, dS} \right)^2 \qquad (2.7.6.12)$$

Minimum (A_L) Leads to Maximum Relative Permeability Value

Referring to equations (2.7.6.8) and (2.7.6.9). The minimum value for A_L can be obtained if $I = 0.0$ i.e. $A_L = \Sigma W$ and $R_G = \Sigma S = A_G$. This assumption is too limiting and leads to k_L values which are too high. It is assumed that porous media can be represented as an isotropic random packing of grains and interfaces must exist between the gas and liquid and non of the three surface areas, I, R_G and R_L is zero.

The lowest value of I/R_G can be evaluated using equation (2.7.6.9) leads to a minimum value of I, A_L and consequently, to maximum value of K_{rL} . It was shown that;

$$\frac{I}{R_G} \rangle \frac{S_L \phi}{1 - \phi} \left[\frac{P_m}{P_c} \right]^2 \qquad (2.7.6.13)$$

Where P_c is the capillary pressure at any saturation and P_m the mean value of P_c for the saturation range S_L to S_{wi}. This leads to the following minimum areas;

$$A_{L(min)} = \left[\Sigma W + \frac{2 \Sigma S}{1 + \frac{1-\phi}{S_L \phi} \left(\frac{P_c}{P_m} \right)^2} \right] \qquad (2.7.6.14)$$

Thus, the maximum relative permeability for the wetting phase will be as follows:

$$k_{rwt(max)} = \frac{\left(\frac{S_{wt} - S_m}{1 - S_m}\right)^2 \left(\int_1^{s_m} P_c \; dS\right)^2}{\left[\int_{s_{wt}}^{s_m} P_c \; dS + \frac{2\int_1^{s_{wt}} P_c \; dS}{1 + \left(\frac{1-\phi}{S_{wt}{}^{\phi}}\right)\left(\frac{P_c\,(S_{wt} - S_m)}{\int_{s_{wt}}^{s_m} P_c \; dS}\right)^2}\right]} \qquad (2.7.6.15)$$

S_m= minimum irreducible saturation of the wetting phase from a drainage capillary pressure data.

2.7.7 Wyllie-Sprangler, and Wyllie-Gardener

Wyllie and Sprangler [141] presented two equations for computing gas and oil relative permeability. Their equations can be expressed as follows:

$$k_{ro} = \left(\frac{S_o}{1 - S_{wi}}\right)^2 \frac{\int_0^{S_o} dS_o/P_c{}^2}{\int_0^1 dS_o/P_c{}^2} \qquad (2.7.7.1)$$

$$k_{rg} = \left(1 - \frac{S_o}{S_m - S_{wi}}\right)^2 \frac{\int_{S_o}^1 dS_o/P_c{}^2}{\int_0^1 dS_o/P_c{}^2} \qquad (2.7.7.2)$$

Where, S_m represents the lowest oil saturation at which the gas phase is discontinuous:

$$S_m = (1 - S_{gc})$$

Obviously values of S_m are required for oil and gas relative permeabilities computing which made the method can not be generalized for the wetting and the non-wetting phase to suit oil-water system.

Wyllie and Gardner[135] presented two equations for oil and gas relative permeability calculations. This model was based on statistical approach (statistical model) which gave the following:

$$k_{ro} = \left(\frac{S_L - S_{wi}}{1 - S_{wi}}\right)^2 \frac{\int_{S_{Wi}}^{S_L} \frac{dS_w}{P_c^{\,2}}}{\int_{S_{Wi}}^{1} \frac{dS_w}{P_c^{\,2}}} \qquad (2.7.7.3)$$

$$k_{rg} = \left(\frac{1 - S_L}{1 - S_{wi}}\right)^2 \frac{\int_{S_L}^{1} \frac{dS_w}{P_c^{\,2}}}{\int_{S_{Wi}}^{1} \frac{dS_w}{P_c^{\,2}}} \qquad (2.7.7.4)$$

Where S_L is the total liquid saturation ($S_L = S_o + S_w$), the previous equations were generalized for wetting and non-wetting phase relative permeabilities. If the oil is the wetting phase and the gas is non-wetting phase then S_L will be the wetting phase saturation, Equations (2.7.7.3) and (2.7.7.4) will be identical to Burdine Equations (2.7.5.18) and (2.7.5.19).

2.7.8 Timmerman

Timmerman[142] introduced two empirical equations for oil and water relative permeabilities calculations from capillary pressure data. It can be presented as Purcell (Gates and Lietz) equations in the following modified forms;

$$k_{ro} = S_o \left(k_{RO}\right)^{2.5} \qquad (2.7.8.1)$$

$$k_{rw} = S_w \left(k_{RW}\right)^{2.5} \qquad (2.7.8.2)$$

Where, k_{RO} and k_{RW} are oil and water relative permeabilities calculated using Purcell (Gatez and Lietz) mathematical models. Timmerman suggested the following equations;

$$k_{ro} = S_o \left[\frac{\int_0^{S_o} dS/P_c^{\,2}}{\int_0^1 dS/P_c^{\,2}} \right]^{2.5} \qquad (2.7.8.3)$$

$$k_{rw} = S_w \left[\frac{\int_{S_O}^1 dS/P_c^{\,2}}{\int_0^1 dS/P_c^{\,2}} \right]^{2.5} \qquad (2.7.8.4)$$

2.7.9 Fatt and Dykstra

Fatt and Dykstra[143] developed an equation based on the Purcell equation, considering that the lithology factor (λ) was a function of saturation. The lithology factor is essentially a correction for the deviation of the path length from the length of the porous medium.

It was assumed that λ is a function of the radius of the conducting pores, so that:

$$\lambda = \frac{a}{r^b}$$

Where a and b are constants for the material and r is the radius of the conducting pores.

The relative permeability equation for the wetting phase (k_{rwt}) then becomes as follows:

$$k_{rwt} = \frac{\int_{s=0}^{s=S_{Wt}} \frac{dS}{P_c^{\;2(1+b)}}}{\int_{s=0}^{s=1} \frac{dS}{P_c^{\;2(1+b)}}} \tag{2.7.9.1}$$

Fatt and Dykstra assumed that b = ½, therefore, equation (2.7.9.2) can be reduced to:

$$k_{rwt} = \frac{\int_{s=0}^{s=S_{Wt}} \frac{dS}{P_c^{\;3}}}{\int_{s=0}^{s=1} \frac{dS}{P_c^{\;3}}} \tag{2.7.9.2}$$

2.7.10 Other Correlations

Corey[144] developed two relative permeability equation for gas-oil systems. His contribution was mainly simplifying Burdine's equation . He approximated $1/P_c^2$ by a linear function as follows:

$$\frac{1}{P_c^{\;2}} = C\left[\frac{S_o - S_{or}}{1 - S_{or}}\right]$$

Where C is a constant, S_o and S_{or} are the oil saturation and irreducible oil saturation respectively. The main weakness of this method is that not all capillary pressure curves in the form of $1/P_c^2$ can be approximated using his linear equation.

Torasco and Wyllie[145] presented one equation for gas-oil relative permeability (k_{rg}/k_{ro}) for water wet sandstone. Their equation was based on Cory's equation. Frick[146] summarized some empirical relative permeability equations. Person[147] developed two equations for wetting and non-wetting phase relative permeabilities based on petrophysical considerations. Many others[148-157] have developed equations for relative permeability calculation or methods for the simultaneous determination of capillary pressure and relative permeability data.

CHAPTER 3

EXPERIMENTAL APPARATUS AND PROCEDURE

3.1 Rock Sample Preparation

Various sandstone rock samples, covering a wide range of porosity and permeability have been selected based on visual examination (for homogeneity) as the primary screening method[148,149]. The plugs were cut horizontally, parallel to the bedding planes, to represent the direction of flow. The trimming was done with great care and accuracy to ensure each sample is a true cylinder. The end faces were ground smooth and square to ensure capillary continuity in capillary pressure measurements using a porous plate diaphragm. Each sample was labeled using indelible ink with a unique identifier for future work. Samples dimensions were measured precisely; all were of 3.8cm diameter and about 5-7.5cm long.

3.2 Cleaning and Drying

3.2.1 Sample Cleaning

Samples were cleaned using distillation extraction (Soxhlet extraction Figure 3.1) which is most commonly used for conventional core analysis. Rock samples are placed in the soxhlet, and sandwiched between a glass vessel containing the required solvent at the bottom, and a condenser at the top. The whole assembly sits on an electric heater, and is supported at the top to ensure stability. The soxhlet lid is firmly clipped on to the body and all glass contacts are checked for leaks. The electric heater is switched on, the solvent boils in the lower vessel, and the solvent vapor passes up through the side arm into the condenser where it condenses, then falls down on the samples in liquid phase. Refluxing is continued until the solvent is clean (the solvent must be changed as required), usually 2-4 days.

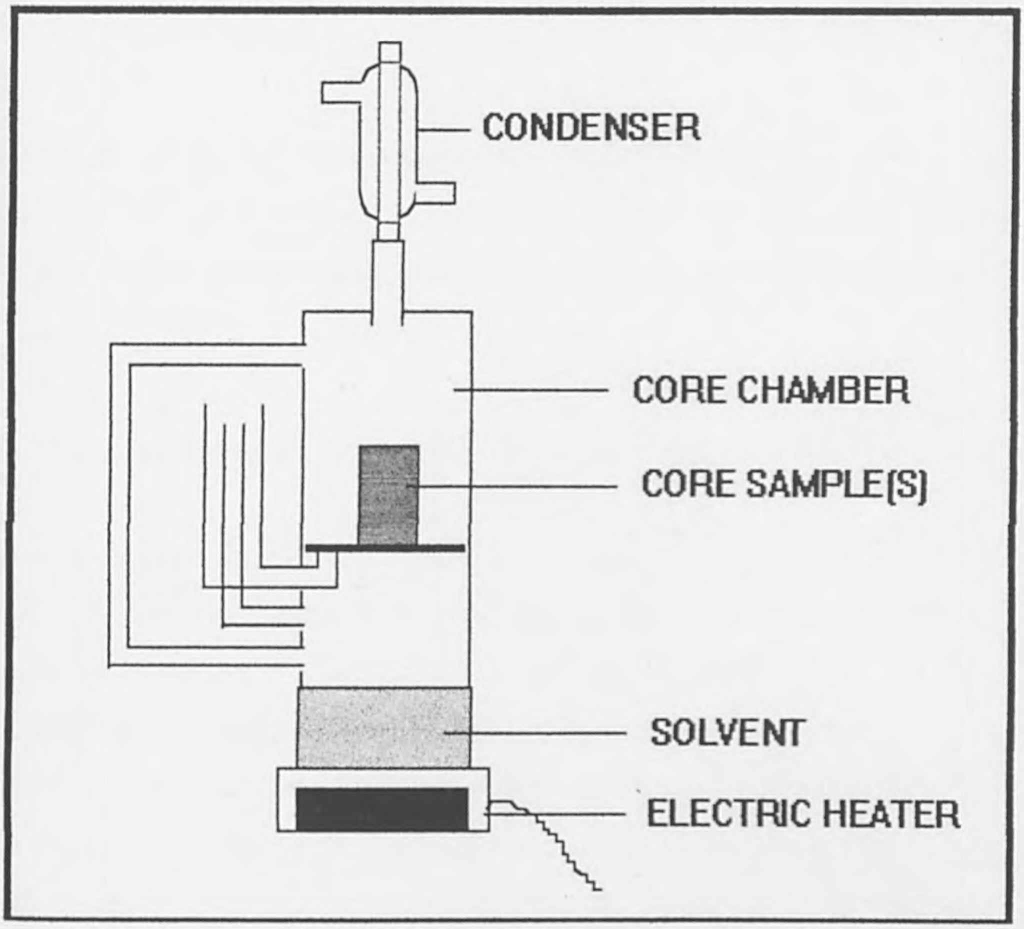

Figure (3.1) Soxhlet refluxing apparatus.

A variety of solvents can be used to remove hydrocarbons, water and salts. The sample cleaning was done with great deal of attention along this project. A mixture of 75% Chloroform (boiling point 61.7°C) and 25% Methanol (its boiling point is 65°C) was used as the first solvent to remove hydrocarbons, salt and water. Core plugs must be checked for oil fluorescence under ultra-violet light, and the solvent must be changed if fluorescence shows oil. The final solvent should always be Methanol, which efficiently removes salts and water. This is continued until tests show the extracted Methanol is clear. Silver nitrate and Barium chloride are used to determine the presence of chlorides and sulphates respectively.

In order to maintain the same rock wettability it is extremely important, that the samples cleaning procedure to be carried out precisely in the same fashion using the same solvents at any stage.

3.2.2 Sample Drying

Individual sample weights are recorded. The samples are then placed in the vacuum oven, typically set to a temperature of 65°C. A vacuum of 4kPa is applied. The sample weights are recorded on a daily basis until stable (this usually takes 2-4 days).

3.3 Construction of Complex Simulated Formation Brine

Brine is required for measuring liquid and CT porosity, air-brine capillary pressure and water-oil relative permeability. Ideally the brine will be recovered from the reservoir for use in the laboratory. Unfortunately, formation brine cannot be recovered in sufficient quantities to satisfy the demands of all the static and dynamic measurements. For this reason it is necessary to make up the required quantity of simulated formation brine. This simulated formation brine is based on a full 10/12 ion water analysis, performed on a water (brine) sample collected in a bottom-hole sampler from a North Sea reservoir. The data required are the individual values in mg/l, for the 5 (7 in 12 ion) cations and 5 anions normally tested for. These are as follows:-

(i) Cations - Na, Ca, Mg, K, Ba, Sr, Li
(ii) Anions - Cl, HCO_3, SO_3, OH

The artificial brine is filtered by passing it into dry clean flask, through a Whatman filter paper (0.45 micron) to remove solid particles. The filtered brine is degassed by attaching a vacuum tube to the flask sidearm and placing a rubber bung in the top aperture. With the mixer bin rotating the vacuum is applied in 2 minutes cycles until no more gas is displaced. Vacuum must not be applied for excessive periods as this causes water to be drawn off, thus concentrating the solution. Two basic properties are measured :- (a) specific gravity using the relative density bottle, (b) viscosity using the rolling ball viscometer. Both properties were measured for a reasonable range of working temperature (from 16° to 24°C). Measurements were taken at every degree Celsius, and the intermediate values were obtained based on a linear relationship. These properties are essential for liquid porosity, air-brine capillary pressure and relative permeability measurements.

3.4 Sample Saturation

The individual weights of the cleaned and dried samples are recorded. The samples are then placed in a chamber which is sealed and evacuated (Figure 3.2) for 30 minutes. A separate but connecting chamber containing the saturant fluid (degassed) is also evacuated. The vacuum in the fluid chamber is then gradually released and fluid is allowed to enter the evacuated chamber containing the rock samples. After allowing sufficient time for in-fill (of the chamber and samples), the chamber containing the samples and fluid is then pressurized to 2000psi (13,790kPa) and allowed a period of circa 16 hours for final saturation.

The pressure is then gradually released to atmospheric pressure and the samples placed in a vessel immersed in degassed saturant.

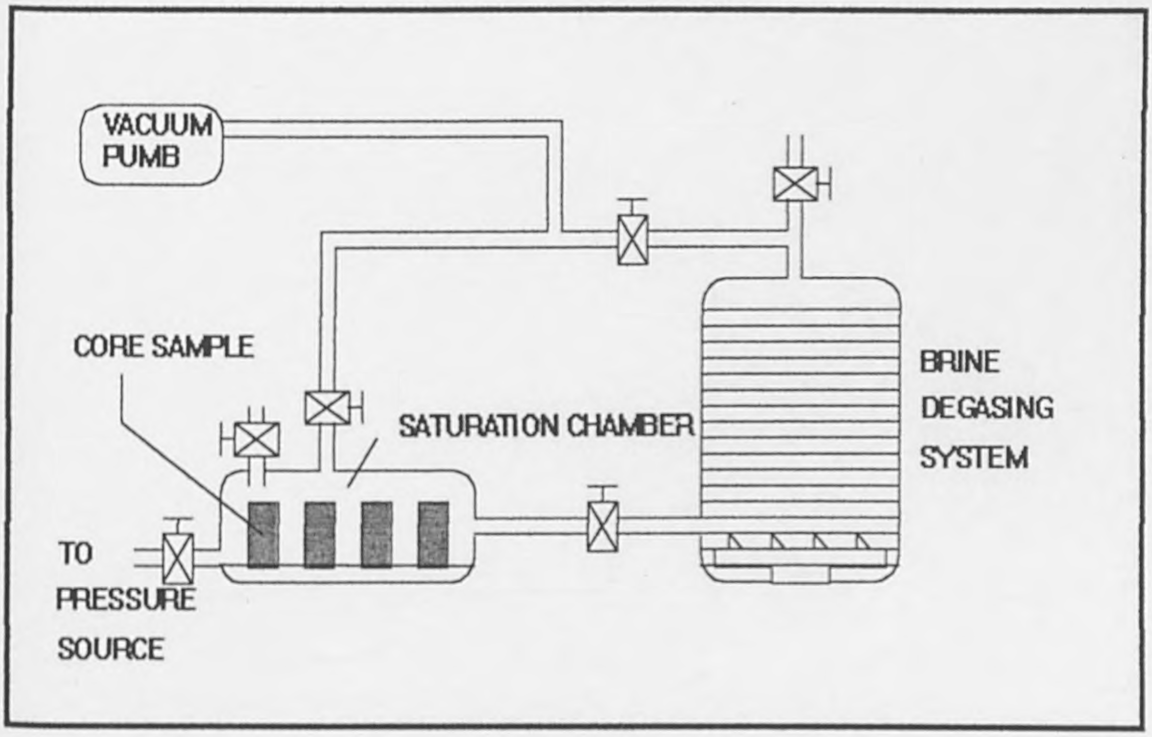

Figure (3.2) Schematic representation of core sample saturation.

3.5 Sample Selection Using CT Scanner

Samples were selected for this study based on a new screening method developed by the author. The most homogeneous sandstone samples were chosen, based on non-destructive porosity measurements within the sample using x-ray computed tomography.

3.5.1 CT Scanner Description

The CT scanner components are distributed over three rooms; (a) the scanning room, (b) the control and computer room, (c) the high voltage room with the x-ray generator. A general illustration of the CT scanner components is shown in Figure 3.3.

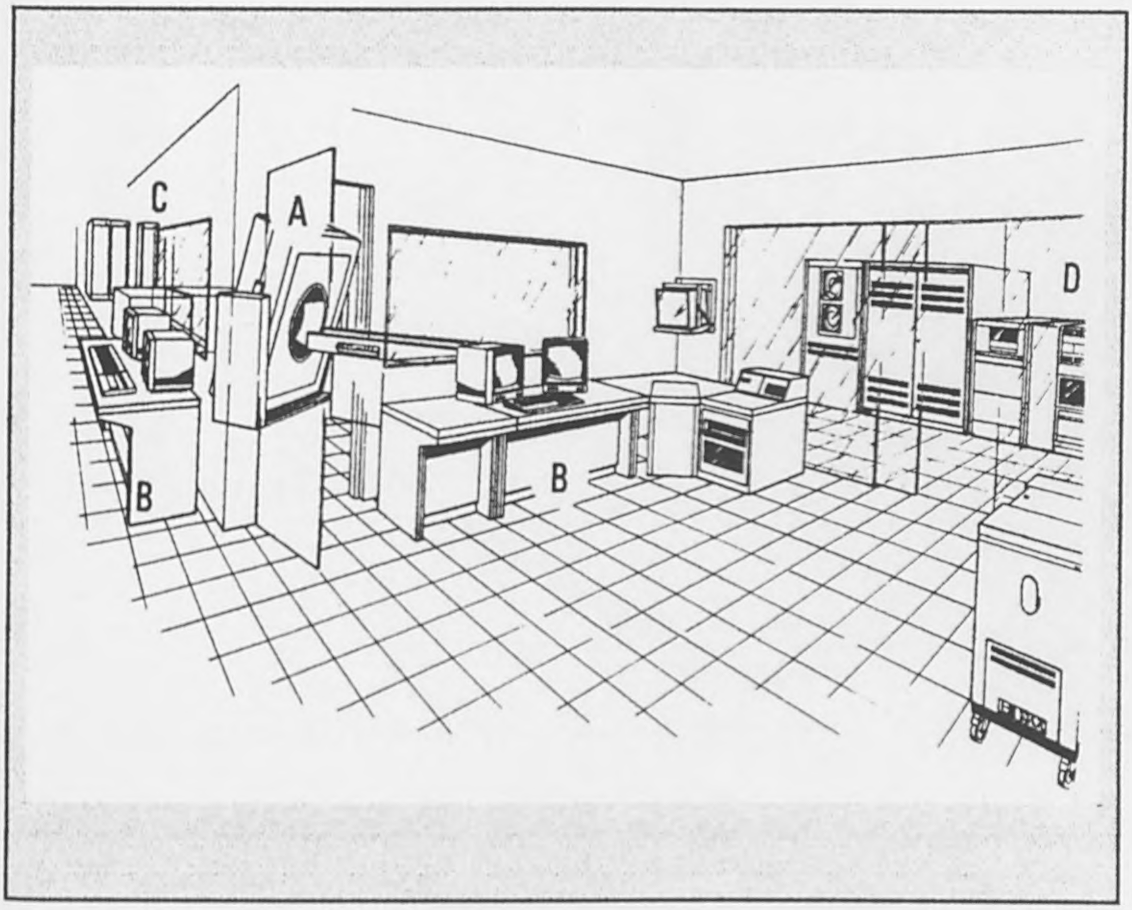

Figure (3.3) General view for the CT scanner components distribution where A, the scanning room, contains the gantry and the patient table, B is the control and computer room and C is the high voltage room.

A Scanning Room

The scanning room contains two main components; (1) the gantry which supports the rotating x-ray source (tube)-detector system with the 3-D light localizer for marking the scanned slice which permits an easy, rapid and precisely reproducible selection of the desired object region; (2) the programmable motor-driven patient (core sample) table with height adjustment, to control the position of the scanned object between the x-ray source and detectors from the operator desk. A general view of the gantry and table is shown in Figure 3.4.

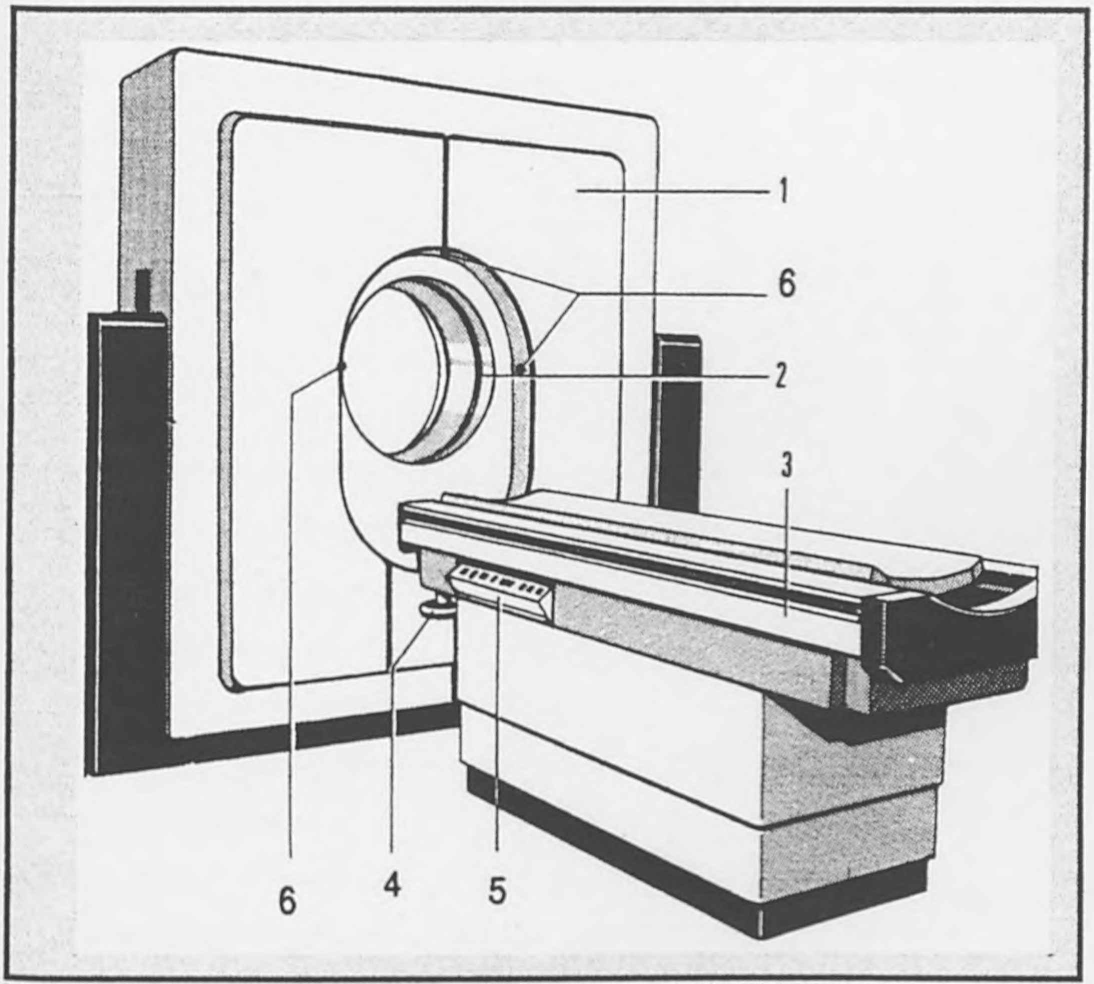

1 GANTRY	4 HANDWHEEL FOR MANUAL HORIZONTAL TABLE MOVEMENT
2 X-RAY SOURCE-DETECTOR ROTATING SYSTEM	5 TABLE CONTROL PANEL
3 MOTOR DRIVEN TABLE	6 POSITIONING LIGHTS (3-D MARKER)

Figure (3.4) General view of the gantry and table.

B Control and Computer Room

All motions of the gantry and table are centrally controlled and monitored from this room. Each time a new operating mode is selected, the current and voltage of the generator are automatically set by the computer. The storage of the measured images on the CT scan computer as well as on external devices such as floppy disk or magnetic tape is also managed by the control computer.

The computerized system of the operator's consoles and data acquisition, storage, image-reconstruction and displaying are shown schematically in Figure 3.5.

C High Voltage Unit

The x-ray tube is connected to a high voltage generator with computer-controlled regulation. It is therefore not necessary to manually operate the generator. Depending on the measuring program, an x-ray tube voltage of 125kV or 140kV can be used.

3.5.2 Procedure

1. After the rock sample is cleaned and dried, scanning positions must be identified, marked and named using indelible ink. The number of scans is generally dependent on the area of interest, the sample length and the CT image thickness. Since the scanner used produces a CT slice of 3.5mm thickness, it is essential to mark the first and last scanning positions at a distance of at least 1.75mm (half of the slice thickness) from the sample end surfaces.
2. The number and position of scanning locations are defined and programmed into the computerized system.
3. The scanner is re-calibrated using a special fused quartz of 1500 HU units (see scanner calibration chapter 4), then the scanner voltage is set at exactly 140kV.
4. The sample is located exactly in the centre of the rotating gantry (between the x-ray source and detectors), and the scanners' 3-D light localizer is accurately overlapped on the first marked scanning position on the sample. **The initial 3-dimensional scanning position must be precisely defined.**
5. The sample is CT scanned by emitting x-rays at 4 positions around the sample (every 45°), and the 2-D image which displays the CT number across the sample is reconstructed and stored into computer. The sample is transported using the

controllable conveyer belt to the next scanning position for CT imaging, and each 2-D slice x-ray attenuation data is reconstructed and stored in the same manner.

6. The sample is 100% saturated with brine as described previously in section (3.4), then CT scanned (following steps 3 to 5) in the same fashion while dry, the its attenuation data is stored. It is extremely important that the saturated sample initial scanning position is identically located to the dry condition initial scanning position.
7. The CT image is displayed on the television monitor for each 2-D slice for both conditions, i.e. while dry and while 100% saturated. Average CT numbers are measured for identical sub-areas of 11mm^2 (corresponding to a rock volume of about 40mm^3).
8. Porosity values for interior sub-volumes along and across the rock sample are calculated by the subtraction method (see chapter 4) (also called dual scan method).
9. Sample selection is carried out based on the quantitative description of the fractional variation in porosity for the volume elements

For each sample selected, the variation in porosity was less than ±0.3%. Details for sample screening using CT scan are given in Chapter 4.

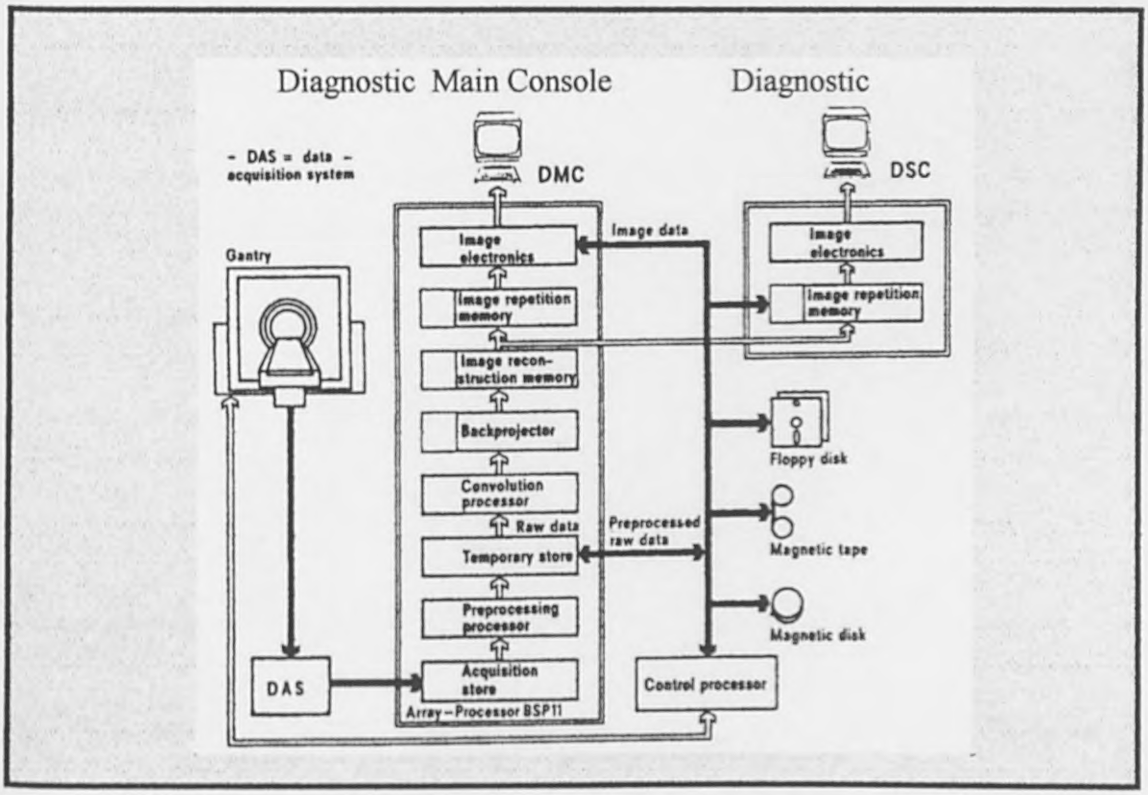

Figure (3.5) Schematic of the CT scanner operating system.

3.6 Conventional Measurements

3.6.1 Helium Porosity

Helium porosity is measured using the helium gas expansion porosimeter. A schematic of the apparatus is shown in Figure 3.3. To measure the grain volume, the standard (reference) volume is filled with helium to a pressure of approximately 200psi (1379kPa), and the transducer reading allowed to stabilize for approximately 30 seconds before recording the initial pressure (P_1). Then the rock sample is placed in the sample chamber, and the helium is expanded from the reference volume into the sample chamber. The transducer reading may take several minutes to stabilize, depending on the porosity/permeability of the sample, and then the final pressure is recorded (P_2). The grain volume (V_g) is then calculated from Boyle's Law, which describes the isothermal expansion of an ideal gas (PV = constant). Helium gas gives the most accurate porosity because of its small atomic size which enables it to penetrate the small interconnected pores. The bulk volume (V_b) is measured using the mercury displacement method:

$$\phi = \frac{V_b - V_g}{V_b}$$

It is important to calibrate the system using stainless steel discs of known volumes prior to making sample porosity measurements.

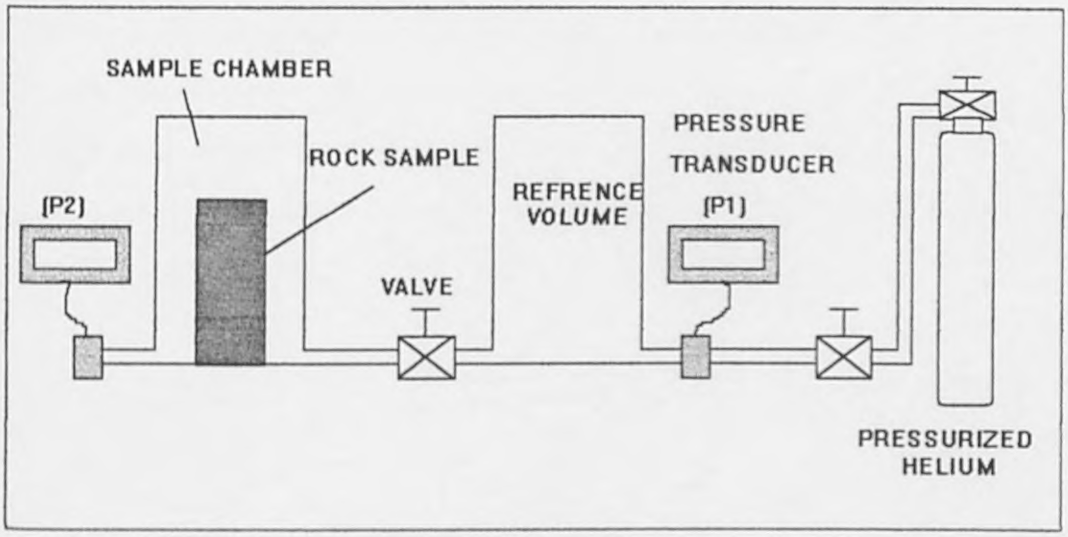

Figure (3.6) Porosity measurement from grain volume determination using the helium expansion method.

3.6. 2 Liquid Porosity

The dry sample is weighed, then saturated with the desired saturant using the method explained in Section 3.4. The saturated sample is weighed first in air (wt_1) and then when immersed in the saturant (wt_2) using a stirrup. The stirrup weight is (w_3). The bulk volume (V_b) can be calculated using Archimedes Principle. Sample pore volume (V_p) and hence porosity can be calculated as follows;

$$V_b = \frac{wt_1 - wt_2 - wt_3}{\text{saturant density}}$$

$$V_p = \frac{wt_1 - \text{dry wt.}}{\text{saturant density}}$$

$$\phi = \frac{V_p}{V_b}$$

3.6.3 Gas Permeability

A Hassler cell permeameter is used for absolute permeability (K) measurement under laboratory conditions. Dry nitrogen gas flows at a constant rate (Q); upstream and downstream pressure (P_1 and P_2) are recorded. Knowing the gas viscosity at laboratory temperature (μ), the sample length (L), atmospheric pressure (P_a) and the end face cross sectional area (A), the absolute permeability is calculated from the following equation:

$$K = \frac{2\mu P_a LQ}{A\left(P_1^{\,2} - P_2^{\,2}\right)}$$

3.7 Wettability Measurements

Wettability can be defined as the tendency for the fluid to spread on or adhere to a solid surface in the presence of other immiscible fluids. In this study the solid surface is that of the individual mineral grains which comprise the rock sample, and the fluids used for flooding are water (brine) and oil.

Different methods are used to measure this property. The used methods are called Amott and combined Amott/USBM wettability tests. The procedures for these methods are as follows:

3.7.1 Amott Wettability

1. The core sample is saturated with brine as in Section 3.4.

2. The sample is weighed, loaded in the hydrostatic core holder and flushed with mineral oil until the effluent is free of brine, thus attaining the residual water saturation (S_{wi}).

3. The plug is placed in the Amott Imbibition Vessel (Figure 3.7), and the sample is submerged completely in the simulated formation brine. With the lid in place, the vessel is inverted so that the oil displaced by the spontaneous imbibition of the brine is caught in the graduated receiving tube. The amount of displaced oil is recorded as a function of time. The sample remains in the tube under brine until no further oil flows out. (all samples are observed for 4 weeks).

4. On achieving production equilibrium, the plug is placed again in the hydrostatic core holder and flushed with the simulated formation brine to achieve residual oil saturation (S_{Or}).

5 The plug is returned to the Amott Imbibition Vessel and immersed completely in the refined mineral oil. The lid is attached and the vessel is placed in the clamp stand with a graduated tube beneath the sample chamber to collect the displaced brine. The sample is observed for 4 weeks.

6 Again on achieving equilibrium, the plug is replaced in the hydrostatic core holder and flushed with the refined mineral oil the residual water saturation (S_{wi}).

7 The Amott Wettability Indices are calculated as follows:

i) $\text{Water Wettability Index} = \frac{A}{A+B}$

Where, A = Water Imbibed (% pore volume)
B = Oil Displaced Dynamically (% pore volume)

ii) $\text{Oil Wettability Index} = \frac{C}{C+D}$

Where, C = Oil Imbibed (% Pore volume)
D = Water Displaced Dynamically (% pore volume)

iii) Amott/Harvey Relative Displacement Index = Water Index - Oil Index

The Amott/Harvey Relative Displacement Index combines the Amott Indices in single wettability index that varies from +1 for complete water wetness, to -1 for complete oil wetness. Any rock sample is water wet when the index varies from +1 to +0.3, of intermediate wettability when it varies from +0.3 to -0.3, and oil wet in the range -0.3 to -1.

3.7.2 Combined Amott/USBM Wettability

1 Follow steps 1-3 of the Amott method.

2 On achieving equilibrium, the plug is placed in the centrifuge container and flushed with the simulated formation brine to achieve the residual oil saturation (S_{or}) using the centrifuge. The capillary pressure is measured in small increments. The area under the capillary pressure curve is calculated.

3 The plug is returned to the Amott Imbibition Vessel and immersed completely in the refined mineral oil. The lid is attached and the vessel is placed in the clamp stand with a graduated tube beneath the sample chamber to collect the displaced brine. The sample is observed for 4 weeks.

4 On achieving equilibrium again, the plug is replaced in the centrifuge container and flushed with the refined mineral oil to the residual water saturation (S_{wi}) using the centrifuge. The capillary pressure is remeasured in small increments. The area under the capillary pressure curve is recalculated from the data obtained.

The USBM Wettability Index is calculated as follows:

$$\text{USBM Wettability Index} = \text{Log}\left(\frac{\text{area under oil drive}}{\text{area under brine drive}}\right)$$

A USBM Wettability Index around zero means the core is neutrally wet. The higher the value of wettability index is the more water wettability preference and vice versa. Furthermore, using this method will allow all the results obtained by Amott method.

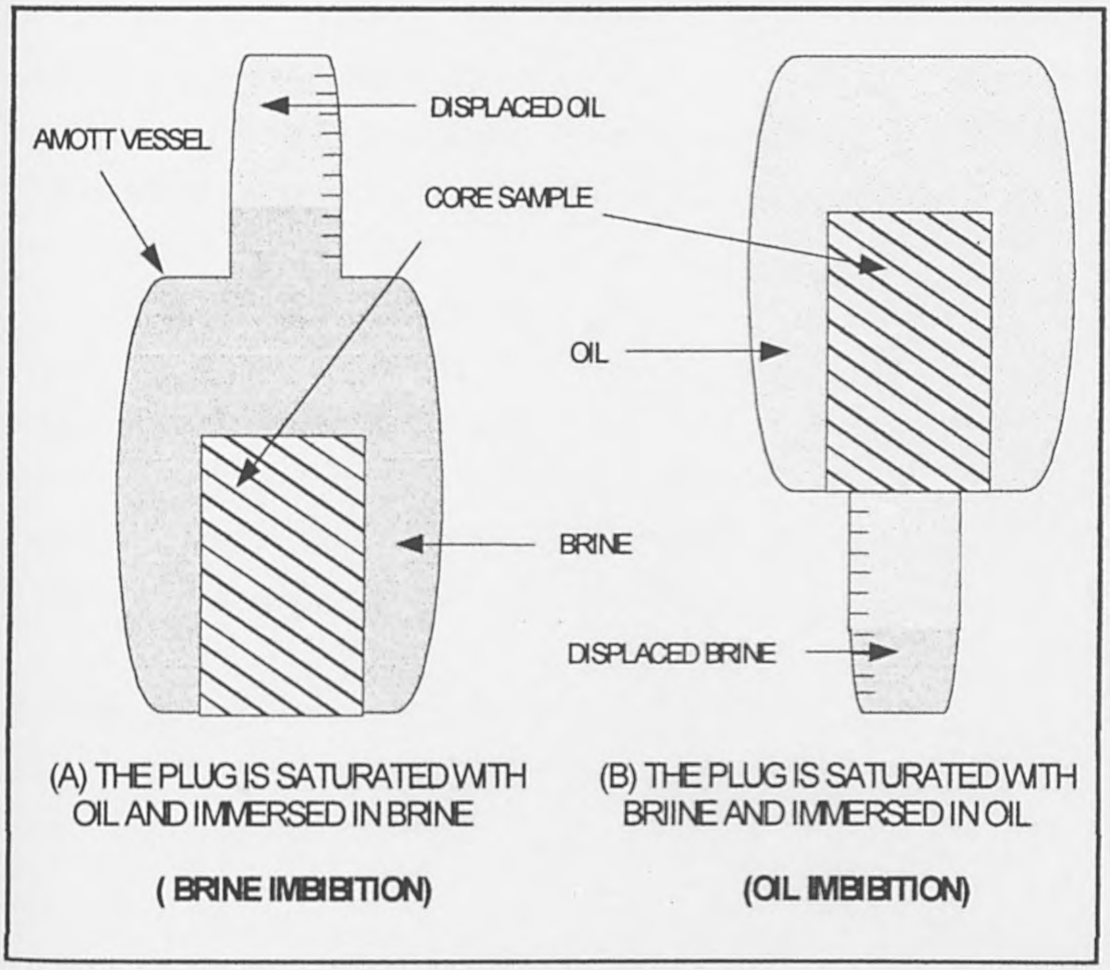

Figure (3.7) Amott imbibition vessel.

3.8 Capillary Pressure Measurements

3.8.1 Air-Brine Capillary Pressure Using Porous Diaphragm

The sample capillary pressure is measured using the air-brine porous plate technique. Samples are cleaned and fully saturated with simulated formation brine. The sample is placed on a brine saturated porous plate (as shown in Figure 3.8), permeable to brine but impermeable to air.

Moist air is confined above the diaphragm, and the brine is expelled from the sample by use of successively higher pressures. The saturations are measured at the following pressure points:- 0.5 (3.4), 1 (7), 2 (14), 4 (28), 8 (55), 16 (110), 32 (220), 64 (441), 120

(827kPa) and 200psi (1379kPa). A special vessel was used for pressures above 50psi (344kPa). The semi-permeable ceramic porous plates have a pressure rating for gas breakthrough, as set by the manufacturer, dependent on their pore size. Consequently a range of porous plates are used to aid turnaround time, with the following pressure ratings:- 50, 100, 500 and 1500kPa.

To ensure proper capillary connection between the rock sample and the porous plate, the sample is dabbed onto a layer of diatomaceous earth which provides a conductive path for the expelled fluid. A sheet of very fine tissue must be used to separate the earth from the sample to avoid sample contamination. To ensure stabilization each reading is taken after 6 days i.e. the total elapsed time for a test is about 60 days.

The fluid saturation is measured by weighing the sample, the relationship between the capillary pressure and fluid saturation can thus be obtained, and the capillary pressure curve is generated for each sample.

3.8.2 Oil-Brine Capillary Pressure Using Centrifuge

In preparation, routine measurements are carried out and samples saturated with simulated formation brine as described in section (3.4). Gravimetric checks must be carried out to insure full saturation.

Then samples are placed individually in a centrifuge rotor insert, which is mounted into the centrifuge container as shown schematically in Figure 3.9. The container is filled completely with a refined mineral oil. Each sample is entirely covered.

Samples are subjected to centrifugal force at constant rotational speed which is equivalent to a pressure value. The centrifuge is run at constant speed for a minimum of 6 hrs to ensure saturation equilibrium. The centrifuge is then stopped, the saturation is measured gravimetrically and the same procedure is followed at a higher speed.

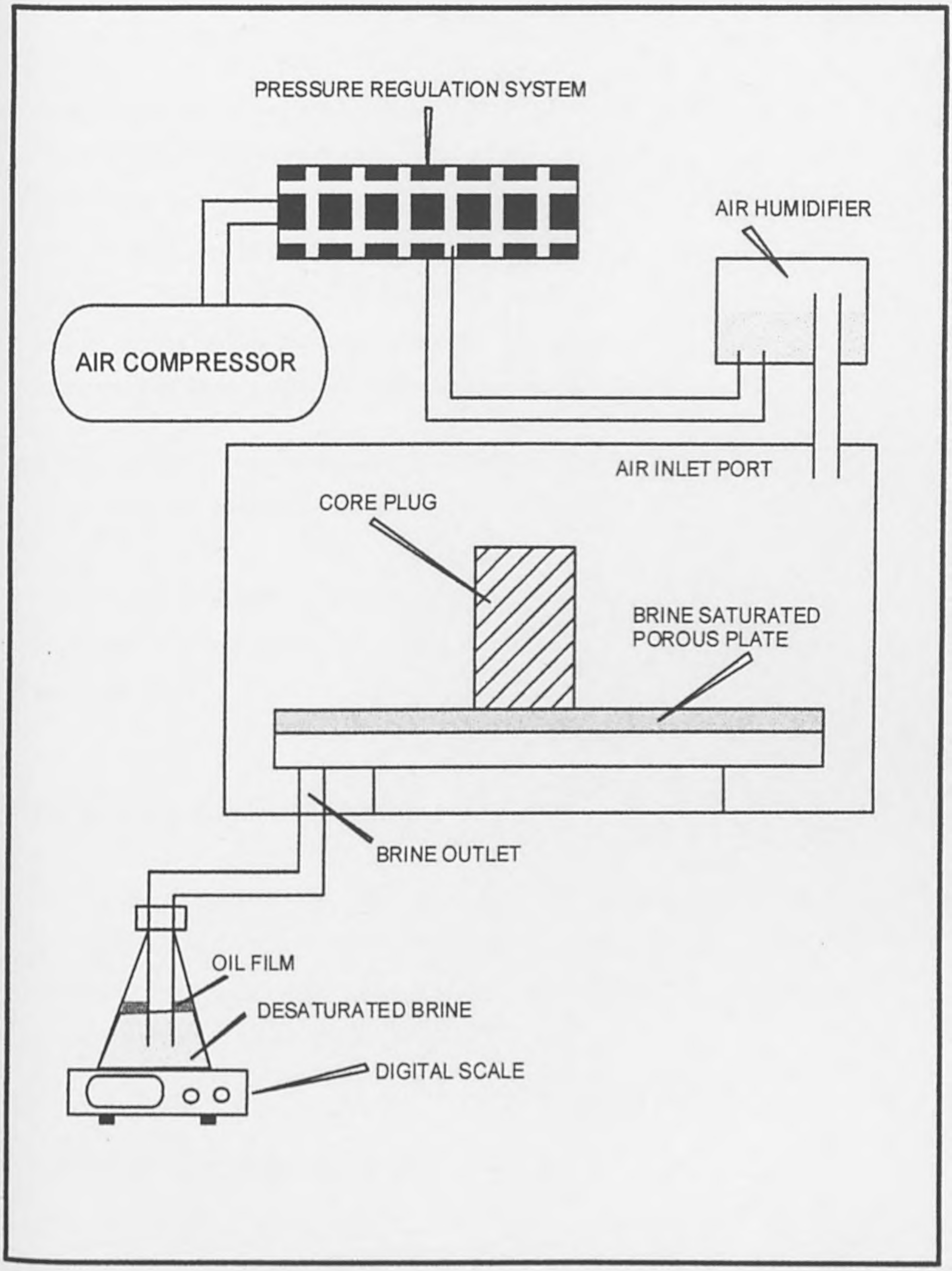

Figure (3.8) Air-Brine Capillary pressure measurement using porous plate System.

3.8.3 Mercury Injection Capillary Pressure

After the sample is cleaned, dried and its porosity measured, it is placed into the rock chamber within the mercury injection apparatus shown in Figure 3.10. The rock sample is evacuated using a vacuum pump. The mercury is pumped into the sample chamber until the rock sample is entirely submerged into the mercury and the reference mark is reached. The mercury is injected into the tested samples by pumping a measured additional volume into the sample chamber. The mercury injection is continued in small increments of known volumes until maximum pressure is reached.

On completion of the drainage cycle, imbibition data can be obtained by releasing the pressure in steps and measuring the retained volumes of mercury.

The injected and retained mercury volumes are divided by total pore volume to be expressed as a percentage of sample saturation, and capillary pressure curves are generated.

3.9 Relative Permeability Measurement

After great difficulties had been experienced in carrying out relative permeability measurements at the laboratories of the collaborating body, (since in this facility there is constantly demand for commercial work) unsteady and steady state relative permeability rigs were designed and assembled by the auther.

3.9.1 Unsteady State Relative Permeability

A low flow rate/high pressure pump (0.001-150ml/min, up to 300kg/cm^2 (29.420×10^{3}kPa), with a flow rate accuracy of ±2% and a flow rate stability of ±0.5%) is connected to the hydrostatic core holder, pressure gauges, etc as shown in Figure 3.11.

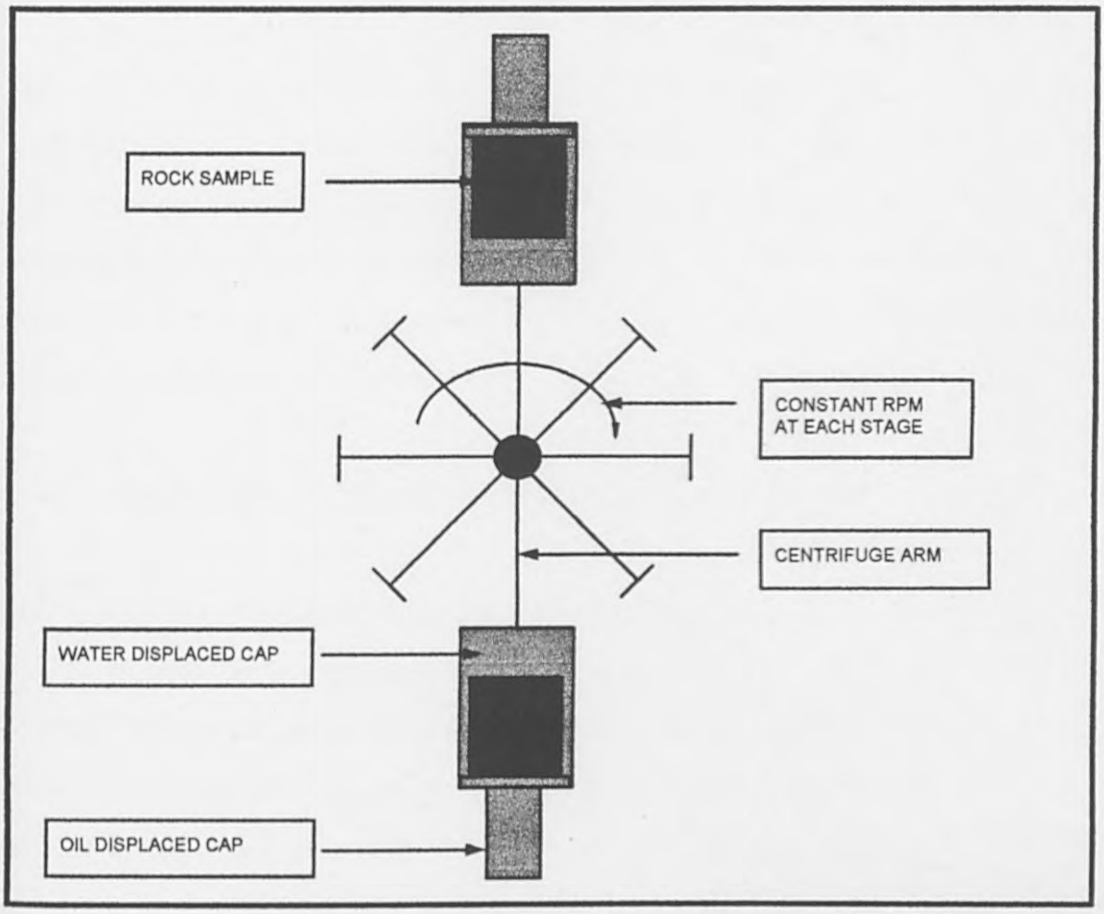

Figure 3.9 Centrifugal capillary pressure test.

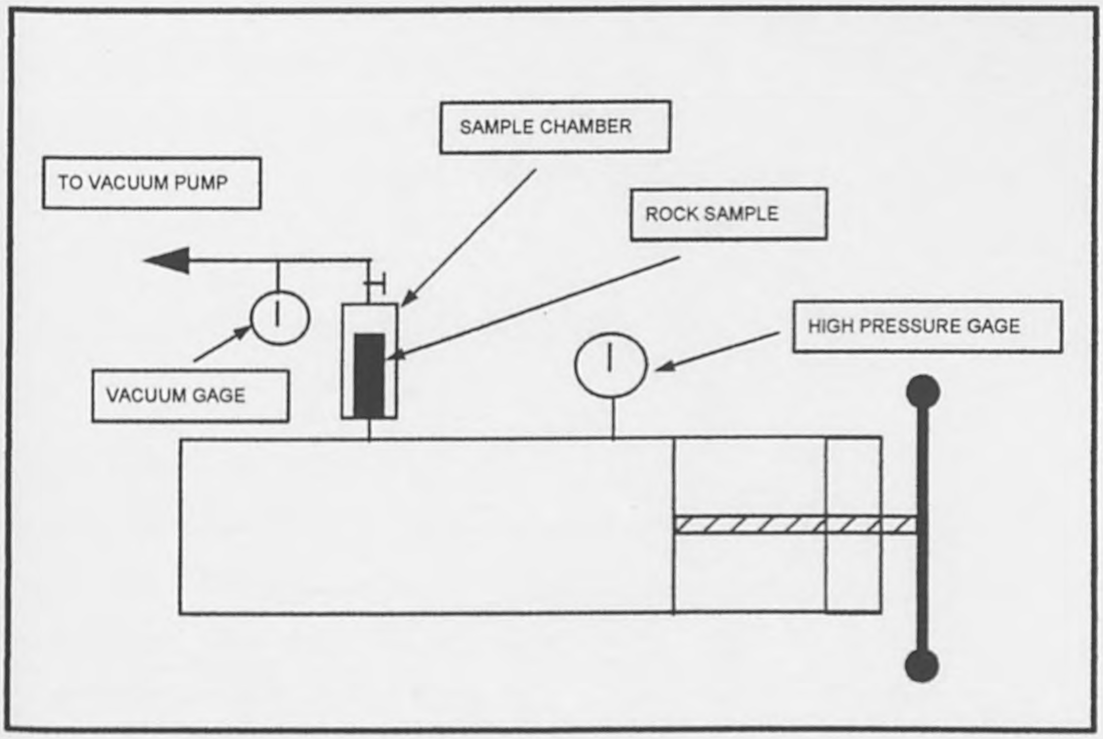

Figure 3.10 Mercury injection capillary pressure test.

3.9.1.1 Drainage Unsteady State Relative Permeability

The sample is prepared (by cleaning, dried then routine measurements were carried out) then saturated with the wetting phase (brine in water wet samples) and placed in the hydrostatic core holder. The wetting phase is displaced by the non-wetting phase (mineral oil) at a constant flooding rate of 6cc/min. Pressure, wetting and non-wetting flow rates are recorded at measured time intervals. Flooding is continued until no further wetting phase is recovered.

3.9.1.2 Imbibition Unsteady State Relative Permeability

The sample is saturated with the non-wetting phase (mineral oil) at irreducible water (brine) saturation while drainage flooding (section 3.9.1.1), still in the core holder). The sample is then flooded with the wetting phase (brine) (so displacing the non-wetting phase) at 6 cc/min, until no further non-wetting phase is recovered. Pressure, time, and recovered volumes of the wetting and non-wetting phases are recorded.

Both drainage and imbibition relative permeability were run under overburden pressure (effective stress ≈ 1730kPa). A high flow rate was used to ensure that viscous forces were large in comparison with capillary forces in order to eliminate the capillary end effect and to avoid distortion of data. The relative permeability is calculated from the flooding experiments using the JBN (Johnson, Bossler, Nauman)[21] method.

3.9.2 Steady State Relative Permeability

Two low flow rate-high pressure pumps (as described in the unsteady state rig) are connected to a hydrostatic core holder, pressure gauges and transducers, etc as shown in Figure 3.12. Two Berea Sandstone samples are used as upstream and downstream mixing heads. Similarly, all steady state relative permeability measurements were run under overburden pressure (effective stress ≈ 1730kPa), and at 6cc/min flow rate.

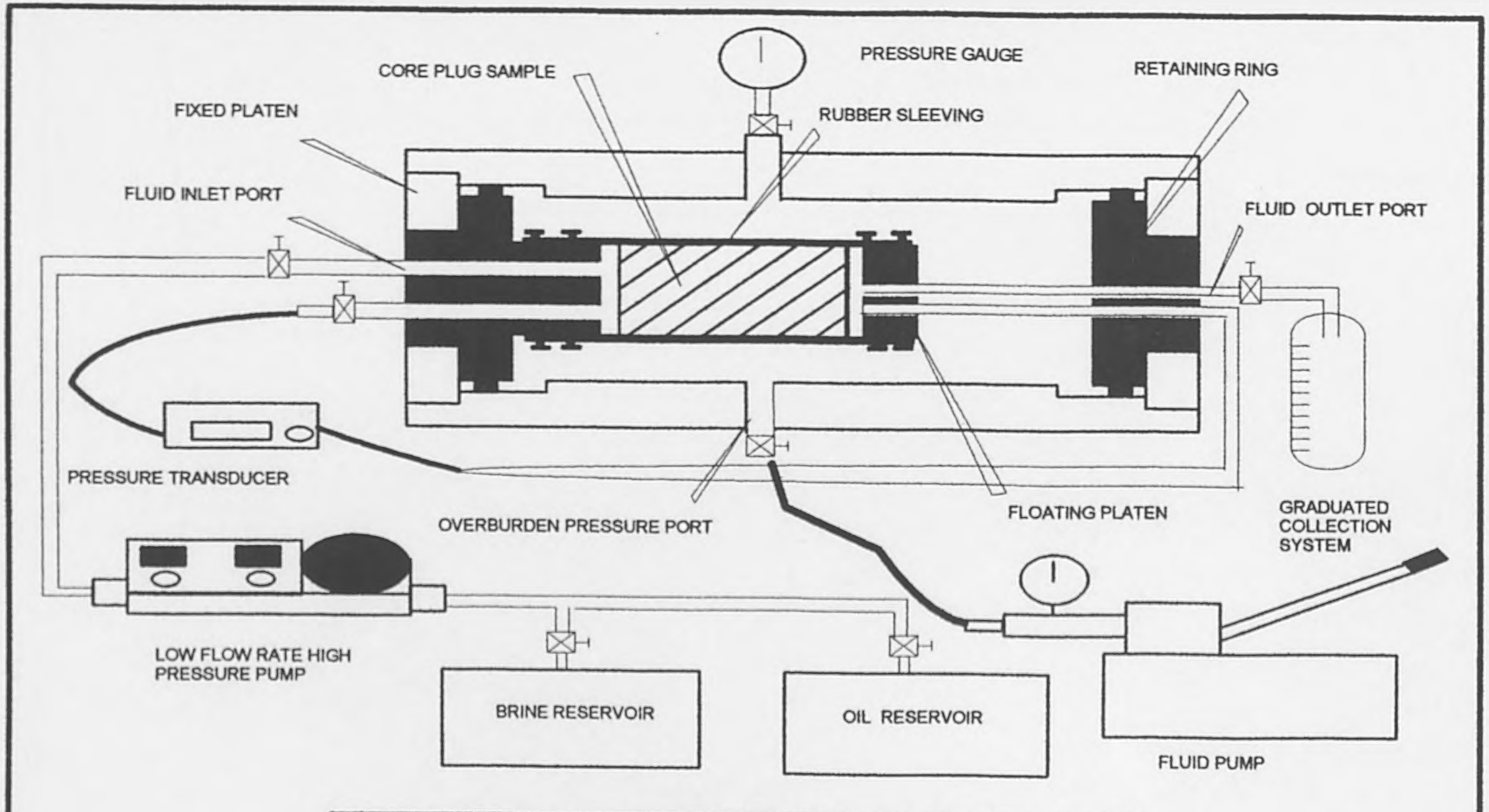

FIGURE (3.11) UNSTEADY STATE RELATIVE PERMEABILITY

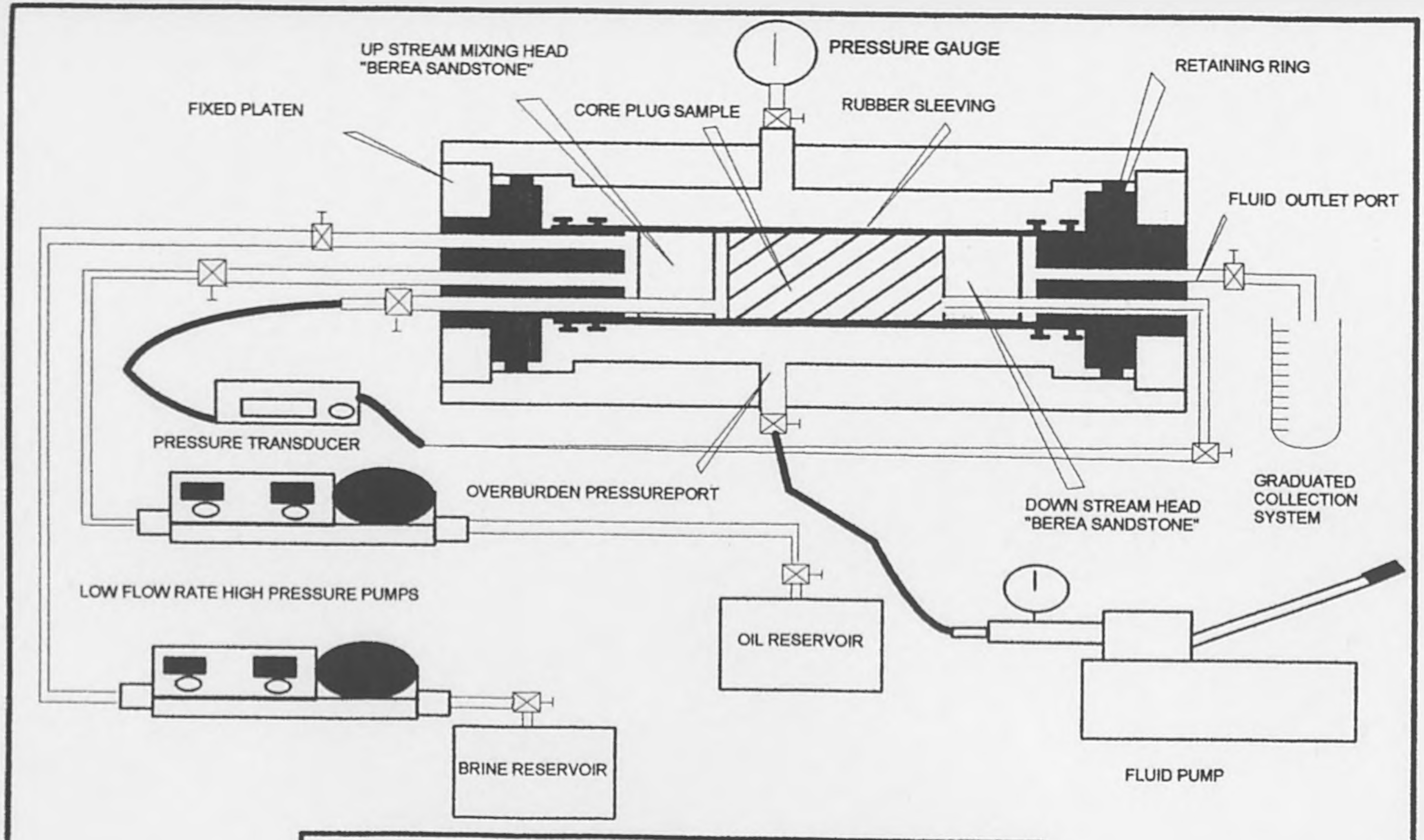

FIGURE (3.12) STEADY STATE RELATIVE PERMEABILITY RIG

3.9.2.1 Imbibition Steady State Relative Permeability

After routine measurements, the sample is fully saturated with the non-wetting phase (oil for water wet samples), and placed in the core holder. The absolute permeability is measured using 100% oil. Steady state tests are carried out by injecting oil/brine mixtures having the following ratios; 2.5% brine -97.5 oil, 10% brine -90% oil, 50% brine -50% oil, 70% brine –30% oil, 90% brine -10% oil, and finally 100% brine which represents the water permeability at irreducible oil saturation. At each oil/brine ratio the flow is held steady and the pressure differential is monitored. When the pressure differential is stable for an extended period, the steady state condition is judged to be reached, thus, pressure and flow rate are measured, and the sample is off loaded for gravimetric saturation measurements. The same steps are repeated for each oil/brine ratio. Oil and brine relative permeability is measured by direct application of Darcy's law.

3.9.2.1 Drainage Steady State Relative Permeability

Drainage steady state procedure is almost identical to the imbibition one. The main differences are;

1. It starts at the end point of imbibition relative permeability, i.e. the sample was saturated with non-wetting phase.

2. The wetting phase saturation is increased, simply reversing the injection of oil/brine mix ratios at the imbibition case. It is started at 100% brine injection (the end point of drainage displacement), then 90% brine -10% oil, 70% brine -30% oil, 50% brine -50% oil, 10% brine -90% oil, 2.5% brine -97.5% oil, and finally 100% oil which represents oil permeability at irreducible water saturation.

CHAPTER 4

CORE SAMPLE EVALUATION USING X-RAY COMPUTED TOMOGRAPHY

4.1 Introduction

X-ray Computed Tomography (CT Scan) is a radiological imaging technique which was developed in 1972 by Hounsfield[160]. X-ray CT is being used increasingly in the oil industry, particularly in saturation monitoring in core analysis[161-169]. The technique allows images of pre-selected slices of core material to be produced non-destructively. The images, obtained by computer reconstruction, show the variation of the x-ray stopping power (attenuation coefficient of the material) in a thin slice of rock.

The aim of using this technique was to select the most homogeneous sandstone samples (to avoid core heterogeneity[170]) for investigation and to establish a basis for the use of x-ray CT for porosity estimates on whole core. Although the attenuation coefficient (η) depends on a number of factors, such as chemical composition and density, the variation in η for a range of similar rocks is dominated by the proportions of solid grains and pore space in the rock, i.e. the porosity (ϕ).

The work done using x-ray computed tomography falls into five parts:-

1 A new calibration procedure for the medical CT scanner was developed, adapted to scanning oil reservoir rock materials rather than the human body.

2 The porosities of selected rock plugs (ranged from 7.5 to 30 percent porosity), were measured by conventional and CT methods to validate porosity measurements obtained by the CT technique and to establish a new relationship between x-ray attenuation coefficient and porosity from a single scan, so that any subsequent measurements of η on sandstone sample (regardless of whether the rock sample is dry or saturated) could be used to evaluate porosity.

3 The establishment of a soundly based non-destructive method for using the CT scanner as a powerful tool to assess the degree of homogeneity of cores for use in core screening based on non-destructive 3-D porosity measurements for small sub-volumes within the rock samples.

4 A set of homogeneous sandstone plug samples, exhibiting a wide porosity range, was obtained by selecting those which showed minimal variation of the x-ray attenuation coefficient (porosity) throughout their volume.

5 The newly developed CT method was used to measure the variation of porosity with depth in poorly consolidated dry sandstone whole core; the results are compared with helium porosity data obtained by plugging the whole core.

4.2 Technical Background

When an x-ray beam passes through a homogeneous medium its intensity will decrease due to absorption and scattering as shown in Figure 4.1. The decrease in intensity of the beam (dI) is proportional to the traversing distance[171-176] (*dl*), hence:

$$-dI = \eta I dl \tag{4.1}$$

Where, I is the intensity of the beam

η is a factor of proportionality called the attenuation coefficient (cm^{-1}). This represents the fraction of energy removed from the beam per centimeter of path traveled.

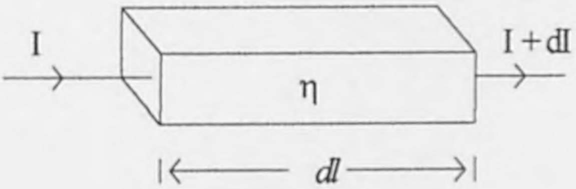

Figure (4.1) An x-ray beam traversing a uniform object. The reduction in intensity represents the attenuation through the whole object.

Then

$$\frac{\mathrm{dI}}{\mathrm{I}} = -\eta dl \tag{4.2}$$

and on integration this becomes

$$\mathrm{I} = \mathrm{I}_0 \mathrm{e}^{(-\eta l)} \tag{4.3}$$

Where I_0 is the initial intensity of the beam and I is the beam intensity after traversing a thickness l of the material.

If x-rays pass through a non-uniform (inhomogeneous) object with (n) different elements (Figure 4.2) of equal lengths l, but with different attenuation coefficients (η_1, η_2, η_3, η_4,....η_n), then

$$\mathrm{I} = \mathrm{I}_0 \mathrm{e}^{l(\eta_1+\eta_1\ +\eta_3+\eta_4 \cdots\cdots\eta_n)} \tag{4.4}$$

The calculation of ($\eta_1+\eta_2+\eta_3+\eta_4+....\eta_n$) is the main principle underlying x-ray computed tomography.

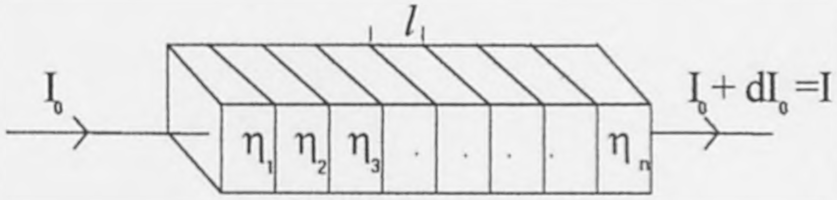

Figure (4.2) An x-ray beam traversing a non-uniform object. The reduction in intensity representing the sum of attenuations through all the elements forming the object.

In CT Scanning, the picture is composed of elements in the matrix called "Pixels". The main objective of developing computed tomography is to determine the attenuation coefficient of the object in each picture element (pixel) and then present these values for viewing on a monitor. As the x-ray beam traverses a non-uniform object, its attenuation will vary from one pixel to another. Hounsfield solved this complicated problem in his first CT scanner using a rotating source and detectors. The measurements were made at 1° intervals up to 180° and carried out 160 times at each angle[173]. The scanning position is defined by the angle θ and distance p as shown in Figure 4.3. To determine the attenuation coefficient at every pixel, consider Figure 4.3, which shows a cross-sectional view of the head superimposed upon a rectangular matrix. Let $\eta(x,y)$ be the average attenuation coefficient in the pixel (x,y) for the radiation emitted by the x-ray source (S), and the radiation transmitted (detected by detector D) I is related to the incident radiation, I_0 by:

$$I = I_0 e^{-\Sigma\eta(X,Y)\Delta l(X,Y)} \tag{4.5}$$

and can be re-arranged as follows

$$\ln(I_0/I) = \Sigma\eta(x,y)\Delta l(x,y) \tag{4.6}$$

Where $\Delta l(x,y)$ is the path length through the pixel (x,y) and summation is carried out along the x-ray beam from A to B. For the ray shown in Figure 4.3, 6 pixels [(1,1), (2,1), (3,2), (4,2), (4,3) and (5,3)] are involved. Full scanning will yield $N_T = 160 \times 180 = 28{,}800$ transmission measurements and 28,800 linear equations similar to Equation (4.6). The CT picture (image) was reconstructed over a square area containing $N_P = 80 \times 80 = 6400$ pixels. Since N_P is smaller than N_T a solution is possible. Although in principle these equations could be solved by standard matrix inversion techniques, it is impractical to do so due to the large number of unknowns. The equations are solved using a back projection algorithm, thus the attenuation coefficient can be determined at any pixel forming the reconstructed CT image.

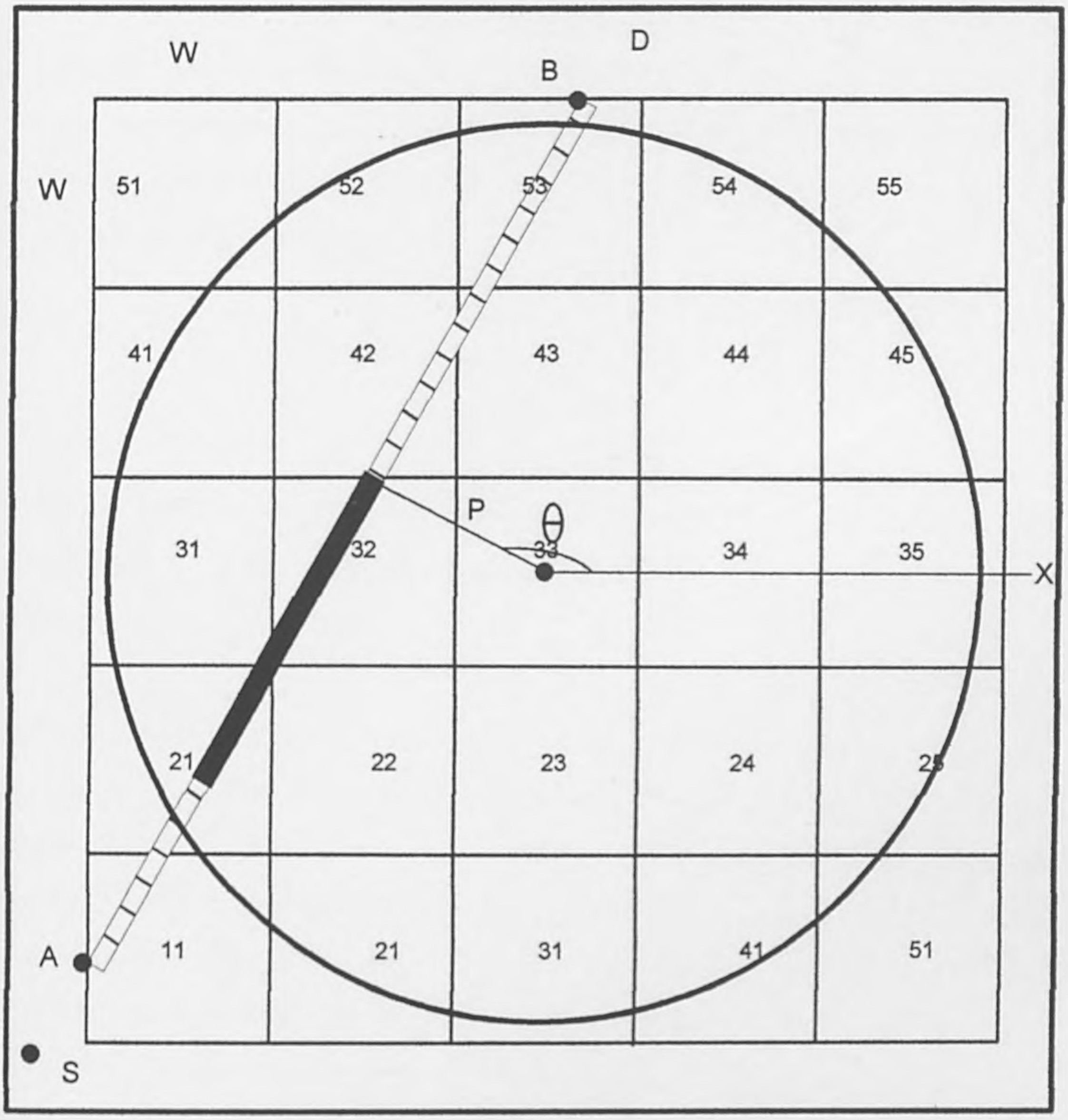

Figure (4.3) Schematic representation of pixels with a cross section of the head superimposed. A typical ray from the source S to the detector D is shown. It can be represented by the parameter P and the angle θ. The path through each of the pixels is illustrated.

To collect the data necessary for image reconstruction[177,178] using a scanner of recent design, an x-ray source and detector system rotate around the sample (or the sample is rotated in a fixed x-ray system) so that many different views of the slice contents may be obtained (see Figure 4.4) (for commercial scanners the slice thickness is typically 1-12mm). From a set of these projections, a cross sectional image is reconstructed using a back projection algorithm 4-9 in the scanner's computer. By convention, inherited from medical applications, the numerical values of η are presented in an internationally standardized scale called Hounsfield units (HU). The scale is defined by the range -1000 HU in air and zero HU corresponding to the attenuation coefficient of water. For the human body, HU units are generally much lower than any reservoir rock such as sandstone or carbonates. Most human body tissues lie in the range -100 to +100 with fat slightly negative and muscle slightly positive. The Hounsfield number (HU) is related to η according to the following formula:

$$HU = 1000\,(\eta_x/\eta_w - 1) \tag{4.7}$$

Where, η_x is the linear attenuation coefficient of the medium occupying the volume element and η_w is the attenuation coefficient of water and η_x/η_w is the CT number (CTN).

The reconstructed CT image is displayed on a monitor, either as shades of gray (black and white), or in color. The viewing scale is set by any two points depending on the region of interest. For instance when using a black and white system for scanning human tissue, it is convenient to select a range such that a Hounsfield units of -200 is dark black and +200 is clear white. In rock imaging it is essential to set a very wide viewing scale to include fractures as well as dense rocks. Usually the range is set as follows; black at air (-1000 HU) and white at dense rocks (≈25000 HU). In a color system HU can be displayed in different colors e.g. blue represents HU from -1000 to -500, red from -500 to 0.0, brown from 0.0 to 500...etc, the range can be set according to the regions of interest.

The reconstructed images can be stored permanently on disk or tape. Therefore it can be displayed on a television monitor or printed out whenever it is required.

The importance of using X-ray Computed Tomography is highlighted by Heaviside and Salt[179], and others[15,158] Detailed discussions can be found in the work of Wellington *et al*[168], Ringen *et al*[169] and Withjack[162].

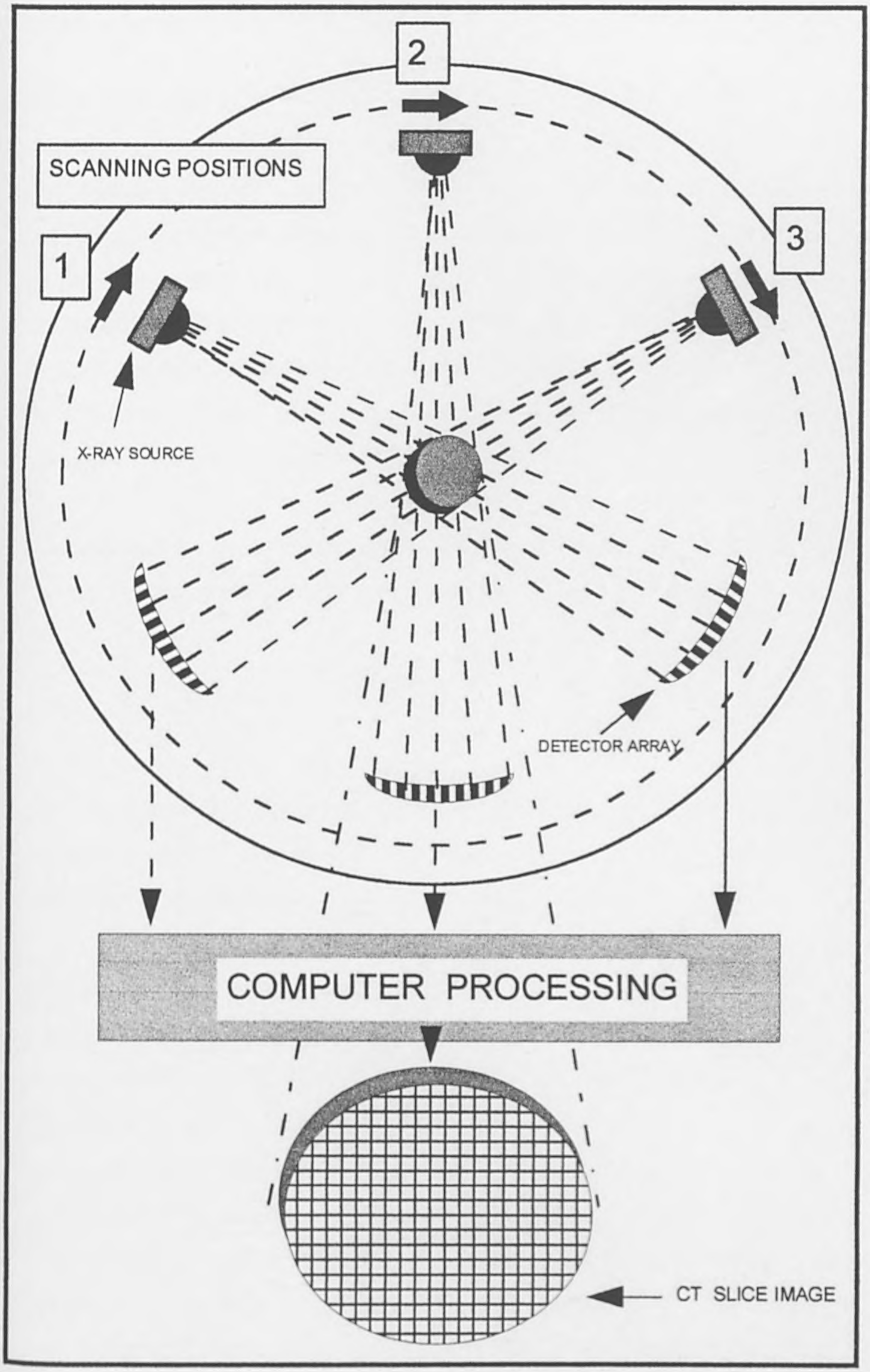

Figure (4.4) Schematic representation of the basic principles of x-ray computed tomography.

4.3 CT Scan Calibration

For medical uses of X-ray Computed Tomography calibration is carried out using the International Standard Reference Points, air and water, since the Hounsfield units (HU) for these are defined. Figure 4.5 shows the use of air and water in CT scanner calibration for medical purposes. As the x-ray attenuation coefficient at the medical region of interest is very close to the upper and main reference point (water), small errors at the calibration point will not be amplified while scanning the human body. As a result the reproducibility of scanning data will not be distorted. Therefore using air and water as reference points for medical scanner calibration is very convenient, and adequate for obtaining reliable and accurate results.

The equivalence between attenuation coefficients and CT numbers is shown by the linear relationship in Figure 4.5, which can be described as follows;

$$\mathrm{HU} = d\left(\eta / \eta_{\mathrm{water}} \right) - 1000 \qquad (4.9)$$

So, small deviations at the main reference point (HU water = 0) will thus lead to significant errors in the region of geological interest, which varies from around 1000 to 2500 HU, depending on rock type and bulk density i.e. porosity.

The CT technique is being used in this project for scanning a group of sandstone rock samples which have HU around 1500. In this region, a deviation of ±1.0% in $(\eta/\eta_{\mathrm{water}})$, will correspond to a difference of 25 HU. The CT number varies from -1000 HU in air (density $\approx$ 0.0 gm/cc) to 0.0 HU in water (density = 1.0 gm/cc), each Hounsfield unit representing a 0.1% change in bulk density. Therefore an error of ± 25 HU leads to an error of ± 2.5% in porosity measurements, which cannot be neglected in reservoir engineering. For this reason, a medically calibrated CT scanner is not convenient for CT measurements for reservoir rock samples and results will not be very reliable, especially as conventional rock scanning requires measurements to be run while samples are dry and then when 100% saturated with desired fluid. This means that in the reproducibility of attenuation data, accuracy is crucial to obtain correct quantitative results.

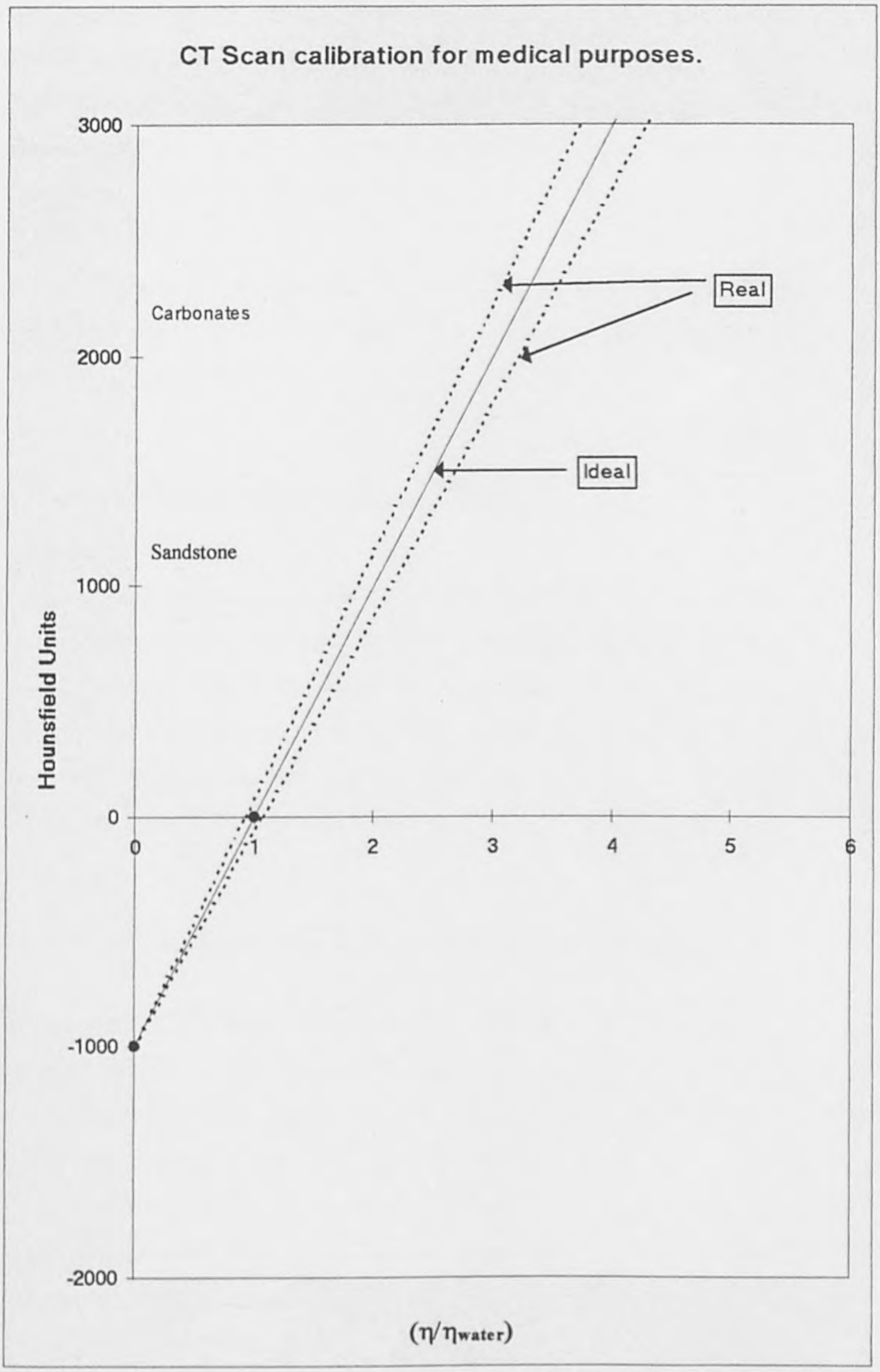

Figure (4.5) CT scanner calibration for medical purposes using air and water as the principle reference points.

In rock imaging, it is very desirable to work with a secondary standard, which provides a calibration point in the region typical of reservoir rock HU. Therefore, the scanner has been re-calibrated using a special fused quartz (1500 HU), of typical rock HU, rather than water. This will eliminate the error amplification and ensure the reproducibility of CT measurements for reservoir rock samples.

Figure 4.6 shows the importance of using a calibration standard with CT number within the region of interest and how the use of the proper calibration point minimizes the errors in CT measurements.

4.4 Porosity Measurements Using CT Scan

X-ray Computed Tomography is one of the latest technologies which has been used to determine reservoir rock porosities. Porosity can be obtained from CT measurements on core material using either a single-scan or multiple (dual) scan technique; each has its own advantages and limitations. The author has developed a new single scan method[181-182] in order to minimize time and cost, and to make the technique more informative and useful in core analysis, especially on whole core.

4.4.1 Porosity Measurement Using Multiple-Scan Technique

Morgan *et al* (1950)[180] employed the commonly used 1-D x-ray attenuation principle for porosity estimation. X-ray CT imaging permits the extension of the method to very precise and non-destructive measurement of porosity for small sub volumes within an interior region of 2mm^2 or less of the rock. In essence the measurement depends on the subtraction of the measured attenuation coefficients for the same sub-volume for dry rock and rock fully saturated with fluid. Knowing the x-ray attenuation coefficient of the saturating fluid permits calculation of the volume of fluid in the rock and hence its porosity.

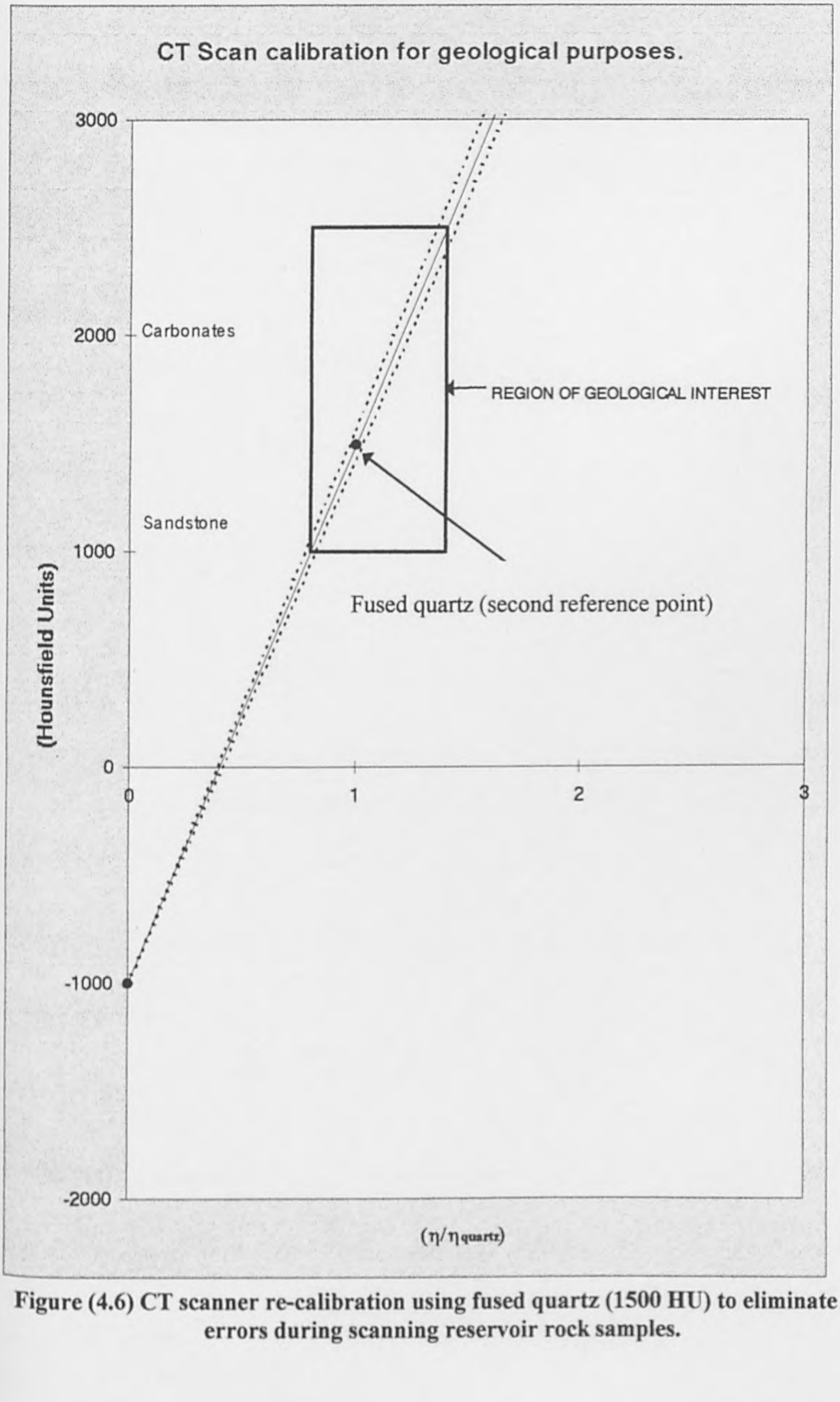

Figure (4.6) CT scanner re-calibration using fused quartz (1500 HU) to eliminate errors during scanning reservoir rock samples.

The evaluation of porosity using the multiple scan technique, i.e. scanning the rock samples twice, once while dry and then when fully saturated with liquid, proceeds as follows: the attenuation coefficient (η) for a sub-volume of imaged rock is the sum of contributions from the rock grains (η_g) and the saturating liquid (η_f) so the measurement on a dry sample (100% saturated with air, where η_{air} is effectively zero) yields

$$\eta_1 = (1-\phi)\eta_g + \phi\eta_{air} \qquad (4.10)$$

The measurement on 100% liquid saturated rock yields

$$\eta_2 = (1-\phi)\eta_g + \phi\eta_f \qquad (4.11)$$

so the porosity is given by

$$\phi = \frac{\eta_2 - \eta_1}{\eta_f - \eta_{air}} \qquad (4.12)$$

Where, η_1 and η_2 are the direct measurements of rock attenuation coefficient while the sample is dry and saturated respectively; η_f can be obtained by scanning a sample of the rock saturating fluid.

Since the CT number (CTN) is defined as $\frac{\eta_x}{\eta_w}$, equation 4.7 can be written in the following form:

$$\mathrm{CTN} = \frac{\eta_x}{\eta_w} = \frac{\mathrm{HU}}{1000} + 1 \qquad (4.13)$$

by combining equations 4.12 and 4.13, the porosity can be expressed as follows:

$$\phi = \frac{\mathrm{CTN}_2 - \mathrm{CTN}_1}{\mathrm{CTN}_f + 1000} \qquad (4.14)$$

Where, CTN_1 and CTN_2 are the directly measured CT numbers on the rock sample while dry and saturated respectively, and CTN_f is the CT number of the fluid saturating the sample. Obviously, from the way equations 4.12 and 4.14 are derived, porosity determination using the multiple scan technique requires a vast amount of effort compared with the conventional methods of helium or liquid porosity. In order to use the dual-scan technique it is essential to scan the sample twice, first dry, then saturated. This requires significant time and effort such as; sample cleaning, drying and saturation (see Chapter 3, Sections 1, 2 and 4, Sample Cleaning, Drying and Saturation). On the other hand, no conventional method could measure porosity for any sub-volume within rock samples non-destructively, i.e. porosity variation cannot be monitored within a single sample. For this reason the CT method is a unique and superior technique to measure porosity variation within the whole sample.

4.4.2 Porosity Measurement using the Single-Scan Technique

The single-scan technique can measure a rock's porosity by scanning only once, regardless of whether the rock sample is dry or saturated. Both sample conditions are convenient and acceptable; the only requirement is to obtain a specimen of the saturating fluid if the sample is not dry, but usually rock samples are kept dry and a sample of the saturating fluid is always available. Since sample saturation is not required, this makes the technique very speedy and convenient. Furthermore, it can be run on whole core before it is sectioned, plugged and/or affected by any other treatments. This technique can take measurements within rock material non-destructively for any sub volume size, exactly as for the multiple-scan technique.

The new single-scan technique has been developed based on the fact that the grain x-ray attenuation coefficient (η_g) is reasonably consistent for the same rock type, e.g. grains which form any sandstone rock have the similar η_g. Thus the variation in η for any sandstone rock sample is due to the contained pore space within the sample, and relates directly to the porosity (ϕ = pore volume/bulk volume). From Equations 4.11 and 4.12 the attenuation coefficient for the rock grains is given by;

$$\eta_g = \frac{\eta_1 \eta_f}{\eta_f + \eta_1 - \eta_2} \tag{4.15}$$

From Equations 4.13 and 4.15 rock grains CT number (CTN_g) can be obtained as follows:

$$CTN_g = \frac{(CTN_1 + 1000)(CTN_f + 1000)}{CTN_f + CTN_1 - CTN_2 + 1000} \tag{4.16}$$

Equation 4.16 has been used to calculate the average rock grains CT number (CTN_g) for sandstone samples. When CTN_g is known for any rock type, porosity can be obtained by a single CT scan measurement using the following equations:-

1. **Dry sample**. Knowing CTN_g and CTN_1, and combining Equations 4.10 and 4.13, porosity is calculated as follows:

$$\phi = \frac{CTN_g - CTN_1}{CTN_g + 1000} \tag{4.17}$$

2. **Saturated sample.** If rock sample is fully saturated with single phase fluid, knowing CTN_g and CTN_2 and combining Equations 4.11 and 4.14, porosity is calculated as follows:

$$\phi = \frac{CTN_g - CTN_2}{CTN_g + CTN_f} \tag{4.18}$$

When a rock sample is saturated with more than one fluid, such as water, oil and/or gas, the measured x-ray attenuation coefficient is made up of contributions from the rock matrix (grains forming the rock) and the fluid(s) filled pore space system. The following equation describes the relationship:

$$\eta_3 = (1 - \phi)(S_w\eta + S_o\eta_o + S_g\eta_{gas}) \qquad (4.19)$$

Where, η_3, η_g, η_w, η_o and η_{gas} are attenuation coefficients for saturated rock sample, rock grains, water or brine, oil and gas respectively, and S_w, S_o and S_{gas} are water or brine, oil and gas saturations respectively. The porosity can be defined from Equation 4.19 using CT number (Equation 4.13) by the relationship

$$\phi = \frac{CTN_g - CTN_3}{CTN_g - \left(S_w CTN_w + S_o CTN_o + S_g CTN_{gas}\right)} \qquad (4.20)$$

Porosity can be measured using the newly developed single-scan method, based on previous knowledge of CTN_g and rock sample status while scanning. Equations 4.17, 4.18 and 4.20 are applicable for dry samples, samples saturated with one fluid and samples saturated with more than one fluid respectively.

4.5 CT Scan Validation

After CT scan re-calibration using a secondary reference point (fused quartz), it is very important to verify the validity of the obtained data. The main aim of utilizing this advanced technique was to select a group of the most homogeneous sandstone core plugs based on 3D porosity measurements for small sub-volumes within the rock samples. Therefore, porosity was measured by a CT scanner for different sandstone rock samples including tight, medium and very porous samples. Results were compared with data obtained conventionally at the routine core analysis laboratory to demonstrate the validity of the method. The CT method showed good agreement with conventional methods; some data is displayed in Figure 5.1 Chapter 5.

4.6 Comparison between Single and Multiple Scan Techniques

Both techniques are capable of measuring rock porosity non-destructively at any interior sub-volume. The multiple scan technique has been employed to establish the foundation for the single-scan method. In this work, the average sandstone grain attenuation coefficient (η_g) was obtained from data produced by multiple scanning for a group of different sandstone samples. This represents the corner stone of the method. The accuracy of the single-scan method depends on the reasonable consistency of η_g for each rock type, where η_g is irrelevant in the dual scanning technique. For this reason, the accuracy of the single-scan method is not comparable with the dual scan method for non homogeneous materials. The single scan technique does not require a change in sample condition, such as cleaning, drying, saturation or subtraction of x-ray attenuation for the same sub-volume. This gives two major benefits to this technique for porosity measurements, 1) it can be carried out using native state whole cores, and 2) it is much faster than the dual scan technique. A summarized comparison between single-scan and dual-scan method is made in Table (4.1).

MULTIPLE-SCAN METHOD	**SINGLE-SCAN METHOD**
Sample position must be precisely defined and both scans must be carried out exactly at the same place	Position identification is not required for porosity measurements
Requires change in saturation (two scans are required for each CT slice image)	Measurements are obtained at any existing saturation (Only one scan is required per CT slice image)
Porosity measurements are independent of grain x-ray attenuation coefficient	Porosity measurements are affected by grain x-ray attenuation coefficient
Suitable for homogeneous and non-homogeneous rock samples	It is necessary to introduce a correction factor for non-homogeneous rock samples
Not suitable for native whole cores	Very convenient for native whole cores
Time consuming	Very quick, measurements can be obtained in few minutes
Relatively expensive	At least 50% cheaper than the multiple scan method

Table (4.1) A summarized comparison between X-ray Computed Tomography Single and Dual-Scan Techniques.

4.7 Core Heterogeneity and Sample Screening

The main purpose of this work was the establishment of a soundly based method to employ x-ray computed tomography to assess rock heterogeneity quantitatively, rather than the usual qualitative description, and to assist in core sample screening. The method has been used to select a group of the most homogeneous sandstone rock samples for investigating the capillary pressure-relative permeability relationship.

As a CT image shows the variation in x-ray attenuation resulting from variation of mineralogy and/or bulk density, then heterogeneity can be simply described qualitatively by looking at CT 2-D images obtained from a single scan output. The quantitative variation in CT number is represented on the displayed image by colour variation; black for low density, getting whiter for more dense material. Within one image, colour may vary from dark (black) which represents fractures, to clear white for a high density mineral bed. Figure 5.7 shows some x-ray CT images that were taken at different locations along a whole core. The qualitative heterogeneity assessment relied on the variation in average x-ray attenuation for each rock sub-volume of 2mm^2 sub-area by 3.5mm slice thickness. It is very efficient in primary screening where the selection of homogeneous rock samples is important. Obviously non-homogeneous samples are removed immediately after single-scanning and no further measurements for porosity variation within the rock sample are required.

The quantitative information in CT images obtained by dual scanning rock samples while they are dry and saturated provides a basis for assessment of sample heterogeneity. The method used for assessing the samples in this study was to measure the average CT value for sub areas of 11mm^2 (corresponding to a rock volume of about 40mm^3 for the slice thickness) within the slice as well as averages over the slice area. Two CT images for each slice of rock material (while it was dry and saturated) were obtained, at exactly the same position, and the porosity for each sub-volume was obtained directly by the CT number subtraction method.

In order to obtain reliable average CT values for a slice of core sample, it is necessary that the CT scanner is re-calibrated at each stage using the same fused quartz of typical rock density to ensure reproducibility of measurements and to avoid any error in sub-volume porosity evaluation.

The rock sample heterogeneity has been classified as most homogeneous, homogeneous and non homogeneous, based on porosity measurements for sub-volumes of 40 mm^3 within and along the rock samples. In the most homogeneous plug samples studied, the variation in porosity was restricted to not more than ±0.3 % porosity, samples with

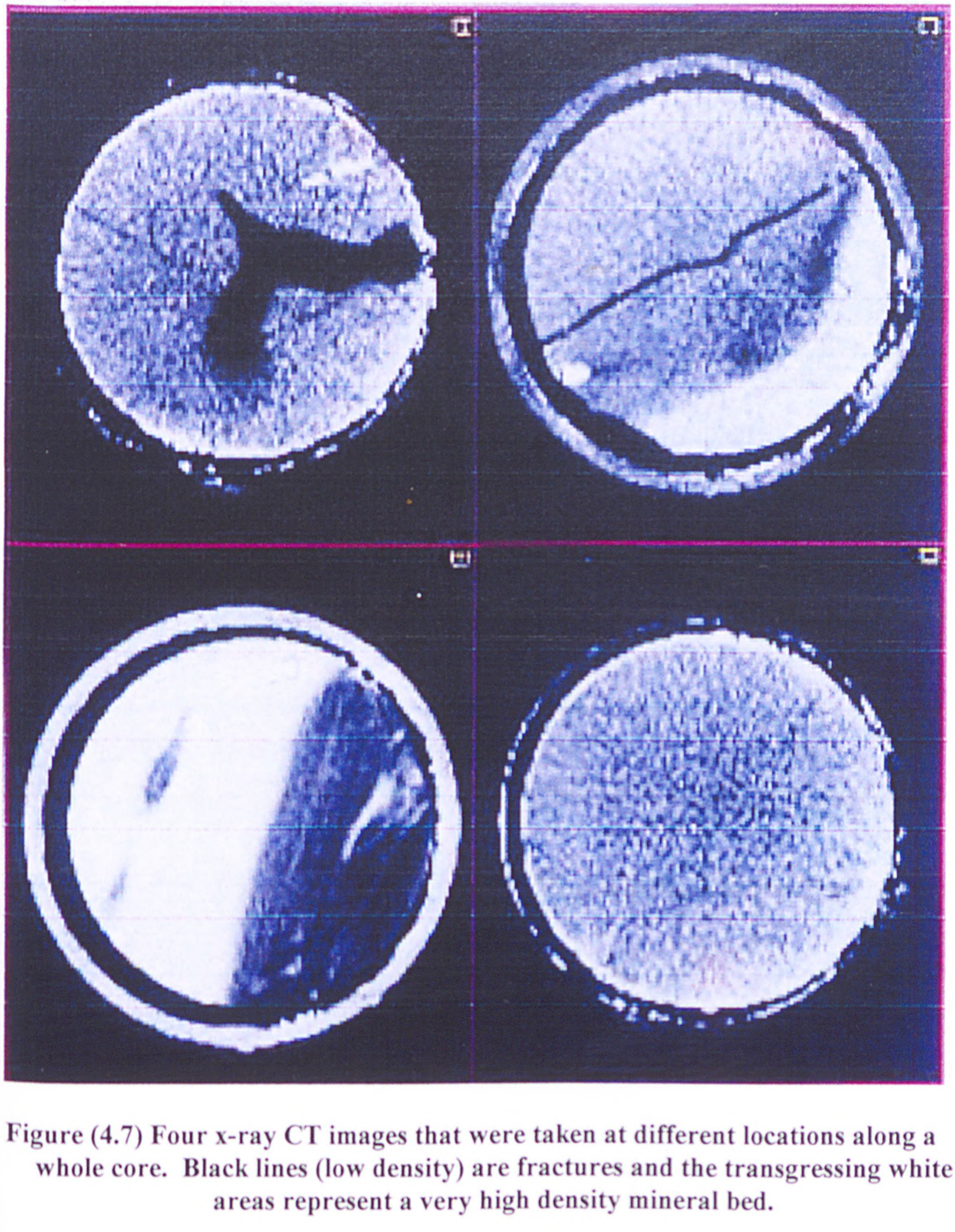

Figure (4.7) Four x-ray CT images that were taken at different locations along a whole core. Black lines (low density) are fractures and the transgressing white areas represent a very high density mineral bed.

porosity variation from 0.3 to 1.0% were classified as homogeneous and all samples with porosity variation over 1.0% were classified as non-homogeneous. Various homogenous sandstone rock samples were selected, based on this assessment, to study the relationship between relative permeability and capillary pressure.

4.8 Porosity Logs of Whole Core

The relationship between x-ray attenuation coefficients and porosity, developed previously based on the single scanning technique, can form the basis of the use of CT as a means for logging the porosity of whole core. It is a direct application of the newly developed single scan method for porosity measurements using Equation 4.18 or 4.20. The porosity log can be performed immediately after whole core recovery from the well and before any man-made intrusion, e.g. sectioning, plugging ...etc. CT images are obtained by scanning along the whole core, the porosity is obtained from CT number measurements at any desired area within the whole core cross section, then porosity values obtained from CT number measurements are plotted against the depth of the cored zone. Two whole core porosity logs together with conventional helium porosity measurements for comparison are presented in Chapter 5.

To obtain rapid porosity evaluations of wet core, the CT log clearly requires corrections for contained fluids. To correct for the fluid content of the core it is necessary to make some assumptions, (e.g. 80% oil saturation and 20% water saturation), together with knowledge, or estimates, of the oil or brine attenuation coefficients. Alternatively, a limited plugging strategy based on CT selected rock regions can be used to obtain reference points on the CT porosity graph.

CHAPTER 5

CT SCAN RESULTS AND DISCUSSION

5.1 CT Scan Re-calibration

X-ray computed tomography was originally developed for medical purposes. Medical scanners are calibrated using two reference points, air and water. Adoption of this technology in core analysis is **only** adequate for producing qualitative images for reservoir samples. For obtaining quantitative results such as rock porosity or fluids saturation measurements it has been found that the use of the ordinary medical scanner leads to significant errors due to the poor reproducibility of data within the geological region of interest. The new calibration method (presented in Chapter 4) using a fused quartz standard has proved to be the key point in error elimination, and hence a major achievement in adapting the CT scan to give an accurate quantitative measurements on reservoir core samples.

5.1 Porosity Measurements Using CT Scan

Porosity values were obtained for various sandstone rock samples, with a wide range of porosity values (from ≈7.5% to ≈30%), using the CT method using the dual-scan technique, and were compared with conventional helium and liquid porosity measurements to demonstrate the precision and reliability of the CT method. As shown in Figure 5.1, over the complete range of porosity values, there is excellent agreement between CT and liquid porosity measurements. Results from CT scanning also showed very close agreement with helium porosity measurements, within 0.5% porosity for low porosity samples (≈7.5%) increasing to 2% porosity at high porosity (≈30%).

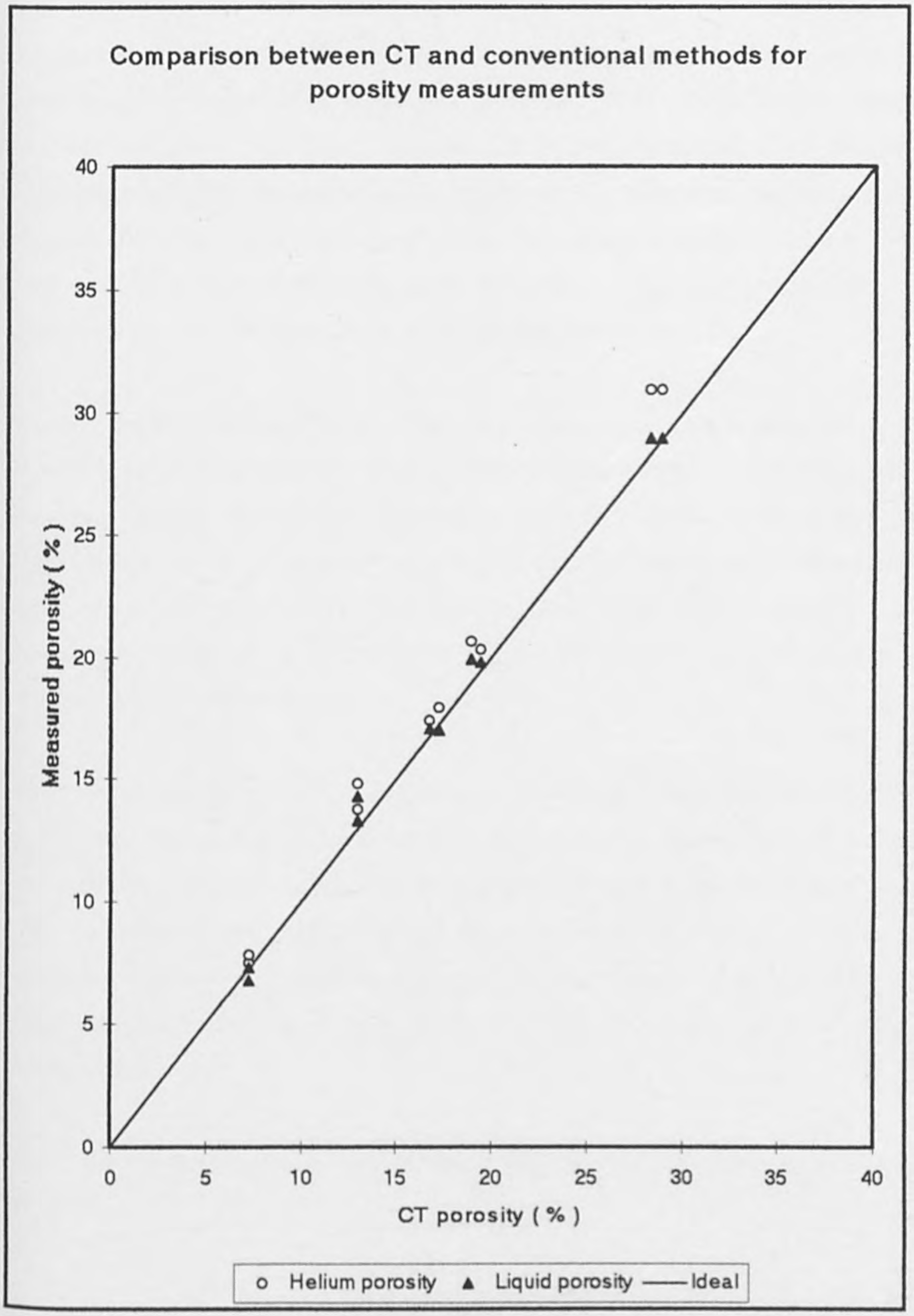

Figure (5.1) Comparison of x-ray CT porosity obtained by the dual-scan technique with conventional liquid and helium porosity measurements.

It is usual for helium porosity measurements to give higher values than liquid porosity measurements due to the ability of helium gas to invade the very fine pores within any rock sample by reason of its small atomic number. It is very difficult to achieve absolute saturation with liquid. As the CT porosity represents fluid saturation measurements which are equivalent to liquid porosity rather than helium porosity, deviation from the helium porosity values does not indicate an error in the CT method. Evaluation of the method must realistically be based on comparison with conventional liquid porosity measurements, which are, in this case, almost identical.

Porosity has been measured for the same group of sandstone samples using the newly developed single scan technique based on previous measurements of the sandstone CT number. The data obtained was compared with dual scan measurements, as shown in Figure 5.2. A very close agreement between both techniques can be seen over the entire range of rock sample porosities. This highlights the accuracy and the capacity of the new method and proves its comparability with the CT dual scan technique, as well as with the conventional methods.

Since the wave length of x-rays is dependent on the scanner voltage, thus the attenuation coefficient. Therefore, a change in scanning voltage leads to a variation in CT number measurements. It is extremely important to carry out scanning of the rock samples using the x-ray computed tomography at a fixed voltage, especially when using the single scan method. The scanning voltage must be identical to that used while the rock grains attenuation coefficient (η_g) is being measured, otherwise a significant error will be introduced.

All of the CT measurements in this work were carried out at a constant voltage of 140K V.

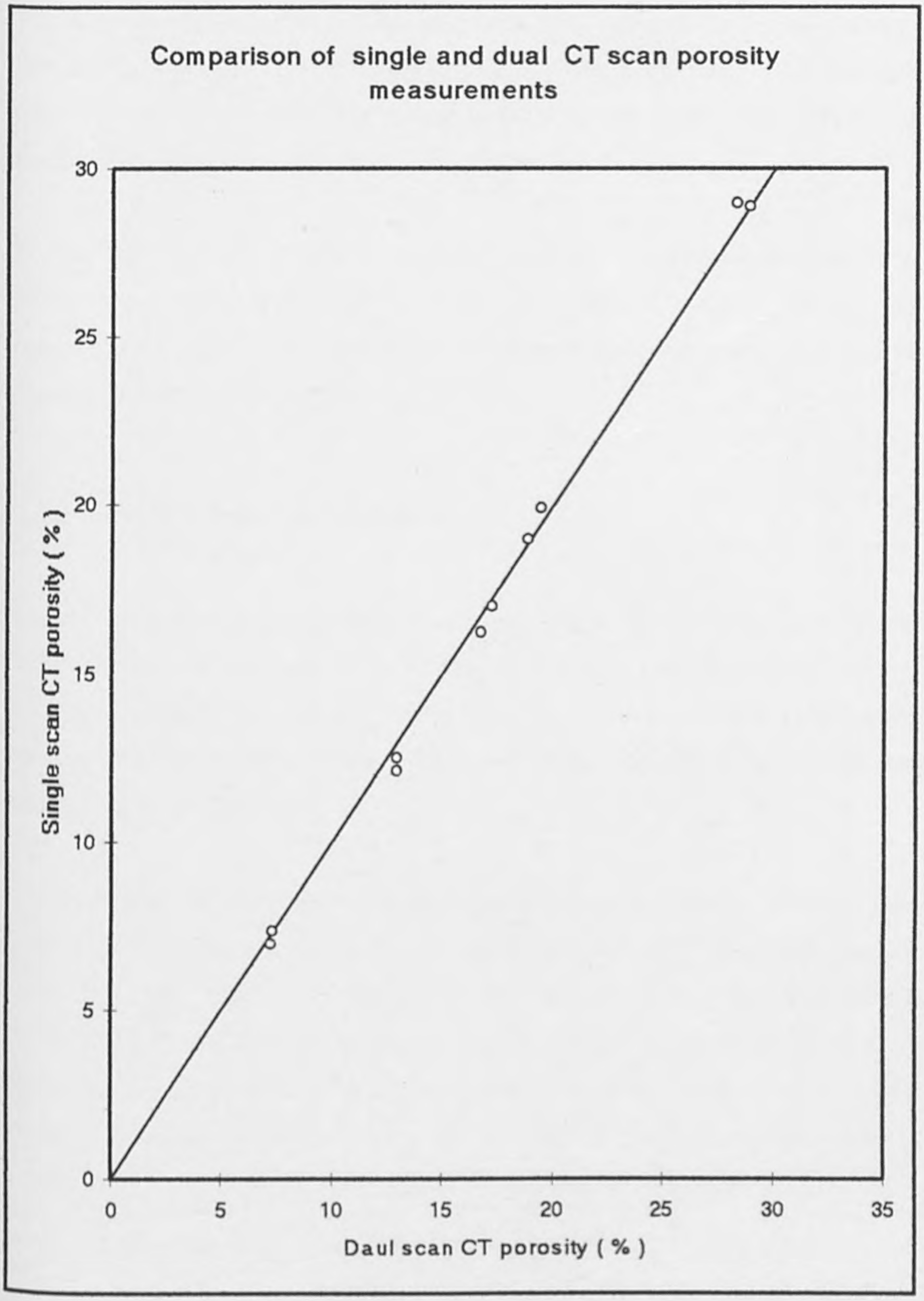

Figure (5.2) Comparison between single-scan and dual-scan porosity measurements using x-ray computed tomography.

5.2 Selection of the Most Homogeneous Rock Samples

The relative permeability concept has been introduced, based on the crucial assumption that the reservoir can be approximated to a single homogeneous bed. This assumption cannot be verified visually, due to the inability to see inside rock samples non-destructively, therefore a visual qualitative description is not adequate.

In this work the CT technique has been employed successfully to quantify the homogeneity of the rocks and to verify this assumption based on CT value measurements for interior rock sub-volumes (non-destructively) and porosity measurements derived therefrom.

5.2.1 Sample Screening Procedures

The new technique allows qualitative, as well as quantitative, descriptions of rock heterogeneity. Both descriptions have been employed to select a group of the most homogeneous sandstone rock samples for capillary pressure and relative permeability measurements and to study the relationship between these variables. Sample selection was carried out in three stages:

The **first stage** was a primary screening based on a visual evaluation. Many samples such as shown in Figure 5.3 are easily rejected at this stage due to the visually apparent variation in rock structure. Samples showing no obvious variations have been taken to the **second stage** of screening which is basically a qualitative description from single scan images obtained while the rock samples were dry. Where images showed obvious variation in x-ray attenuation the samples were rejected directly and no further scanning carried out.

Figure 5.4 shows an excellent example of the x-ray ability to reveal detailed structures and barriers within a core sample which appeared to be homogeneous to visual inspection. It is also important that samples are scanned longitudinally as well as cross sectionally, especially for samples with parallel beddings.

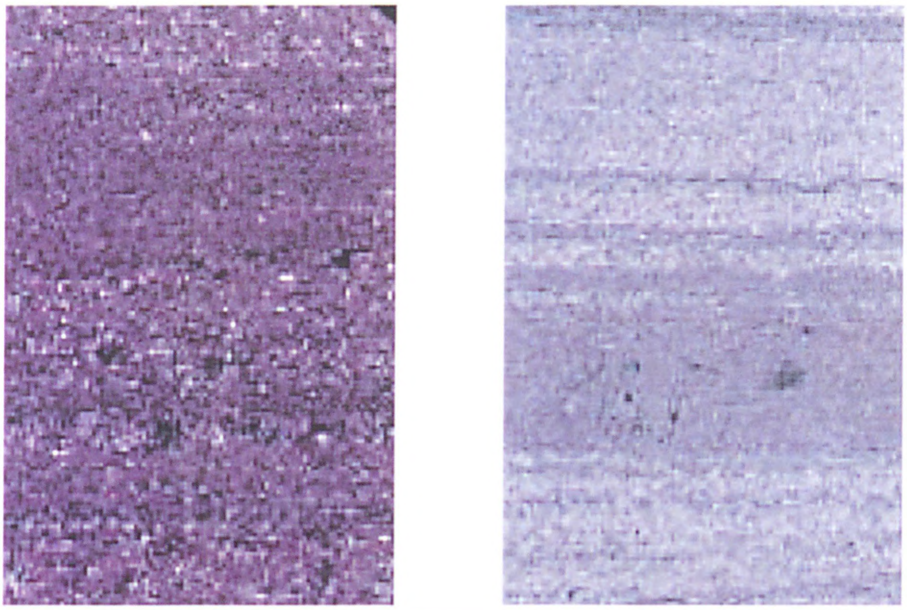

Figure (5.3) Conventional photographs for apparent heterogeneous core samples.

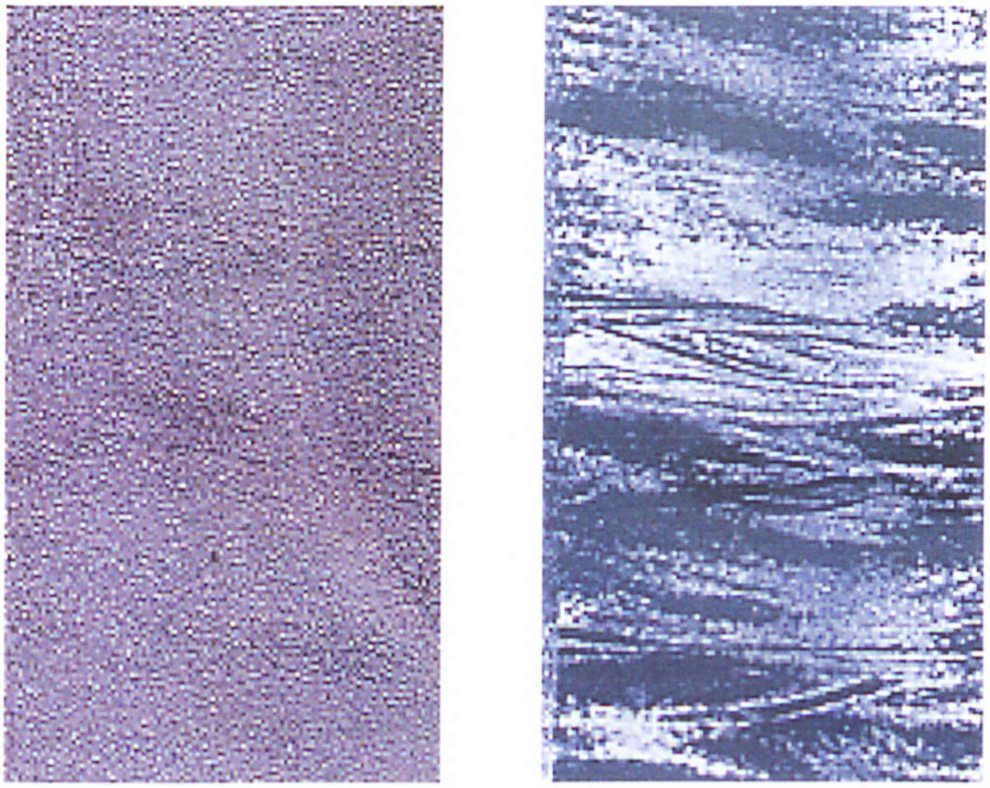

Conventional photograph showing apparently homogeneous sandstone core sample.

X-ray of the same core, revealing detailed structures and permeability barriers

Figure (5.4) Comparison between conventional photograph and x-ray scan for a non-homogeneous sandstone core sample.

Figure 5.5 shows longitudinal and transverse images of a non-homogeneous sandstone sample which was rejected at the secondary screening stage. The 2-D displayed images show significant variation in CT values, especially in the longitudinal image where scanning was carried out perpendicular to the beddings. All the different bedding layers were included in one longitudinal image and, as a result, variation in CT values was much more noticeable for this image than for the cross-sectional images.

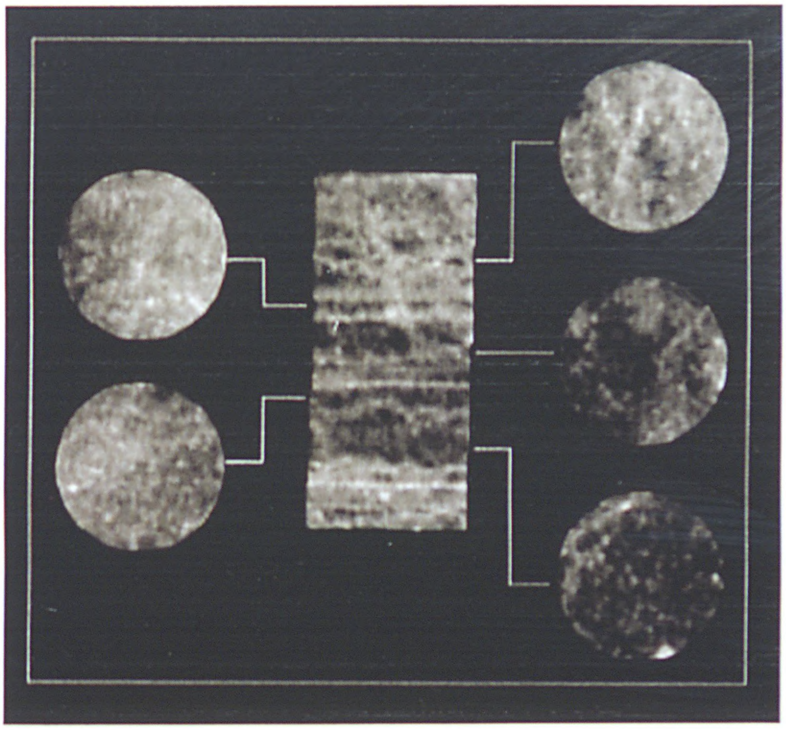

Figure (5.5) Longitudinal and some transverse CT slice images of an inhomogeneous sandstone core plug (diameter 37 mm, length 78 mm). The slice width is 3.5 mm and the in-plane resolution is 2 mm^2.

Samples showing insignificant variation at the first and second scans have been taken to the **third stage** of screening, where samples were saturated and dual scanned for sub-volume porosity measurements.

5.2.2 Heterogeneity Scaling

The CT scan technique demonstrated high precision in measuring porosity variation for $40mm^3$ sub-volumes within, and along the rock samples. Variations of less than 0.3% in porosity were easily monitored. This demonstrates that the x-ray computed tomography technique is a very powerful tool in core screening, with the ability to work efficiently within the newly introduced quantitative heterogeneity scale.

Rock sample heterogeneity has been classified based on 3-D porosity variation for a sub-volume of $40mm^3$ as follows:

1. Samples with a porosity variation less than 0.3% porosity classified as most homogeneous.
2. Samples with porosity variation from 0.3 to 1.0% porosity classified as homogeneous.
3. Any rock sample with a variation greater than 1.0% porosity classified as non-homogeneous or heterogeneous.

Figure 5.6 compares the porosity variation obtained by the CT scan in three samples that may be described as most homogeneous, homogeneous and non homogeneous. The porosity variation in the most homogeneous sample was extremely small (less than 0.3% porosity) and less than 1.0% porosity in the homogeneous sample. In the non-homogeneous sample the porosity variation was quite marked (over 15%).

A qualitative description for rock homogeneity must be always associated with a sub-volume unit, such as in the previous heterogeneity scale. Porosity variation was monitored within a unit volume of $40mm^3$. However it was found that rock homogeneity is not an absolute property and porosity variation is dependent on the reference sub-volume size. For the most homogeneous samples porosity variations can be significantly higher for smaller unit volumes.

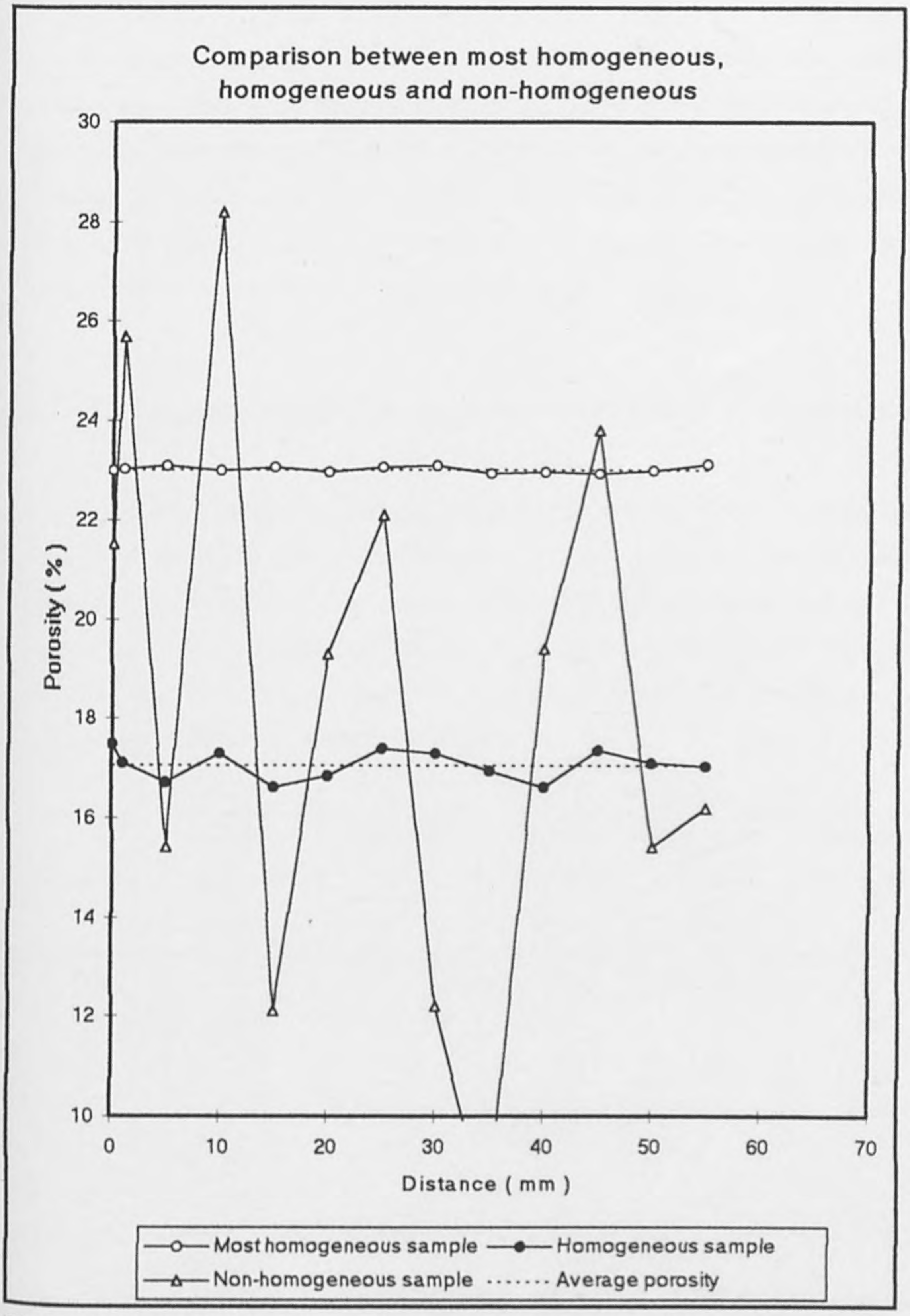

Figure (5.6) Porosity distribution along most homogeneous, homogeneous and non-homogeneous samples.

Figures 5.7 & 5.8 show 2-D CT images for most homogeneous and inhomogeneous rock samples respectively together with a porosity profile for each sample with the scale of porosity variation calculated from the foregoing calibration experiments. The resolution of these data is 2mm^2 of surface corresponding to a rock volume of 7mm^2 for the 3.5mm slice width. From Figures 5.7 and 5.8, it is obvious that porosity can vary in the most homogeneous rock samples such as Berea Sandstone as the sub-volume unit decreases. Up to ± 2% porosity variations were detected in the most homogeneous rock sample, while very wide variations were found in the inhomogeneous samples.

5.2.3 Comparison of some Homogeneous Samples with Berea Sandstone

A group of most homogeneous core plugs from UK lands classified on the previous basis have been compared to the Berea Sandstone which is widely considered as a standard on account of its homogeneity. The porosity distributions measured by the dual scan CT method as shown in Figure 5.9, porosity values for all the samples fall within the classified range of the most homogeneous samples, i.e. the maximum variation is below 0.3% porosity. Data are summarized in Table 5.1.

Sample	**Average porosity (%)**	**Minimum porosity (%)**	**Maximum porosity (%)**	**Maximum difference (%)**	**Maximum deviation (%)**
A1	17.29	17.11	17.41	0.3	0.18
A8	28.8	28.64	28.94	0.3	0.16
A10	7.28	7.19	7.43	0.24	0.15
A15	12.94	12.82	13.1	0.28	0.16
C1	18.5	18.37	18.65	0.28	0.15
B1	19.4	19.29	19.58	0.29	0.18

Table (5.1) Summary of porosity distributions displayed in Figure 5.9.

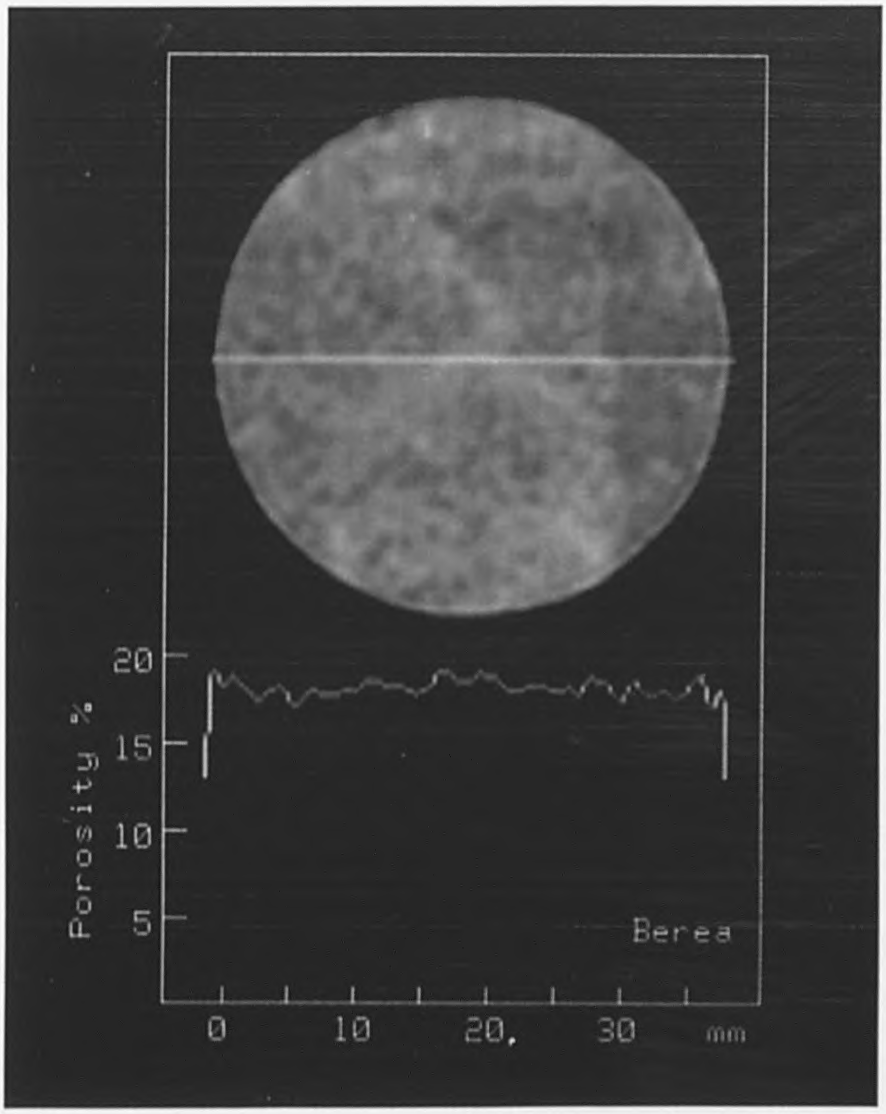

Figure (5.7) A porosity profile across one of the most homogeneous sandstone plug samples (Berea 1). Data represent sequential porosity values for volume elements (sub-volumes) of 2 mm^2 x 3.5 mm .

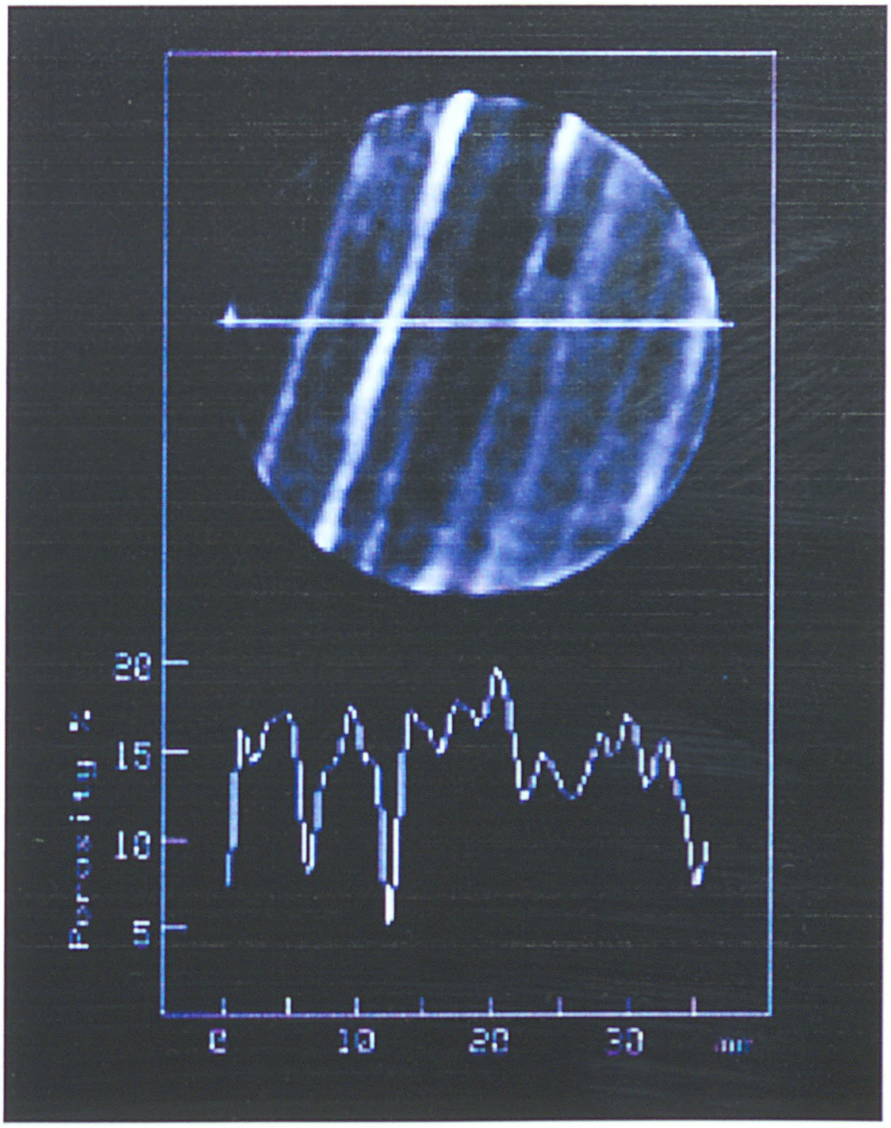

Figure (5.8) A porosity profile across an inhomogeneous (heterogeneous) sandstone plug sample. Data represent sequential porosity values for volume elements (sub-volumes) of 2 $mm^2 \times 3.5$ mm.

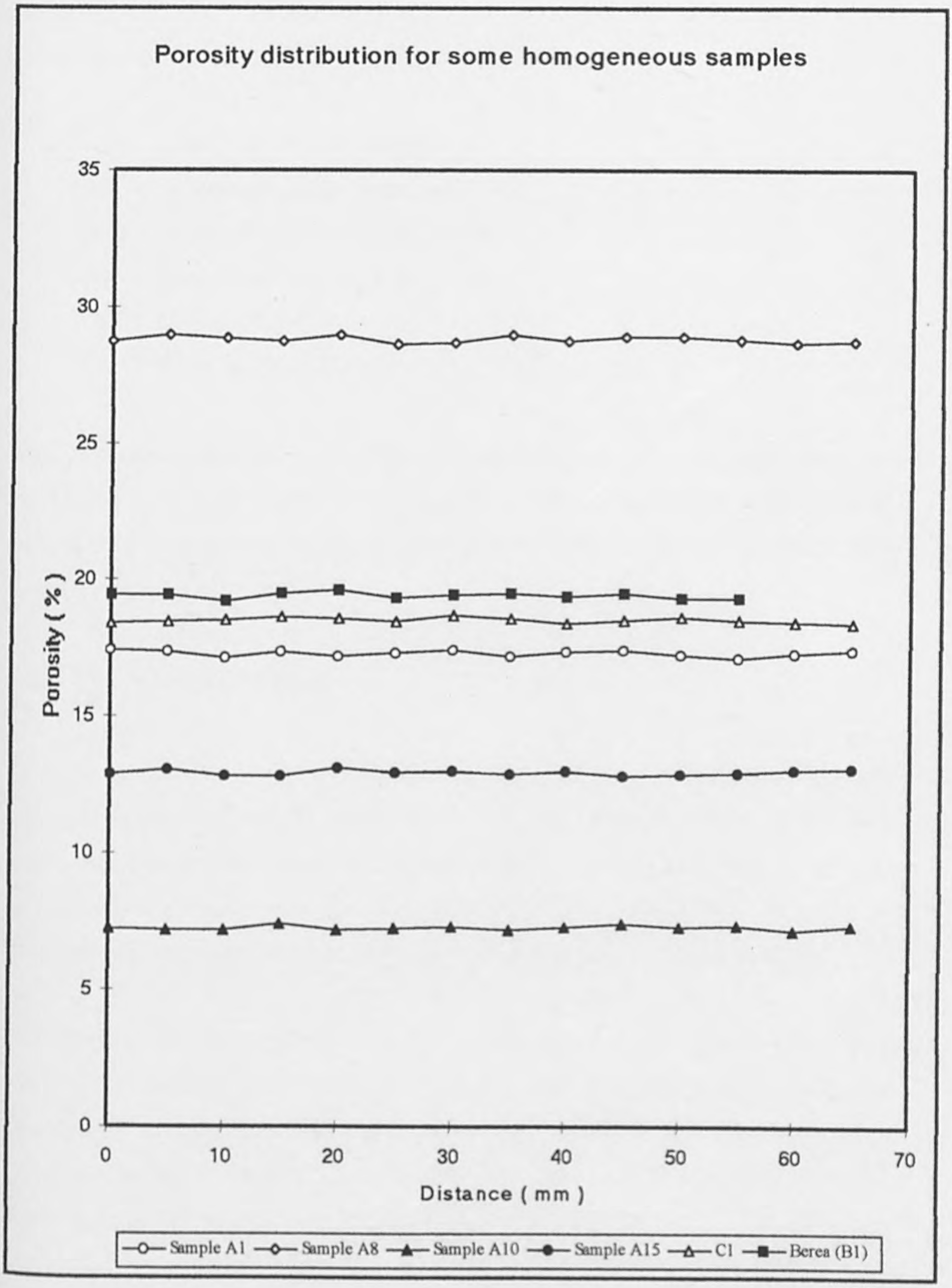

Figure (5.9) Porosity distributions for some homogeneous sandstone rock samples based on CT measurement in comparison with Berea Sandstone (B1).

As shown in Table 5.1 some samples demonstrated lower variation than the Berea Sandstone sample. The samples shown are the following:

A1	Lower Carboniferous Sandstone
A8	Sandstone from St. Bees (Bank End)
A10	Upper Carboniferous Sandstone
A15	Lower Permian Penrith Sandstone
C1	Clashach Sandstone
B1	Berea sandstone

One of the most interesting results of this study is that samples from the upper and lower carboniferous, lower Permian Penrith Sandstone and Clashach were **all found to be of comparable homogeneity to Berea Sandstone** and can be considered as standard samples with great confidence.

5.2.4 The Selected Samples

Since the rock homogeneity is a crucial assumption for the relative permeability concept, the samples selected for the study of the capillary pressure/relative permeability relationship were chosen with a great deal of attention. From data obtained by the x-ray CT scanning of a huge number of sandstone rock samples, a small number were selected showing variation of less than 0.3% porosity and classified as most homogeneous.

The selection was still restricted to **the more homogeneous core plugs** and an effort was made to identify those with the minimum porosity variation in order to verify this assumption. It is extremely important in this study to include samples with a wide range of porosity as well as permeability which made the sample screening very laborious and time consuming . Selected samples therefore range in porosity values from 13.8% to 30.9% and permeability values from less than 100md to 2500md. Average x-ray attenuation and porosity distribution for some selected samples are shown in Figures 5.10 and 5.11.

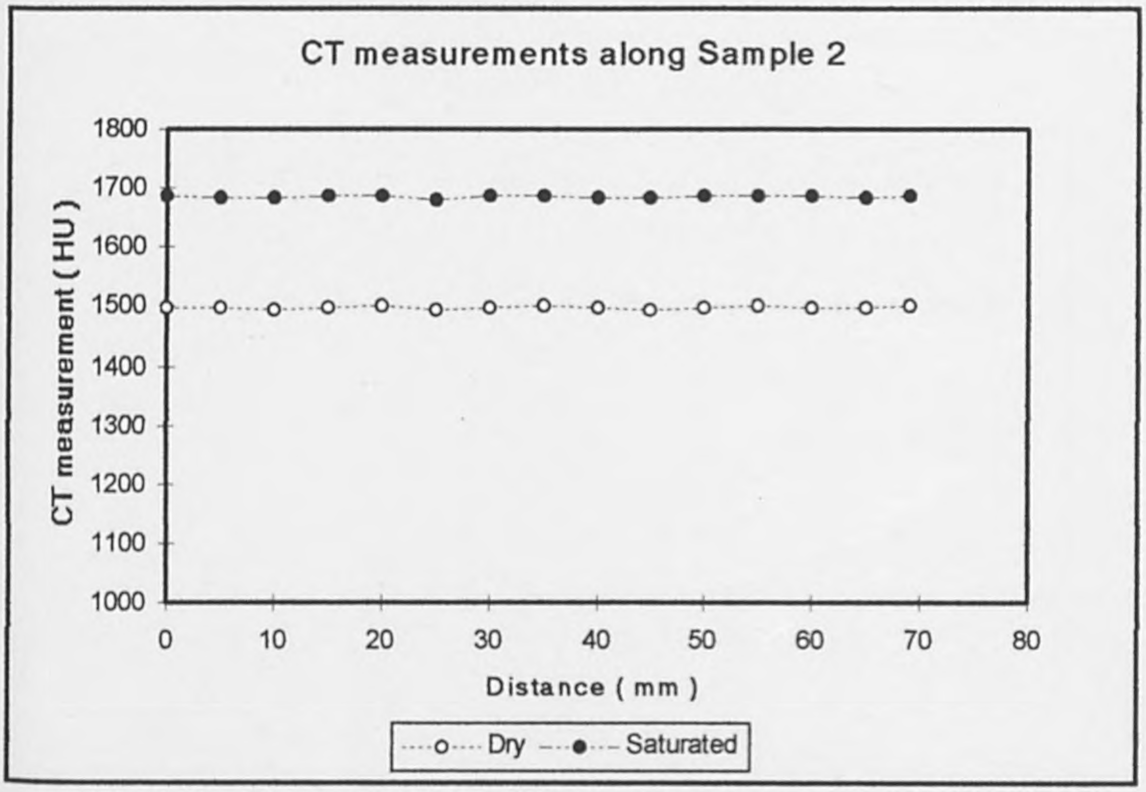

Figure (5.10a) CT measurements (HU) along sample 2 while dry and 100 % saturated with brine.

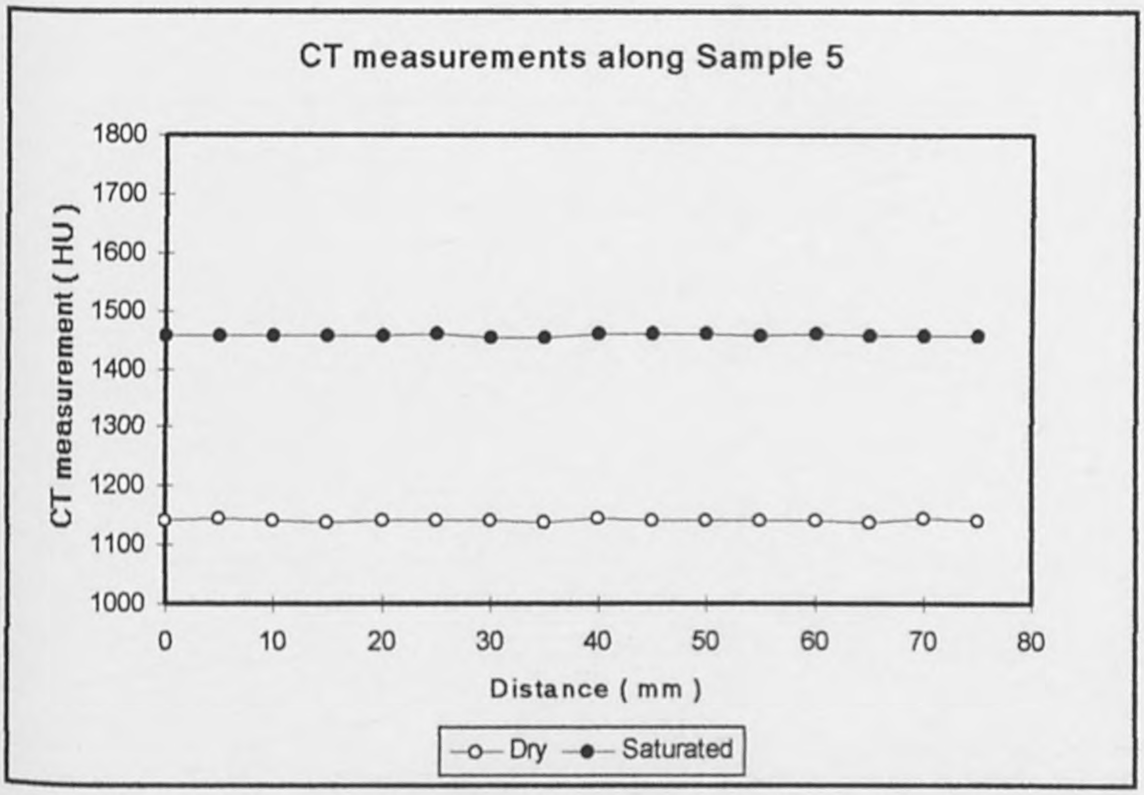

Figure (5.10b) CT measurements (HU) along sample 5 while dry and 100 % saturated with brine.

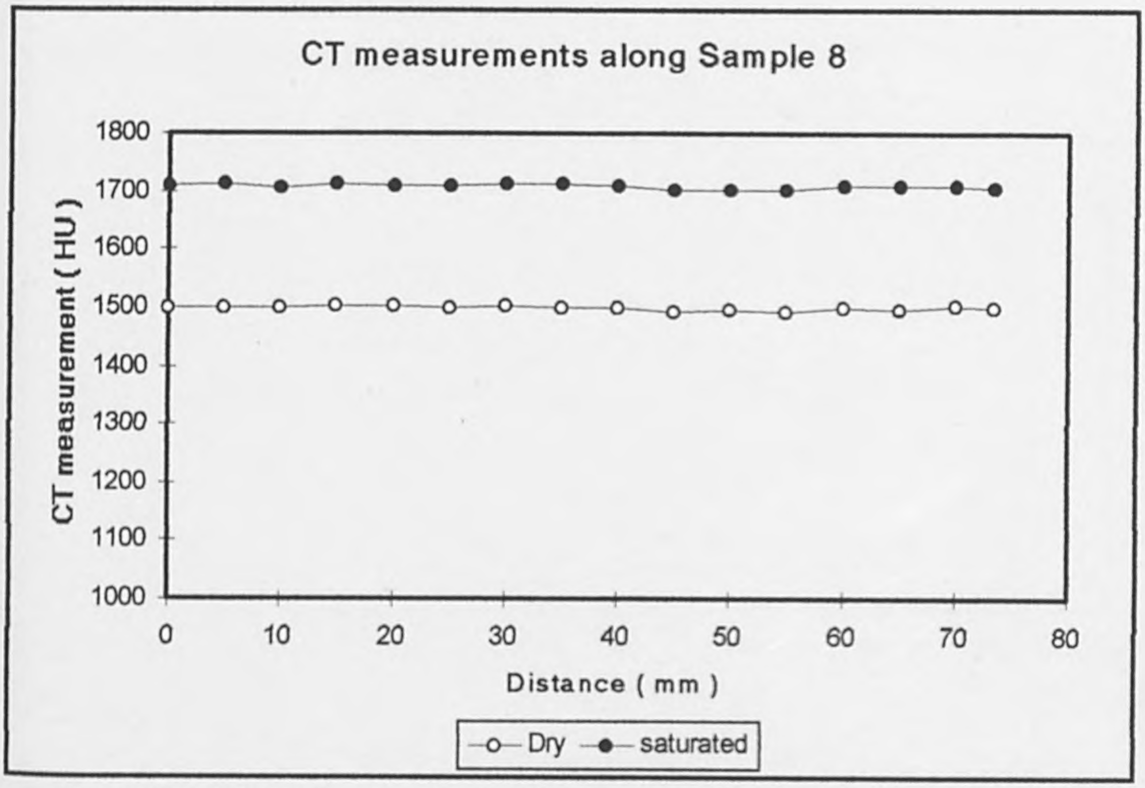

Figure (5.10c) CT measurements (HU) along sample 8 while dry and 100 % saturated with brine.

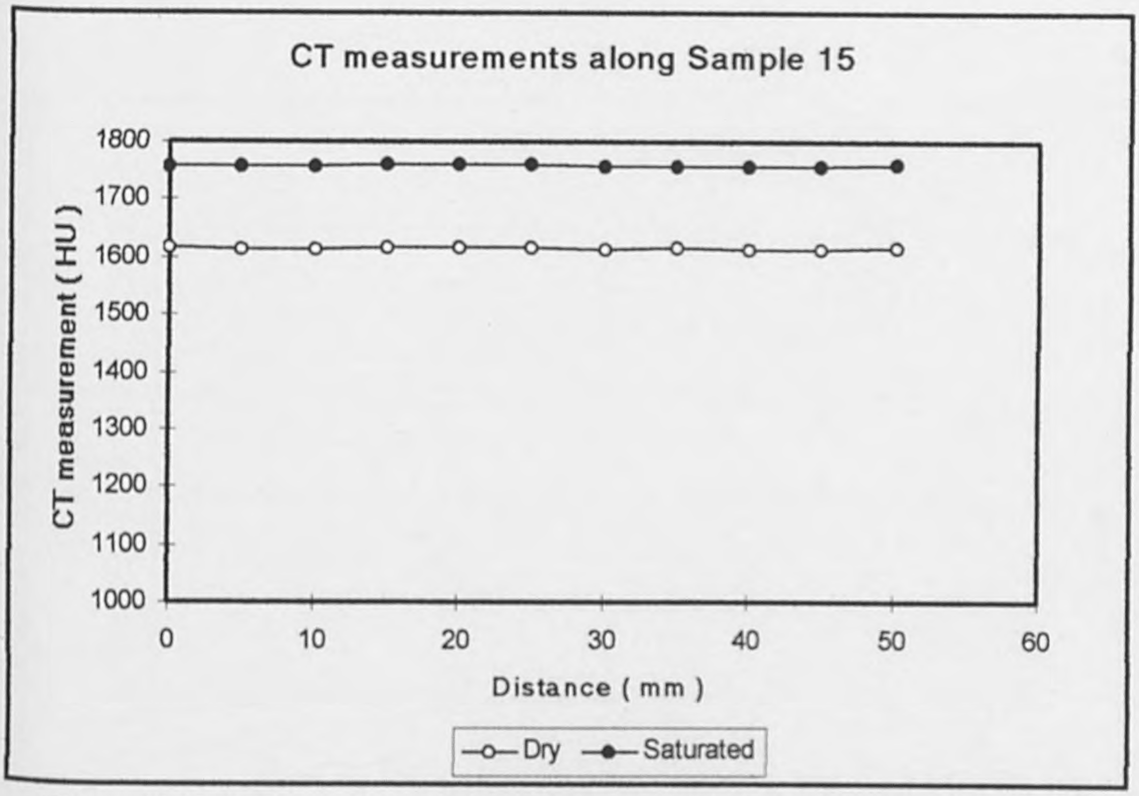

Figure (5.10d) CT measurements (HU) along sample 15 while dry and 100 % saturated with brine.

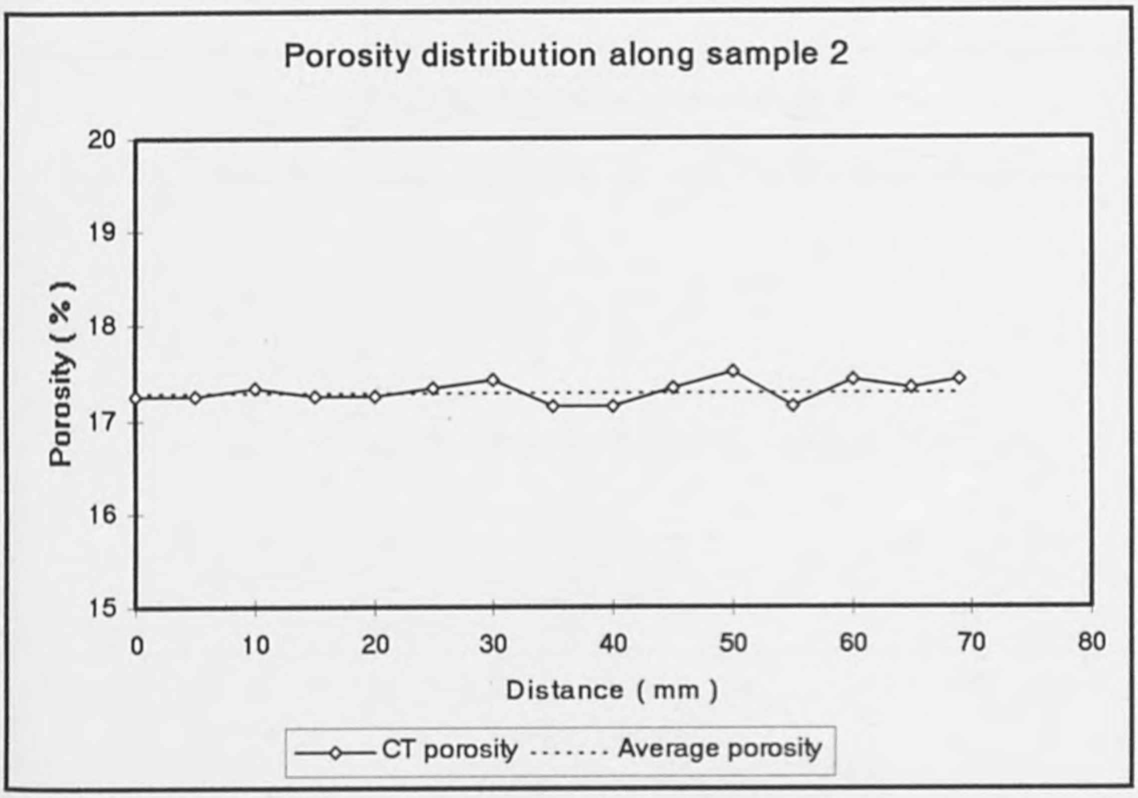

Figure (5.11a) Porosity distribution along sample 2 obtained from x-ray computed tomography dual scanning

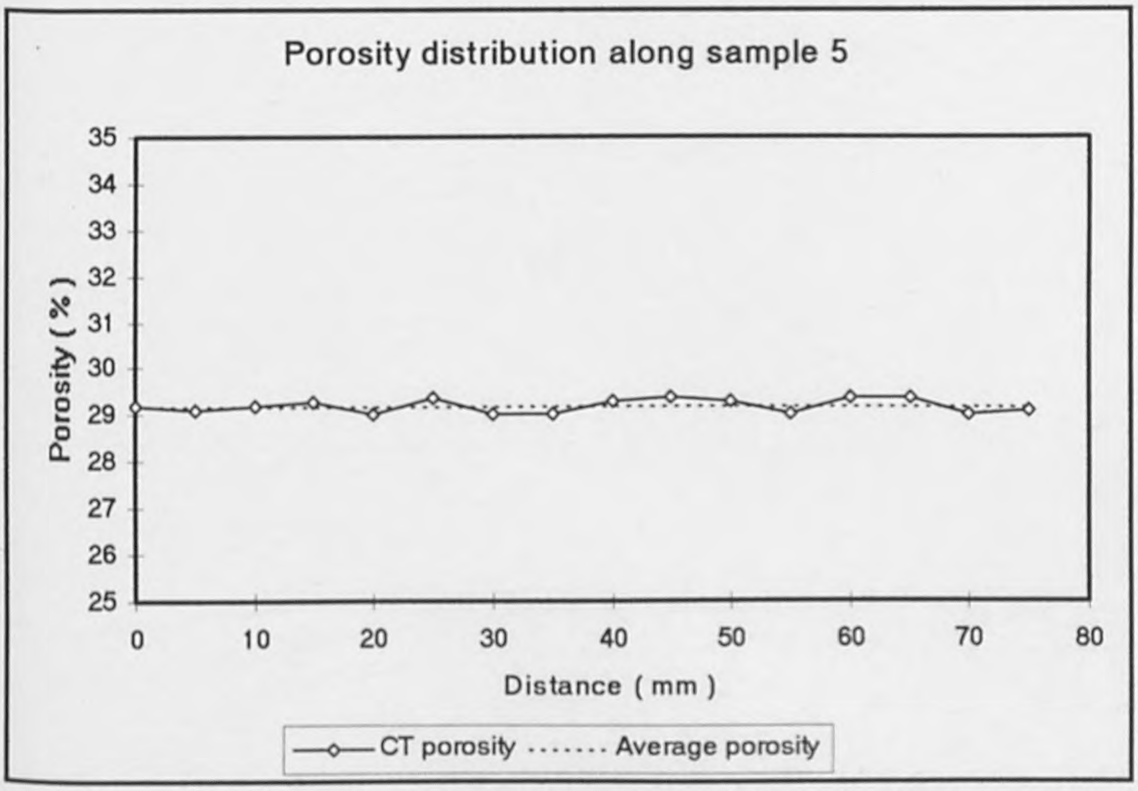

Figure (5.11b) Porosity distribution along sample 5 obtained from x-ray computed tomography dual scanning.

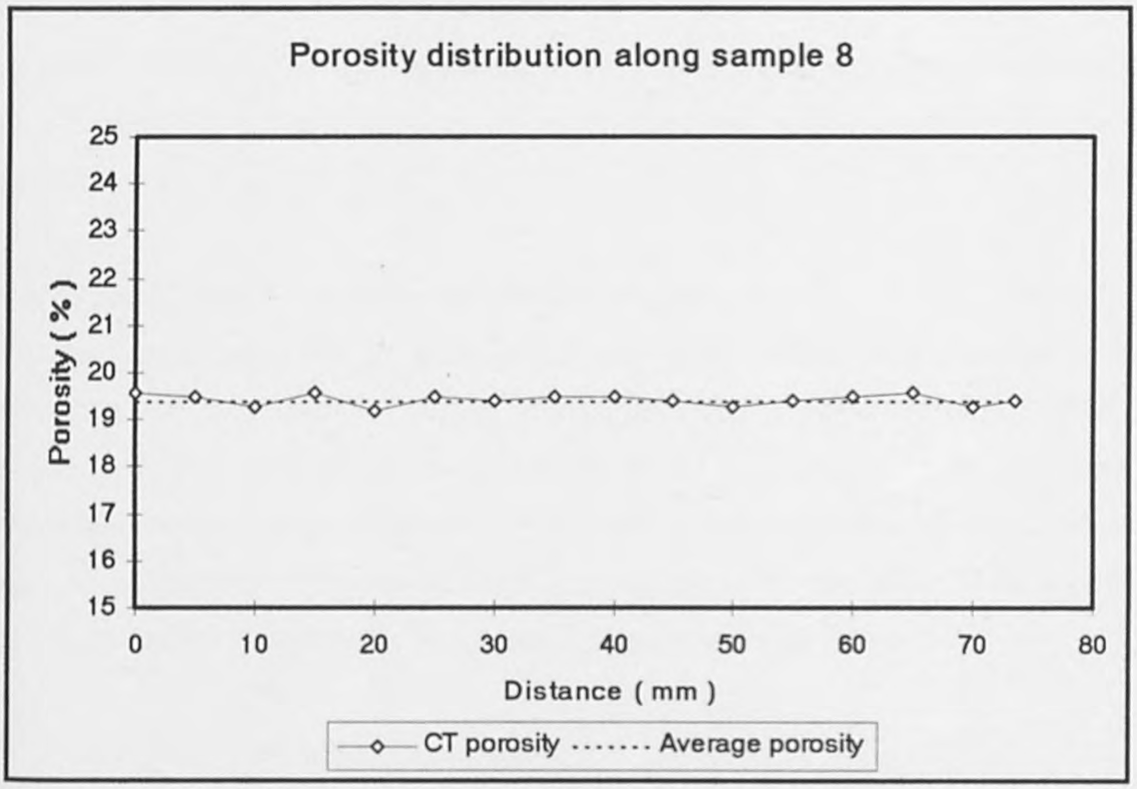

Figure (5.11c) Porosity distribution along sample 8 obtained from x-ray computed tomography dual scanning.

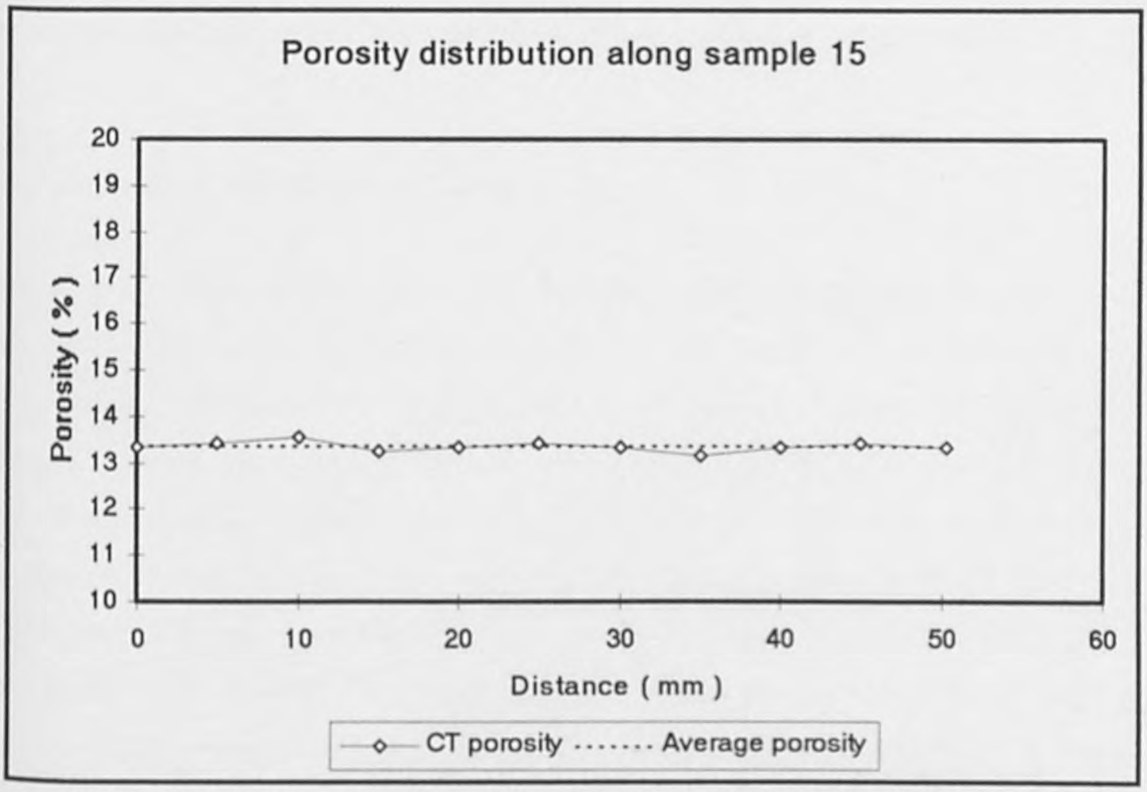

Figure (5.11d) Porosity distribution along sample 15 obtained from x-ray computed tomography dual scanning.

CT values were almost constant along all the selected samples, both, while dry and 100% saturated with brine. The consistency in CT measurements led to a negligible variation (less than 0.3%) in porosity values for longitudinal and transverse sections of these samples.

It is noticeable that CT measurements for dry sandstone vary from around 1450 HU in Sample 5 up to over 1700 HU in sample 15, and greater values were measured while saturation with brine. Samples with higher CT values have the lower porosity, due to the stopping power of rock grains which increases the x-ray attenuation as the pore space fraction decreases. As the difference in CT values increases between dry and saturated statues, the rock porosity increases and vice versa, this is directly related to the amount of saturating fluid present in the pore space. The samples are as follows;

Sample 2	Clashach Sandstone
Sample 5	Lower Carboniferous Sandstone
Sample 8	Sandstone from St. Bees (Bank end)
Sample 15	Lower Permian Penrith Sandstone

A summery of measurements for selected samples are presented in Appendix 1.

5.3 Porosity Logs of Whole Core

Based on the relationship between x-ray attenuation coefficients and porosity, developed previously, CT porosity logs have been performed for 24 and 27foot sections of poorly consolidated sandstone whole cores in fiber glass sleeving. Subsequently 26 and 30 plugs have been removed respectively from the scanned positions along the whole cores. Conventional helium porosity data was acquired from subsequent plug measurements. Figures 5.12 and 5.13 show the comparison between the single scan CT measured porosities and helium porosities for the previous whole cores. The CT data shows good agreement with the conventional measurements including small trends within the narrow porosity range. Furthermore, the CT Scan includes all the cross sections of the whole core. It measures an average porosity rather than that of the plugged area only.

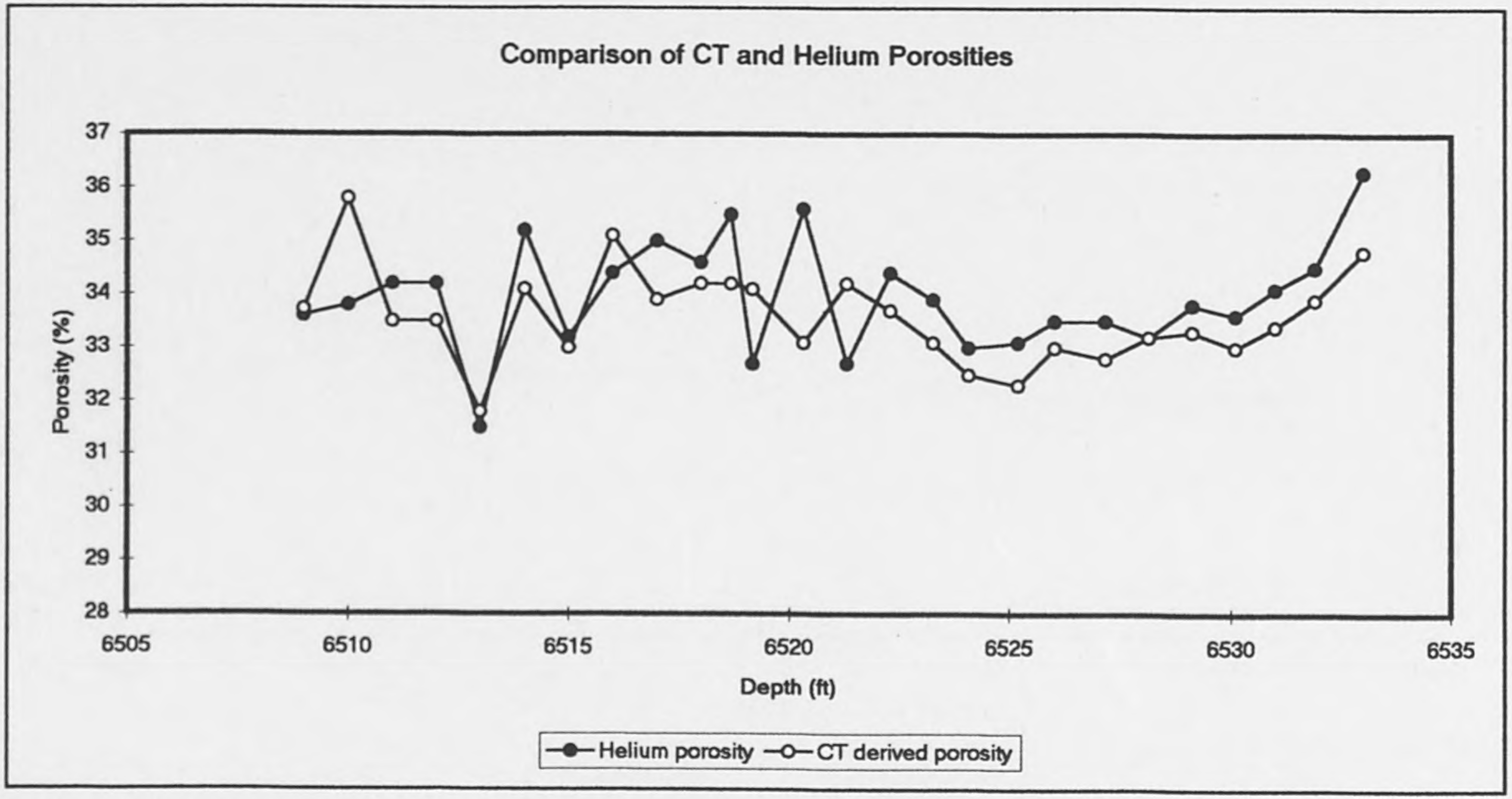

Figure (5.12) Comparison of single-scan CT and conventional helium porosity measurements on poorly consolidated sandstone whole core (length 24 ft). Helium porosity was measured on 26 core plugs extracted from the scanned zones.

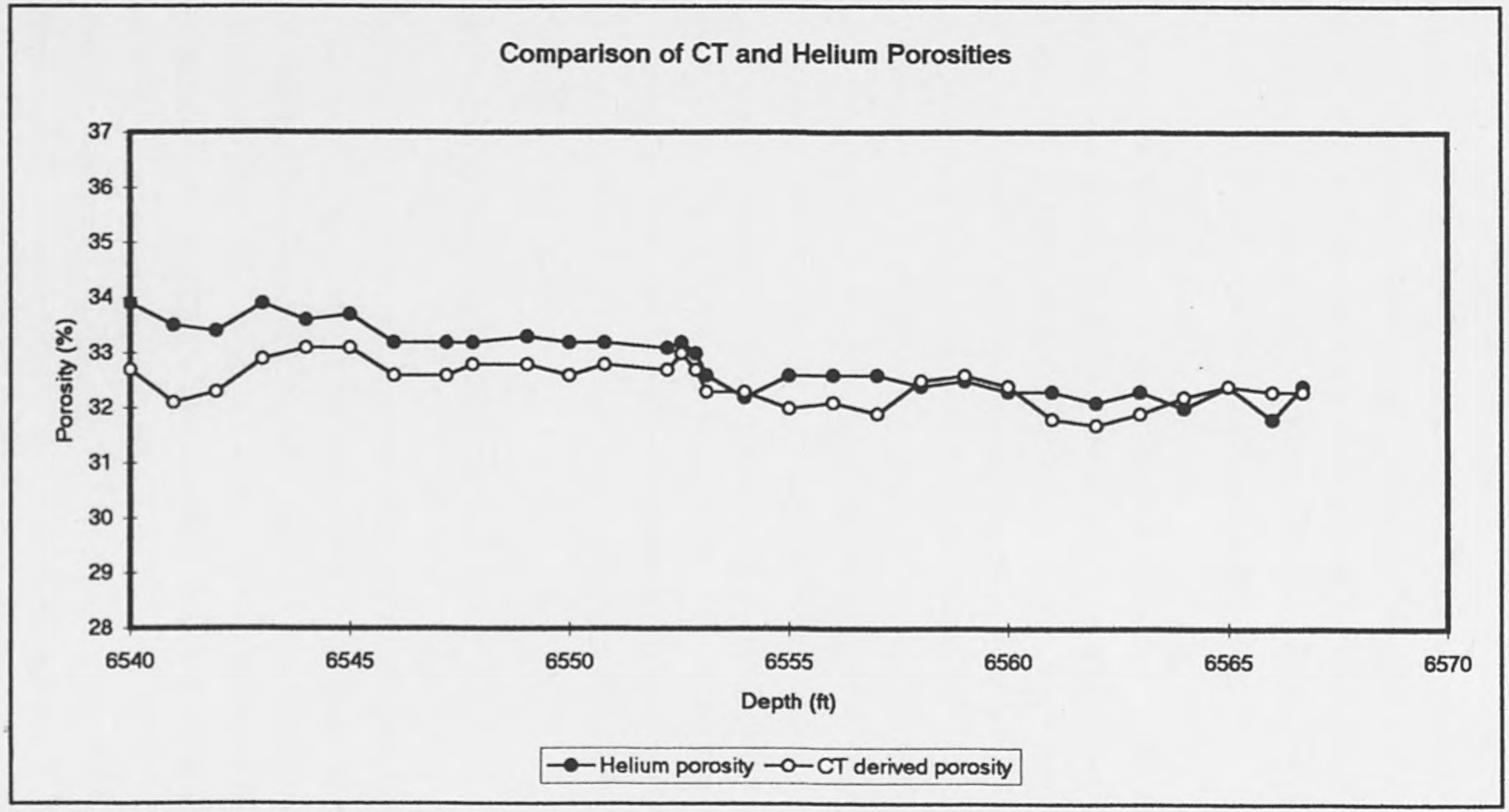

Figure (5.13) Comparison of CT and helium porosity measurements on sandstone whole core (length 27 ft). Helium porosity was measured on 30 core plugs extracted from the CT scanned zones.

It is clear in Figure 5.12, where porosity variation is significant, that in the region of depth from 6517 to 6522 ft, CT porosity values show less scater than the helium porosity measurements. It is obvious that core plugs were removed from zones with different porosity values. Conventional helium porosity values vary from 32.8 to 35.5% but the CT measurements showed some consistency at around 34% over this section. It is an outstanding example to demonstrate the advantage of including the entire cross-section of whole core using CT technique rather targeting small core plugs.

The CT measurements, apart from the speed of acquisition, have the additional advantages that measurements can be made from parts of images whilst avoiding man-made damage (such as coring or sectioning damage or mud invasion) or features revealed in the rock which would corrupt a conventional plug measurement. Figure 5.14 shows two CT transverse images taken from the same whole core of 10cm diameter, with CT values measured across both slices. In slice (a) the Hounsfield units varies from ≈1000 HU at the virgin zone in the middle of the core increasing toward the edges to ≈ 2000 HU due to mud invasion. The depth of mud invasion can be measured precisely from the screen as well as from the print out (it is 2cm in slice (a)). As a result, mud contaminated formation can be easily avoided and virgin zones which represent native reservoir formation can be targeted accurately while plugging for core analyses. Slice (b) was taken at a non invaded zone, where CT measurements were constant (≈1000 HU) through out the CT image cross section.

5.4 Construction of 3-D Images Using CT Scan Data

Some of the existing CT scanners can only produce sequential 2-D cross sectional image slices as the object is moved through the scanner and a 3-D image can only be interpreted visually from the obtained 2-D images. Figure 5.15 is a part of 3-D data set of 6inches (15.2cm) whole core showing cross sections taken at 5mm intervals along the core. All the images were displayed in order to assist in 3-D image construction. By examining these images starting from slice number 1, it can be seen that black lines and areas indicate fractures and holes respectively and the transgressing white line represents a high density mineral bed. The big fracture or hole on the left side of slice 1 is decreasing gradually at slices 2, 3 and 4 then disappears completely at slice 5. The high

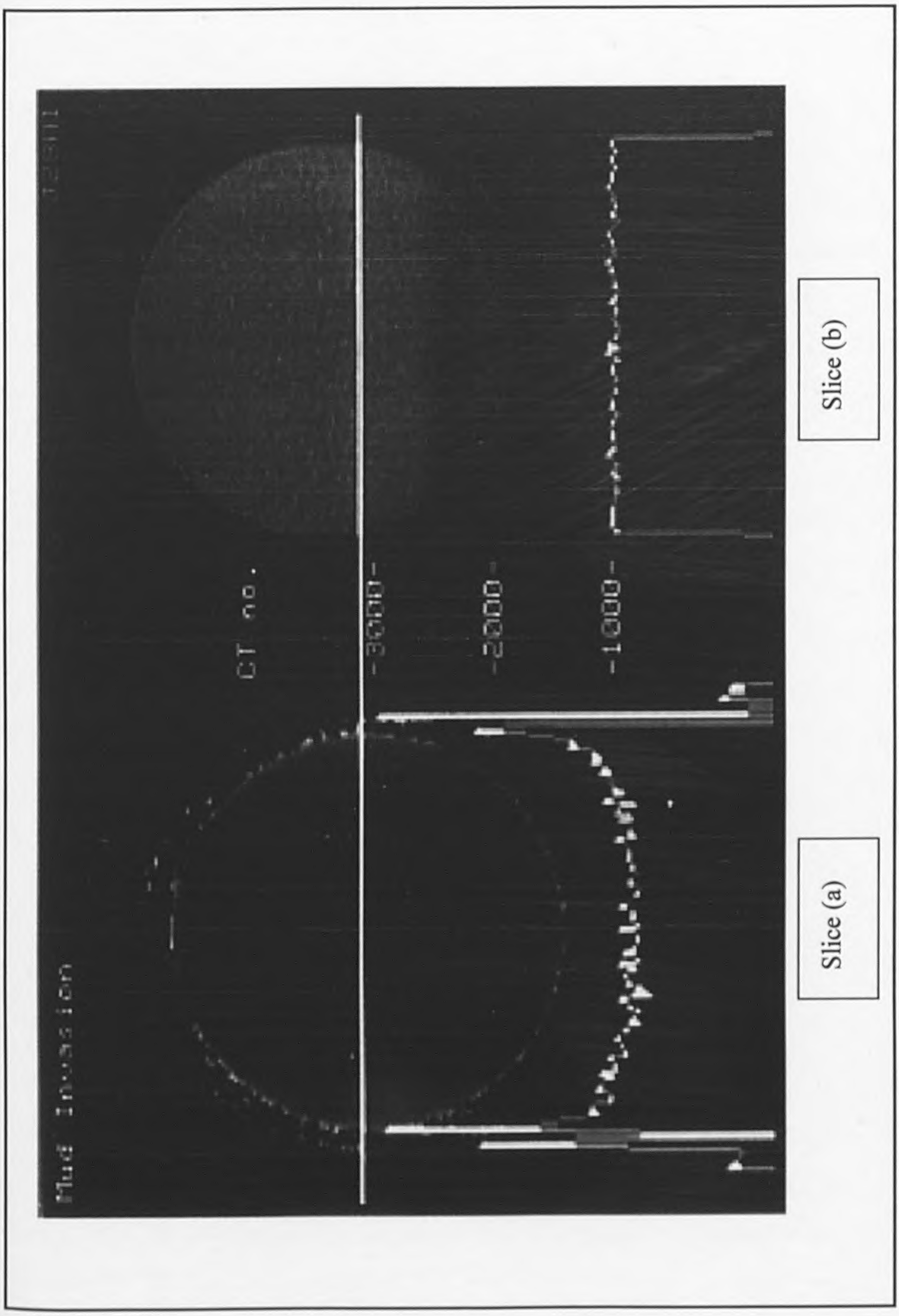

Figure (5.14) CT number profile across whole core (10 cm diameter). CT slice image (a) shows variation in CT values due to the mud invasion. Image (b) shows non-invaded zone, CT values are constant (≈ 1000 HU).

density mineral bed appeared at every slice (from slice 1 to 30) moving downward at a constant angle. The angle was measured and found to be 24 degrees.

As the distance between the scanned slices and/or slice thickness representing the Z axis is known any point co-ordinates i.e. X,Y positions can be measured precisely from the displayed image on the screen as well as on the print out. Any point can be well defined by 3-D (X,Y,Z) values and the 3-D image can be described or reconstructed manually. In the new generation of CT scanner, once the 3-D data set (the sequential CT images) has been acquired, the 3-D image can be reconstructed automatically by the computer and any plane through the object can be viewed as shown schematically in Figure 5.16.

5.5 Limitations of Using X-ray Techniques for Dynamic Displacement Experiments

X-ray techniques are being increasingly used in core analysis generally and in saturation monitoring particularly, where it is considered as the state of the art method. It was intended to use x-ray computed tomography and the 1-D x-ray technique (which is the most common technique for saturation monitoring) for relative permeability measurements carried out in this study. However, it was discovered early on that using both techniques in dynamic displacement experiments can lead to significant errors. Each technique will be discussed individually in the following sections.

5.5.1 CT Scan Deficiency

Despite the associated errors, x-ray computed tomography has been proven to be one of the most powerful tools in static core analysis. Adopting a medical scanner for dynamic displacement in core analysis however, is a serious mistake. Unsteady state relative permeability measurement requires one of the following dynamic displacement processes; (1) water displacing oil (for water/oil relative permeability data) or (2) gas displacing oil (for gas/oil relative permeability data). These are the most common displacements used.

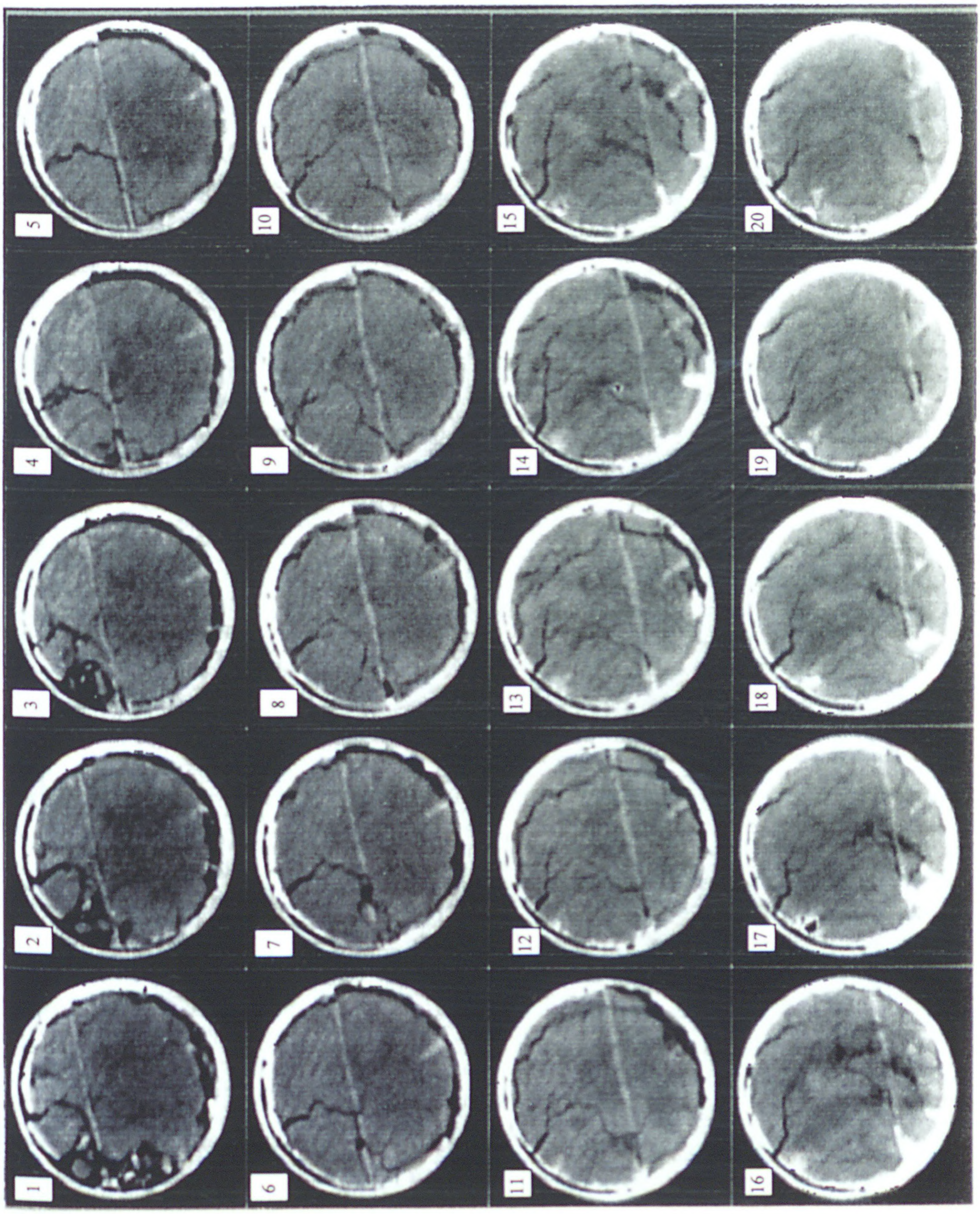

Figure (5.15) Part of 3-D CT data set for a 6" whole core sample showing cross sections at 5 mm intervals along the core. Black lines (low density) are fractures and the transgressing white line is a high density mineral bed.

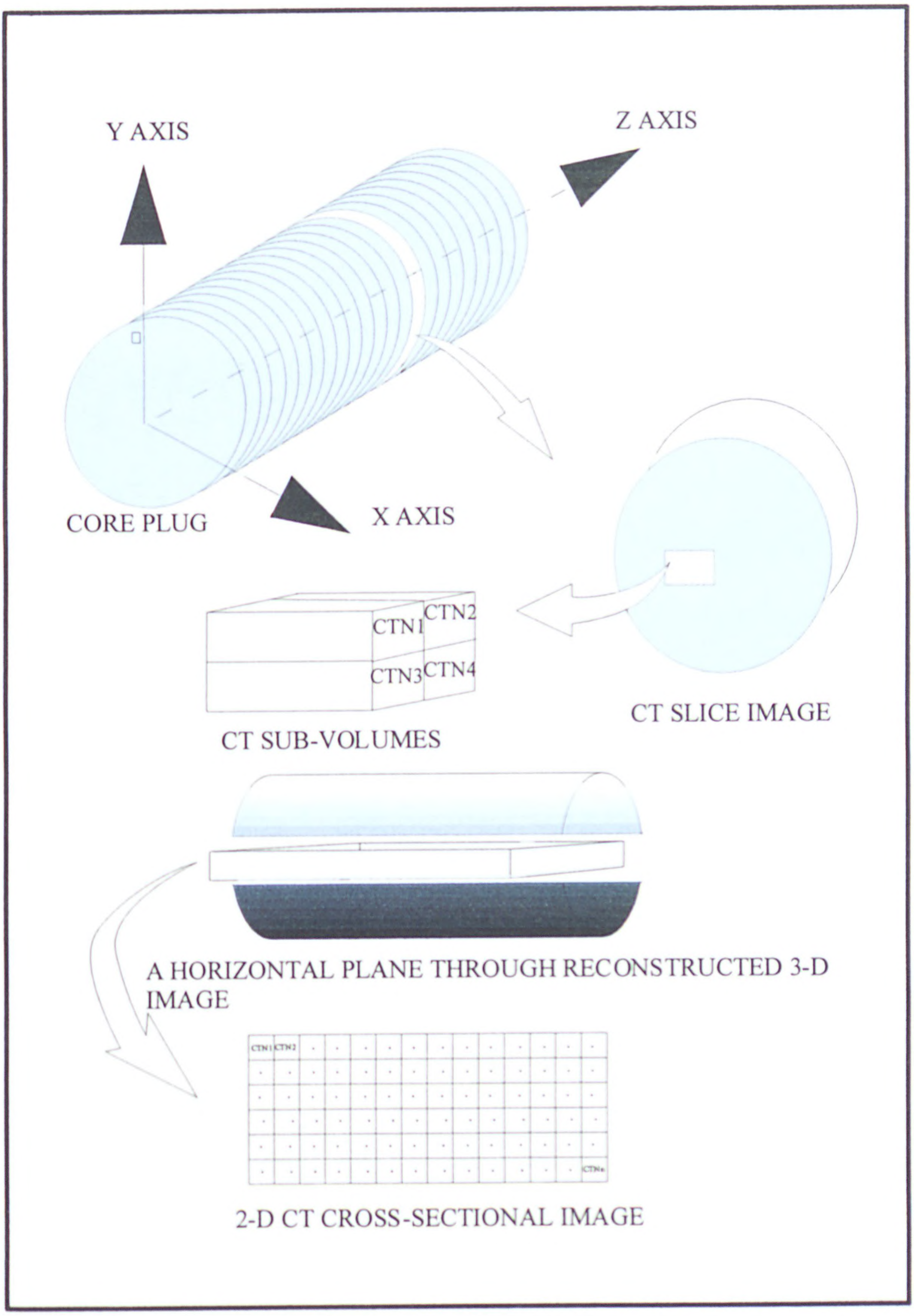

Figure (5.16) Computerized 3-D image construction using advanced CT Scanner.

The basic operation of the CT scanner is an x-ray source-detector system rotating around the scanned object to different predetermined positions, or the object rotats around a fixed x-ray system. The number of stationary positions varies from one scanner to another and from one generation to another, however, the main concept of the computed tomography is still the same. At each position the source emits x-rays at a certain intensity (I_0) and the traversing beam intensity (I) is measured by the detectors. Consequently, enormous numbers of equations are generated and solved by the computer using a back projection algorithm in order to obtain and display x-ray attenuation values as a 2-D image. To illustrate the significant error in using the available medical CT scanner for dynamic measurement, the following simplification is required;

As shown in Figure 5.17, an x-ray source/detector system is rotating around an object (sample) containing four volume elements of equal dimensions of length (L). At each position (1 and 2) x-rays of the same intensity (I_0) are emitted. Meanwhile the traversed beams intensity are measured (I_{11}, I_{12}, I_{21}, I_{22},) using the detectors, generating the following equations;

$$I_{11} = I_o\, e^{-L(\eta_{11} + \eta_{12})} \qquad (5.1)$$

$$I_{12} = I_o\, e^{-L(\eta_{21} + \eta_{22})} \qquad (5.2)$$

$$I_{21} = I_o\, e^{-L(\eta_{21} + \eta_{11})} \qquad (5.3)$$

$$I_{22} = I_o\, e^{-L(\eta_{22} + \eta_{12})} \qquad (5.4)$$

The previous equations (5.1 to 5.4) cannot be generated at single scanning position or at the same time. Equations 5.1 and 5.2 are generated as a result of measurements obtained at the first position, while Equations 5.3 and 5.4 are generated from scanning at position 2, i.e. after the x-ray system rotates to the second position. In order to calculate

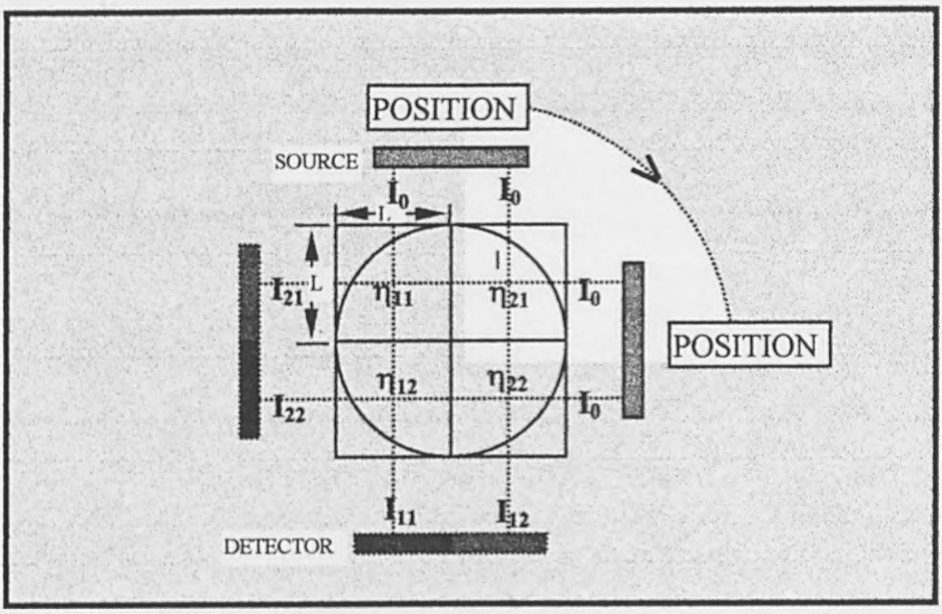

Figure (5.17) Illustration for the basic principles of how x-ray computed Tomography generates the required mathematical equations by changing the scanning position which has a significant effect on dynamic displacements.

the x-ray attenuation coefficient (η) for each volume element, it is necessary to solve the previous four equations simultaneously. Obviously, all the attenuation coefficients for every volume element (η_{11}, η_{12}, η_{21}, η_{22}) must be included in the generated equations from scanning at positions 1 and 2. For static or steady conditions they are always constant, consequently, the equations can be solved accurately.

In the dynamic or unsteady state condition, as water is displacing oil in this case, water and oil saturation values are changing as soon as the scanned slice is invaded with multiphase flow, hence, η_{11}, η_{12}, η_{21} and η_{22} will not remain constant after the scanner rotates to the following scanning position. For this reason, dynamic displacement data obtained by any ordinary medical scanner is not valid unless the displacement is carried out at an extremely low rate, which is an indisputably undesirable situation, as the fluid flow in the porous medium will then be dominated by the capillary forces. As a result of this the test is no longer representative.

The previous discussion is dealt only with the errors associated with one CT slice image (regardless of whether it is transverse or longitudinal) resulting from the time lag when the x-ray system changed from position 1 to position 2. The average saturation within the sample can be measured from one longitudinal image based on the sole assumption that fluid saturations are distributed evenly across the tested sample; this cannot be verified easily. This assumption will confine errors exclusively to the above addressed problem. To eliminate any other errors resulting from saturation variations across the core sample, it is suggested that the whole sample should be scanned, and the summation of saturation values used including all the sample slices. The necessary adaptation for the medical scanner to suite the unsteady state displacements are presented in the following section.

5.5.2 Modifying CT Scan for Dynamic Displacement

In order to eliminate errors when using the medical scanner in dynamic displacement experimentation, the following modification is essential. The x-ray source and detector system must be replicated to give the equivalent number of scanning positions (i.e. a multi x-ray source-detector system must be used). For instance, if the original scanner is required to rotate to three different positions, as in Figure 4.4, two extra x-ray source-detector systems must be added, one at each scanning position as shown in Figure 5.18

This action eliminates the necessity of rotation which creates a time lag problem when using the normal scanner. All the sources emit x-rays of known intensity at the same time, and the intensity of all the traversing beams are measured simultaneously using the multi detector system. This modification will enable the CT scanner to truly generate simultaneously the required equations for producing a complete CT slice image- i.e. "snap shot". Accordingly, the technique will allow corresponding (constant) x-ray attenuation coefficients to be solved for in the simultaneously generated equations and consequently, the significant errors described earlier in using x-ray computed tomography for unsteady state displacement experiments are removed. **Completion of this modification will allow the medical CT scanner to be used efficiently in heart imaging.**

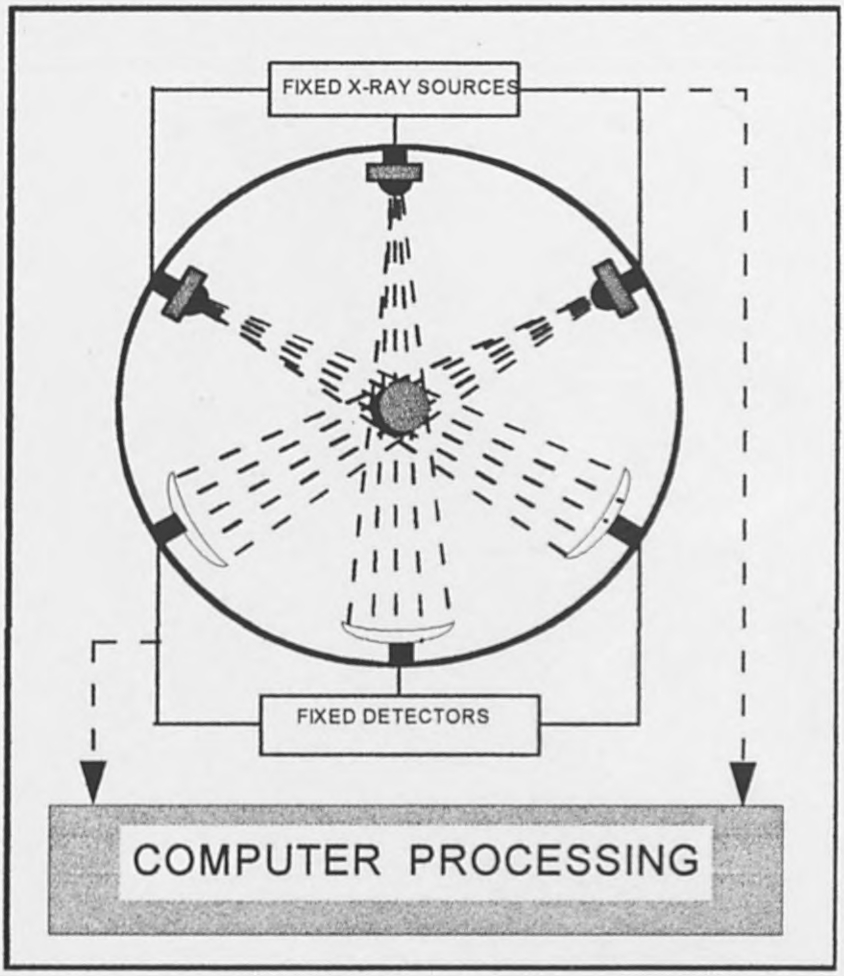

Figure (5.18) The basic principles of the multi source-detector scanner.

Furthermore, to obtain an exact average saturation, it is essential to produce sequential slice images for the whole core sample instead of using a single longitudinal image. To avoid any other time lag problem it is necessary to address the scanning of the whole sample. Conventionally whole sample scanning occurs by moving the tested sample through the multi source-detector system or moving the system along the tested sample. It can be argued that the multi source-detector system itself must be replicated to cover the tested sample completely. This will allow the scanner to be capable of producing a true 3-D image "snap shot" for the entire sample at any time step and excluding all of the previously discussed errors. The new modification, together with use of pressure transducers along the tested sample (as shown in Figure 5.19), will make the technique an excellent tool not only for accurate saturation measurements but also for micro modeling i.e. 3-D monitoring of fluid saturations distributions within the rock sample along with pressure measurements along the sample at any time step or injected pore volume.

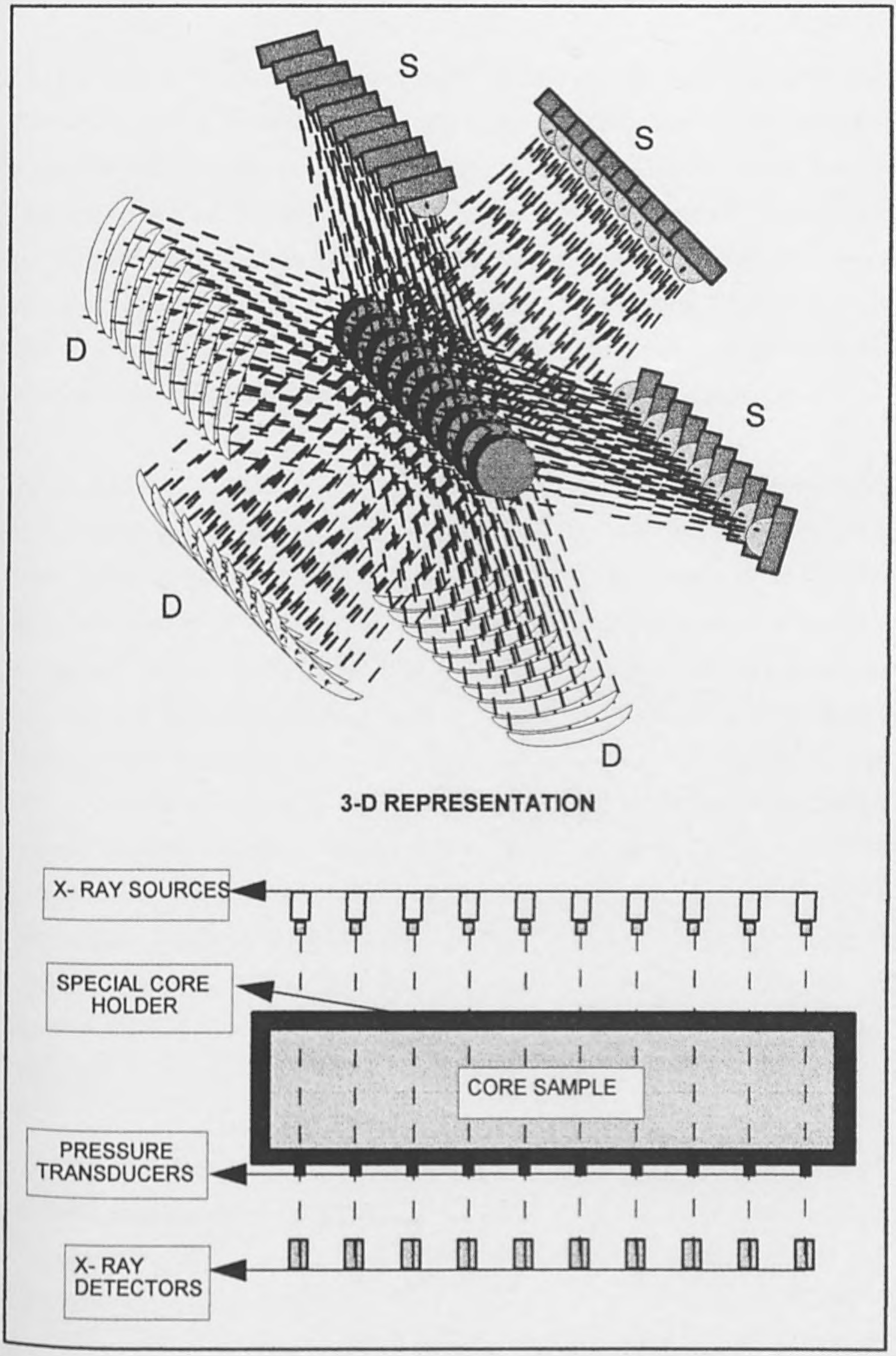

Figure (5.19) CT scan modification for micro modeling.

5.5.3 Limitation of The 1-D X-ray Technique

The 1-D x-ray technique is the most common method of using x-rays in core analysis. The basic concept of the technique is similar to that of CT scanning, the main difference is that the 1-D technique consists of a single x-ray source-detector system traveling along the sample, i.e. 1-D data can be obtained along the whole sample. The technique has many advantages in static tests, such as the measurement of irreducible oil and water saturation along the sample rather than the routine average values. This method also used for steady state displacements, which can be acceptable based on the assumption that flow paths and saturations are unchanging at stabilized flow condition.

Unfortunately, the technique is being commercially used in dynamic displacements, which mainly involve unsteady state relative permeability measurements. It should be noted that using this technique for this type of measurement leads to those identified above errors in the CT scanning method. In this case the main errors are in measuring the average fluid saturation for the whole sample. The average saturation obtained is considered as the summation of saturation measurements along the sample which is collected while the system is moving along the tested sample. One scan cycle needs some time to allow the x-ray system to complete its journey along the entire sample. In dynamic displacement, the fluids saturations are continuously changing as the x-ray system travels, especially at a high injection rates which is the most desirable and representative condition in core flooding. The measured average saturation therefore does not represent the real sample saturation and the method cannot be correct except in one hypothetical scenario where fluids are frozen until the sample scanning is completed.

The following are some core flooding examples at different scenarios to illustrate the occurrence and significance of errors in using the technique in dynamic displacements;

Tested sample length = 7cm
Diameter = 3.75cm
Scanning time = 20sec
Porosity = 10%

The extra pore volumes injected before completing the sample scanning are the main source of errors and directly related to the displacing fluid rate or velocity. Although the most common rate is 6cc/min, many tests are carried out at so-called "bump flood" rates which are around 10cc/min. As shown in Table 5.2 the errors in saturation measurement increases as the injection rate increases, the change in sample saturation goes up to 50% at bump flood rates before one scan cycle is completed. This significant change cannot be neglected.

Flow rate (cc/min)	**Extra pore volumes injected during scanning (% pore volume)**
2	10
4	20
6	30
10	50

Table 5.2 The effect of flow rate in saturation measurement using 1-D x-ray technique.

Sample porosity also has a great influence on the accuracy of the method. It can be noted that as the porosity decreases the errors increase and vice versa. To demonstrate the porosity effect, it is assumed that similar samples (with identical dimensions to the above sample), with different porosities varying from 5% to 30% have been flooded at a constant flow rate of 6cc/min. As shown in Table 5.3 the error magnitude is also directly related to the core sample porosity. The saturation measurements will therefore be distorted generally and especially at low porosity values.

The length of the tested sample will have some effect on the percentage errors in using the 1-D x-ray technique. The sample length has an effect only when the injected fluid velocity is different from the x-ray system velocity. When the injected fluid and the system travel at the same velocity, the sample length has no influence at all. If the x-ray system moves at higher velocity, the longer the sample the lower the error. If the injected fluid moves at higher velocity, the shorter the sample the lower the error.

Core sample porosity (%)	Extra pore volumes injected during scanning (% pore volume)
5	60
10	30
15	20
20	15
25	12
30	10

Table 5.3 The effect of porosity variations in saturation measurement using 1-D x-ray technique.

5.5.4 Modifying the 1-D X-ray System for Dynamic Displacement

As has been discussed in the previous section, the main errors in using the 1-D x-ray technique for dynamic displacement results from the time necessary to complete one scan cycle, in other words, the time required for the system to travel along the whole sample during scanning. To eliminate these errors requires the use of a stationary system, which completely covers the tested sample. This is can be achieved by using a multi 1-D x-ray system with units distributed evenly along the tested sample. This new modification would allow instant saturation measurements along the entire sample, thus removing the principal errors discussed earlier.

CHAPTER 6

RELATIVE PERMEABILITY/CAPILLARY PRESSURE RESULTS AND DISCUSSION

6.1 Sample Ageing

On completion of routine measurements (porosity, absolute permeability, grain density ..etc) shown in Table1 (Appendix I), the selected samples were evacuated and fully saturated using simulated formation brine. Full saturation was verified by gravimetric measurements.

The saturated samples were placed individually in a hydrostatic core holder, and 250psi (1,724kPa) net overburden pressure was applied. Each sample was primarily flushed using refined mineral oil until the effluent was free of brine, then flooded using filtered dead crude oil. The system was locked in, 2000psi (13,790kPa) pressure and 200°F (193°C) were applied. Samples were allowed 40 days for aging as an ideal method for samples to restore their original wettability which is commonly altered by sample cleaning, cutting and handling.. etc. The core material wettability preference has a great influence on relative permeability measurements, accordingly, it is very important to restore the original wettability of samples before further investigations are carried out.

6.2 Wettability of Rock Samples

Since most of the mathematical models for deriving the relative permeability from the capillary pressure data relies on the wetting and the non-wetting phase determination, it is crucial that wetting and the non-wetting phase to be identified by measuring samples wettability. Omitting the sample wettability will lead to misuse of the existing models especially in intermediate and oil wet reservoir samples. Whatsoever, the input data must be clearly identified, and the water (brine) cannot be considered as the wetting phase in every oil/water rock system without performing wettability tests, thus, using random samples with no wettability assessment will cause serious errors in intermediate and oil wet reservoir samples. For this reason the wettabilitied of the selected rock samples were measured in order to identify the wetting and the non-wetting phase. Intermediate and oil wet samples have been presented to demonstrate the importance of performing these tests; assuming that water is the wetting phase in all cases may lead to very serious errors.

After the restoration process is completed the samples were flooded by refined mineral oil to irreducible water saturation and then the wettability of each sample was measured using the Amott/USBM method[36,45,66]. The tests were carried out in four steps:

1- **Spontaneous brine imbibition.** The oil saturated samples were immersed under brine and the volume of brine imbibed freely was measured versus time. The samples were monitored until equilibrium was attained (up to 4 weeks).

2- **Brine drive**. Samples were subjected to brine drive by centrifuge where the capillary pressure curves for brine drive generated.

3- **Spontaneous oil imbibition**. The brine saturated samples were immersed under refined mineral oil and the volume of oil imbibed freely was measured versus time. The samples were monitored until equilibrium was attained (again up to 4 weeks).

4- **Oil drive**. Samples were subjected to oil drive by centrifuge where the capillary pressure curves for oil drive generated.

The generated data and results (presented in Tables 6.2 and 6.3) from the combined Amott/USBM wettability testing performed on the selected samples have been examined and can be summarized as follows;

To assess the generated data, Amott/Harvey Relative Displacement Indices (AHRDI) have been used (= Water Index - Oil Index). This combines the two Amott Indices in a single wettability index which varies from +1 for complete water-wetness, to -1 for complete oil-wetness; the system is water-wet when $+0.3 \leq \text{AHRDI} \leq +1.0$, intermediate-wet when $-0.3 < \text{AHRDI} < +0.3$, and oil-wet when $-1 \leq \text{AHRDI} \leq -0.3$. In addition, the USBM Wettability Indices were calculated from areas under oil and water drive as shown in Figure 6.1. Samples 2, 5, 8, and 15 have the following Relative Displacement Indices; 0.444, 0.624, 0.67, 0.565, -0.143 and -0.491 respectively, and the following USBM wettability Indices; 0.45, 0.64, 0.78, 0.72, -0.146, and -0.458 respectively. The data indicate that rock samples 2, 5, 8, and 15 are clearly water-wet. Sample MW1 is an intermediate-wet (with a small trend toward oil wet). Sample OW1 is clearly oil-wet. As a result, for samples 2, 5, 8, and 15 water (brine) is the wetting phase and oil is the non-wetting phase, where, in sample OW1, oil is the wetting phase and water is the non wetting phase.

On wettability data analysis, the following trends were indicated;

- The fraction of **brine spontaneously imbibed** has a higher values for water wet samples and decreases dramatically as oil wet preference increases; it increases as rock porosity increases. This can be attributed to the large size of the contained pores in high porosity core samples, where the imbibition forces can easily overcome the previously existing capillary forces. As pore sizes (porosity) decrease their capillarity increases, hence, the resistance for the invading fluid will increase and this leads to a lower percentage of imbibition.

- The fraction of **oil spontaneously imbibed** increases as oil wet preference increases and decreases significantly as water wet preference increases.

- The ratio of area under oil drive to the area under water drive increases as water wet preference increases (> 1), and decreases as oil wet preference increases. For intermediate wet samples, area under oil drive is equal or very close to area under water drive i.e. the ratio is around 1.

- Good agreement between Amott/Harvey Relative Displacement and USBM wettability Indices is seen throughout all the tested samples.

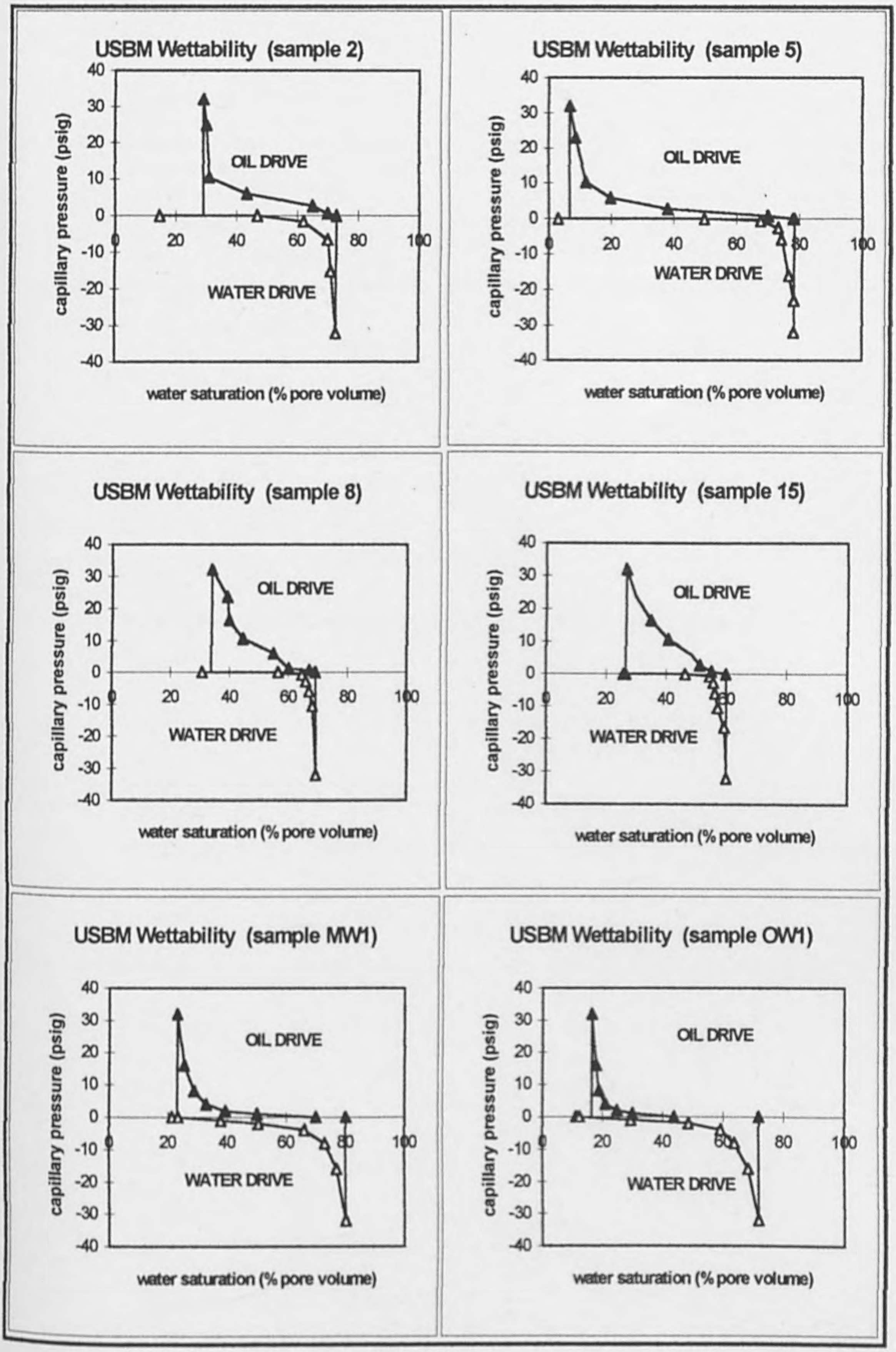
USBM Wettability (sample 2)

USBM Wettability (sample 5)

USBM Wettability (sample 8)

USBM Wettability (sample 15)

USBM Wettability (sample MW1)

USBM Wettability (sample OW1)

Figure (6.1) Water and oil drive for wettability measurements.

Sample	Brine imbibed spontaneously (% pore volume)	Oil displaced (% pore volume)	Oil imbibed spontaneously (% pore volume)	Water displaced (% pore volume)	(Area under oil drive) / (area under water drive)
2	32.4	40.5	traces	43.7	2.8
5	49.6	29.38	0.1	96.0	4.4
8	25.78	12.58	0.06	38.57	6.04
15	20.47	15.74	0.01	35.25	5.3
MW1	2.1	56.8	10.3	47	0.714
OW1	1.2	59.5	28.3	27.2	0.348

Table 6.1 The combined Amott/USBM wettability experimental data.

Sample	Amott water wettability index	Amott oil wettability index	Amott/Harvey relative displacement index	USBM wettability index
2	0.444	0.0	0.444	0.45
5	0.628	0.004	0.624	0.64
8	0.672	0.0016	0.67	0.78
15	0.565	0.0003	0.565	0.72
MW1	0.036	0.179	-0.143	-0.146
OW1	0.018	0.509	-0.491	-0.458

Table 6.2 The combined Amott/USBM results summary.

6.3 The Experimental Relative Permeability Data

The experimental relative permeability data was measured using both the unsteady state and steady state techniques. Both drainage and imbibition relative permeabilities were carried out at a high flow rate (6cc/min) to create a large pressure gradient in order to eliminate the capillary end effect[79,183] which can distort the experimental measurements. All relative permeability data were calculated using two reference values; (1) K= water permeability at 100% saturation, (2) K= oil permeability at S_{wi}.

6.3.1 The Unsteady State Relative Permeability Data

The relative permeability measurement by the unsteady state method does not attain the saturation equilibrium; thus it is the quickest laboratory method. Only few hours are required to complete the displacement process, and the long time required is due the sample preparation which takes more than one week. While flow rate is maintained constant, the pressure drop and effluent (oil and water) volumes are continuously monitored from the time of the displacing phase breakthrough to the end of the test, then the Johnson-Bosseler-Numan method is used to calculate the relative permeability data.

Using a low viscosity oil in measuring the relative permeability of core samples by the unsteady state technique led to a favorable mobility ratio which caused a piston like or nearly piston like displacement. In piston like displacement water (brine) displaces 100% of the movable oil at a square shock front, where only one phase can be produced at the out flow boundary during the entire displacement process, i.e. no water can be produced at the out flow boundary before the movable oil is totally recovered. The relative permeability calculations using this method require simultaneous production of oil and water at the out flow end. This made it impossible to obtain any relative permeability data apart from the two end point relative permeabilities (oil relative permeability at irreducible water saturation and water relative permeability at irreducible oil saturation).

Since full curves of experimental relative permeability data are definitely required in this project for comparison against data obtained by mathematical models, it is essential to induce simultaneous flow of water and oil at the out flow end as long as possible. Therefore the piston like displacement was disturbed by using a very viscous oil (μ_o= 20cp). Using a high viscosity oil created a reasonable amount of relative permeability data, but, it is still impossible to obtain a full curve using the ordinary unsteady steady state method, **and any full relative permeability curve obtained using this technique (as commonly done) relies on questionable extrapolation**. This is attributed to the mechanism of these tests which can be explained as follows;

Generally, unsteady state tests start while the sample is oil saturated, then water is injected to displace oil. A significant amount of water is required before any water is recovered (oil/water simultaneous flow) at the outlet end; for this reason, no multi phase flow can occur before the displacing phase breakthrough, and it is impossible to collect any data to calculate the relative permeability at low water saturations falling between S_{wi} and water saturation at breakthrough. To obtain full relative permeability curves using the unsteady state method, the following technique has been attempted; on completion of the commonly used displacement (water displacing oil) the oil is re injected to displace the water. This gives simultaneous production of oil and water at low water saturations, as a result, relative permeabilities can be calculated for water saturations as low as S_{wi}. The experimental data using both types of displacement were compiled and presented in Figures 6.2-6.9.

For water wet samples, data obtained during the first displacement cycle is known as imbibition relative permeability, where the wetting phase (water or brine) is displacing the non-wetting phase (oil), i.e. the wetting phase saturation is increasing. The data obtained by the reversed displacement cycle is known as drainage relative permeability, where the wetting phase is displaced by the non-wetting phase (the non-wetting phase saturation is increasing).

In oil reservoirs, water is always the displacing phase, therefore, the water/oil relative permeability is the most representative data and using the reversed displacement just a reasonable attempt to obtain some questionable data for a range of water saturations that cannot be covered using the conventional unsteady state tests. Combining the drainage and the imbibition relative permeability data for the selected samples covers the important range of water saturations which varies from irreducible water saturation to (1- irreducible oil saturation). Water saturation below S_{wi} and above $(1-S_{or})$ will never be encountered in any oil reservoir and can only be obtained in the core laboratories.

Some samples such as sample 2 and sample 5 demonstrated unusual k_o at S_{wi} which is higher than the sample's absolute permeability using a high viscosity oil, this leads to k_{ro} at S_{wi} values greater than 1.0. This is incompatible with the commonly known range of relative permeability values $(k_{ro} + k_{rw} <)1.0$. One author[18] reported similar results for high viscosity oil, and he explained the increase in the oil permeability at S_{wi} as a result of the interstitial water saturation working as a lubricant, which decreases the amount of the pressure drop and increases the oil permeability. Oil permeability at S_{wi} was measured for samples 2 and 5 using low viscosity oil of 2cp rather than using the 20cp oil, but normal results were obtained.

6.3.2 The Steady State Relative Permeability Data

In steady state technique water and oil are injected simultaneously at constant rates until saturation equilibrium is attained i.e. the test is extended at the same injection rates until the pressure drop across the tested samples becomes constant. This may require several hours or days at each saturation point. On equilibrium achievement, the rates, the pressure drop and fluid saturations are measured, then Darcy's law is applied directly to calculate oil and water effective permeabilities.

Although the steady state method is time consuming and may require several weeks to produce a complete relative permeability curve for any rock sample, its main advantage is that it produces the most reliable data and a full curve can be obtained at any oil/water viscosity ratio especially at low values where this is impossible using the unsteady state method. For water wet samples, tests are conventionally termed 'drainage'. if the injected oil percent is increasing and 'imbibition' when this is decreasing i.e. (the water percent is increasing). Both drainage and imbibition relative permeabilities have been measured for all selected samples and are presented in Figures 6.10 - 6.17.

The drainage and imbibition steady state relative permeabilities were obtained for all the selected samples over the complete range of water saturations. Figures 6.10 - 6.17 show very good agreement between the data obtained by drainage and by imbibition flooding. The agreement between the drainage and the imbibition relative permeabilities using the steady state technique proves that there is no fundamental difference between these tests and that the relative permeability at any saturation value is constant regardless of whether the saturation value is attained in increasing or decreasing fashion. For instance, 40% water saturation for any sample can be attained either by increasing the injected water fraction gradually (decreasing the oil percent) in case of imbibition or by the gradual increase of the injected oil fraction (increasing the oil percent) in case of drainage. The relative permeabilities of oil and of water at this saturation are not influenced by the direction of the saturation change.

This experimental data was obtained for comparison with the calculated relative permeability data obtained from the capillary pressure measurements. The steady state data were considered more reliable than unsteady state, for reasons which will be discussed later in this chapter

6.4 Generation of Capillary Pressure Curves

Capillary pressure measurements are essential in using the mathematical models for relative permeability predictions. The capillary pressure curves (plots of capillary pressure vs saturation) for the selected water wet samples were generated using the three common well-established methods which are porous plate (porous diaphragm), centrifuge and mercury injection.

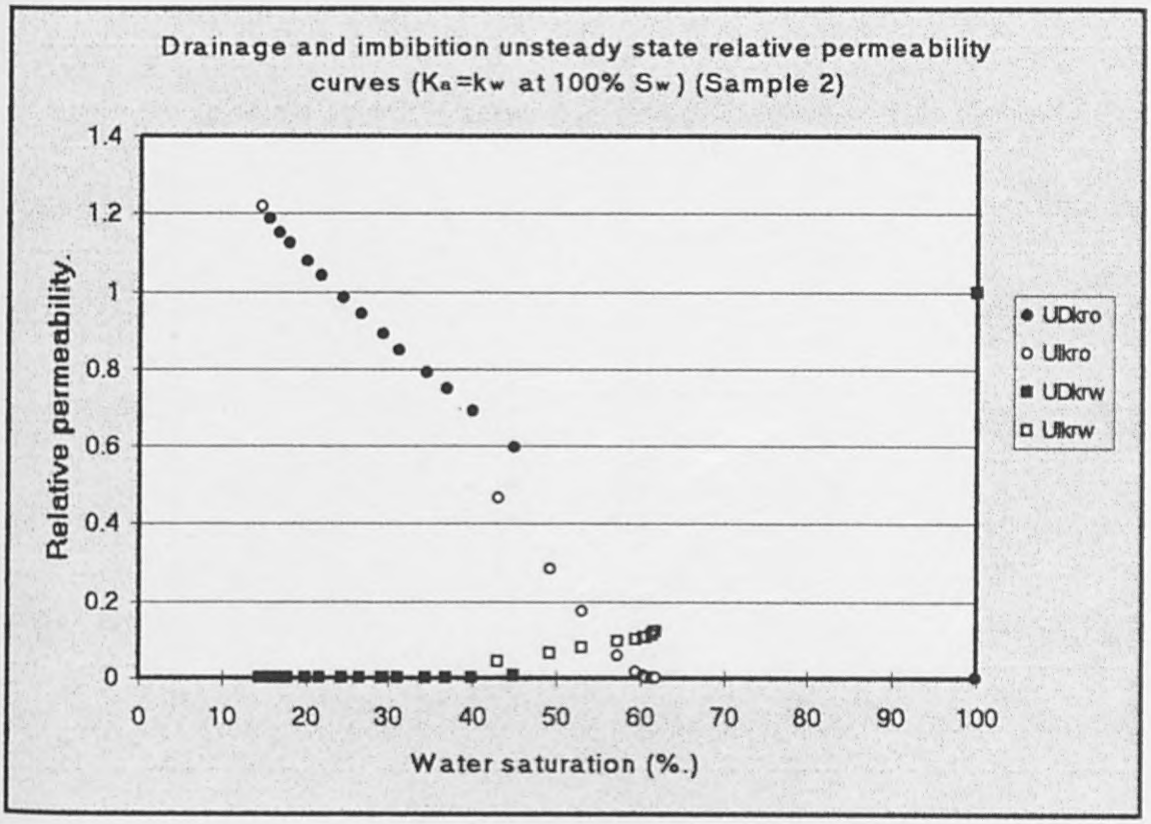

Figure (6.2) Unsteady state relative permeability data for Sample 2 ($K_a = k_w$ at 100% S_w).

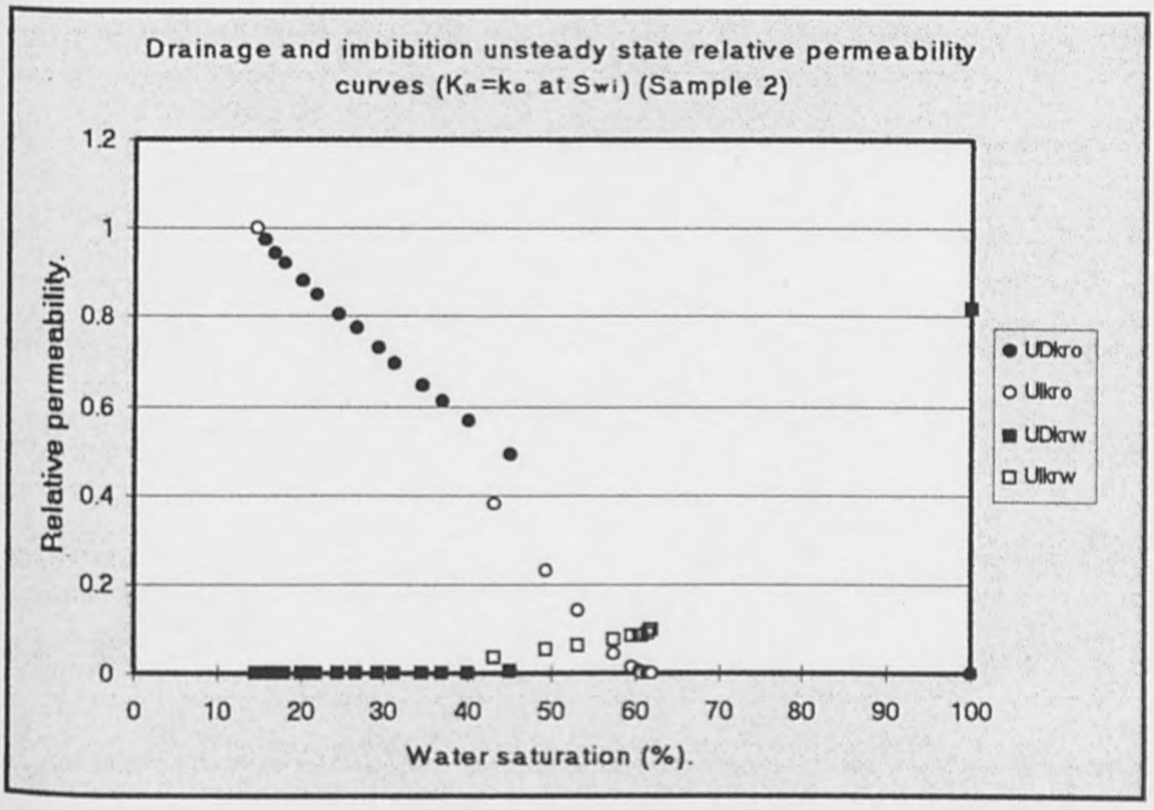

Figure (6.3) Unsteady state relative permeability data for Sample 2 ($k_a = k_o$ at S_{wi}).

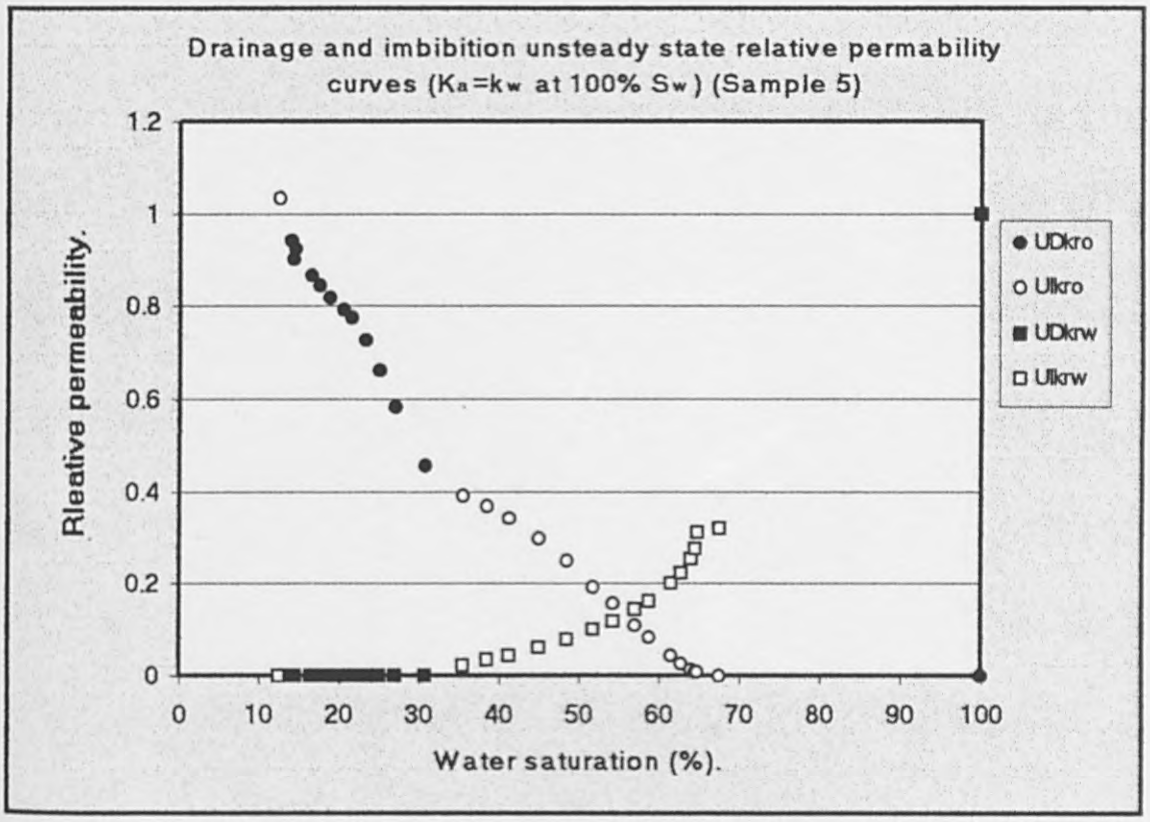

Figure (6.4) Unsteady state relative permeability data for Sample 5 ($K_a = k_w$ at 100% S_w).

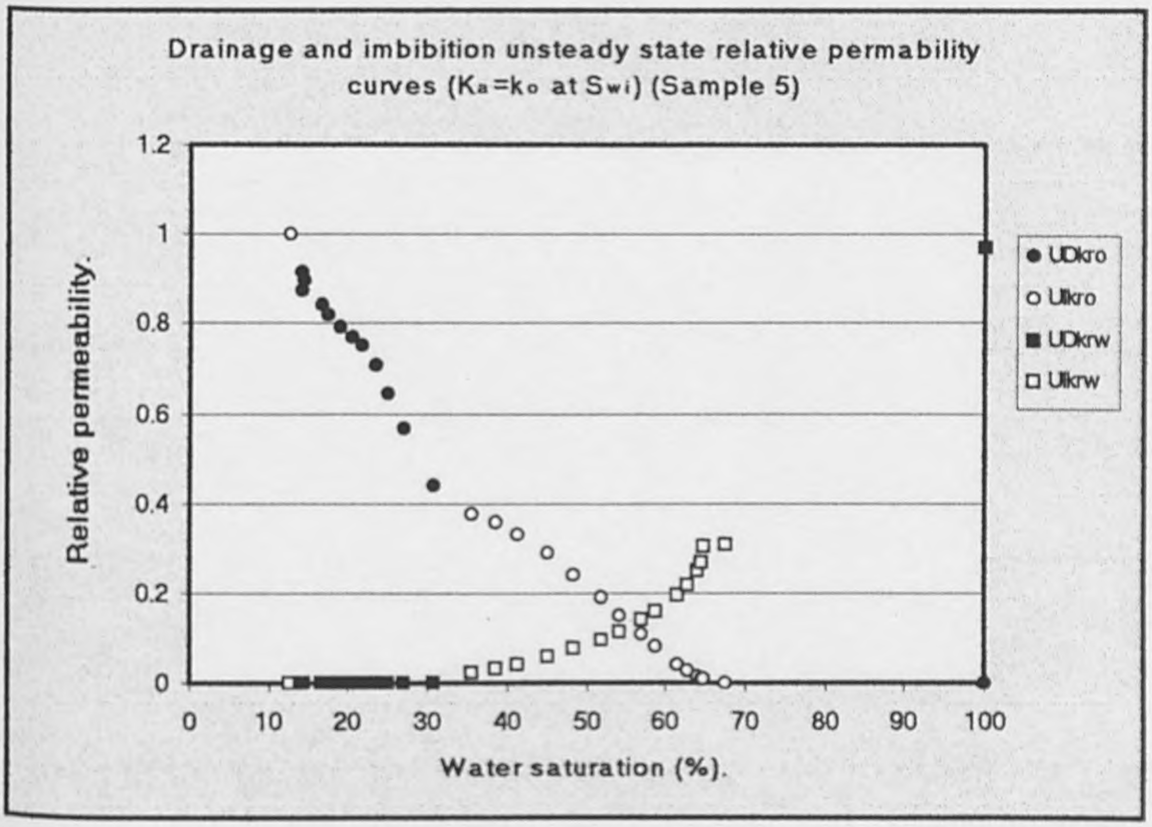

Figure (6.5) Unsteady state relative permeability data for Sample 5 ($k_a = k_o$ at S_{wi}).

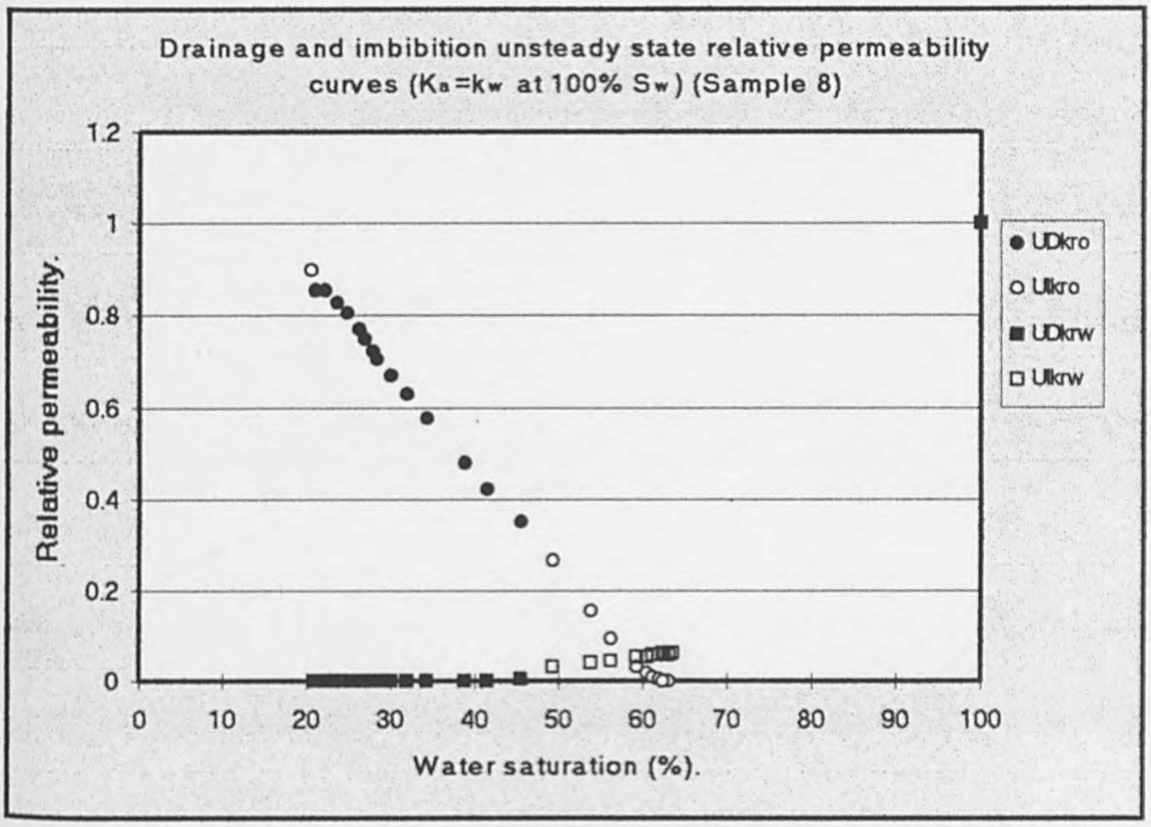

Figure (6.6) Unsteady state relative permeability data for Sample 8 ($K_a = k_w$ at 100% S_w).

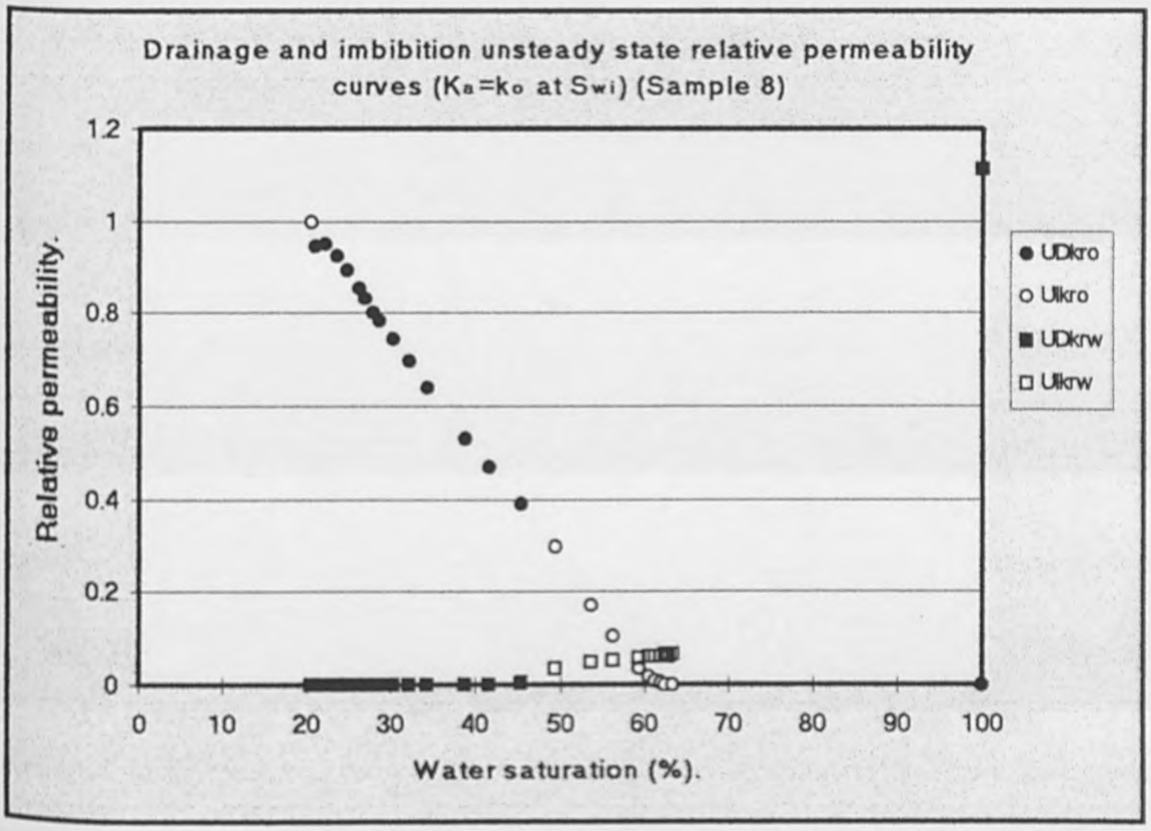

Figure (6.7) Unsteady state relative permeability data for Sample 5 ($k_a = k_o$ at S_{wi}).

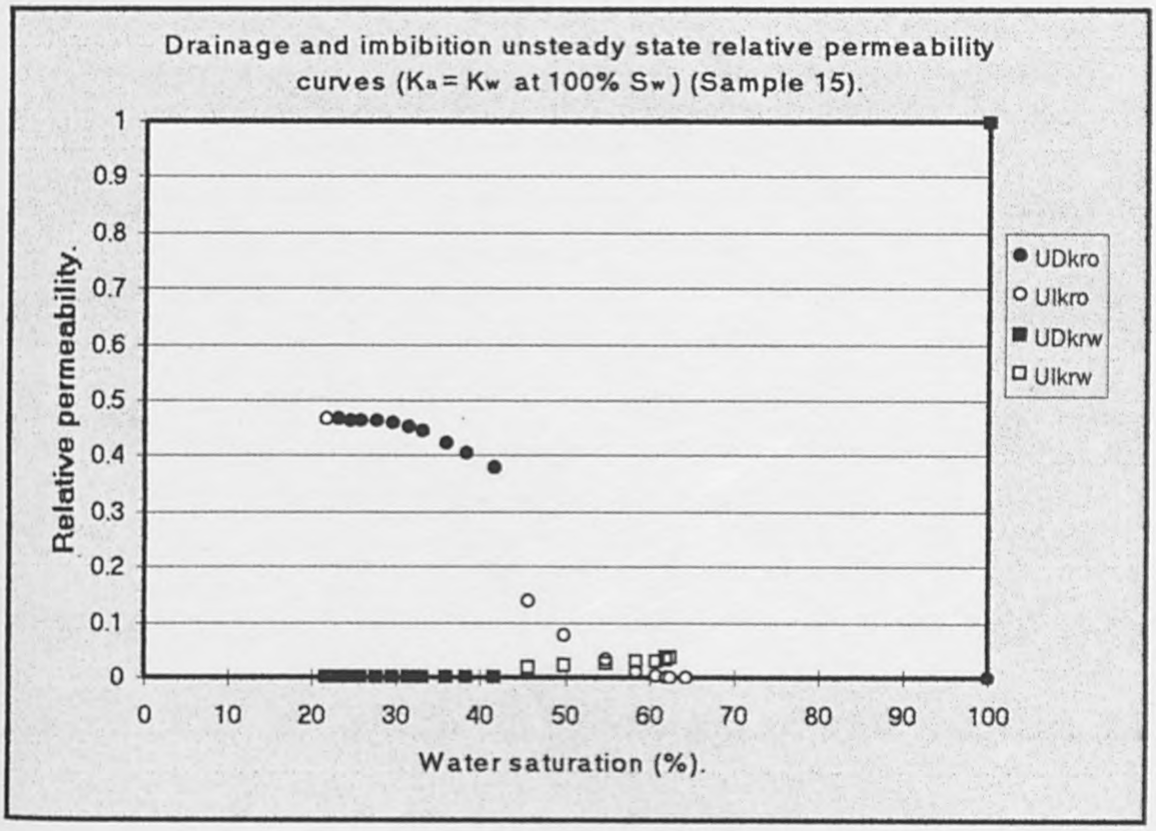

Figure (6.8) Unsteady state relative permeability data for Sample15 ($K_a = k_w$ at100% S_w).

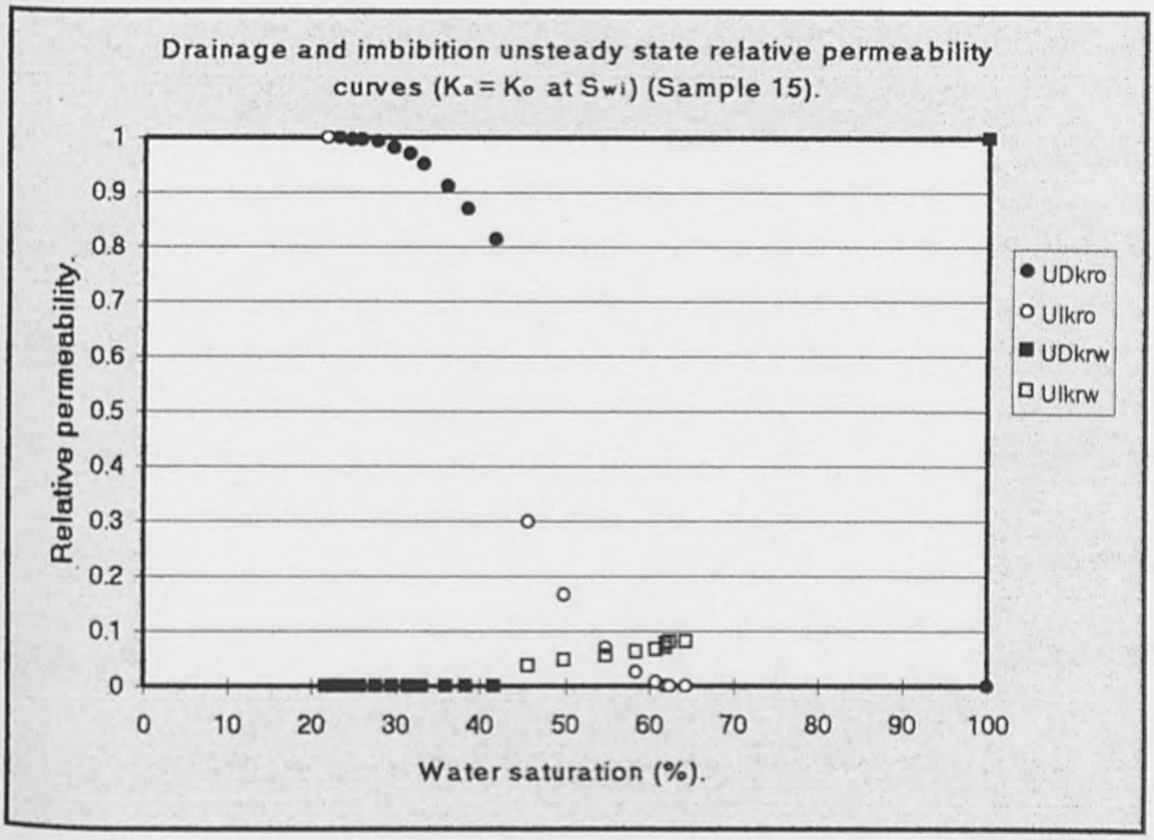

Figure (6.9) Unsteady state relative permeability data for Sample 15 ($K_a = k_o$ at S_{wi}).

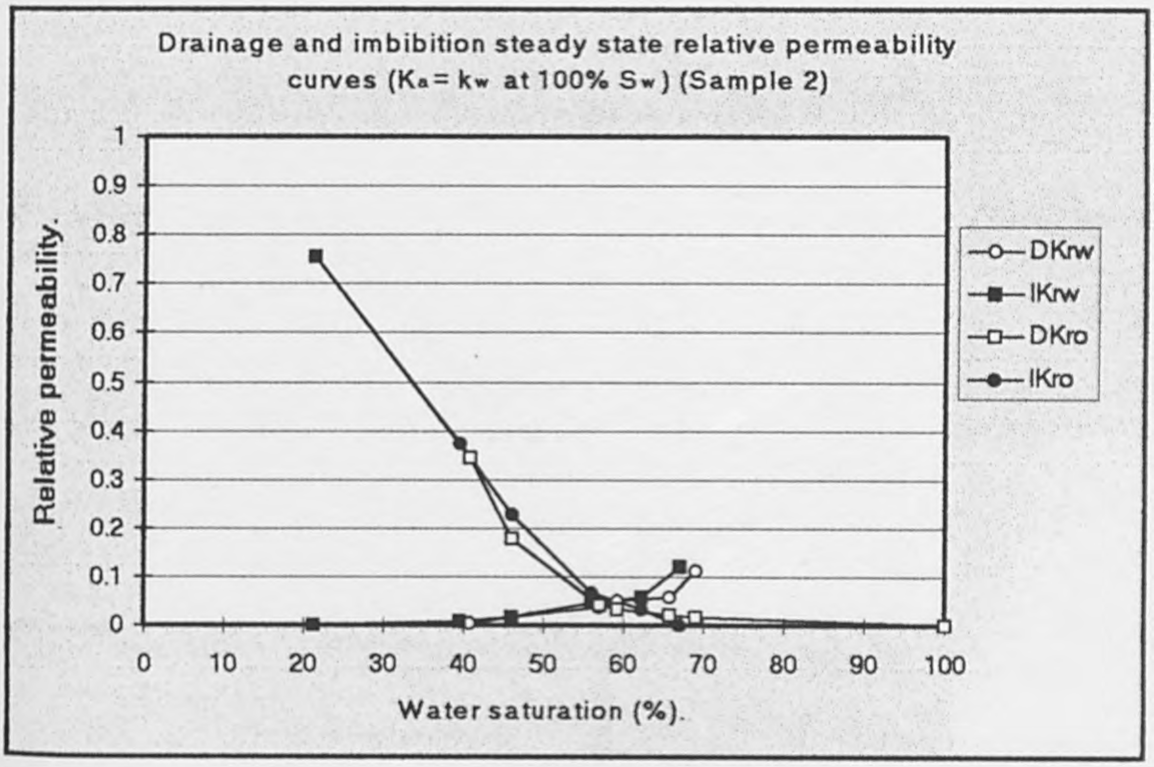

Figure (6.10) Steady state relative permeability data for Sample 2 ($K_a = k_w$ at 100% S_w).

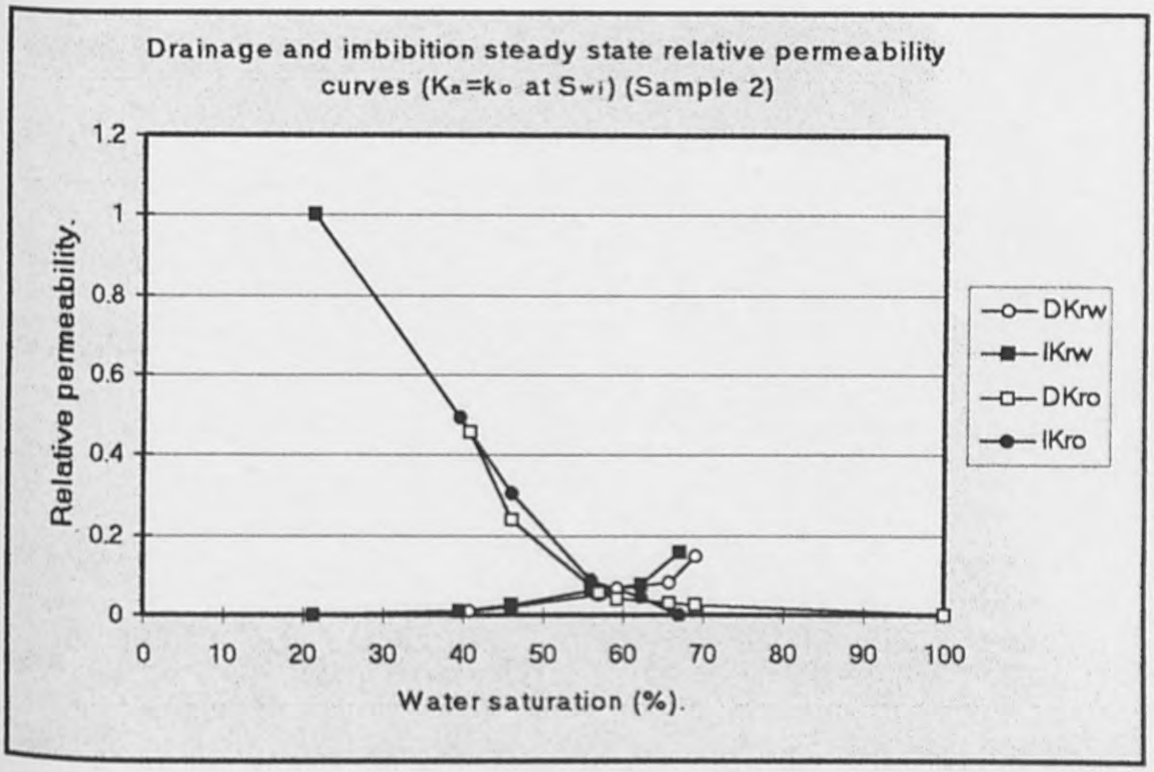

Figure (6.11) Steady state relative permeability data for Sample 2 ($K_a = k_o$ at S_{wi}).

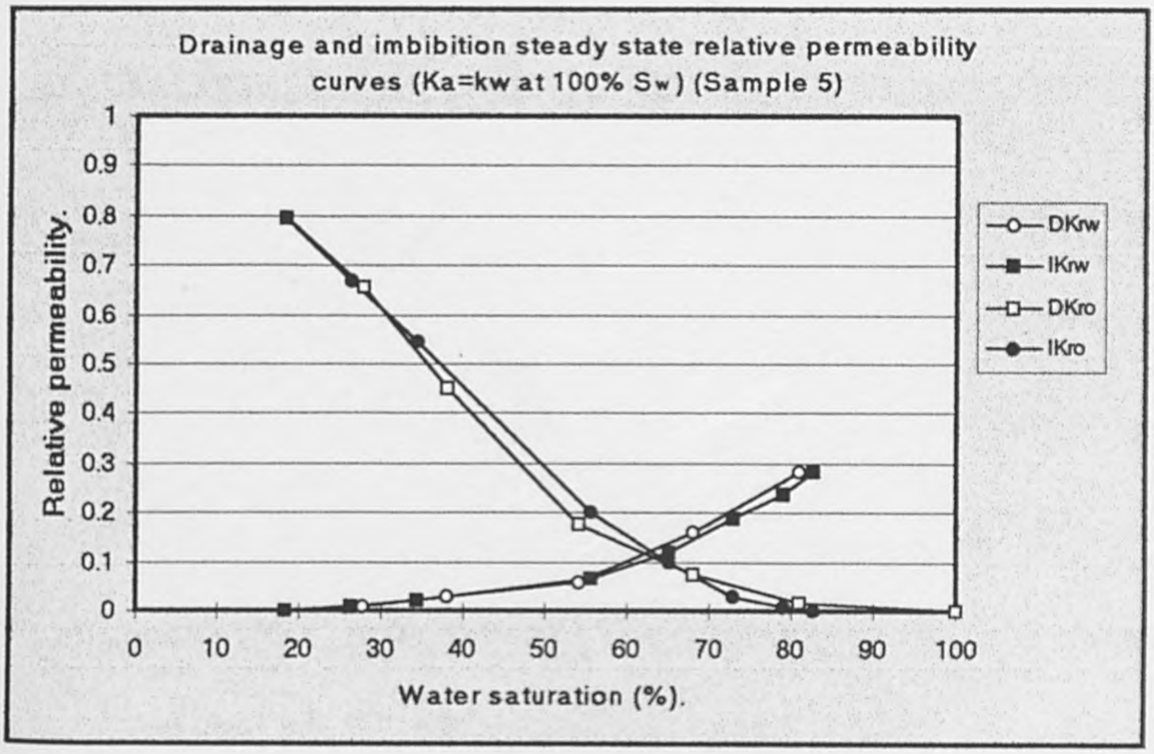

Figure (6.12) Steady state relative permeability data for Sample 5 ($K_a = k_w$ at 100% S_w).

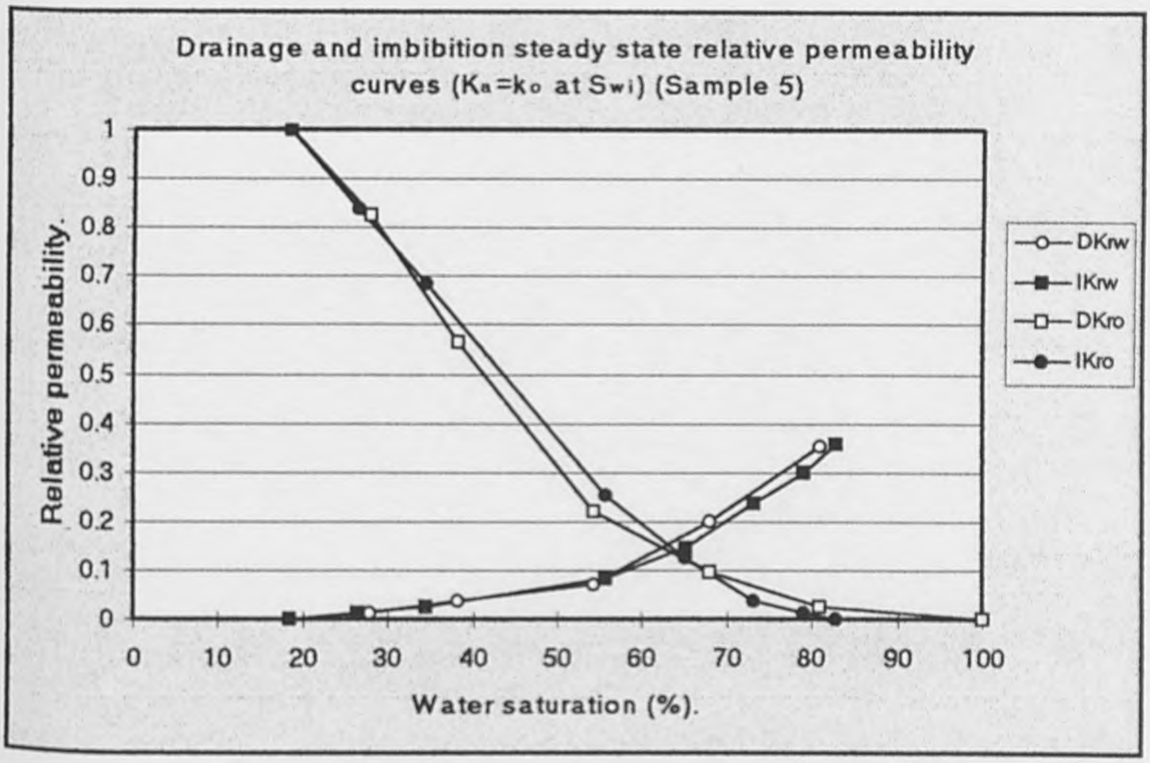

Figure (6.13) Steady state relative permeability data for Sample 5 ($K_a = k_o$ at S_{wi}).

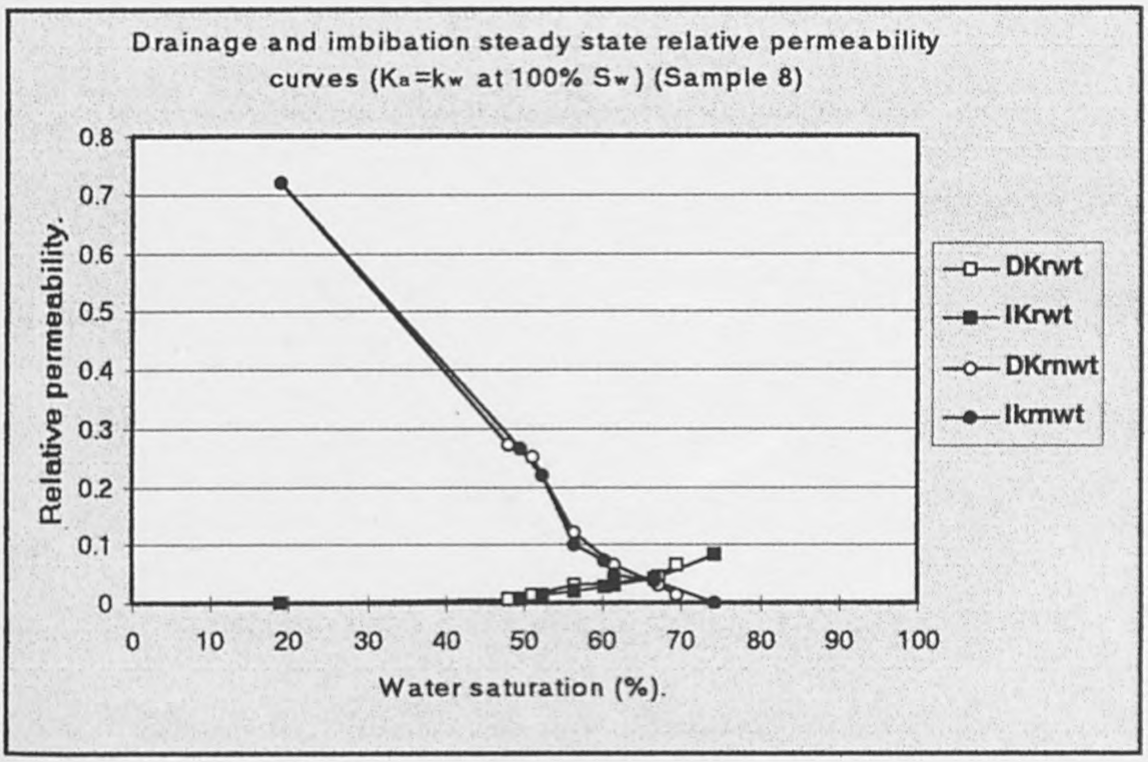

Figure (6.14) Steady state relative permeability data for Sample 8 ($K_a = k_w$ at 100% S_w).

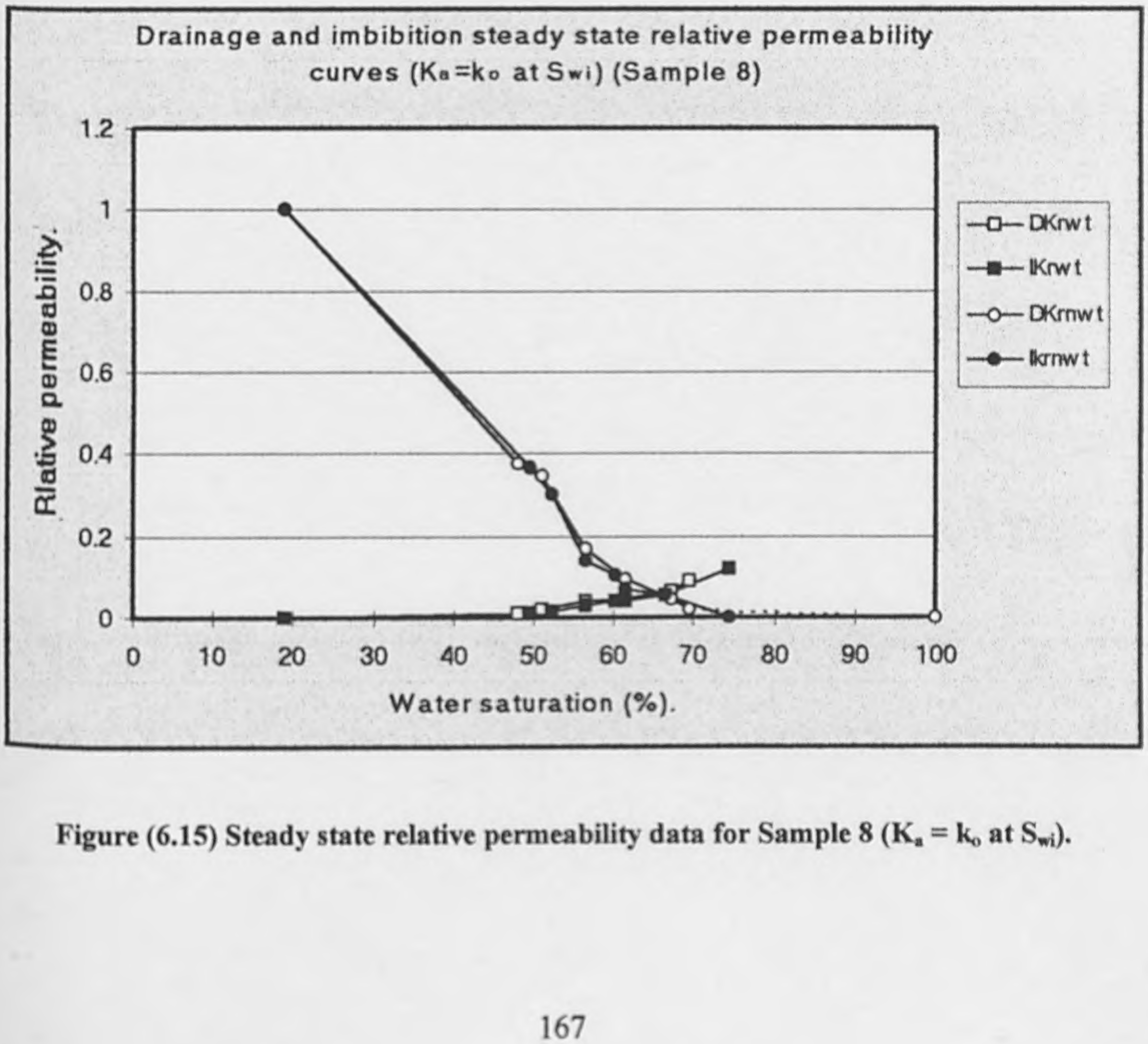

Figure (6.15) Steady state relative permeability data for Sample 8 ($K_a = k_o$ at S_{wi}).

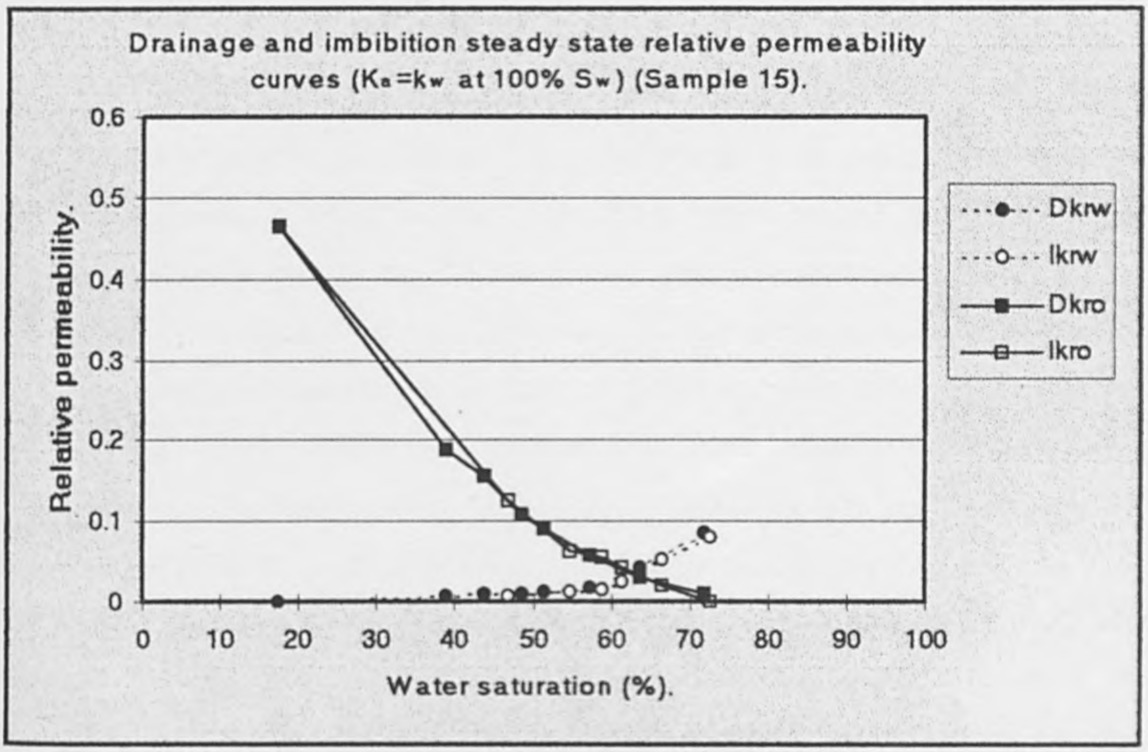

Figure (6.16) Steady state relative permeability data for Sample 15 ($K_a = k_w$ at 100% S_w).

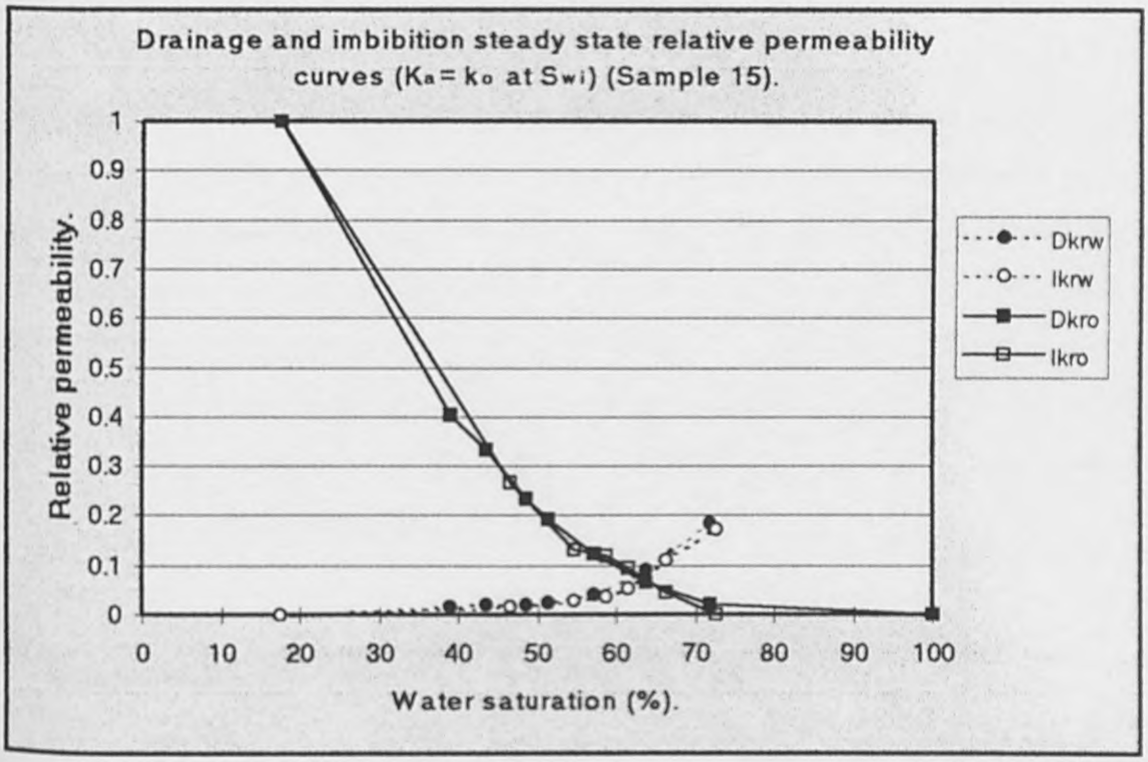

Figure (6.17) Steady state relative permeability data for Sample 15 ($K_a = k_o$ at S_{wi}).

6.4.1 Porous Diaphragm Method

After sample preparation, the fully brine saturated samples were placed "standing up" on the porous diaphragm which is only permeable to brine (impermeable to air). The capillary pressure curves for the selected samples were generated using an air and brine as displacing and displaced fluids respectively. A specially adopted unit was used to allow high pressure desaturation at up to 200psi (1379kPa). A brine saturated tissue was used to ensure good capillary contact between the tested sample and the special clay which connects the sample to the porous plate. Moist air was confined above the diaphragm, and the pressure in the chamber was increased in steps 0.5 (3.4), 1 (6.8), 2 (13.8), 4 (27.5), 8 (55), 32 (220), 64 (441) then 200psi (1397kPa)). Each step may take up to one week to attain capillary equilibrium. Once equilibrium is achieved, the saturation is determined from the changes in the sample weight. Capillary pressure versus saturation plots for the selected water wet samples are displayed in Figure 6.18.

The capillary pressure data obtained by capillary displacement in the porous plate method is considered to be the most reliable[35-38], thus, the data presented in Figure 6.18 was used as the main capillary pressure data in comparing the relative permeability data obtained by the mathematical models against the experimental data. Briefly the porous plate method is the only technique in which the fluid desaturation occurs by capillary displacement. This makes the method is the most representative of the capillary displacement in oil reservoirs. On the other hand, ensuring complete desaturation at each pressure point requires several days, i.e. several weeks are required to produce the full capillary pressure curve. This makes the technique is very time consuming and lacks of the speed of the other methods.

6.4.2 Centrifuge Method

Although, the capillary pressure data obtained by subjecting the samples to a centrifugal force is questionable[35,184], it is included in this project to examine its reliability in using the mathematical models for predicting the relative permeability data where no other capillary pressure data is available.

Figure 6.19 shows the capillary pressure data obtained for the selected samples using the centrifuge. These results demonstrate that the trend of the obtained data is compatible with the classic capillary pressure curves, for instance the higher permeability samples are have water saturations at the same capillary pressure, which leads to lower interstitial water saturation (s_{wi}) for the higher permeability samples. The great weakness of this method is that when a fluid saturated rock sample is centrifuged the fluid filling the pore space is displaced (destructed) in a non uniform manner along the plug's major axis. This was confirmed by resistivity[185], CT imaging[186] and Nuclear Magnetic Imaging (NMR)[187] studies.

6.4.3 Mercury Injection Method

Figure 6.20 shows capillary pressure curves obtained for the selected samples using 2000psi (13,790kPa) mercury injection operation. This technique offers two main advantages over the porous plate and the centrifuge methods. These can be summarized as follows;

1- Capillary pressure data can cover a wide range of saturations compared to the other methods. Furthermore, the technique has the ability of obtaining measurements at any saturation which allow high precision in defining the threshold pressure and transition zone.

2- Complete curve can be generated in few hours rather than several weeks.

The major disadvantage in using the mercury injection method is that it is a destructive test, thus the sample cannot be used for any further investigations. For this reason these tests were carried out as a last step of the experimental programme.

It was found that the connate or interstitial water saturation (S_{wi}) is not really a constant value. For instance it is always significantly lower at 2000psi (13,790kPa) than at 50psi

(345kPa) (which is the test pressure commonly used). The difference can approach 5% in some samples. High pressure capillary desaturation is more representative of the water desaturation by oil in hydrocarbon reservoirs with a large pay zone, therefore it is extremely important to define the reservoir capillary pressure to identify the correct S_{wi} from the capillary pressure curve and the common random use can lead to a significant errors especially in reservoirs with a large thickness and/or transition zone. Melrose[188] belives that is due to wetting films desaturation.

Although it is known that the higher rock porosity and permeability, the lower the connate water saturation and desaturates at lower capillary pressures, some tested samples showed anomalous results. Figures 6.18-6.20 show that sample 15 (13.8% porosity and 125md permeability) had a lower S_{wi} and capillary pressure than sample 8 which is of higher porosity and permeability than sample 8 (20.3% porosity and 183md permeability). The interesting finding is that the same results were obtained using the three different techniques (air-brine, centrifuge and mercury injection). This indicates that interstitial water saturation is not only dependent on porosity and permeability, but also depends on the pore size distribution

6.5 Comparison between Measured and Predicted Relative Permeabilities

Relative permeability curves have been generated for each selected sample using the following mathematical models (detailed in Section 2.4);

1. Purcell
2. Burdine
3. Rapoport and Leas
4. Timmerman
5. Fatt and Dykstra

The above mathematical models have been used to predict the relative permeabilities from the capillary pressure data for all the selected water wet samples. The calculated relative permeability for each sample has been displayed on one graph per sample in

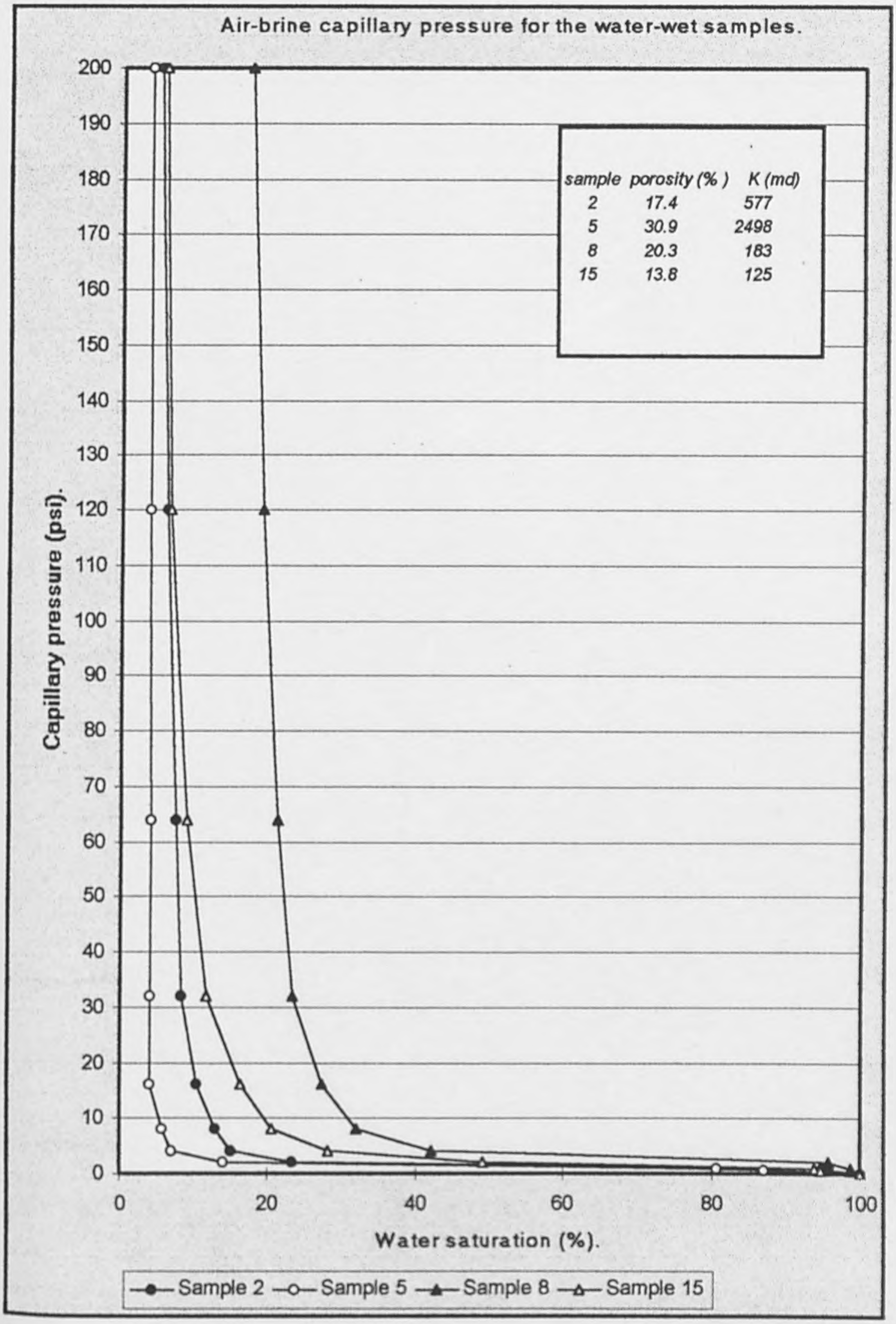

Figure (6.18) Air -brine capillary pressure curves for the selected water wet samples.

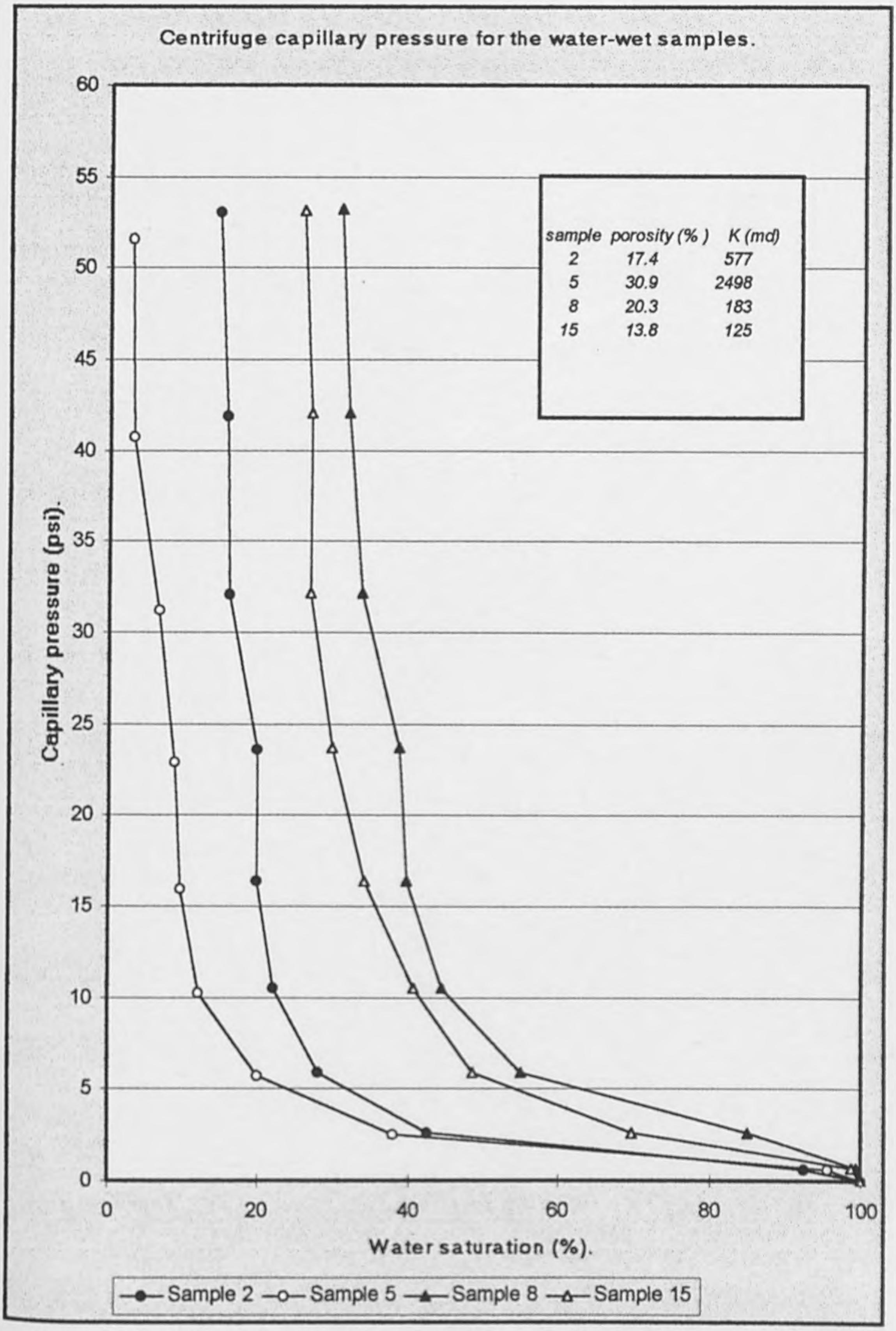

Figure (6.19) Centrifuge capillary pressure curves for the selected water wet samples.

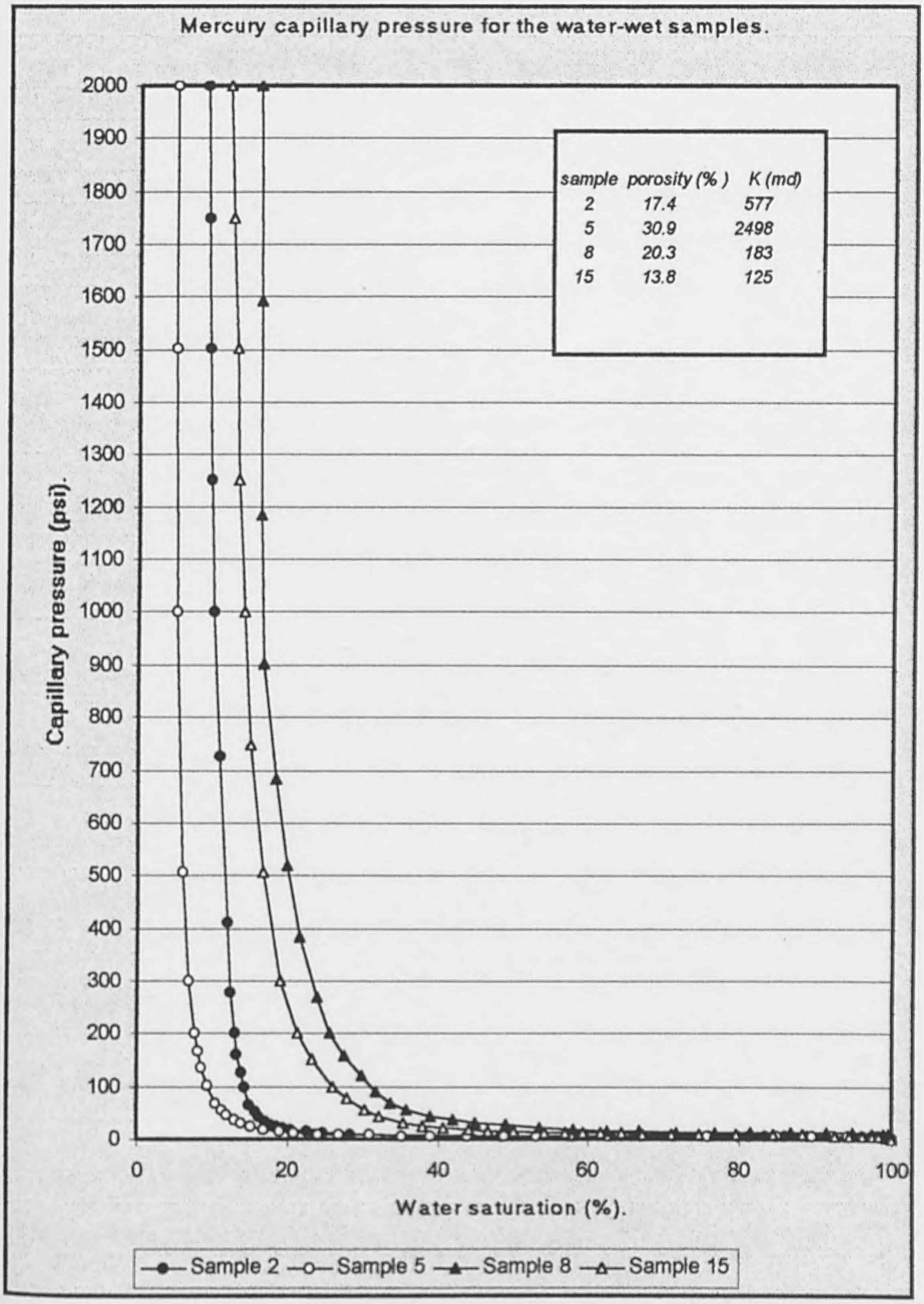

Figure (6.20) Mercury capillary pressure curves for the selected water wet samples.

preparation for comparison with the laboratory unsteady and steady state experimental data. The mathematically derived wetting phase relative permeability data has been displayed against the experimental unsteady state wetting phase relative permeabilities in Figures 6.21-6.24, then against the steady state wetting phase relative permeabilities in Figures 6.25-6.28. Likewise the mathematically derived non-wetting phase relative permeability data is displayed against the experimental unsteady state non-wetting phase relative permeabilities in Figures 6.29-6.32, and against the steady state non-wetting phase relative permeabilities in Figures 6.33-6.36.

As water wet samples, the experimental imbibition data is selected for comparison, since it is more representative of water/oil displacement in oil reservoirs especially the unsteady state data. To asses the validity of the mathematical models, deviation (average error) from the laboratory experimental data has been calculated for each sample as follows;

$$\text{Average error} = \frac{\sqrt{(\text{experimental} - \text{theoritical})^2}}{\text{n}}$$

Where n is number of readings.

6.5.1 Comparison between the Predicted and Unsteady State Relative Permeability

The mathematically generated relative permeability data primarily compared to those measured experimentally by the unsteady state method. The unsteady state relative permeability has been presented in two sets of data; 1- using rock sample permeability to water (k_w at 100% S_w) as reference value, 2- using oil permeability at S_{wi} as reference value. Preliminary comparisons (Figures 6.25 – 6.28) show that the mathematical models are in agreement with the use of oil permeability at irreducible water saturation (k_o at S_{wi}) as reference value. Both, experimental and mathematical results have the same end point relative permeability (k_{ro} at S_{wi}) of 1.0 where using k_w at 100% S_w a reference point led to a significant deviation from all the mathematical models. As shown in Figures 7.5-7.8 the oil relative permeability either higher than 1.0 as in sample 2 or less than 1.0 in all other samples. Therefore it has been decided to compare the predicted data to the unsteady state data set with k_o at S_{wi} as a reference value, the comparison against the unsteady state results with k_w at 100% S_w a reference value is presented in Figures 7.1-7.8. The comparison between the calculated wetting and non wetting phase relative permeability and the unsteady state data is shown in Figures 6.21-628.

6.5.1.1 Wetting Phase Relative Permeability Comparison.

Both mathematically calculated and measured wetting phase relative permeability for samples 2, 5, 8 and 15 have been displayed on one graph per sample as shown in Figures 6.21-6.24. The data derived by mathematical models shows a significant variation from the laboratory experimental measurements. The discrepancy varies from one correlation to another. To evaluate these mathematical models, deviation from the laboratory data has been calculated for each model. A comparison summary is presented in Tables 6.3–6.6.

Comparing the proposed wetting phase relative permeability mathematical models led to the following results;

1. Purcell's model led to a cumulative average error of 18.3% saturation varying from an average error of 8.9% at sample 15 to 27.5% at sample 5.
2. Fatt and Dykstra model's led to a cumulative average error of 13.2% saturation varying from an average error of 3.9% at sample 15 to 22.1% at sample 5.
3. Burdine model led to a cumulative average error of 3.0% saturation varying from an average error of 1.3% at sample 5 to 4.9% at sample 15.
4. Rapoport and Leas's model led to a cumulative average error of 5.8% saturation varying from an average error of 3.5% at sample 5 to 8.5% at sample 8.
5. Timmerman's model led to a cumulative average error of 21.4% saturation varying from an average error of 4.3% at sample 5 to 33.5% at sample 8.

In conclusion, although the results unsteady state flooding leads to some ambiguities, the Burdine equation appears to be the most appropriate for predicting water relative permeability for water wet rock samples.

k_{rw}	Error (saturation %)					
	Purcell	F&D	Burdine	R&L min	R&L max	Timmerman
0.05	17.592	13.966	5.517	3.793	0.692	17.592
0.1	24.138	18.965	0.000	8.276	5.515	24.485
0.125	24.828	19.656	1.380	8.970	6.550	24.050
Avg. error	**22.186**	**17.529**	**2.299**	**7.013**	**4.252**	**22.042**

Table 6.3 Comparison of predicted wetting phase relative permeability (Sample 2).

k_{rw}	Error (saturation %)					
	Purcell	F&D	Burdine	R&L min	R&L max	Timmerman
0.05	26.667	21.336	1.000	10.666	2.334	1.666
0.1	29.340	23.334	1.667	7.667	2.000	4.667
0.15	29.667	24.000	2.666	7.000	2.664	5.666
0.2	28.664	23.163	1.330	3.331	3.000	5.331
0.25	27.334	22.000	1.333	1.003	4.000	4.667
0.3	25.660	20.661	0.661	1.339	5.006	3.994
0.32	25.000	20.331	0.331	2.670	5.336	4.000
Avg. error	**27.476**	**22.118**	**1.284**	**4.811**	**3.477**	**4.284**

Table 6.4 Comparison of predicted wetting phase relative permeability (Sample 5).

k_{rw}	Error (saturation %)					
	Purcell	F&D	Burdine	R&L min	R&L max	Timmerman
0.025	7.241	2.759	8.276	2.758	0.000	24.837
0.05	17.242	11.379	0.000	10.690	7.241	36.552
0.06	19.311	13.448	2.759	12.069	9.311	39.311
Avg. error	**14.598**	**9.195**	**3.678**	**8.506**	**5.517**	**33.567**

Table 6.5 Comparison of predicted wetting phase relative permeability (Sample 8).

k_{rw}	Error (saturation %)					
	Purcell	F&D	Burdine	R&L min	R&L max	Timmerman
0.025	3.674	6.326	8.979	4.082	1.225	15.919
0.05	11.428	1.632	3.674	10.204	8.163	26.939
0.075	11.836	3.673	2.040	8.571	6.938	33.877
Avg. error	**8.979**	**3.877**	**4.898**	**7.619**	**5.442**	**25.578**

Table 6.6 Comparison of predicted wetting phase relative permeability (Sample 15).

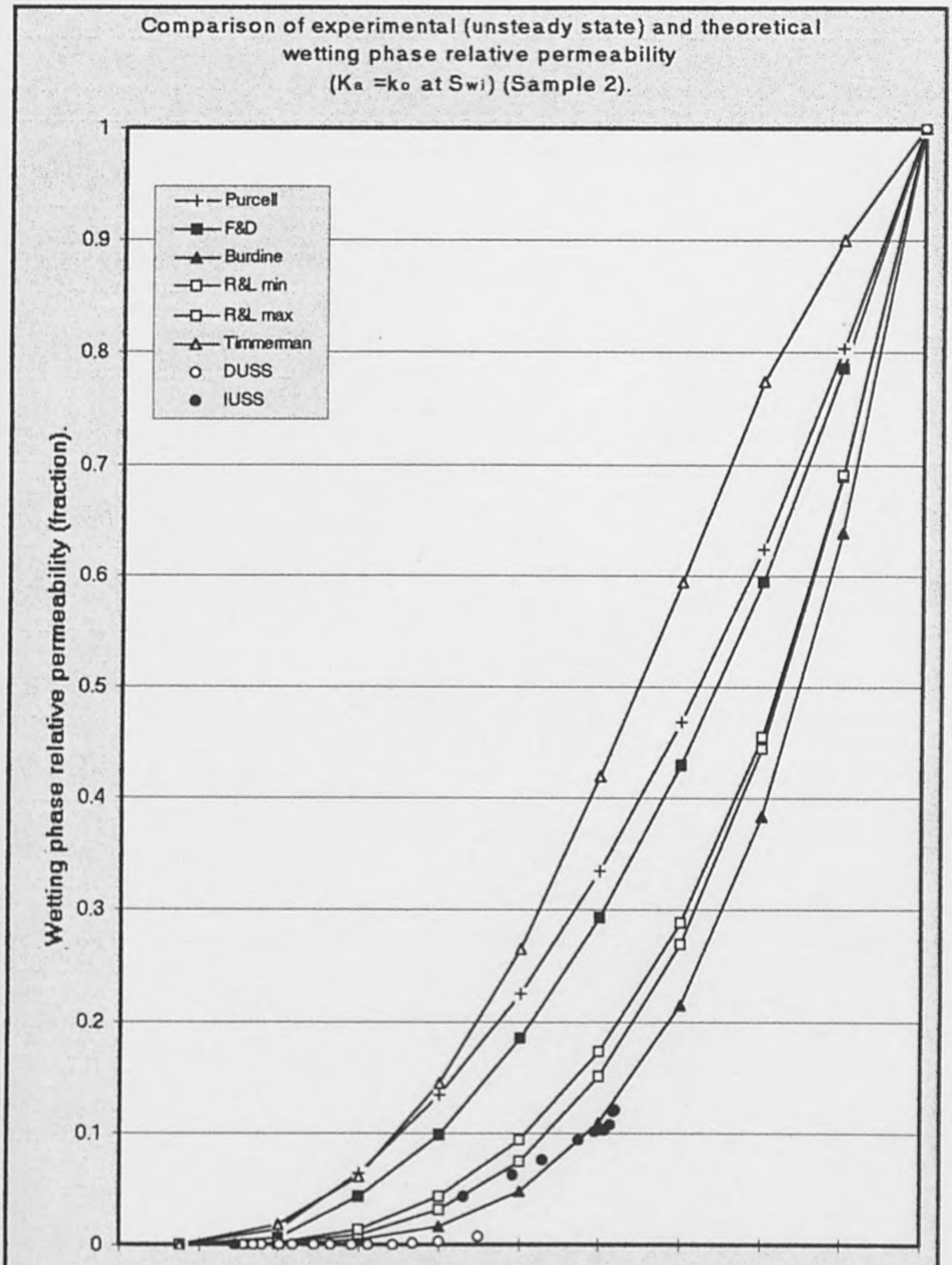

Figure (6.21) Comparison of experimental unsteady state and theoretical wetting phase relative permeability for Sample 2.

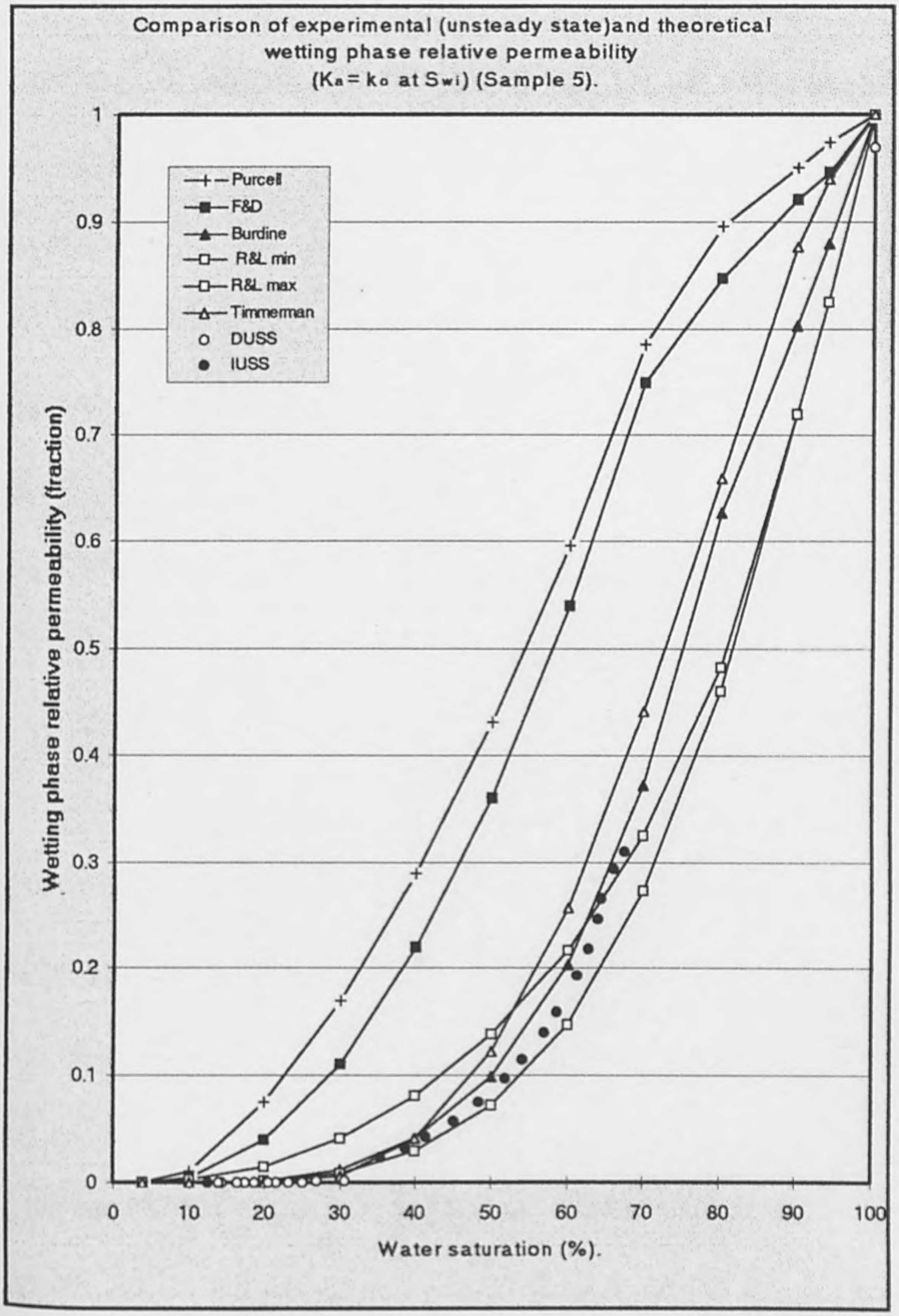

Figure (6.22) Comparison of experimental unsteady state and theoretical wetting phase relative permeability for Sample 5.

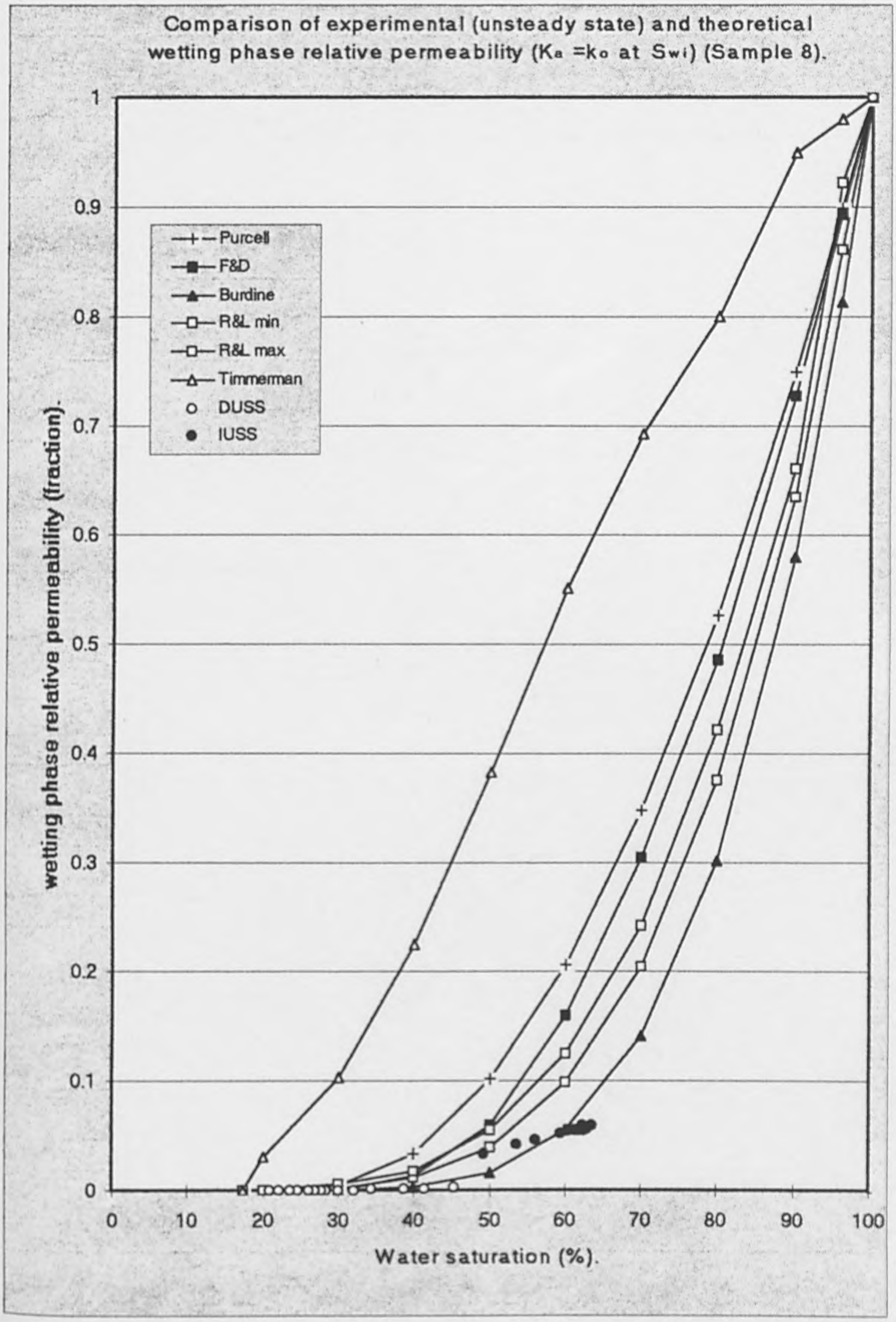

Figure (6.23) Comparison of experimental unsteady state and theoretical wetting phase relative permeability for Sample 8.

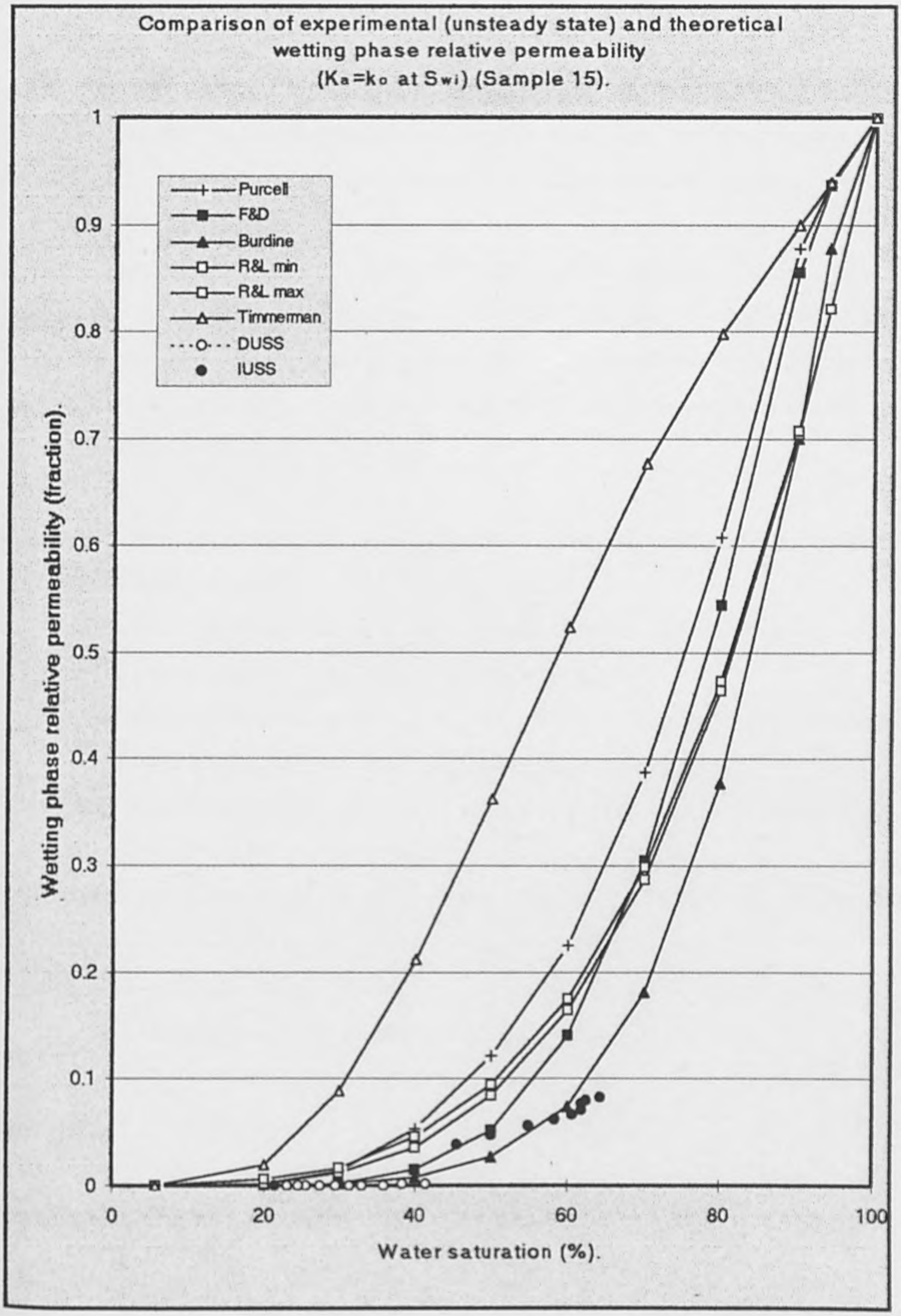

Figure (6.24) Comparison of experimental unsteady state and theoretical wetting phase relative permeability for Sample 15.

6.5.1.2 Non wetting Phase Relative Permeability Comparison.

As for the wetting phase data, the mathematically derived non wetting phase relative permeabilities for the selected water wet samples have been displayed against the experimental unsteady state data on one graph per sample as shown in Figures 6.25-6.28. The oil relative permeability derived from the capillary pressure data by mathematical models showed a wide range of variations from the experimental data. The discrepancy varies from one correlation to another. To evaluate these mathematical models for predicting the non wetting relative permeability, deviations from the laboratory experimental data have been calculated for each model, and a comparison summary is presented in Tables 6.7 – 6.10.

Comparing the proposed non wetting phase relative permeability mathematical models led to the following results;

1. Purcell's model led to a cumulative average error of 34.8% saturation varying from an average error of 22.9% at sample 5 to 39.7% at sample 8.
2. Fatt and Dykstra's model led to a cumulative average error of 36.3% saturation varying from an average error of 26.6% at sample 5 to 40% at sample 2.
3. Burdine model's led to a cumulative average error of 6.2% saturation varying from an average error of 3.6% at sample 5 to 9% at sample 8.
4. Rapoport and Leas's model led to a cumulative average error of 43.2% saturation varying from an average error of 40.4% at sample 8 to 45% at sample 5.
5. Timmerman's model led to a cumulative average error of 23.4% saturation varying from an average error of 9.9% at sample 5 to 32% at sample 8.

Although the oil relative permeability data obtained from unsteady state experiments is of doubtful validity, the Burdine equation appeared to be the most appropriate for predicting oil relative permeability for water wet rock samples.

6.5.1.3 Validity of the Unsteady State Relative Permeability Data.

In spite of the fact that unsteady state water laboratory tests are the closest to the reservoir flooding mechanism, and it can be conducted in a much shorter time compared to the sophisticated steady state tests, the data obtained from unsteady state tests has the following major shortcomings;

1. Inability to produce any intermediate relative permeability values for favourable displacement conditions (mobility ratios ≤ 1.0).

2. Lack of relative permeability data at low water saturations for higher mobility ratios and data falling in a narrow water saturation range below the residual oil saturation.

3. Conducting unsteady state relative permeability tests at adverse oil-water viscosity ratios develops viscous fingering. This invalidates the assumption that flow is one dimensional, upon which classical unsteady state relative permeability interpretation techniques are based.

4. Lack of capillary equilibrium.

5. The absence of upstream and downstream mixing heads in the unsteady state laboratory rigs makes tested samples more exposed to capillary end effects. High flow rates have been used to overcome the capillary end effects, however, the higher the flooding rate the lower capillary equilibrium.

Finally, the use of reservoir waterflood advance rates and matched viscosity ratios is the most appropriate way to represent the reservoir situation, but the capillary end effect in low rate/viscosity ratio core floods will also undermine classical theory. Unfortunately, the effects of capillarity, viscous fingering and failure to obtain relative permeability data for a wide range of water saturations cannot be suppressed simultaneously. This makes the interpretation of the unsteady state floods extremely difficult especially if proper non invasive saturation monitoring diagnoses are not available.

In view of the violations of the underlying assumptions upon which the unsteady state method is based, relative permeabilities obtained from most, if not all, unsteady state displacements must be viewed with great caution. As result of the previous discussion, the proposed mathematical models for predicting the relative permeability data ought to be compared against relative permeability data obtained by the steady state method which is considered to be the most sophisticated and reliable experimental method.

k_{ro}	Error (saturation %)					
	Purcell	**F&D**	**Burdine**	**R&L min**	**R&L max**	**Timmerman**
0.05	40.410	40.410	14.700	42.044	42.043	18.780
0.1	40.002	40.410	8.980	41.634	41.634	24.080
0.15	40.413	41.433	4.903	42.862	42.862	25.300
0.2	39.186	40.410	1.635	42.859	42.859	27.753
0.25	38.777	40.408	0.000	44.082	44.082	28.571
0.3	37.959	39.184	2.041	44.082	44.082	27.755
0.35	37.551	38.776	3.265	44.490	44.490	26.121
0.38	37.143	38.775	3.674	44.489	44.489	24.898
Avg. error	**38.930**	**39.976**	**4.900**	**43.318**	**43.318**	**25.407**

Table 6.7 Comparison of predicted non wetting phase relative permeability (Sample 2).

k_{ro}	Error (saturation %)					
	Purcell	**F&D**	**Burdine**	**R&L min**	**R&L max**	**Timmerman**
0.05	29.00	33.800	3.333	37.666	37.666	8.670
0.1	23.267	29.869	1.000	39.833	39.834	10.673
0.15	20.817	26.417	4.003	41.666	41.666	12.667
0.2	21.00	23.500	4.340	43.666	43.666	12.334
0.25	20.000	22.331	5.333	45.331	45.331	11.669
0.3	21.167	23.494	5.167	47.834	47.834	10.166
0.35	23.006	25.670	3.661	52.006	52.006	7.994
0.3775	25.334	28.001	1.999	52.334	52.667	5.333
Avg. error	**20.949**	**26.635**	**3.605**	**45.042**	**45.084**	**9.938**

Table 6.8 Comparison of predicted non wetting phase relative permeability (Sample 5).

k_{ro}	Error (saturation %)					
	Purcell	F&D	Burdine	R&L min	R&L max	Timmerman
0.05	39.666	39.666	17.666	39.000	40.333	31.334
0.1	42.000	40.000	12.667	39.667	42.000	32.333
0.15	39.667	40.333	9.333	40.333	42.000	34.000
0.2	39.334	40.000	6.333	40.667	41.900	33.000
0.25	39.000	40.000	4.666	41.000	42.333	31.600
0.3	38.667	39.667	3.334	42.001	43.001	29.666
Avg. error	**39.722**	**39.944**	**9.000**	**40.445**	**41.928**	**31.989**

Table 6.9 Comparison of predicted non wetting phase relative permeability (Sample 8).

k_{ro}	Error (saturation %)					
	Purcell	F&D	Burdine	R&L min	R&L max	Timmerman
0.05	35.001	35.17	13.104	38.621	38.621	26.896
0.1	38.172	38.96	12.069	43.448	43.448	25.517
0.15	37.759	38.966	8.276	43.793	43.793	25.862
0.2	38.793	39.999	6.551	45.172	45.172	26.208
0.25	37.586	39.138	2.414	43.793	43.793	27.931
0.3	37.931	39.483	0.689	44.483	44.483	26.897
Avg. error	**37.54**	**38.621**	**7.184**	**43.218**	**43.218**	**26.552**

Table 6.10 Comparison of predicted non wetting phase relative permeability (Sample 15).

6.5.2 Comparison between Predicted and Steady State Relative Permeability

It is ironic that while water/oil relative permeability curves probably represent the most important category of data in special core analysis in general and this project in particular, obtaining valid results also presents the greatest challenges. As discussed in section (6.5.1.3) the data obtained by the unsteady state method has not been credited and the sole alternative is to adopt the very expensive (average of $7000 per sample) and time consuming steady state technique. However, steady state method is considered to be the state of the art when it comes to measurement of water oil relative permeability. The obtained experimental steady state data has the following characterizations:

1. In addition to avoiding many of problems associated with the unsteady state procedure, an important advantage of the method is that it is possible to define

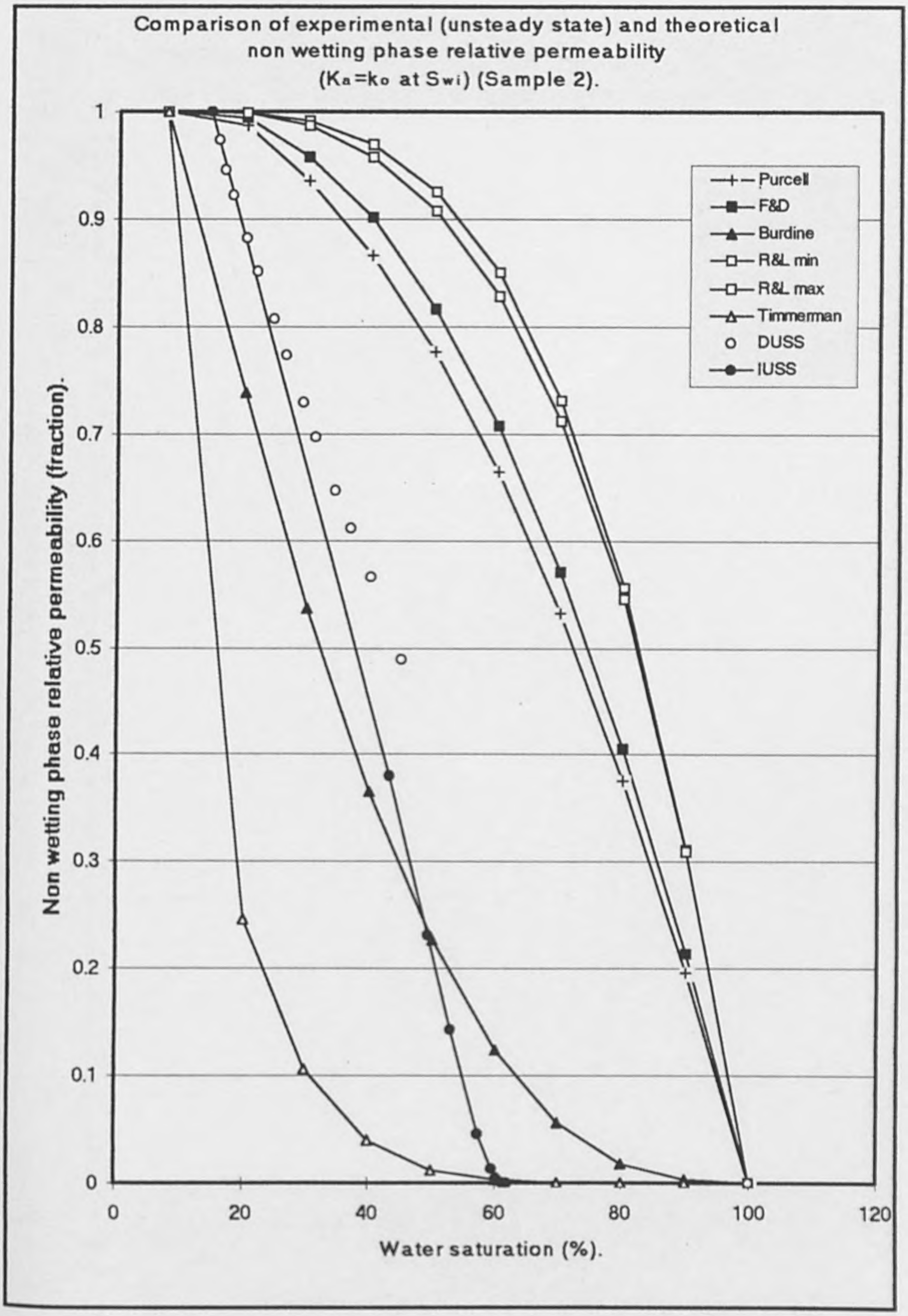

Figure (6.25) Comparison of experimental unsteady state and theoretical non wetting phase relative permeability for Sample 2.

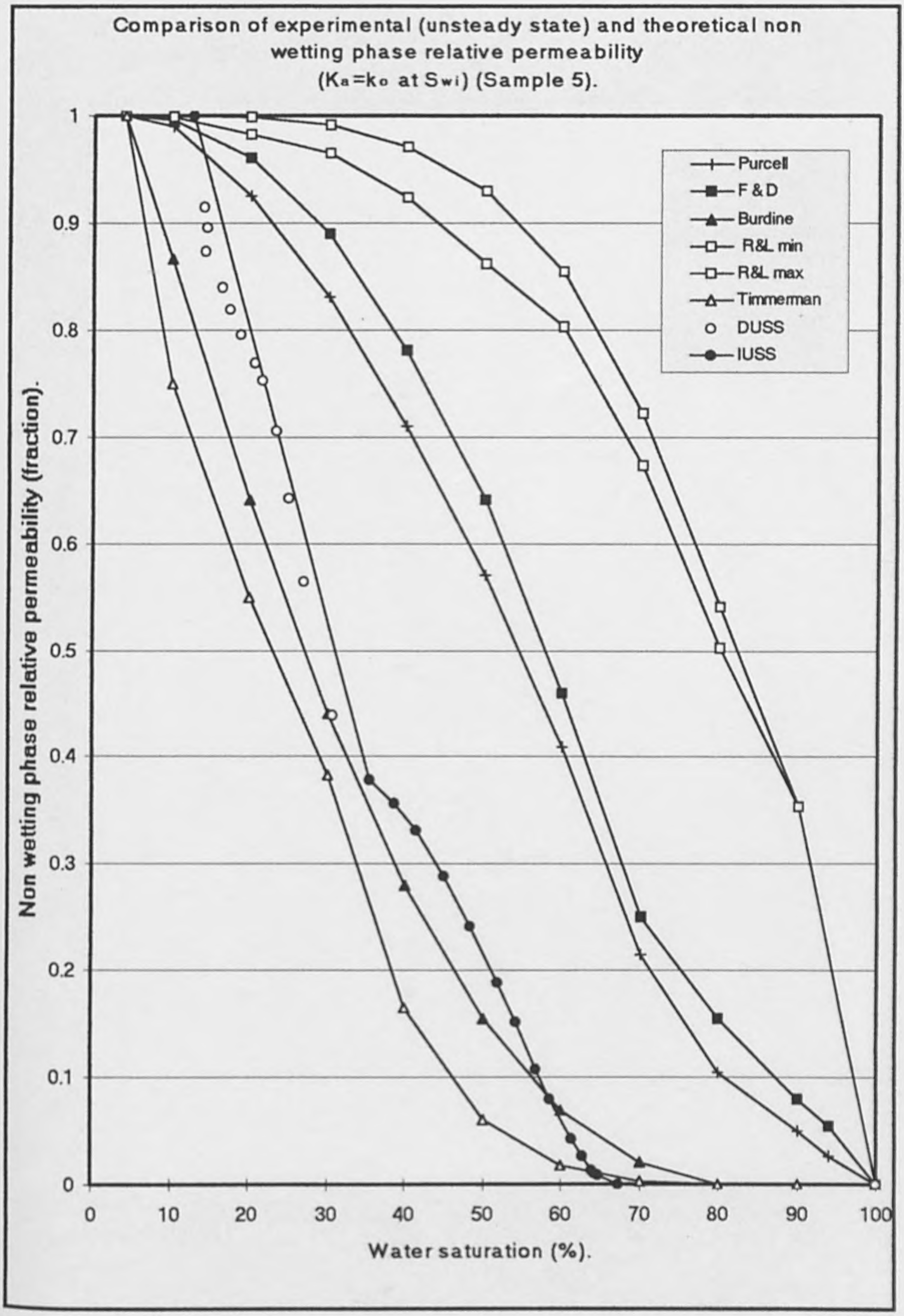

Figure (6.26) Comparison of experimental unsteady state and theoretical non wetting phase relative permeability for Sample 5.

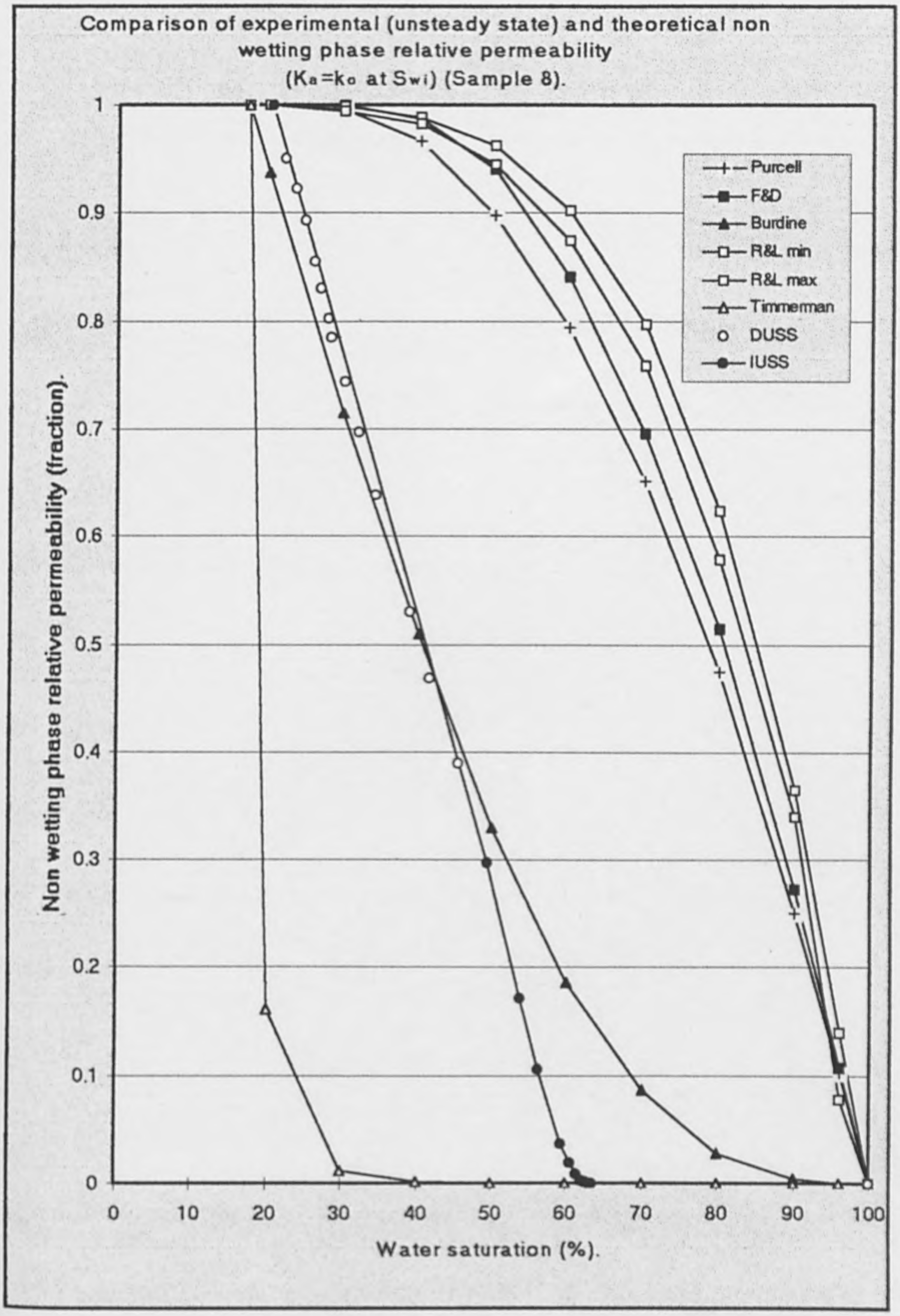

Figure (6.27) Comparison of experimental unsteady state and theoretical non wetting phase relative permeability for Sample 8.

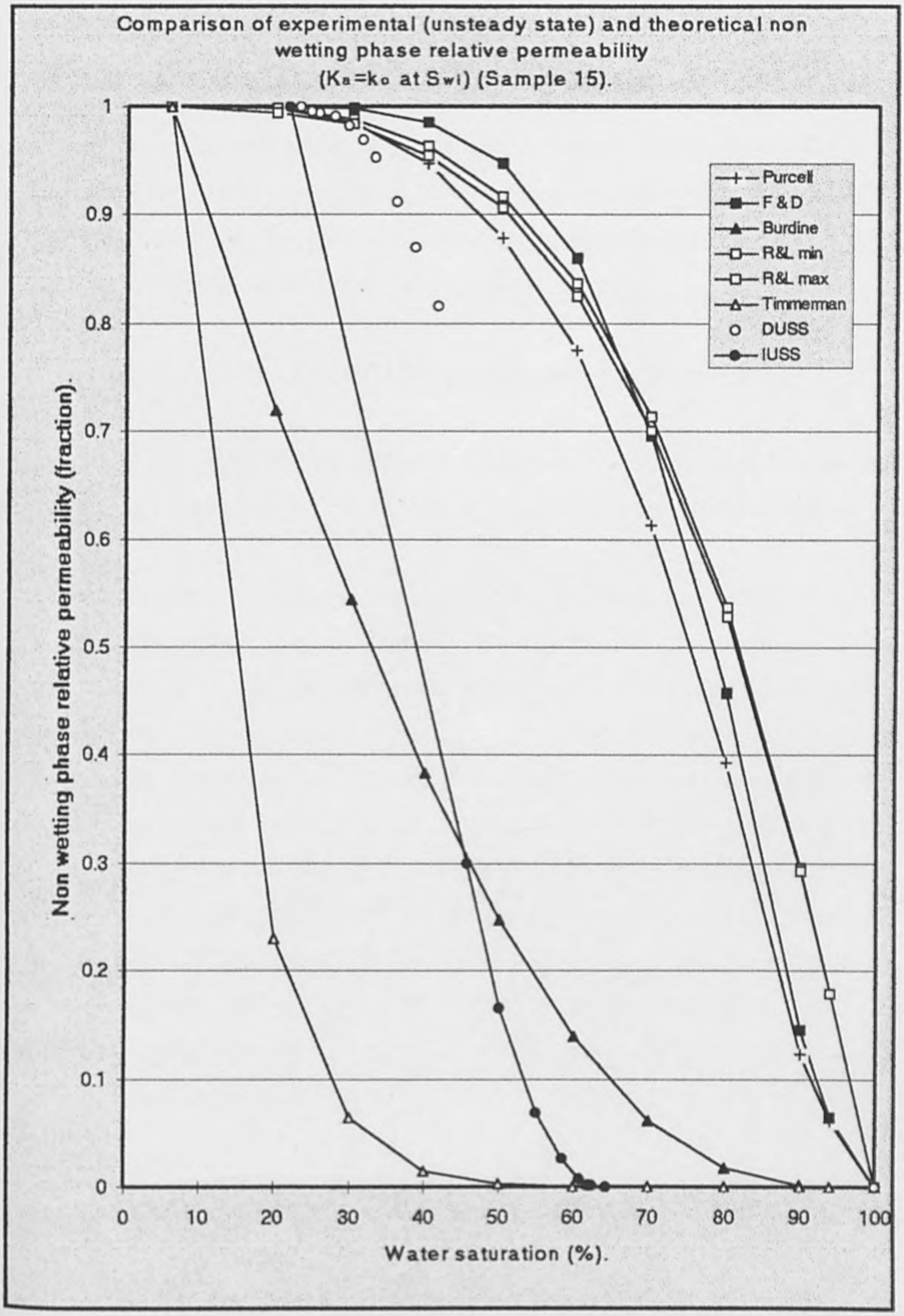

Figure (6.28) Comparison of experimental unsteady state and theoretical non wetting phase relative permeability for Sample 15.

relative permeability across a broader saturation range even for systems with favourable mobility ratios.

2. Use of the steady state technique allows one to calculate relative permeabilities of water and oil directly using Darcy's law. Furthermore, it is possible to ensure that capillary equilibrium has been achieved before making the final readings of flow rate and differential pressure used in the equation.

3. The capillary end effect has been enhanced using sandstone mixing heads.

Consequently, the experimentally measured steady state relative permeability data has been chosen for comparison with data derived by the proposed mathematical models.

The steady state relative permeability also has been presented in two sets of data based on two different reference points; 1- water permeability at 100% saturations, 2- oil permeability at S_{wi}. Preliminary comparisons (Figures 6.29 – 6.36 and Figures A9-A16 Appendix I) show that the mathematical models are in closer agreement with the use of oil permeability at irreducible water saturation (k_o at S_{wi}) as the reference value. The two sets of experimental wetting and non wetting phase relative permeabilities always fall lower than the data derived from the capillary pressure curves using Burdine model which appears to be the closest model to the laboratory data. Since, k_o at S_{wi} values are lower than k_w at 100% S_w, so using k_o at S_{wi} as a reference value will shift the laboratory measured relative permeability data closer (upward) to the mathematically derived data. Furthermore, using k_o at S_{wi} as a reference value makes both experimental and mathematical results have the same end point relative permeability (k_{ro} at S_{wi}) of 1.0.

Accordingly, the experimental steady state data set using k_o at S_{wi} as a reference value was used for comparison with relative permeability curves generated by the mathematical models. It is worth mentioning that although Sample 5 is considered to be a very troublesome sample due to the continuous loss of grains which has a great impact on fluids saturation determination, it is still included as part of this study. The results obtained have been discussed in the following sections.

6.5.2.1 Wetting Phase Relative Permeability Comparison.

The mathematically calculated and experimentally measured wetting phase steady state relative permeabilities for samples 2, 5, 8 and 15 have been displayed on one graph per sample as shown in Figures 6.29-6.36. The data derived by mathematical models showed a significant variation from the laboratory experimental measurements. The discrepancy varies from one correlation to another. To assess these mathematical models quantitatively, deviation from the laboratory data has been calculated in saturation units for each proposed model. A comparison summary is presented in Tables 6.11 – 6.12.

Comparing the proposed wetting phase relative permeability mathematical models to the steady state experimental results led to the following results;

1. Purcell's model led to a cumulative average error of 25.6% saturation varying from an average error of 18.5% at sample 15 to 36.7% at sample 5.
2. Fatt and Dykstra's model led to a cumulative average error of 19.7% saturation varying from an average error of 9.8% at sample 15 to 30.8% at sample 5.
3. Burdine's model led to a cumulative average error of 5.6% saturation varying from an average error of 3.1% at sample 15 to 10.1% at sample 5.
4. Rapoport and Leas's model led to a cumulative average error of 11.43% saturation varying from an average error of 5.3% at sample 5 to 15.6% at sample 15.
5. Timmerman's model led to a cumulative average error of 28.9% varying from an average error of 13% at sample 5 to 41.1% at sample 8.

From the obtained results it can be concluded that Burdine's equation is the most reliable for predicting water relative permeability for water wet rock samples. This is in line with the ambiguous unsteady state results.

k_{rw}	Error (saturation%)					
	Purcell	F&D	Burdine	R&L min	R&L max	Timmerman
0.050	25.784	22.117	3.450	12.117	8.784	26.117
0.100	28.450	23.117	4.784	12.784	9.784	28.784
0.150	24.884	20.884	2.760	9.551	6.550	26.220
0.157	24.120	20.121	2.640	9.121	6.454	25.787
Avg. error	**25.810**	**21.560**	**3.409**	**10.893**	**7.893**	**26.727**

Table 6.11 Comparison of predicted wetting phase relative permeability (Sample 2).

k_{rw}	Error (saturation%)					
	Purcell	F&D	Burdine	R&L min	R&L max	Timmerman
0.050	28.750	23.340	3.334	12.083	0.000	3.750
0.100	35.416	29.167	8.333	15.417	4.167	10.833
0.150	40.000	31.249	10.426	14.166	5.416	13.336
0.200	37.500	31.251	10.000	12.084	5.834	14.167
0.250	38.330	33.330	12.090	12.074	6.660	15.410
0.3	38.744	33.744	13.33	11.244	7.5	17.077
0.35	38.337	33.333	13.547	10.417	7.927	17.084
Avg. error	**36.725**	**30.774**	**10.151**	**12.498**	**5.358**	**13.094**

Table 6.12 Comparison of predicted wetting phase relative permeability (Sample 5).

k_{rw}	Error (saturation%)					
	Purcell	F&D	Burdine	R&L min	R&L max	Timmerman
0.025	17.000	12.667	2.667	13.333	10.667	35.667
0.050	22.327	16.661	5.327	15.994	12.660	41.994
0.075	23.000	17.666	6.666	16.333	3.000	42.666
0.100	22.667	18.000	6.667	15.667	12.000	42.334
0.120	22.000	18.334	6.667	15.000	12.333	43.000
Avg. error	**21.399**	**16.666**	**5.599**	**15.265**	**10.132**	**41.132**

Table 6.13 Comparison of predicted wetting phase relative permeability (Sample 8).

k_{rw}	Error (saturation%)					
	Purcell	F&D	Burdine	R&L min	R&L max	Timmerman
0.025	17.143	6.786	0.000	16.429	13.929	28.929
0.050	21.071	11.071	5.714	20.000	17.857	36.428
0.075	20.357	10.714	3.214	17.500	15.000	35.357
0.100	18.572	10.000	2.857	15.000	13.214	34.643
0.125	17.857	10.000	3.214	14.286	12.857	35.179
0.15	17.5	9.643	3.571	13.571	12.143	35.357
0.171	17.273	10.488	3.345	12.63	11.559	35.845
Avg. error	**18.539**	**9.815**	**3.131**	**15.631**	**13.794**	**34.534**

Table 6.14 Comparison of predicted wetting phase relative permeability (Sample 15).

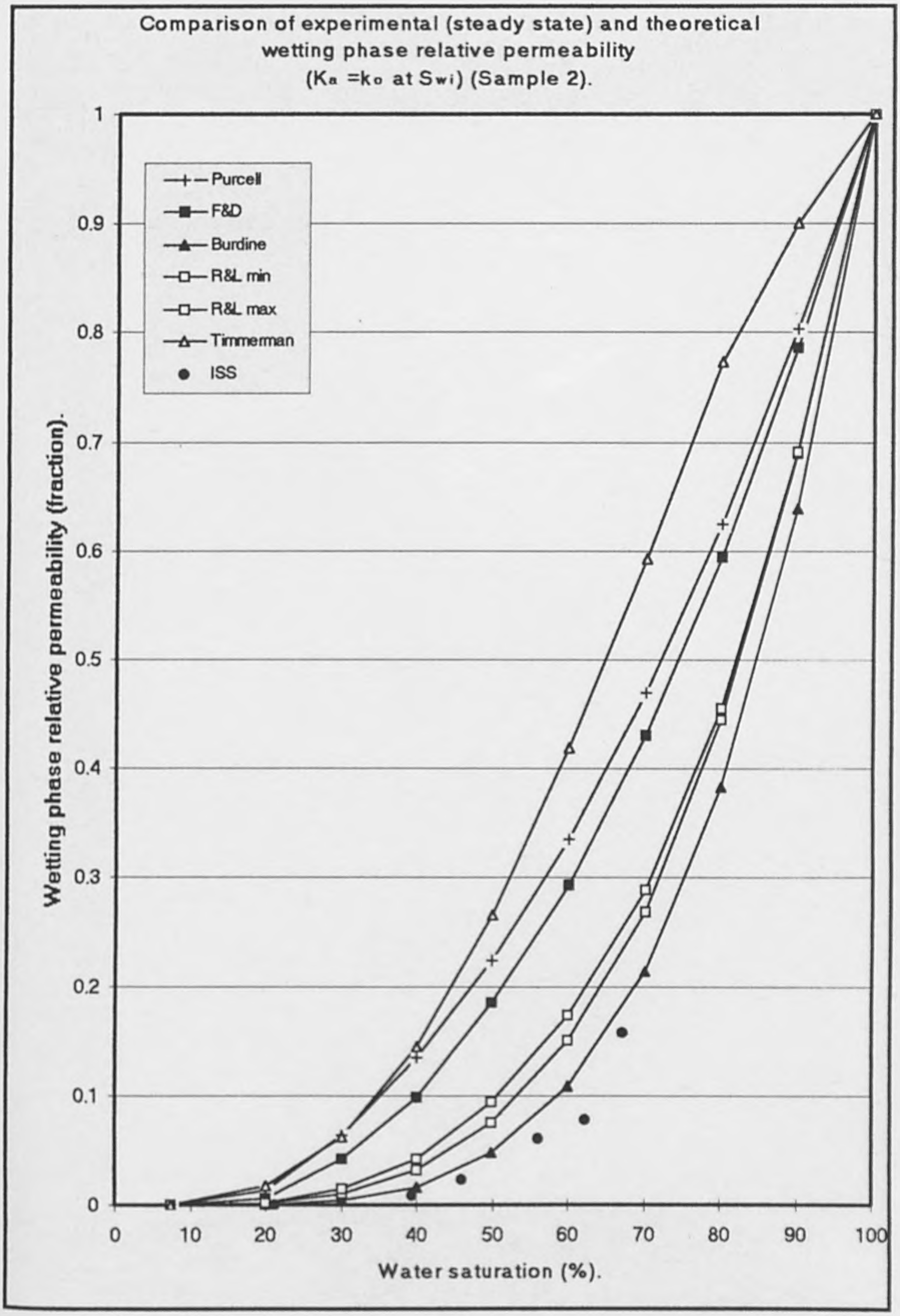

Figure (6.29) Comparison of experimental steady state and theoretical wetting phase relative permeability for Sample 2.

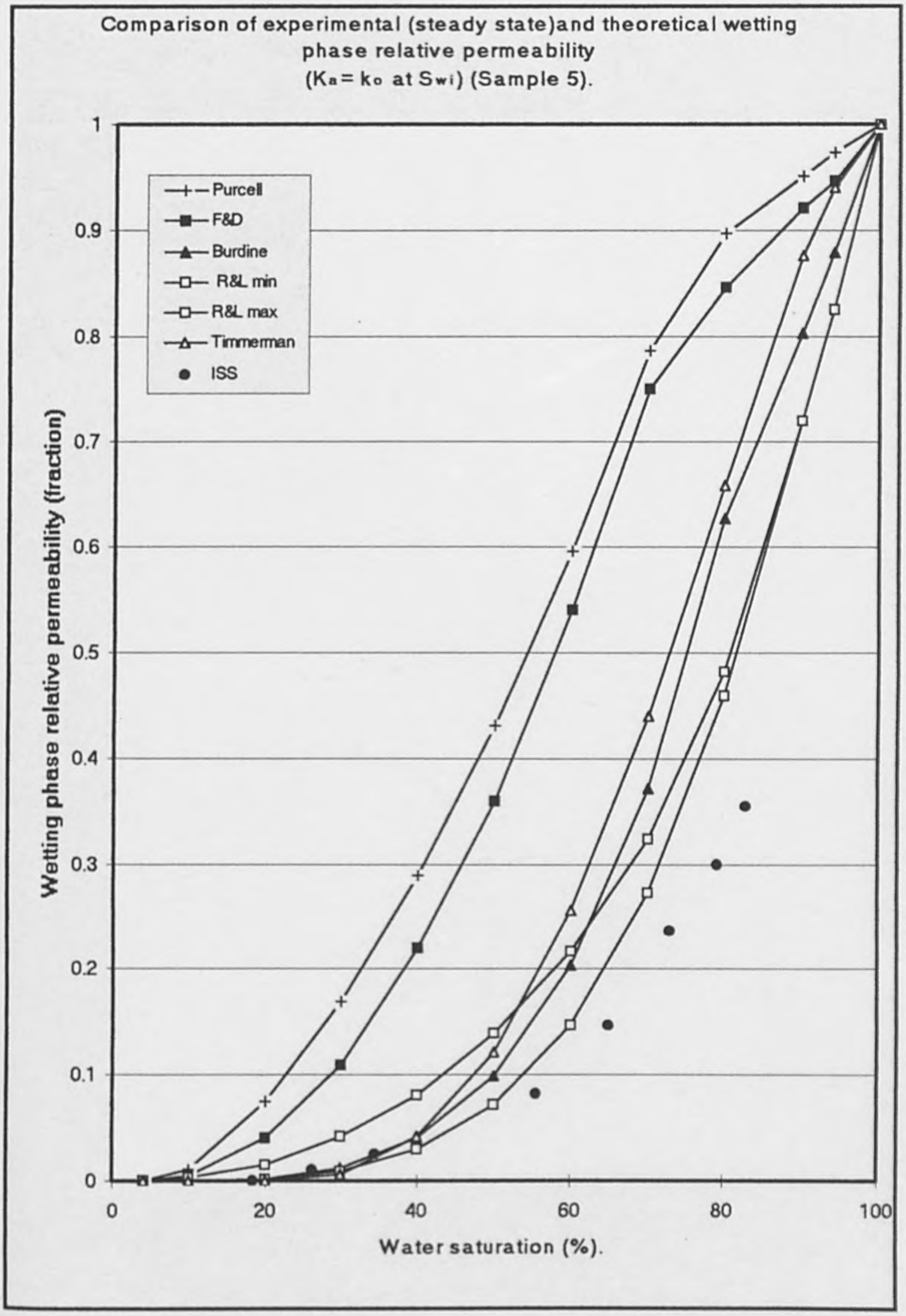

Figure (6.30) Comparison of experimental steady state and theoretical wetting phase relative permeability for Sample 5.

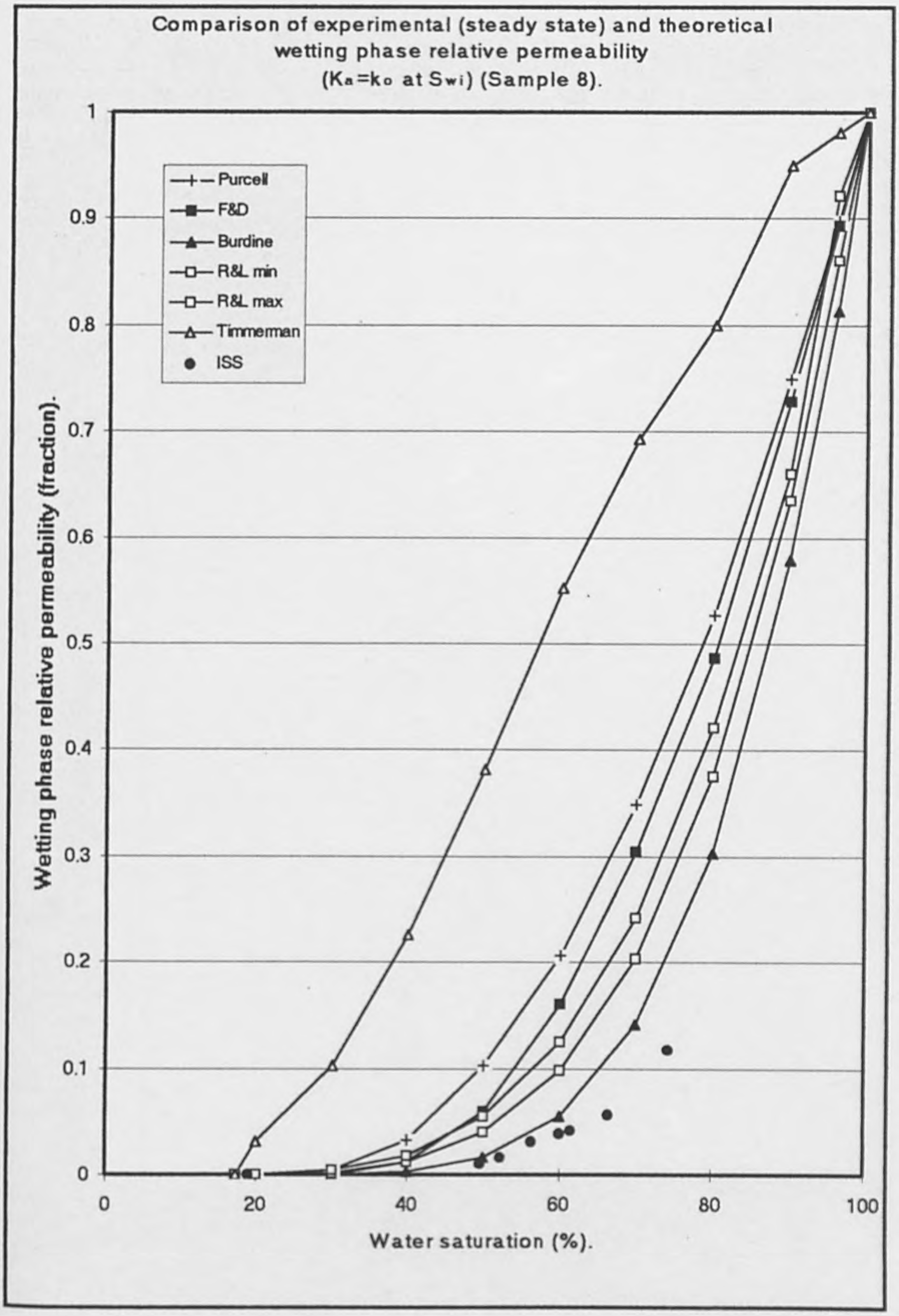

Figure (6.31) Comparison of experimental steady state and theoretical wetting phase relative permeability for Sample 8.

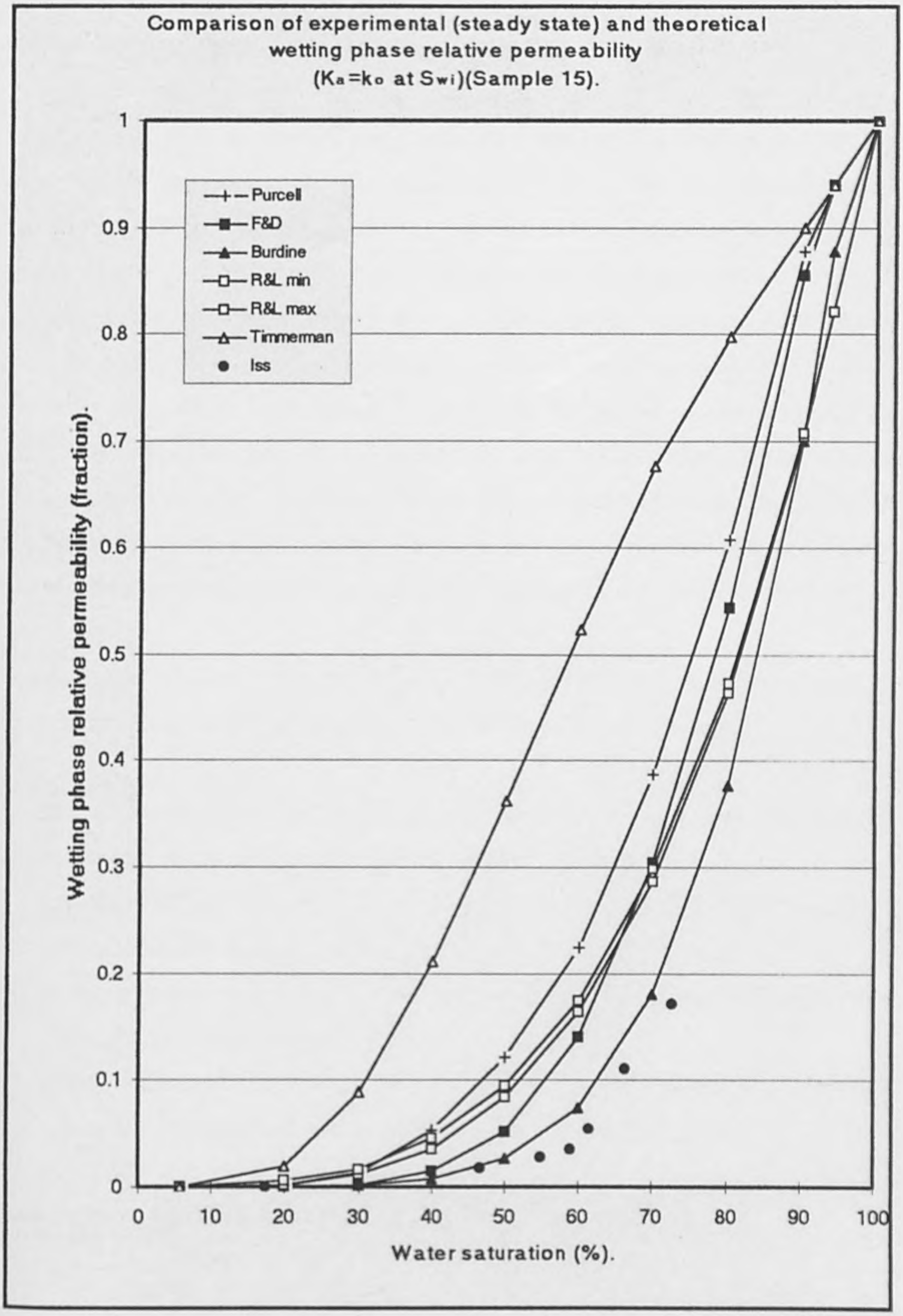

Figure (6.32) Comparison of experimental steady state and theoretical wetting phase relative permeability for Sample 15.

6.5.2.2 Non wetting Phase Relative Permeability Comparison.

In a like manner to the wetting phase data, the mathematically derived non wetting phase relative permeability for the selected water wet samples have been displayed against the experimental steady state relative permeability curves on one graph per sample as shown in Figures 6.33 - 6.36. The oil relative permeability derived from the capillary pressure data by mathematical models showed a very wide range of variations from the experimental data. The discrepancy varies from one correlation to another. Generally all correlations produced a higher error in the oil relative permeability calculations in comparison to the calculated water relative permeability, except Timmerman's correlation. Again, to evaluate these mathematical models for predicting the oil relative permeability, deviation from the laboratory experimental data has been calculated for each model; a comparison summary is presented in Tables 6.15 – 6.18.

Comparing the oil relative permeability generated by the proposed mathematical models to the steady state relative permeability curves led to the following results;

1. Purcell's model led to a cumulative average error of 29.0% saturation varying from an average error of 10.1% at sample 5 to 35.9% at sample 2.
2. Fatt and Dykstra's model led to a cumulative average error of 31.0% saturation varying from an average error of 14.3% at sample 5 to 38.1% at sample 2.
3. Burdine's model led to a cumulative average error of 6.9% saturation varying from an average error of 3.9% at sample 15 to 14.6% at sample 5.
4. Rapoport and Leas's model led to a cumulative average error of 38.8% saturation varying from an average error of 34.3% at sample 5 to 42.3% at sample 2.
5. Timmerman's model led to a cumulative average error of 27.6% saturation varying from an average error of 20.3% at sample 5 to 29.9% at sample 15.

Burdine's equation appeared once more to be the most appropriate for predicting oil relative permeability for water wet rock samples. This also agrees with the unsteady state results. However, this mathematical model, like others, continues producing oil relative permeability values below the residual oil saturation which conflict with the physical reality.

k_{ro}	Error (saturation%)					
	Purcell	**F&D**	**Burdine**	**R&L min**	**R&L max**	**Timmerman**
0.050	35.172	35.172	9.310	36.207	36.207	23.793
0.100	39.655	40.000	8.276	41.379	41.379	24.483
0.150	38.966	39.655	4.828	42.069	42.069	26.207
0.200	38.966	39.655	1.725	42.414	42.414	27.931
0.250	38.276	39.655	0.000	42.759	42.759	28.966
0.300	38.276	39.655	1.724	44.138	44.138	26.897
0.350	37.241	38.966	3.448	44.483	44.483	25.517
0.400	35.862	37.586	4.483	43.792	43.792	25.172
0.45	34.483	36.552	5.862	43.448	43.448	24.138
0.495	22.413	34.483	7.586	42.069	42.413	24.138
Avg. error	**35.931**	**38.138**	**4.724**	**42.276**	**42.310**	**25.724**

Table 6.15 Comparison of predicted non wetting phase relative permeability (Sample 2).

k_{ro}	Error (saturation%)					
	Purcell	**F&D**	**Burdine**	**R&L min**	**R&L max**	**Timmerman**
0.050	18.000	22.800	8.000	26.660	26.660	19.700
0.100	13.267	19.867	11.003	29.997	29.997	20.733
0.150	12.150	17.750	12.670	32.860	32.860	21.340
0.200	12.270	14.770	13.064	34.570	34.570	21.240
0.250	11.610	14.340	13.324	37.010	37.010	20.000
0.300	11.970	14.000	14.670	38.670	38.670	19.670
0.350	12.000	14.340	15.170	39.340	39.340	19.360
0.400	11.340	14.000	15.994	37.940	38.640	19.500
0.450	10.660	13.970	17.000	36.970	38.330	20.430
0.500	10.340	14.170	16.360	36.340	38.340	20.660
0.550	10.003	13.670	16.830	35.660	38.000	21.030
0.600	10.310	14.310	15.990	36.010	38.610	20.500
0.650	8.940	13.673	16.200	35.640	38.000	20.660
0.700	7.530	12.690	15.967	34.360	37.700	20.800
0.750	5.830	12.330	15.597	33.170	36.830	20.830
0.800	3.670	9.330	15.661	31.640	35.340	20.060
0.840	2.660	8.000	15.330	26.970	34.270	18.340
Avg. error	**10.150**	**14.354**	**14.637**	**34.342**	**36.069**	**20.285**

Table 6.16 Comparison of predicted non wetting phase relative permeability (Sample 5).

k_{ro}	Error (saturation%)					
	Purcell	F&D	Burdine	R&L min	R&L max	Timmerman
0.050	31.000	31.000	9.334	30.334	31.334	40.000
0.100	35.666	35.666	8.333	35.333	36.666	36.333
0.150	38.001	38.667	7.667	38.667	39.667	35.666
0.200	37.334	38.000	4.000	38.334	39.667	35.000
0.250	36.667	37.667	2.000	38.667	39.667	33.834
0.300	35.666	36.666	0.334	39.000	39.666	32.667
0.350	34.833	36.099	1.840	39.166	39.833	31.234
0.370	35.167	36.500	1.667	39.333	40.667	30.334
Avg. error	**35.542**	**36.283**	**4.397**	**37.354**	**38.396**	**34.384**

Table 6.17 Comparison of predicted non wetting phase relative permeability (Sample 8).

k_{ro}	Error (saturation %)					
	Purcell	F&D	Burdine	R&L min	R&L max	Timmerman
0.050	29.132	29.311	6.379	32.586	32.586	32.931
0.100	30.739	31.454	4.138	35.966	35.966	32.758
0.150	35.135	35.850	5.172	41.034	41.034	28.966
0.200	36.454	37.525	3.794	42.761	42.761	28.621
0.250	37.247	38.855	2.413	43.793	43.793	28.276
0.270	37.747	39.175	1.379	44.138	44.138	27.586
Avg. error	**34.409**	**35.362**	**3.879**	**40.046**	**40.046**	**29.856**

Table 6.18 Comparison of predicted non wetting phase relative permeability (Sample 15).

6.6 Mathematical Models General Discussions

The present study is restricted to mathematical models that derive relative permeability data from capillary pressure curves. The models considered are;

1. Purcell
2. Burdine
3. Rapoport and Leas
4. Timmerman
5. Fatt and Dykstra

These models were discussed in chapter 2. Precisely, these relative permeability mathematical models fall under one of the following categories;

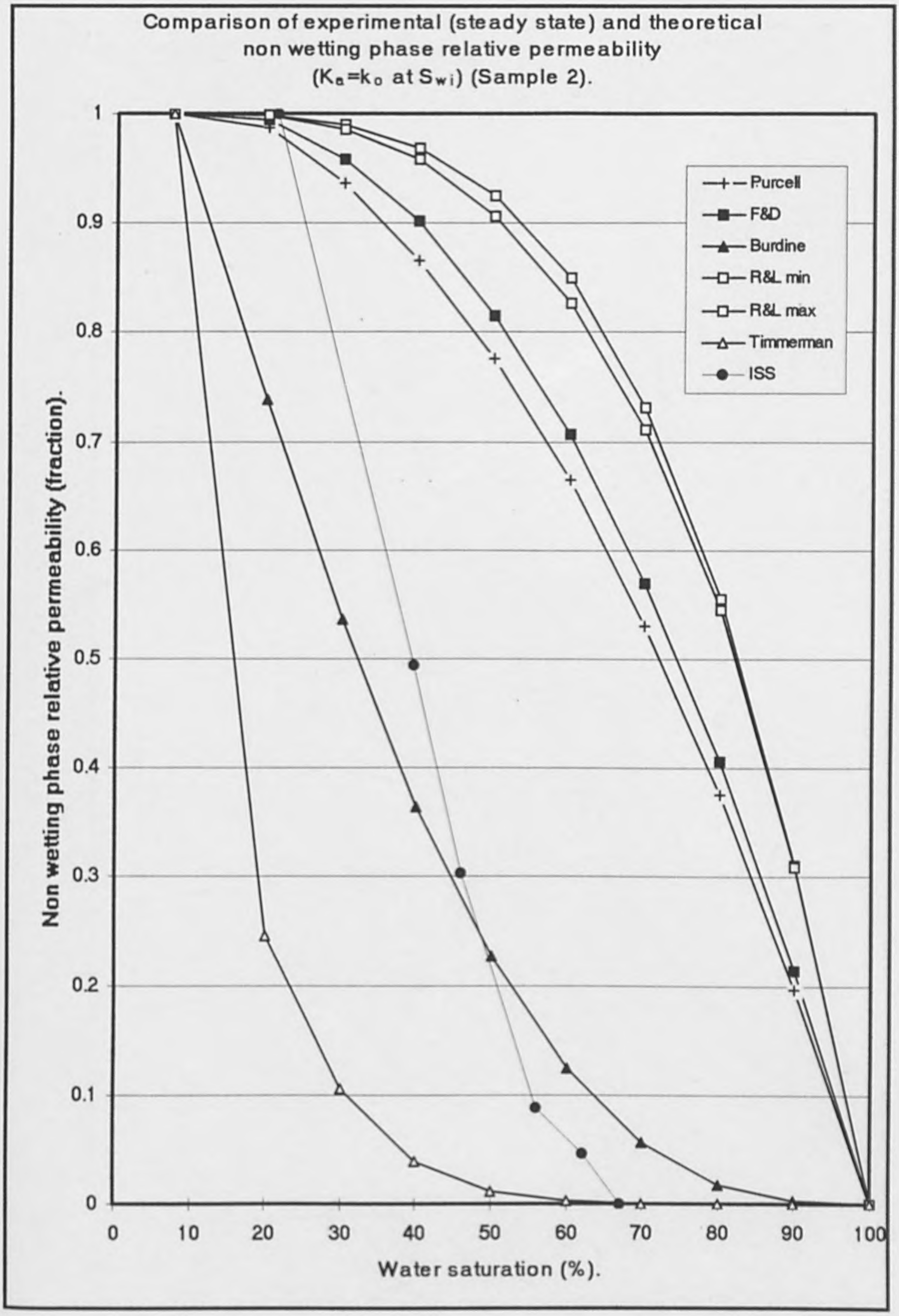

Figure (6.33) Comparison of experimental steady state and theoretical non wetting phase relative permeability for Sample 2.

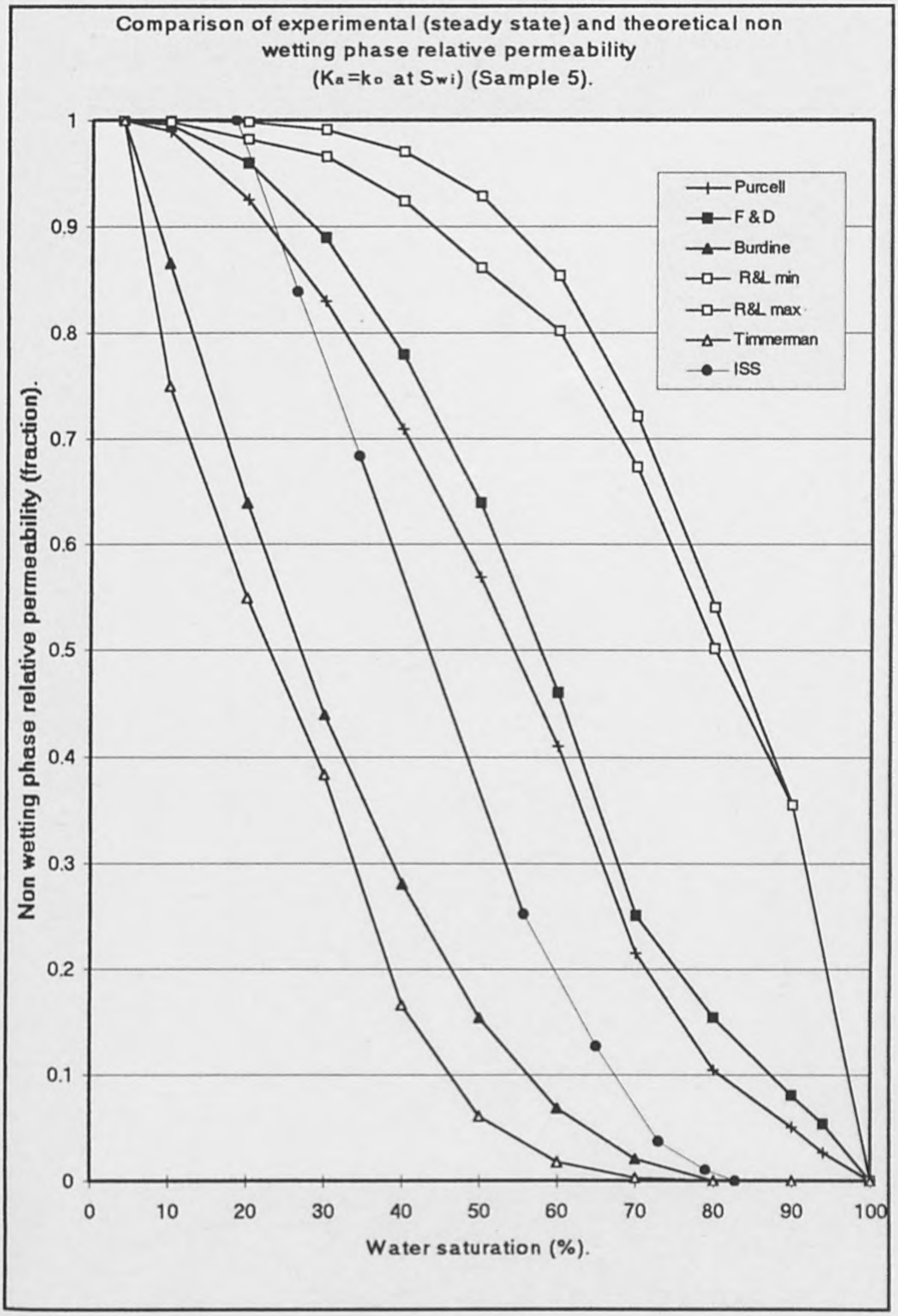

Figure (6.34) Comparison of experimental unsteady state and theoretical non wetting phase relative permeability for Sample 5.

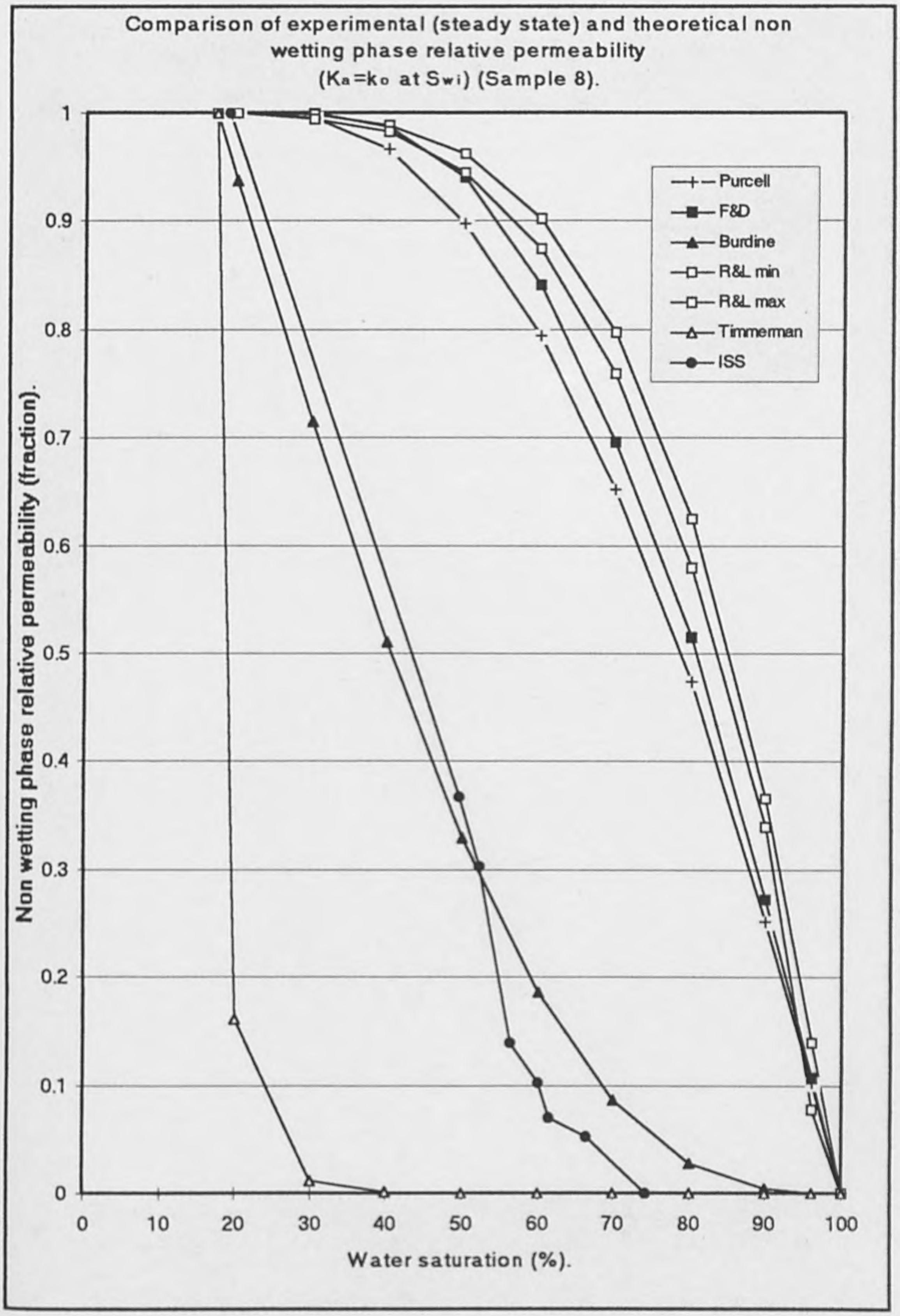

Figure (6.35) Comparison of experimental unsteady state and theoretical non wetting phase relative permeability for Sample 8.

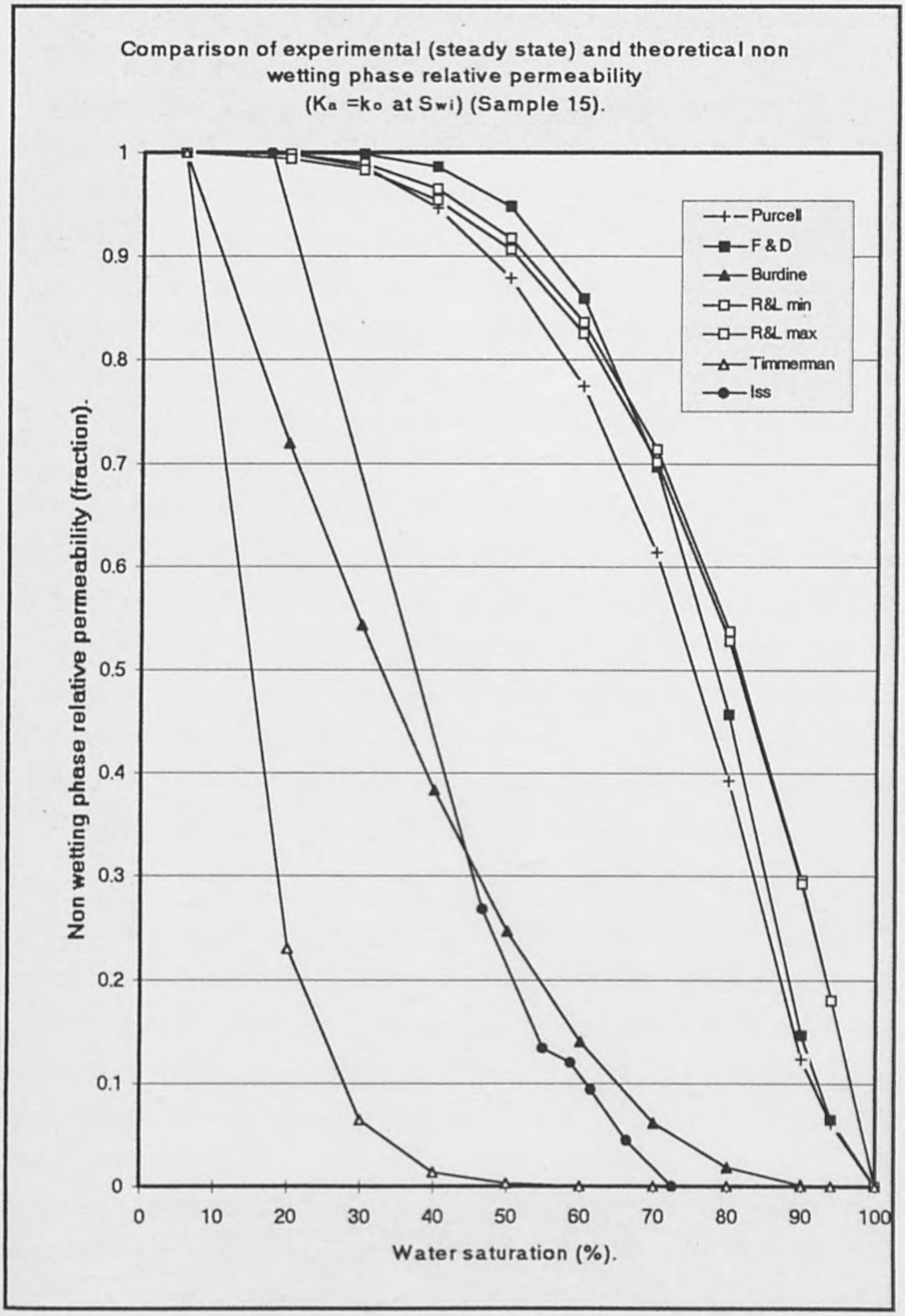

Figure (6.36) Comparison of experimental unsteady state and theoretical non wetting phase relative permeability for Sample 15.

1. **Capillary models**, these models are based on simulating the porous media by a bundle of capillary tubes of various diameters with the fluid path equal to longer than the sample. Capillary models ignore the the interconnected nature of the pores.
2. **Statistical models,** are based on modeling the porous media by a bundle of capillary tubes of various diameters distributed randomly. The model is then divided into a large number of thin slices by planes perpendicular to the axes of the tubes. The slices are rearranged and reassembled randomly. Again the main deficiency of the statistical model is that it is not capable of handling the interconnected pore spaces.
3. **Empirical models,** are based on empirical relationships that fit data obtained experimentally. In general empirical models have provided the most successful approximation[24].
4. **Purcell,** based his mathematical model on the assumption that the porous medium consists of a number of capillary tubes all of the same length but different diameters. This model is classified as a capillary model. Assuming straight capillary tubes completely neglects the tortuosity of the actual flow path and the interconnected pore spaces. One other serious limitations is that it assumes that the summation of wetting and non wetting relative permeability equal to 1.0. This is not true; in practice k_{rwt}+ k_{rnwt} is always less than 1.0. For these reasons, Purcell model failed to provide any satisfactory results for all the water wet selected samples.

Burdine based his mathematical model on the assumption that the porous medium consists of a number of capillary tubes of the same length and of different diameters which is Capillary Model too, but considered each radii interval has an effective length, and apparent length. So, he introduced the concept of tortuosity factor (effective length/apparent length) which is more representative of the flow paths within porous media. Burdine ignored the interconnected nature of the pores within the medium and assumed a constant tortuosity for a given porous medium. The use of the constant value for the tortuosity in Burdine model may allow us to consider this model as a semi-empirical model. Burdine's model produced outstanding results for all selected samples compared to all other mathematical models. Due to the complex nature of the porous media it is believed that empirical or semi-empirical approaches provide the most successful model. Wyllie and Gardner[135], (Section 2.8.7) presented two equations for oil and gas relative permeability calculations. Their model was based on a statistical approach (statistical model). When these equations are generalized for wetting and non-wetting phase relative permeabilities, if the oil is considered to be the wetting phase and the gas is non wetting phase then the equations will be identical to those derived by Burdine.

Fatt and Dykstra presented two equations for the minimum and maximum wetting phase relative permeability. Their equations were based on surface energy relationships and the Kozeny–Carman equation. The equations were presented as defining limits for wetting phase relative permeability. The model implicitly assumed that the porous medium consists of a number of capillary tubes of different diameters from which the areas were calculated. The main weakness of this model is that it carries all the assumptions of the Kozeny–Carman equation, and furthermore the non wetting phase relative permeability is calculated assuming that $k_{rwt}+ k_{rnwt}$ equal to 1.0. As a result the error in the non wetting phase relative permeability is extremely high.

Timmerman presented two equations for oil and water relative permeabilities calculated from capillary pressure data. His equations were based on proposed empirical relationships describing experimentally measured relative permeabilities. The main weakness of this model is that it was developed to fit data for one particular field without allowing for any variations in rock properties, including rock wettability. Generalizing the model led to very poor results.

Fatt and Dykstra developed an equation for predicting the wetting phase relative permeability. It was based on the Purcell equation, which assumes that the porous medium consists of a number of capillary tubes of the same length but different diameters. They introduced a so called lithology factor which is essentially a correction for the deviation of the path length from the length of the porous medium. This model also ignores the interconnected nature of the porous media, and assumes that, the non wetting relative permeability is calculated only by assuming that $k_{rwt} + k_{rnwt} = 1.0$. This explains the deficiency of the model in producing reliable relative permeability in general and the non wetting phase relative permeabilities in particular.

All these mathematical models have another serious weaknesses;

1. They ignore the effect of other rock properties including wettability variations and are assumed to be valid for any wettability including intermediate wettability, where definition of the wetting and non wetting phase is very difficult task.

2. They do not allow for the fact that oil reservoirs have a residual oil saturation. This is a serious misrepresentation, as models definitely produce incorrect oil relative permeability values at water saturations $\geq (1.0 - S_{or})$.

Taking these points into consideration, the Burdine model has been modified to suit water wet reservoir rock samples and to allow for the residual oil saturation. The newly modified model is presented in chapter 7.

CHAPTER 7

APPLICATIONS TO THE PRACTICE OF CORE ANALYSIS

7.1 Introduction

The results obtained show that, the use of existing mathematical models for deriving relative permeability data from capillary pressure curves for water wet reservoir rock samples leads to significant errors. Although Burdine's model exhibited "numerically" a reasonable agreement with the experimental data, yet, using this model in its existing form certainly produces serious errors. In this chapter, Burdine's model will be presented in a newly modified form which suits water wet reservoir rock samples, and allows for the residual oil saturation by normalising relative permeability data between S_{or} and S_{wi}. The modified (semi-empirical) model has been verified, including an error analysis when applied to the representative rock samples, moreover, the validity of the use of centrifuge or mercury injection data has been verified also. This chapter also presents two new approaches for air-brine capillary pressure and permeability measurements.

7.2 The Modified Burdine Model

Based on proposed empirical relationships describing the experimentally obtained relative permeability data for a set of homogeneous water wet sand stone samples and after careful considerations for many rock properties such as wettability and porosity. Burdine model has been successfully modified to fit best the carefully planed steady state experimental data. The new equations for wetting and non wetting phase relative permeability can be presented as follows: -

$$k_{rwt} = \left(\frac{S_{wt} - S_{wi}}{1 - S_{wi}}\right)^{\left(\frac{\alpha_{wt}}{1-\phi}\right)} \frac{\int_{s=0}^{s=S_{wt}} dS/P_c^{\,2}}{\int_{s=0}^{s=1} dS/P_c^{\,2}} \tag{7.1}$$

And,

$$k_{rnwt} = \left(\frac{S_{wt} - S_{wi}}{1 - S_{wi}}\right)^{\left(\alpha_{nwt}(1-\phi)\right)} \frac{\int_{s=S_{wt}}^{s=1} dS/P_c^{\,2}}{\int_{s=0}^{s=1} dS/P_c^{\,2}} \tag{7.2}$$

Where:

k_{rwt} = wetting phase relative permeability

k_{rnwt} = nonwetting phase relative permeability

S_{wt} = wetting phase saturation

S_{wi} = irreducible water saturation

ϕ = porosity

α_{wt} = wetting phase constant (for water wet medium = **2.2)**

α_{nwt} = non wetting phase constant (for water wet medium = **1.4)**

Although the above equations produced very close results in comparison to Burdine's model but still generate oil relative permeability below the residual oil saturation. Therefore, the newly generated relative permeability is normalised as follows;

$$S_w^* = S_w\left((1-S_{or}-S_{wi\text{-}pc})/(1-S_{wi\text{-}wf})\right) + b \tag{7.3}$$

This will restrict the oil relative permeability values to the two real end points, which are 1.0 at S_{wi} and Zero at S_{or}

Where,

S_w^* = normalised water saturation

S_w = measured water saturation

S_{or} = irreducible oil saturation

$S_{wi\text{-}pc}$ = irreducible water saturation from water flood

$S_{wi\text{-}wf}$ = irreducible water saturation from capillary pressure

b = the intercept when assuming a straight line conversion factor

7.2.1 Verification of the Modified Model

Wetting and non wetting phase relative permeabilities for samples 2, 5, 8 and 15 have been generated using the newly modified model. The mathematically obtained data has been compared to the experimental steady state relative permeabilities with oil permeability at the irreducible water saturation (k_o at S_{wi}) as a reference point. The new model also has been compared to the original Burdine model. Similarly, the capillary pressure data used has been obtained by the air-brine method.

7.2.1.1 Wetting Phase Relative Permeability Verification.

The wetting phase relative permeability generated by the newly modified model has been compared to the steady state experimental data as well as the curves generated by Burdine's model. As shown in Figures 7.1-7.4 the data generated by the new model demonstrates excellent agreement with the laboratory data in comparison with the Burdine Model. To assess the new model quantitatively, deviation (in saturation units) from the steady state laboratory experimental data has been calculated and then compared to the corresponding deviation of the Burdine model. Comparison summary is presented in Table 7.1 Comparing the oil relative permeabilities generated by the new model with the steady state relative permeability curves and the Burdine model led to the following results;

The new model led to average errors of 1.3%, 3.1%, 2.3% and 1.2% for samples 2, 5, 8 and 15 respectively, while, Burdine's model led to average errors of 3.4%, 10.1%, 5.6% and 3.1% for samples 2, 5, 8 and 15 respectively. Obviously the wetting phase relative permeability predicted by the new model is in much closer agreement with the experimental data than the Burdine model.

7.2.1.2 Non Wetting Phase Relative Permeability Verification.

In the same manner, the non wetting phase relative permeabilities for the selected water wet samples derived using the new model have been displayed against the experimental steady state data, togather with curves generated by Burdine's model, as shown in Figures 7.5-7.8. The oil relative permeabilities derived from the capillary pressure data by the newly developed model show outstanding agreement with the steady state laboratory data in general and the Burdine model in particular. Again, to evaluate the new model for predicting the oil relative permeability, deviation from the laboratory experimental data has been calculated for each sample, then compared to the Burdine model. A comparison summary is presented in Tables 7.2 Comparing the oil relative permeability generated by the new model to the steady state data and to the Burdine model, led to the following results;

The new model led to average errors of 0.7%, 0.27%, 1.0% and 1.8% for samples 2, 5, 8 and 15 respectively, whereas, Burdine's model led to average errors of 7.8%, 14.6%, 3.1% and 6.2% for the same samples. Definitely, the new model showed outstanding results in general and compared to the Burdine model in particular. This can be explained as follows:

Burdine model does not allow for the residual oil saturation; this is a feature of all other proposed mathematical models for deriving relative permeability from capillary pressure curves. Hence the model continues to generate oil relative permeability data for water saturations > $(1.0 - S_{or})$. This contradicts one of the fundamental concepts of fluid flow in oil reservoirs. The oil flow will cease within a porous medium as soon as its saturation reaches the residual oil saturation (S_{or}), since the oil permeability becomes zero for any oil saturation less than or equal to S_{or}. Using these false relative permeabilities in classical reservoir engineering calculations will incorrectly predict that the reservoir will produce far more oil than is physically possible. Consequently, the predicted oil recovery will be higher than real recoverable oil. In any case omitting the fact that all oil reservoirs must have a residual oil saturation is a serious misrepresentation and models definitely will produce false oil relative permeability values at water saturation $\geq (1.0 - S_{or})$.

Burdine's model also does not allow for wettability variations. It is assumed that it will fit any reservoir rock wettability. The new model has been developed to suit water wet samples only and further investigations are required before utilising it for intermediate or oil wet samples.

7.2.2 Applications of the New Model in Reservoir Engineering

The model has been developed to be efficient and flexible to suit the practical applications of relative permeability data for oil reservoirs. It is recommended that it should be utilised as follows:

1. **No history matching data available;** the model can be used as presented in Equations 7.1 and 7.2 to predict wetting and non-wetting phase relative permeabilities. The results obtained are considered to be the most reliable estimate. To give some room for uncertainty, the model can also be used with upside and downside scenarios as shown in Figures 7.1 –7.2. This can be obtained by changing the wetting phase constant (α_{wt}) to 2.8 for the downside and 2.2 for the upside, and the non-wetting phase constant (α_{nwt}) to 0. 8 for the downside and 1.8 for the upside. This technique will provide reasonable guide for preliminary studies when no data is available for history matching.

2. **History matching data available;** Generally, when using of the relative permeabilities in reservoir simulation, some concerns arise from the scaling of micromodel core plug data to simulation grid size displacement. There are no proven rules for obtaining valid relative permeability data for reservoir modeling[23] hence, relative permeability curves in simulators are checked by history matching. If the history match is not acceptable, the relative permeability curves are modified by "tuning[191]. The new model has been presented in a form that can be easily used in reservoir simulation. Furthermore, the model can readily generate an unlimited number of wetting and non-wetting phase relative permeability curves simply by varying α_{wt} and α_{nwt}. This makes the new model very practical in tuning relative permeability curves for history matching in reservoir simulation as well as in classical reservoir engineering calculations.

7.2.3 Validity of Centrifuge and Mercury Injection Data

All the mathematically obtained relative permeability data presented in this project were derived from air brine capillary data. To verify the validity of using the centrifuge and the mercury injection capillary pressure data in predicting relative permeability curves, the new modified model has been used to generate wetting and non wetting phase relative permeability curves for all selected water wet samples. The applied capillary pressure data was obtained by the centrifuge and mercury injection techniques (Figures 6.19 and 6.20).

Figures 7.9 –7.12 show a comparison of water relative permeabilities derived from centrifuge, mercury injection and air-brine (**data derived from the air-brine capillary pressure is referred to as modified in all figures**) capillary pressure data with the experimental steady state measurements. A comparison summary is presented in tables 7.3-7.4. The results obtained by the three capillary pressure techniques demonstrate excellent agreement. Applying the air-brine capillary pressure data led to a cumulative average error of 2%, using the centrifuge and mercury injection data led to cumulative average errors of 2.8% and 4% respectively. This is in agreement with results obtained by Espach and Fray[190]. Their conclusion was;

> ***"A comparison of mercury-injection method with the restored-state (porous plate) method of measuring capillary pressure showed that the two yielded nearly identical results"***[190]

The oil relative permeabilities derived from the capillary pressure data obtained by centrifuge, mercury injection and air-brine for samples measurements 2, 5, 8 and 15 have also been compared with the experimental steady state oil relative permeabilities as shown in Figures 7.13-7.16. A comparison summary is presented in Tables 7.5-7.6. Again the oil relative permeabilities obtained by the three capillary pressure determination techniques show very good agreement. Applying the air-brine capillary pressure data led to a cumulative average error in oil relative permeability of 0.93%, using the centrifuge and mercury injection data led to cumulative average errors of 1.6% and 2.3% respectively.

From the results obtained, it can be concluded that relative permeability curves can be reliably generated from capillary pressure data obtained by the air-brine, centrifuge or mercury injection methods. This makes the technique more versatile and widely applicable in practice.

7.3 New Experimental Approach for Air-Brine Capillary Pressure Measurements

7.3.1 Introduction

Nevertheless, the capillary pressure measurement is classified as a special core analysis, capillary pressure curves for any reservoir rock must be established. Essentially, three techniques are commonly used to generate this data. The methods are; porous plate (porous diaphragm), centrifuge and mercury injection. Each method has some advantages and disadvantages. The porous plate method is the only technique in which the fluid desaturation occurs by capillary displacement. This makes the method is the most representative of capillary displacement in oil reservoirs. On the other hand, achieving complete desaturation (capillary equilibrium) at each pressure step requires several days. Obtaining a complete air-brine capillary pressure curve will take weeks; using oil/water will take years. This makes the technique very time consuming, and it lacks the speed of the other methods. A new technique is presented in which the time required for capillary equilibrium is significantly reduced. Consequently the total time to obtain the complete air-brine capillary pressure curve can be reduced and adopting the new method can make the use of oil/water porous plate capillary pressure practical.

7.3.2 The new Approach (Background and Results)

The new technique primarily relies on altering the sampling procedure. Conventionally, all tested samples are core plugs of 1-1.5 inches (2.54-3.81cm) diameter and around 2.5 inches (6.35cm) length. Assuming 1.5 inches (3.81cm) diameter, gives an average core plug bulk volume of 4.4in^3 (72cm^3). As samples are placed upside during capillary pressure measurements, the apparent flow path (ignoring tortuosity) varies from

2.5inches (6.35cm) at the top, decreasing towards the contact surface with the porous plate It is believed that reducing the fluid path length will allow desaturation to occur more rapidly. Shortening conventional core plug samples will reduce the bulk volume dramatically, consequently, apart from the misrepresentation of the short samples due to this reduction in volume, accurate saturation measurements becomes impossible. To obtain representative samples with sufficient bulk volume and having a very short flow path, small disks must be targeted from the whole core rock ample. The whole core disks can provide a reliable bulk volume for very thin samples. For instance, 0.22inches (0.55cm) length disk of 5inches (12.7cm) diameter whole core gives 4.4in^3 (72cm^3) bulk volume. This is equivalent to the average core plug volume. Using large size cores will expose a larger area of the test rock sample for desaturation and the fluid travels for a shorter distance. This makes it possible to achieve complete desaturation (capillary equilibrium) in a shorter time. To verify the new method, the following experimental work has been carried out: -

1. Three 5 inch diameter whole core disks with different thicknesses (Disk 1 = 1inches (2.54cm), Disk 2 = 0.35inches (0.9cm), and Disk 3 = 0.12inches (0.3cm)) and one conventional 1.5inches (3.81cm) diameter core plug (2.5inches (6.35cm) long) were cut from a Clashach Sandstone rock sample.
2. The retrieved core plug and disks were cleaned and saturated with brine. Routine measurements are presented in Table 3, Appendix I.
3. Using the porous plate method, capillary pressure has been applied on all disks and core plug at six pressure steps (0.5 (3.44), 1.0 (6.89), 3.0 (20.68), 8.0 (55.15), 16 (110.3) and 32psi (220.63kPa)). The fluid desaturation was monitored thoroughly against time for each pressure step. Obtained results are presented in Figures 7.17-a - 7.17-e. Results can be summarized as follows;

Disk 3 appeared to be the first sample that attains capillary equilibrium almost over the complete range of pressure steps followed by Disk 2 and Disk 3 respectively. For instance, as shown in Figure 7.17-a at 0.5psi (3.4kPa) desaturation pressure. Disk 3 stabilised before 40 hrs, where Disk 2, Disk 1 and the core plug stabilized at 64, 72 and 96hrs respectively. Similar results were obtained at 1.0 (6.9), 3.0 (20.7) and 8psi

(55kPa). (Figures 7.17-b to7.17-d in agreement with 7.17-a). Figures 7.17-b and 7.17-c exhibited interesting results in that no significant variation in time of equilibrium between the core disks and/or core plug as samples approach the irreducible water saturation (S_{wi}) at higher pressures (16 and 32psi) (110 and 220kPa). From previous results the following can be concluded: -

- Using thin large diameter whole core disks definitely reduces time of capillary equilibrium especially at high fluid saturations. This reduces the time and the cost of the porous plate capillary pressure measurements.
- It was notable that the time of equilibrium has a proportional relationship with the disk thickness. Therefore using very thin disks can dramatically strengthen the inherited weakness of the technique. Additionally the new approach may allow the use of water/oil capillary pressure measurements to be practical rather than theoretical. If the technique proved to be success in water/oil system it would be a big breakthrough in core analyses.
- As water saturation approach S_{wi} the effect of sample size becomes negligible, This can be attributed to the fact that as water saturation becomes closer to S_{wi} and the displaced volume is extremely small hence, will be no fluid accumulation on the contact surface.

7.4 New Approach for Permeability Measurements

Permeability is one of the most essential rock properties for petroleum engineers. It is the key factor in production and well completion optimization, moreover, it is essential in overall reservoir management and development. Despite its importance no in-situ measurement can be obtained without resorting to the complicated and expensive pressure testing or coring. However, the most common and widely used measurement technique is core analysis. In liquid (oil or water) permeability Darcy's law is directly applied as follows:-

Oil or water flows at a constant rate (Q) through the rock sample; upstream and downstream pressure (P_1 and P_2) are recorded. Knowing the fluid viscosity (μ), the sample length (L) and the end face cross sectional area (A), the liquid permeability (K_L) is calculated from the Darcy equation as follows:-

$$K_L = \frac{Q\mu L}{A(P_1 - P_2)} \tag{7.4}$$

The equation assumes a constant pressure gradient through the tested rock sample. In practice, the pressure gradient along the conventional core plug is usually higher at the inflow end. Therefore the application of Darcy's Law for permeability measurements using the upstream and downstream pressure values may lead to some errors, especially in the following cases:-

1. Low permeability samples.
2. Formation damage assessment

In both cases pressure gradient varies along the tested rock sample. As illustrated below,

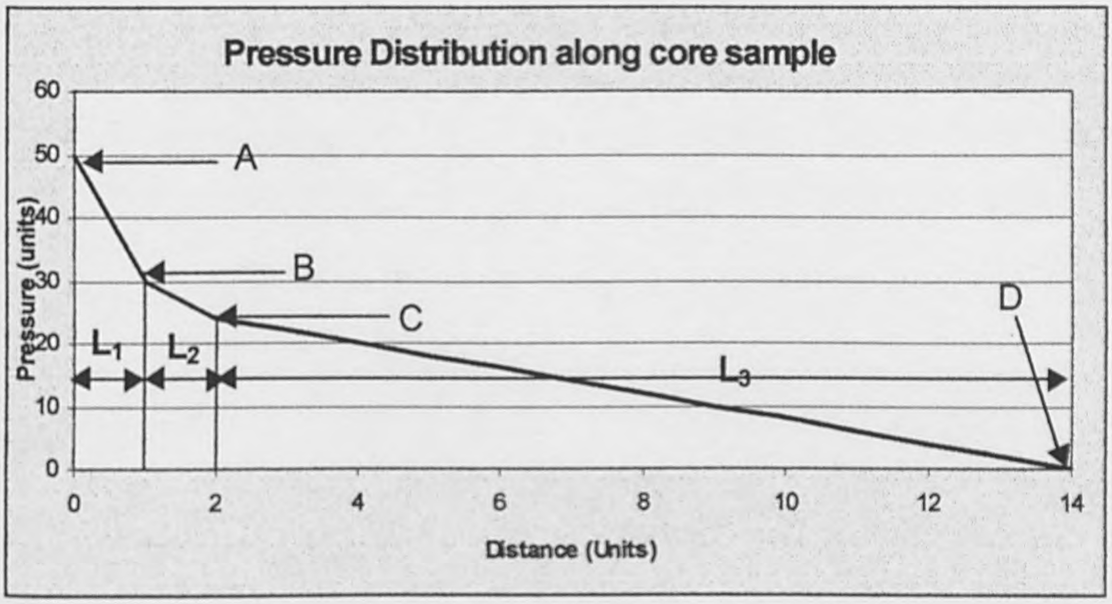

pressure gradient is high near the inflow end, but stabilizes towards the outflow end. Conventionally the pressure gradient = $(P_A - P_D)/L$ where $L = (L_1 + L_2 + L_3)$. In reality (as illustrated above) there is at least another three different gradients which are:-

Gradient 1= $(P_A - P_B)/L_1$

Gradient 2= $(P_B - P_C)/ L_2$

Gradient 3 = $(P_A - P_D)/ L_3$

Each gradient will give a different permeability. Using the conventional gradient leads to incorrect permeability and makes the permeability varies with sample length. In homogeneous rock samples, permeability must be measured using the stabilized pressure gradient, i.e. the pressure drop due to the inflow end effect ($P_A - P_C$) and the corresponding sample length ($L_1 + L_2$) must be ignored. Consequently, Darcy's Equation should be used in the following form:-

$$K_L = \frac{Q\mu(L - L')}{A(P_1 - P' - P_2)} \tag{7.5}$$

Where

$L' = L_1 + L_2$

$P' = P_A - P_C$

Similarly, in formation damage assessment the depth of mud invasion must be allowed for.

This approach is presented only for discussion. It requires some experimental work a using multi-pressure sensor core holder. Resources were not available to curry this out during the present project, but the intention is to undertake the work in the near future.

Sample 2			Sample 5			Sample 8			Sample 15		
Error (Saturation%)			Error (Saturation%)			Error (Saturation%)			Error (Saturation%)		
k_{rw}	Burd.	Mod.	k_{rw}	Burd.	Mod.	k_{rw}	Burd.	Mod.	k_{rw}	Burd.	Mod.
0.05	3.450	0.343	0.050	3.334	9.480	0.025	2.667	0.666	0.025	0.000	2.143
0.1	4.784	1.037	0.100	8.333	4.425	0.050	5.327	2.330	0.050	5.714	1.786
0.15	2.760	1.725	0.150	10.426	2.860	0.075	6.666	3.000	0.075	3.214	1.428
0.157	2.640	2.190	0.200	10.000	2.240	0.100	6.667	2.334	0.100	2.857	0.714
			0.250	12.090	0.355	0.120	6.667	3.167	0.125	3.214	0.357
			0.300	13.330	0.710				0.150	3.571	0.357
			0.358	13.547	1.883				0.171	3.345	1.380
Avg. Error	**3.409**	**1.324**	**Avg. Error**	**10.151**	**3.136**	**Avg. Error**	**5.599**	**2.299**	**Avg. Error**	**3.131**	**1.166**

Table 7.1 Comparison between Burdine and the modified model wetting phase relative permeability.

Sample 2			Sample 5			Sample 8			Sample 15		
Error (Saturation%)			Error (Saturation%)			Error (Saturation%)			Error (Saturation%)		
k_{ro}	Burd.	Mod.	k_{ro}	Burd.	Mod.	k_{ro}	Burd.	Mod.	k_{ro}	Burd.	Mod.
0.050	9.310	3.769	0.050	8.000	0.340	0.050	9.343	2.330	0.050	6.379	3.189
0.100	8.276	0.172	0.100	11.003	0.173	0.100	8.333	0.667	0.100	4.138	1.761
0.150	*4.828*	*1.103*	*0.150*	*12.670*	*0.160*	*0.150*	*7.667*	*1.661*	*0.150*	5.172	*1.921*
0.200	1.725	1.034	0.200	13.064	0.231	0.200	4.000	0.006	0.200	3.794	2.168
0.250	0.000	1.366	0.250	13.324	0.500	0.250	2.000	1.003	0.250	2.413	2.783
0.300	1.724	0.607	0.300	14.670	0.170	0.300	0.334	2.000	0.300	0.361	2.504
0.350	3.448	0.538	0.350	15.170	0.040	0.350	1.840	3.170	0.350	1.071	2.500
0.400	4.483	0.759	0.400	15.994	0.040	0.400	1.660	2.330	0.400	2.143	2.143
0.450	5.862	1.034	0.450	17.000	0.030	0.450	1.640	1.640	0.450	3.571	1.786
0.500	6.897	0.665	0.500	16.360	0.040	0.500	2.000	1.340	0.500	5.357	1.428
0.550	8.000	1.000	0.550	16.830	0.030	0.550	2.670	1.000	0.550	5.715	2.143
0.600	8.700	0.700	0.600	15.990	0.010	0.600	2.830	1.160	0.600	6.429	1.786
0.650	9.300	0.300	0.650	16.200	0.040	0.650	2.990	0.990	0.650	7.143	1.786
0.700	10.000	0.570	0.700	15.967	0.700	0.700	2.670	0.330	0.700	8.035	1.786
0.750	10.400	0.000	0.750	15.597	0.770	0.750	2.670	0.000	0.750	8.928	2.143
0.800	11.200	0.000	0.800	15.661	0.330	0.800	2.340	0.000	0.800	9.286	1.428
0.850	11.830	0.030	0.850	14.994	0.940	0.850	2.330	0.000	0.850	10.000	1.428
0.900	12.400	0.000	0.900	15.000	0.700	0.900	2.000	0.000	0.900	10.357	1.071
0.950	13.300	0.000	0.950	15.010	0.160	0.950	1.330	0.000	0.950	11.071	0.357
1.000	*13.970*	*0.000*	*1.000*	*14.300*	*0.000*	*1.000*	2.340	*0.000*	*1.000*	*11.786*	*0.000*
Avg. Error	**7.783**	**0.682**	**Avg. Error**	**14.640**	**0.270**	**Avg. Error**	**3.149**	**0.981**	**Avg. Error**	**6.157**	**1.806**

Table 7.2 Comparison between Burdine and the modified model non wetting phase relative permeability.

Sample 2				Sample 5			
Error (Saturation%)				Error (Saturation%)			
k_{rw}	Air-Brine	Mercury	Centrifuge	k_{rw}	Air-Brine	Mercury	Centrifuge
0.05	0.343	0.883	1.883	0.050	9.480	11.33	8.660
0.1	1.037	0.12	0.12	0.100	4.425	5.497	2.997
0.15	*1.725*	*1.78*	*1.44*	*0.150*	*2.860*	*3.914*	*0.884*
0.157	2.19	29.54	1.546	0.200	2.240	2.666	0.830
				0.250	0.355	1.009	1.160
				0.300	0.710	0.173	2.500
				0.358	1.883	1.251	2.917
Avg. Error	**1.324**	**8.081**	**1.247**	Avg. Error	**3.136**	**3.691**	**2.850**

Table 7.3 Comparison between wetting phase relative permeabilities derived from capillary pressure data using different techniques (Samples 2 & 5).

Sample 8				**Sample15**			
Error (Saturation%)				**Error (Saturation%)**			
k_{rw}	**Air-Brine**	**Mercury**	**Centrifuge**	**k_{rw}**	**Air-brine**	**Mercury**	**Centrifuge**
0.025	0.666	5.333	7.667	0.025	2.143	6.428	10.714
0.05	2.330	0.340	3.673	0.050	1.786	0.714	2.857
0.075	*3.000*	*0.334*	*2.001*	*0.075*	*1.428*	*1.786*	3.929
0.100	2.334	0.667	1.000	0.100	0.714	3.036	4.286
0.120	3.167	1.333	0.000	0.125	0.357	2.600	3.214
				0.150	0.357	2.143	2.678
				0.171	1.380	1.513	1.834
Avg. Error	**2.299**	**1.601**	**2.868**	**Avg. Error**	**1.166**	**2.603**	**4.216**

Table 7.4 Comparison between wetting phase relative permeabilities derived from capillary pressure data using different techniques (Samples 8 & 15).

Sample 2				**Sample 5**			
Error (Saturation%)				**Error (Saturation%)**			
k_{ro}	**Air-Brine**	**Mercury**	**Centrifuge**	**k_{ro}**	**Air-Brine**	**Mercury**	**Centrifuge**
0.050	3.769	2.414	4.487	0.050	0.340	1.300	0.000
0.100	0.172	1.379	0.692	0.100	0.173	1.657	0.003
0.150	*1.103*	*0.687*	*1.213*	*0.150*	*0.160*	2.330	*0.000*
0.200	1.034	0.172	1.379	0.200	0.231	2.270	0.430
0.250	1.366	0.001	1.366	0.250	0.500	3.000	1.340
0.300	0.607	0.688	0.607	0.300	0.170	3.000	1.170
0.350	0.538	1.034	0.008	0.350	0.040	2.670	1.340
0.400	0.759	0.516	0.349	0.400	0.040	2.340	1.000
0.450	1.034	0.516	0.345	0.450	0.030	2.000	1.000
0.500	0.665	1.035	0.035	0.500	0.040	2.670	0.040
0.550	1.000	0.630	0.000	0.550	0.030	2.330	1.330
0.600	0.700	0.900	1.000	0.600	0.010	3.340	4.670
0.650	0.300	1.050	1.050	0.650	0.040	3.500	3.000
0.700	0.570	0.930	0.900	0.700	0.700	3.860	2.690
0.750	0.000	1.300	1.300	0.750	0.770	3.830	2.770
0.800	0.000	1.150	1.150	0.800	0.330	2.840	2.840
0.850	0.030	1.100	1.100	0.850	0.940	3.330	4.140
0.900	0.000	0.860	0.860	0.900	0.700	2.360	2.530
0.950	0.000	0.140	0.100	0.950	0.160	1.330	1.300
1.000	*0.000*	*0.079*	*0.079*	*1.000*	*0.000*	*0.000*	*0.000*
Avg. Error	**0.682**	**0.829**	**0.901**	**Avg. Error**	**0.270**	**2.498**	**1.580**

Table 7.5 Comparison between non wetting phase relative permeabilities derived from capillary pressure data using different techniques (Samples 2 & 5).

Sample 8				Sample1 5			
Error (Saturation%)				Error (Saturation%)			
k_{ro}	Air-Brine	Mercury	Centrifuge	k_{ro}	Air-Brine	Mercury	Centrifuge
0.050	2.330	0.251	2.853	0.050	3.189	0.382	1.761
0.100	0.667	3.460	0.701	0.100	1.761	3.025	1.046
0.150	*1.661*	*4.345*	*2.276*	*0.150*	*1.921*	*5.850*	*2.635*
0.200	0.006	3.092	1.540	0.200	2.168	5.739	3.596
0.250	1.003	2.873	0.460	0.250	2.783	5.997	3.497
0.300	2.000	1.793	0.276	0.300	2.504	5.718	3.932
0.350	3.170	0.879	1.190	0.350	2.500	5.893	4.286
0.400	2.330	1.320	0.404	0.400	2.143	5.715	4.286
0.450	1.640	2.286	0.217	0.450	1.786	5.358	4.286
0.500	1.340	2.172	0.448	0.500	1.428	4.821	3.572
0.550	1.000	2.271	0.719	0.550	2.143	5.357	4.286
0.600	1.160	2.199	0.820	0.600	1.786	4.643	3.929
0.650	0.990	2.630	1.251	0.650	1.786	4.643	3.929
0.700	0.330	2.876	1.497	0.700	1.786	4.643	3.572
0.750	0.000	2.448	1.413	0.750	2.143	3.929	3.215
0.800	0.000	2.359	1.325	0.800	1.428	3.285	3.214
0.850	0.000	1.596	1.251	0.850	1.428	2.500	2.500
0.900	0.000	0.822	0.822	0.900	1.071	2.143	2.143
0.950	0.000	0.394	0.394	0.950	0.357	1.072	1.072
1.000	*0.000*	*0.635*	*0.635*	*1.000*	*0.000*	*0.000*	*0.000*
Avg. Error	**0.981**	**2.035**	**1.025**	**Avg. Error**	**1.806**	**4.036**	**3.038**

Table 7.6 Comparison between non wetting phase relative permeabilities derived from capillary pressure data using different techniques (Samples 8 & 15).

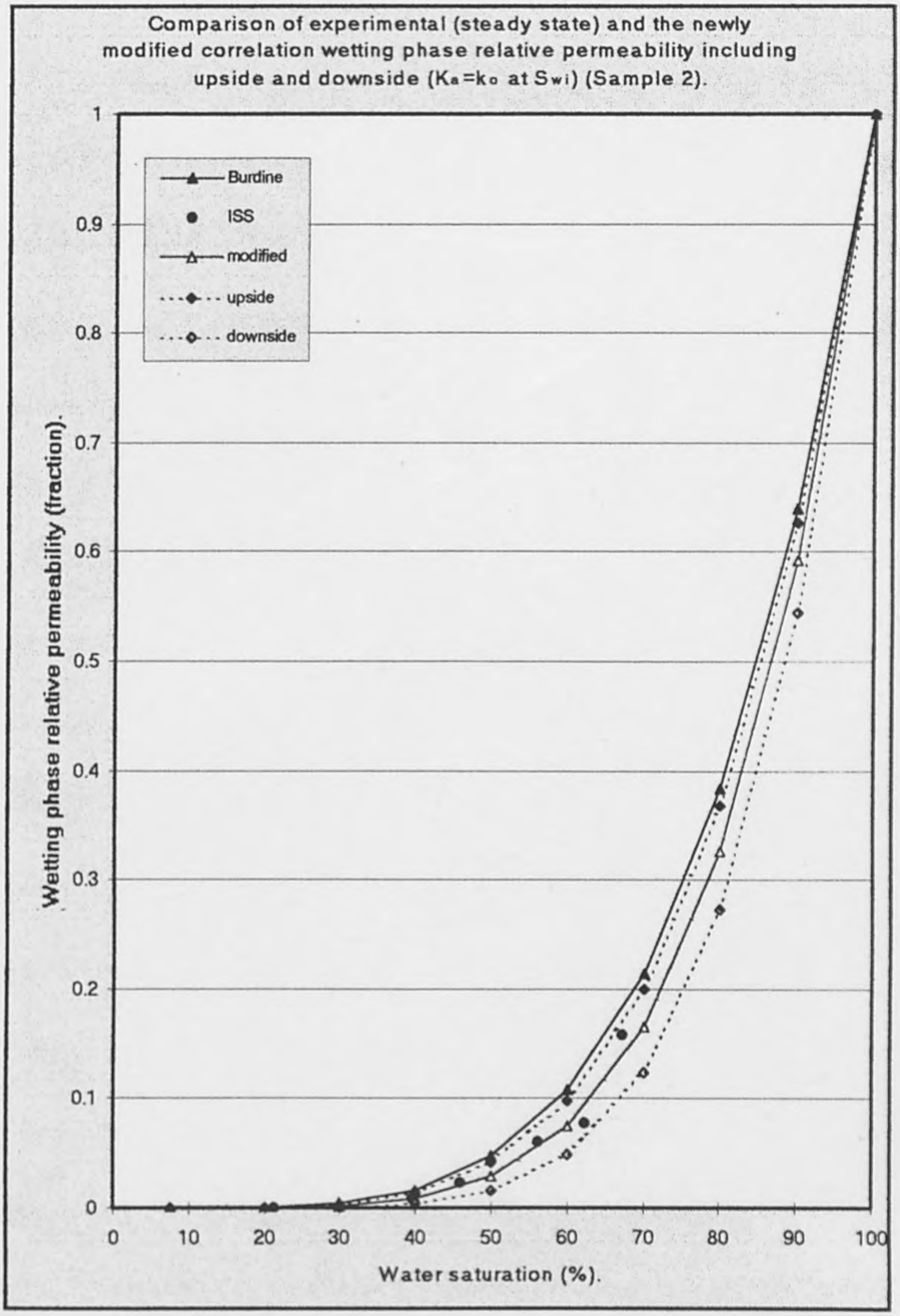

Figure (7.1) Comparison of experimental steady state and theoretical (Burdine & the modified model) wetting phase relative permeability for Sample 2.

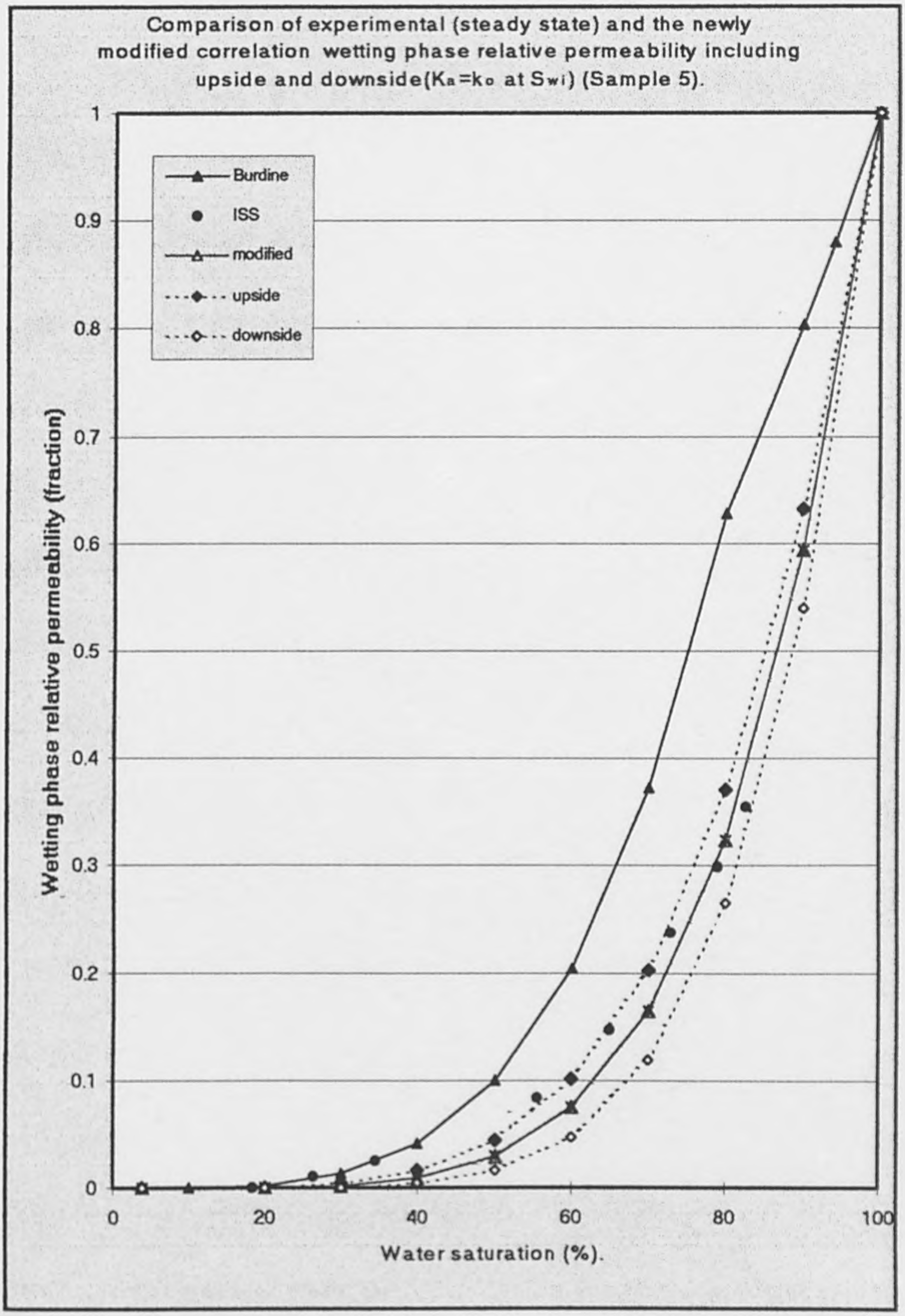

Figure (7.2) Comparison of experimental steady state and theoretical (Burdine & the modified model) wetting phase relative permeability for Sample 5.

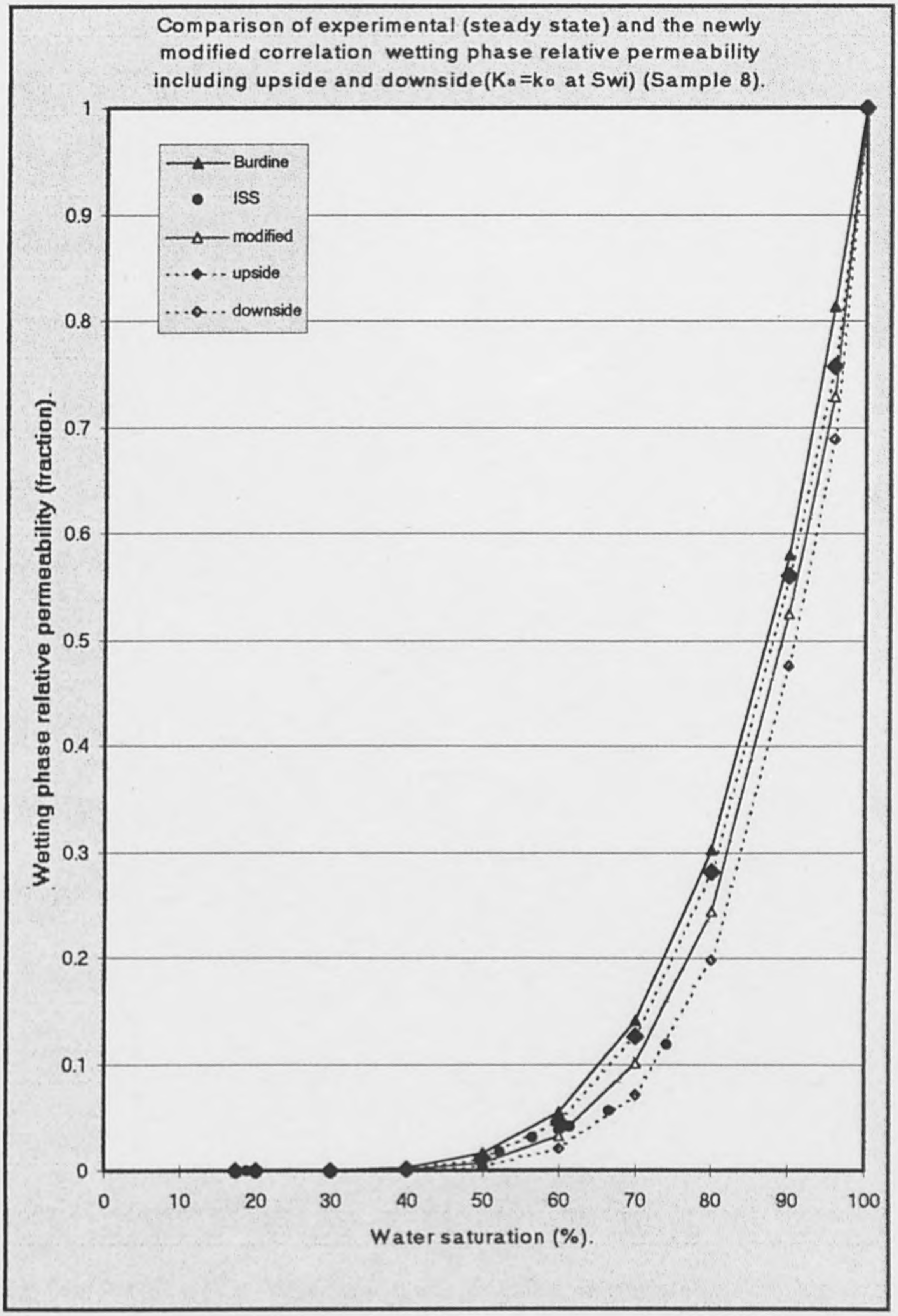

Figure (7.3) Comparison of experimental steady state and theoretical (Burdine & the modified model) wetting phase relative permeability for Sample 8.

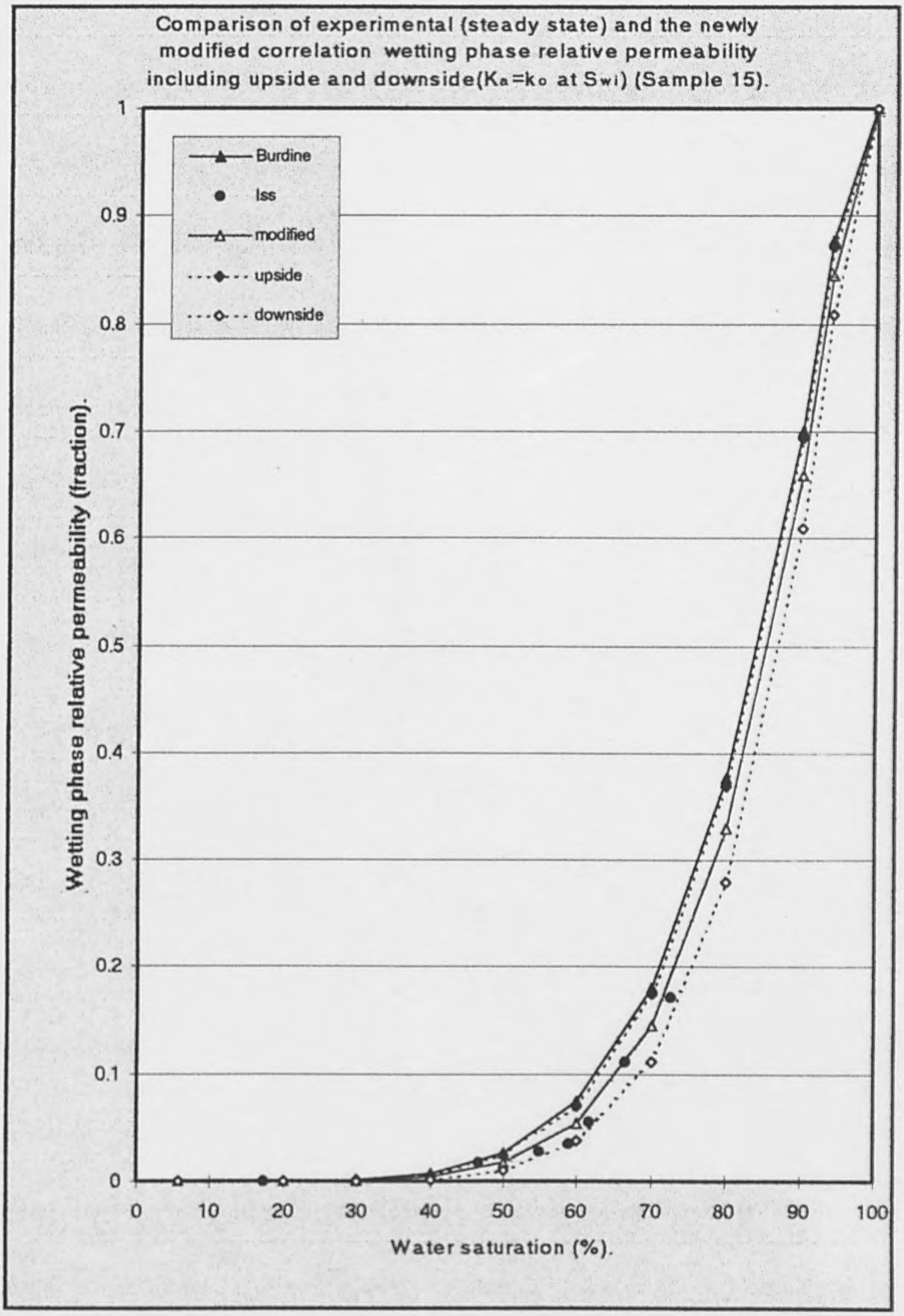

Figure (7.4) Comparison of experimental steady state and theoretical (Burdine & the modified model) wetting phase relative permeability for Sample 15.

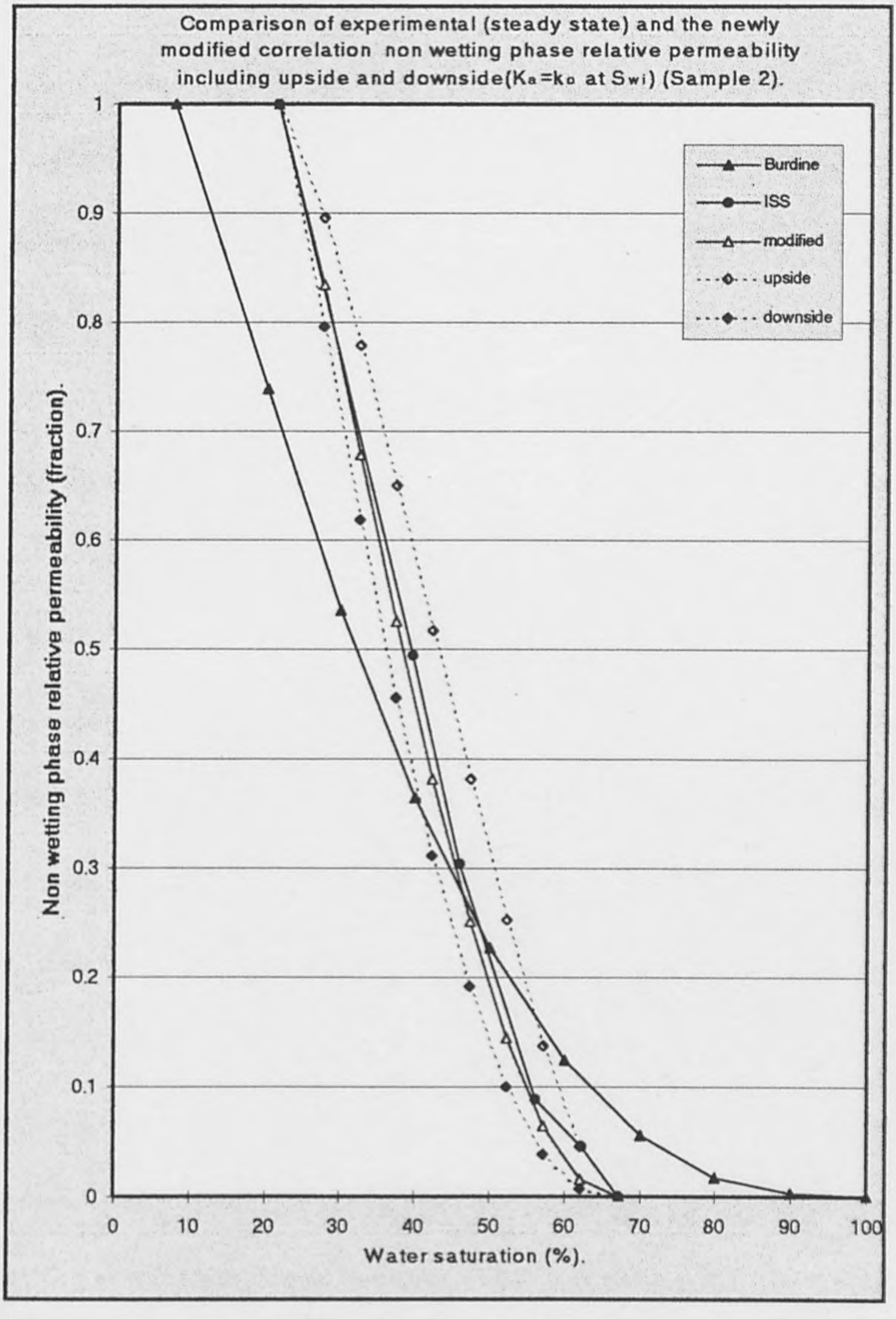

Figure (7.5) Comparison of experimental steady state and theoretical (Burdine & the modified model) non wetting phase relative permeability for Sample 2.

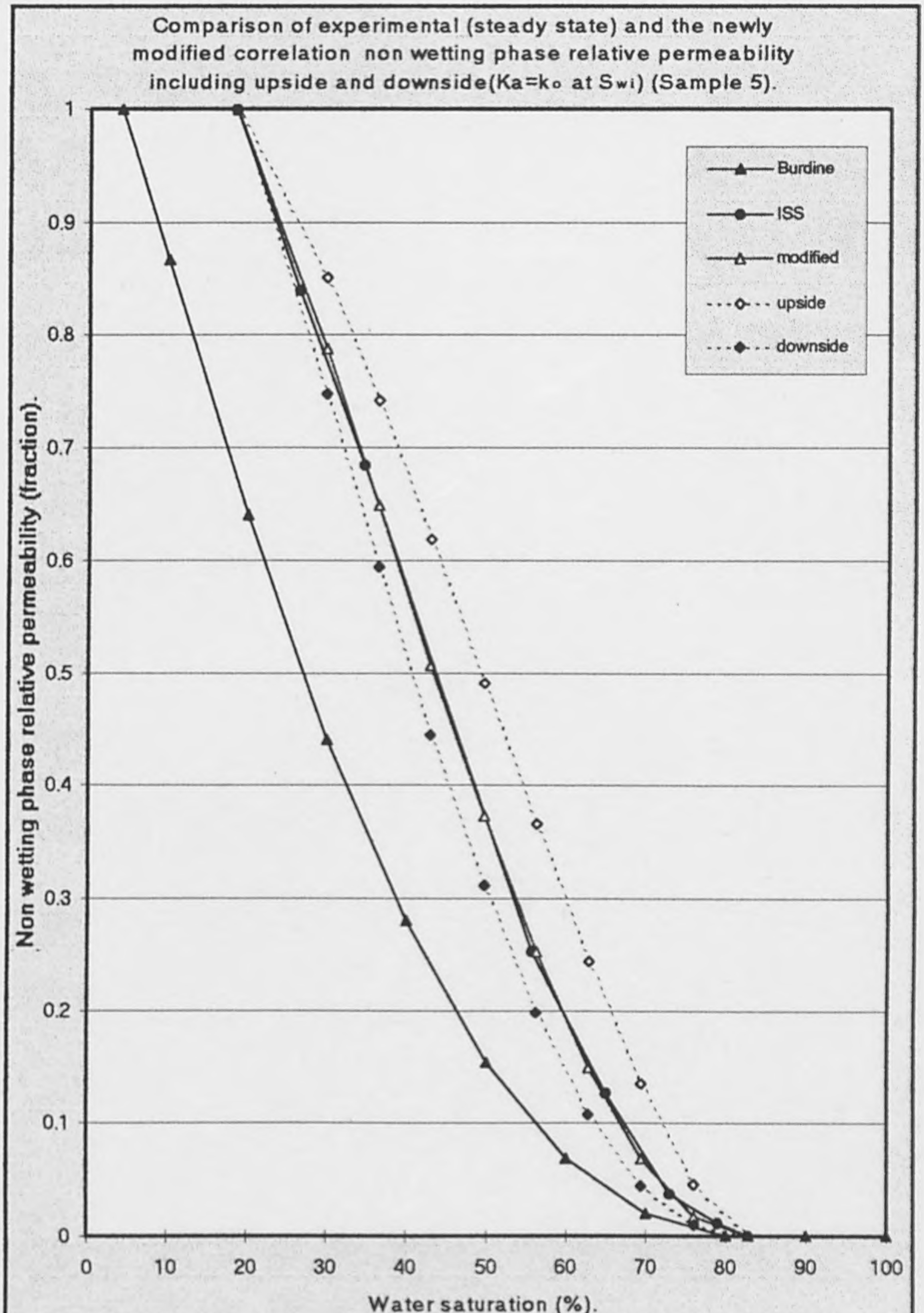

Figure (7.6) Comparison of experimental steady state and theoretical (Burdine & the modified model) non wetting phase relative permeability for Sample 5.

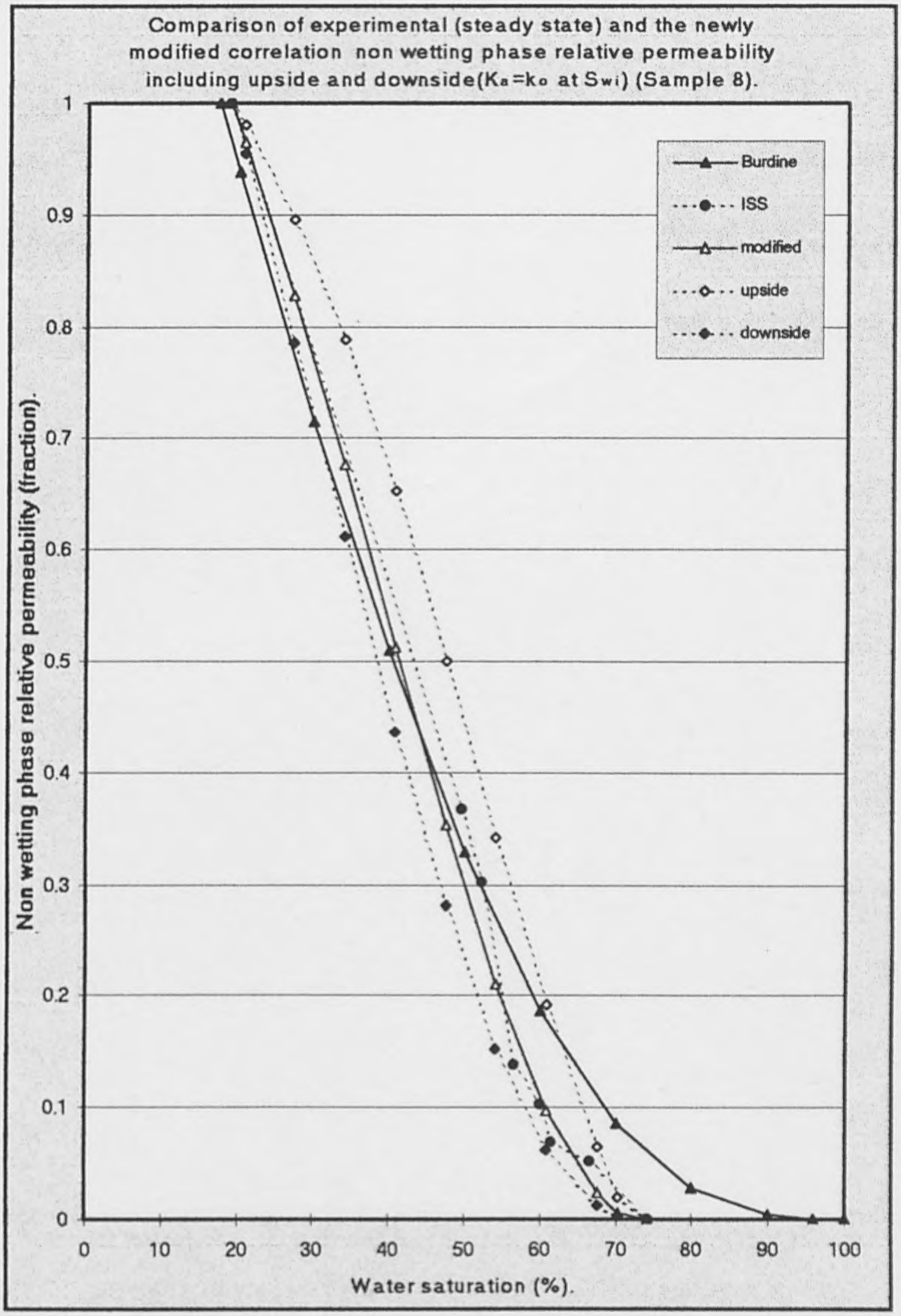

Figure (7.7) Comparison of experimental steady state and theoretical (Burdine & the modified model) non wetting phase relative permeability for Sample 8.

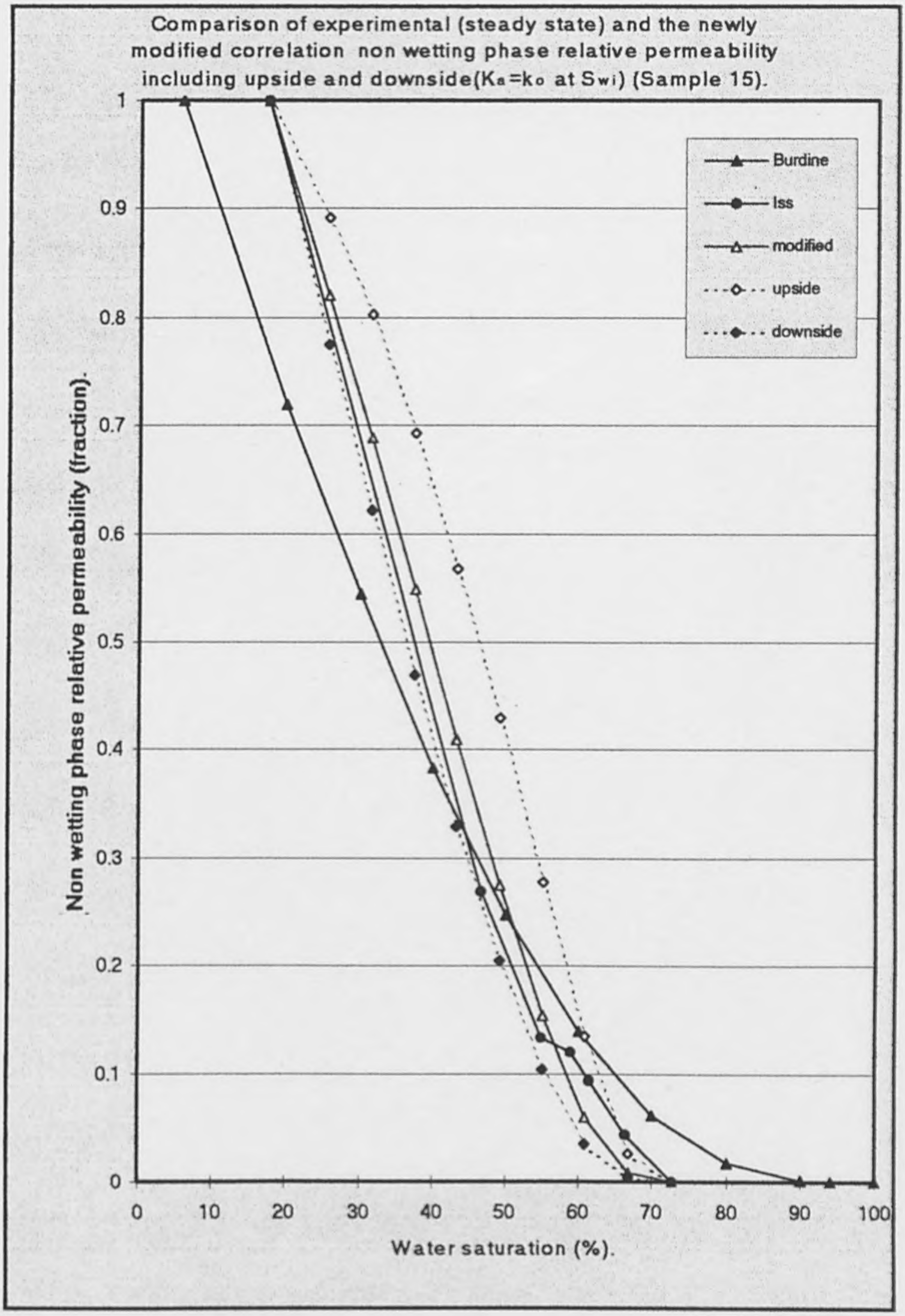

Figure (7.8) Comparison of experimental steady state and theoretical (Burdine & the modified model) non wetting phase relative permeability for Sample 15.

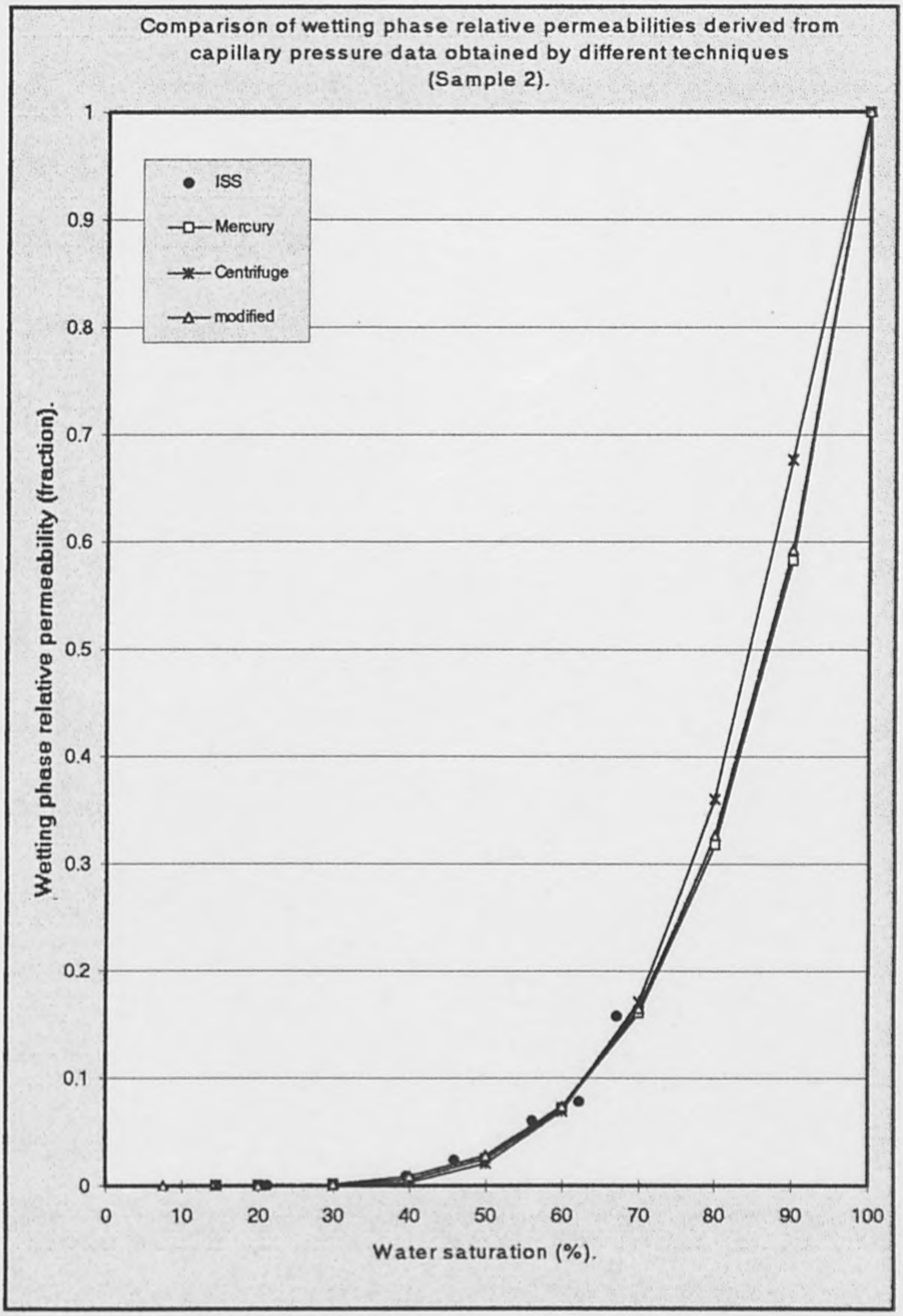

Figure (7.9) Comparison of wetting phase relative permeabilities derived from different capillary pressure technique for Sample 2.

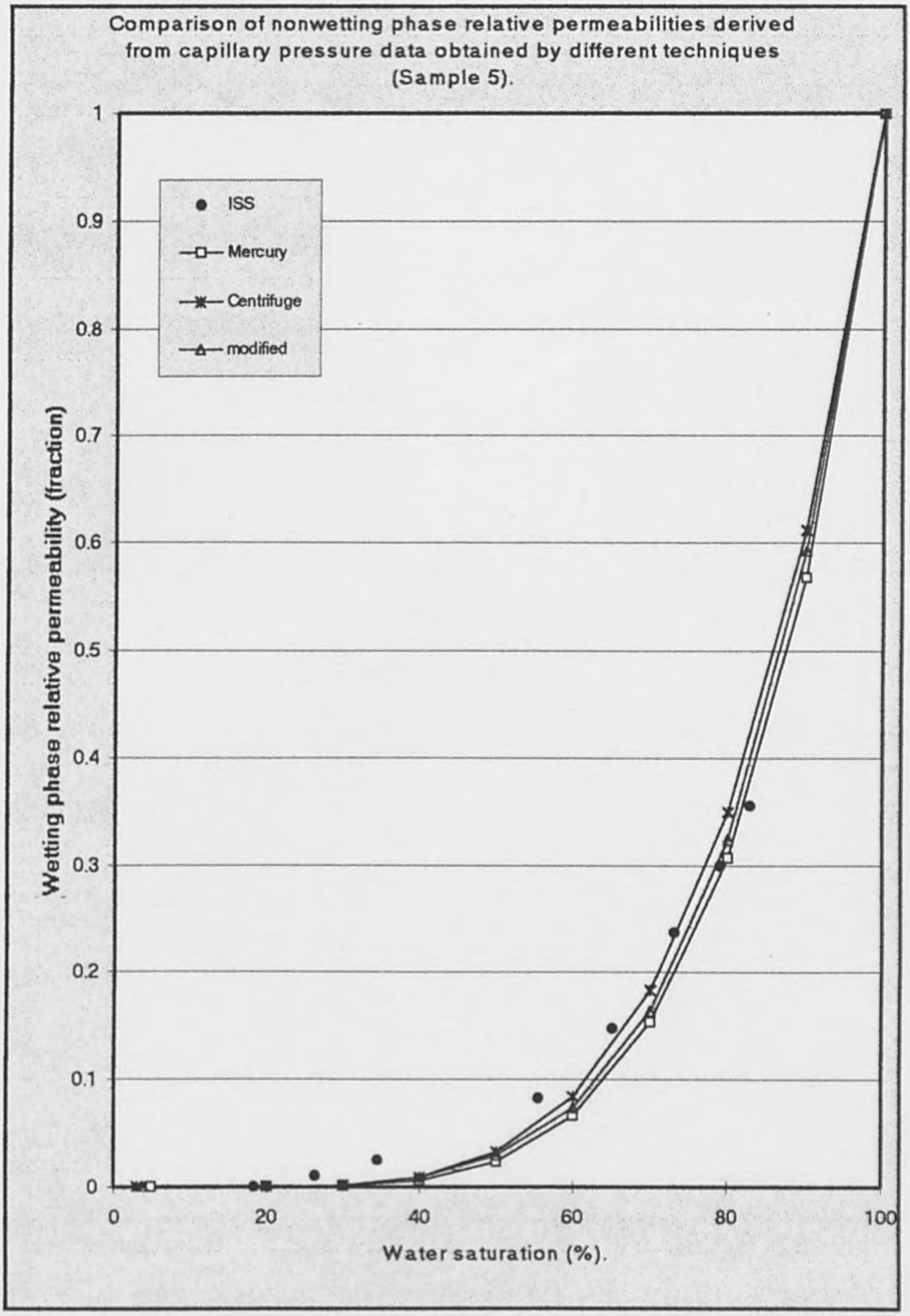

Figure (7.10) Comparison of wetting phase relative permeabilities derived from different capillary pressure technique for Sample 5.

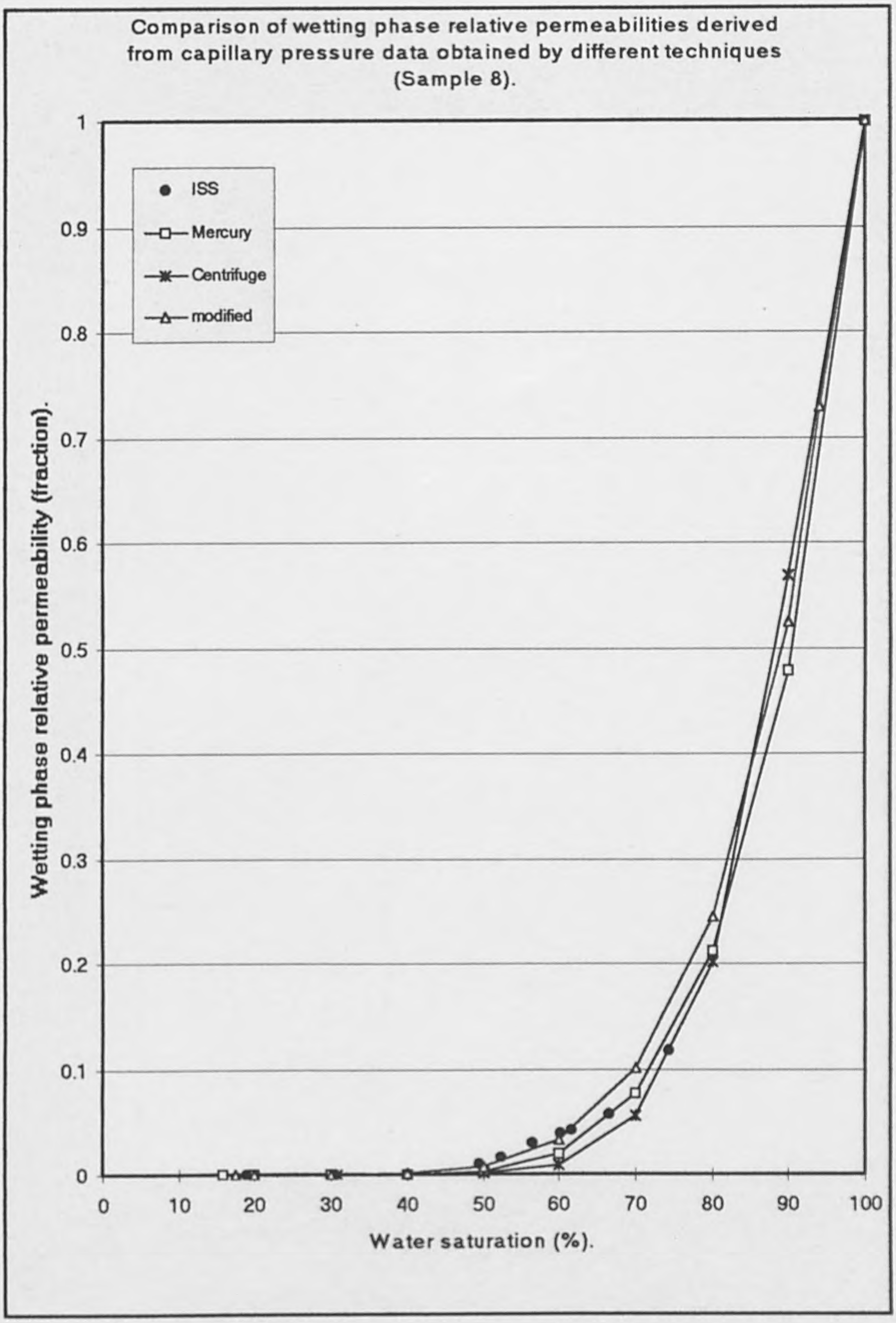

Figure (7.11) Comparison of wetting phase relative permeabilities derived from different capillary pressure technique for Sample 8.

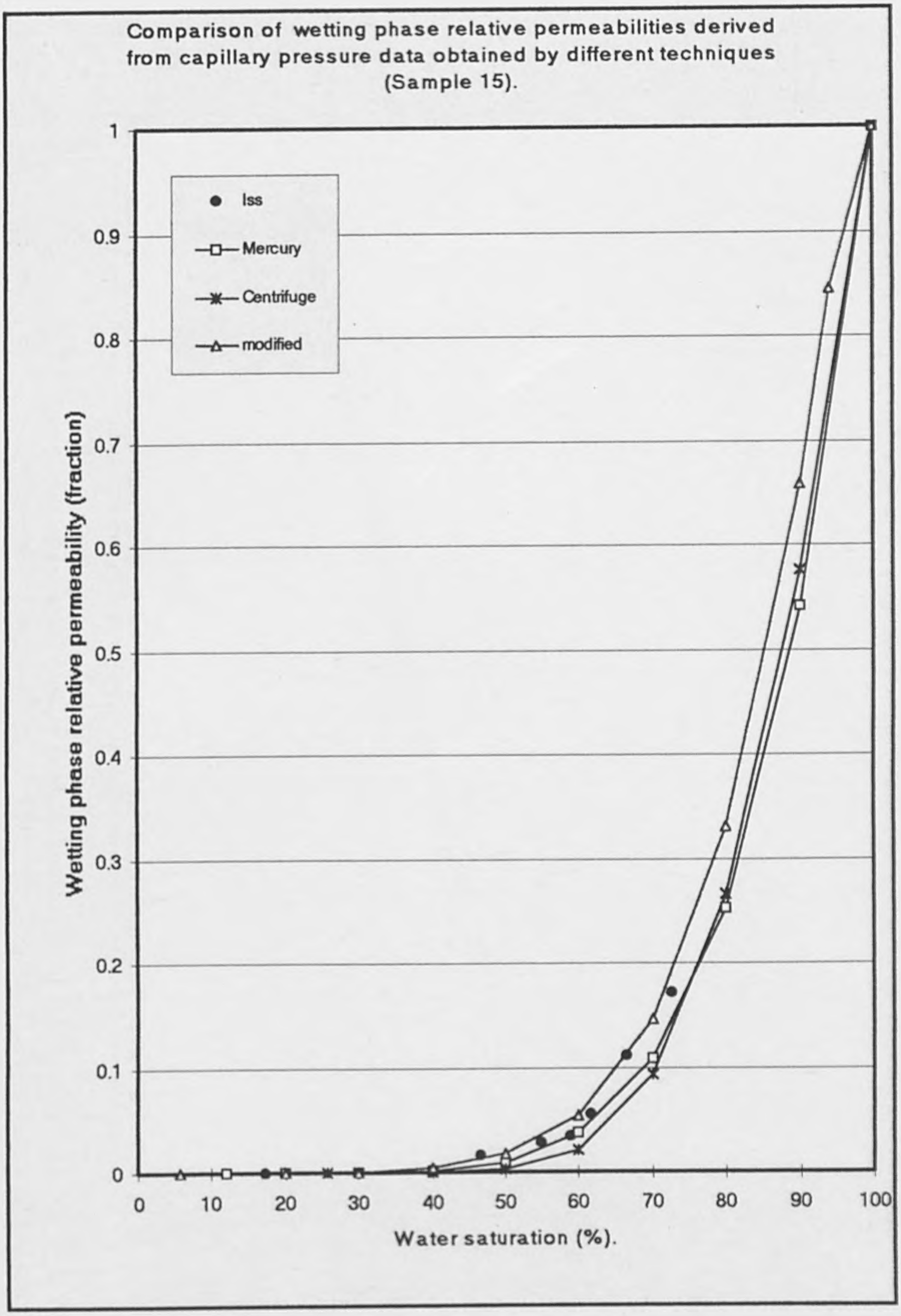

Figure (7.12) Comparison of wetting phase relative permeabilities derived from different capillary pressure technique for Sample 15.

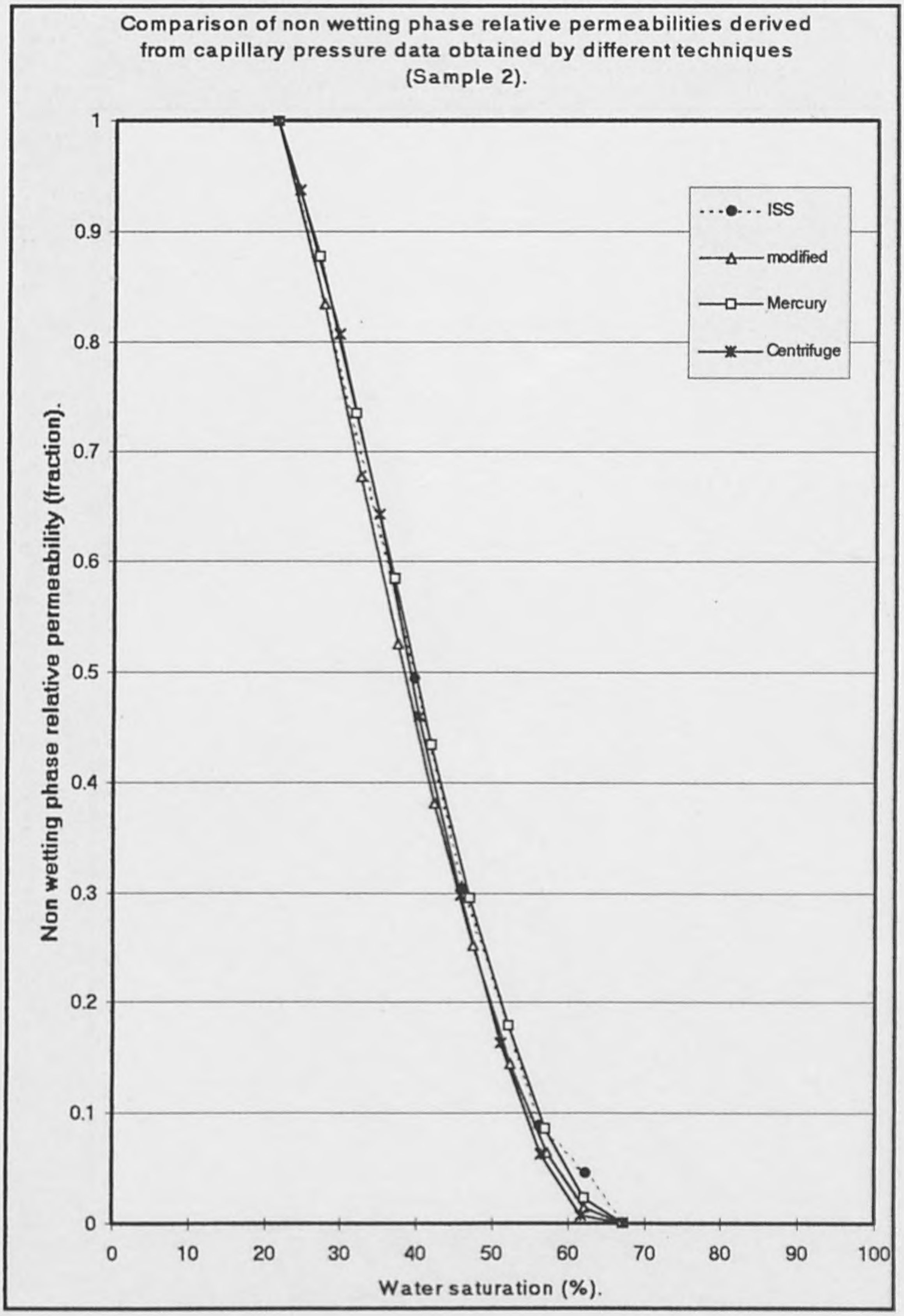

Figure (7.13) Comparison of non wetting phase relative permeabilities derived from different capillary pressure technique for Sample 2.

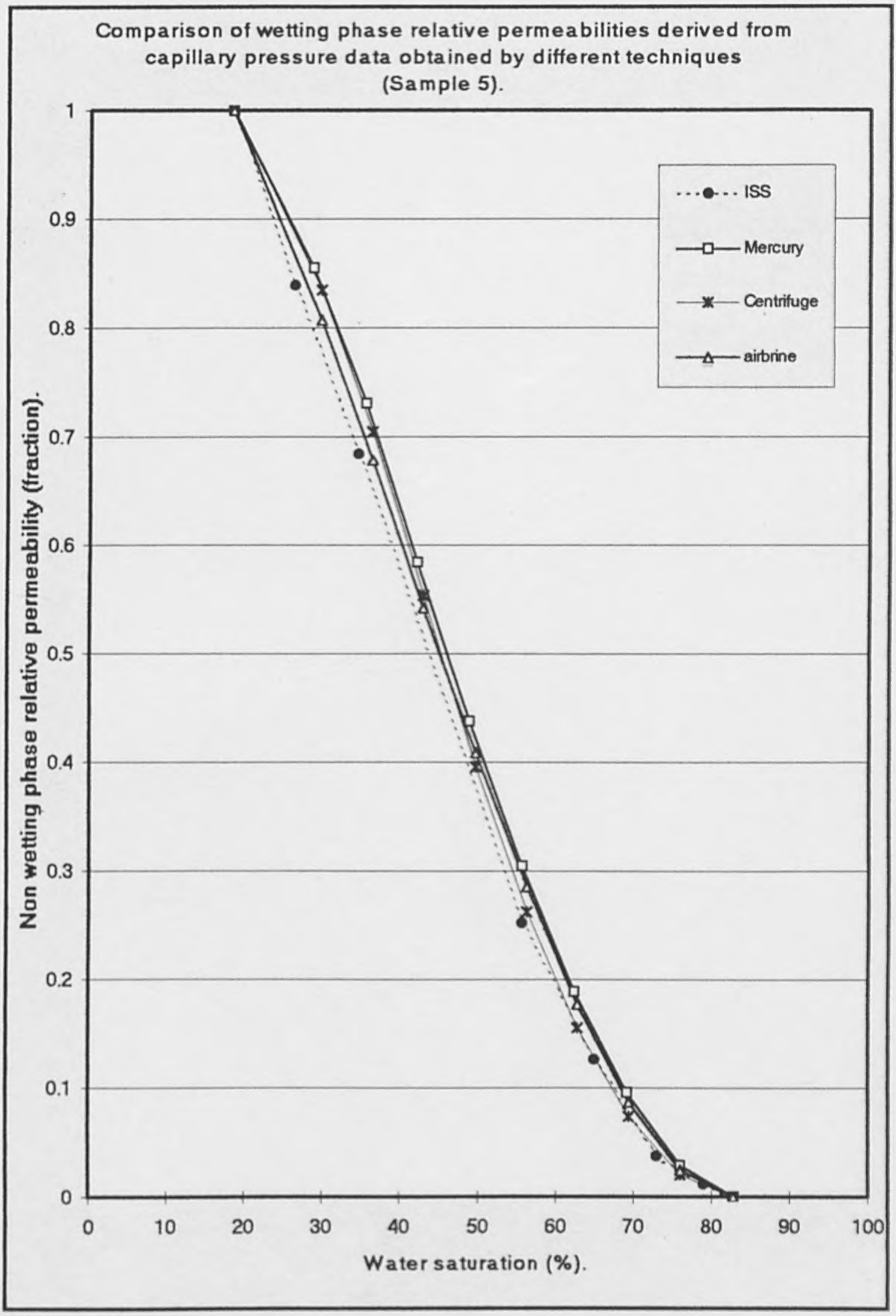

Figure (7.14) Comparison of non wetting phase relative permeabilities derived from different capillary pressure technique for Sample 5.

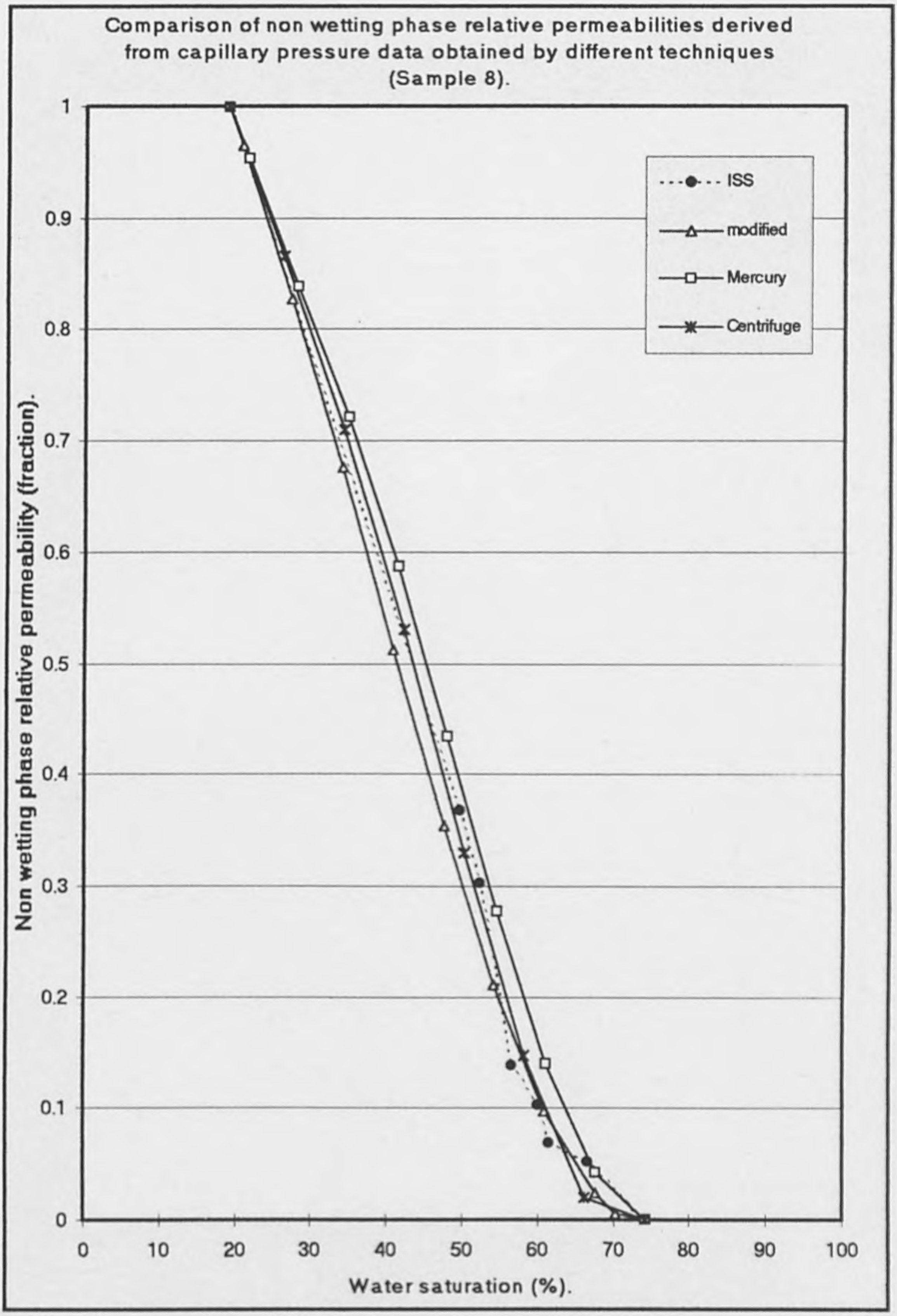

Figure (7.15) Comparison of non wetting phase relative permeabilities derived from different capillary pressure technique for Sample 8.

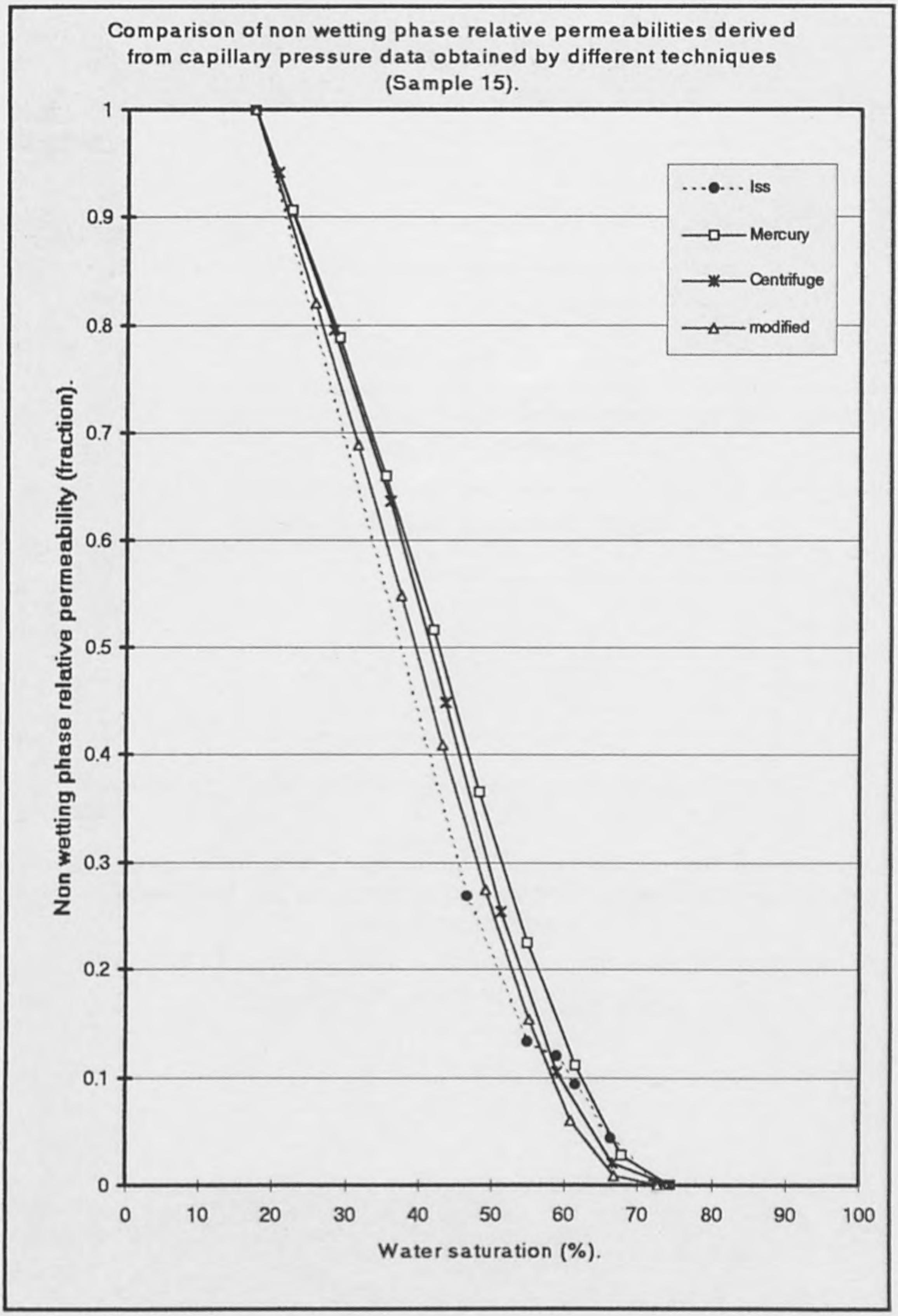

Figure (7.16) Comparison of non wetting phase relative permeabilities derived from different capillary pressure technique for Sample 15.

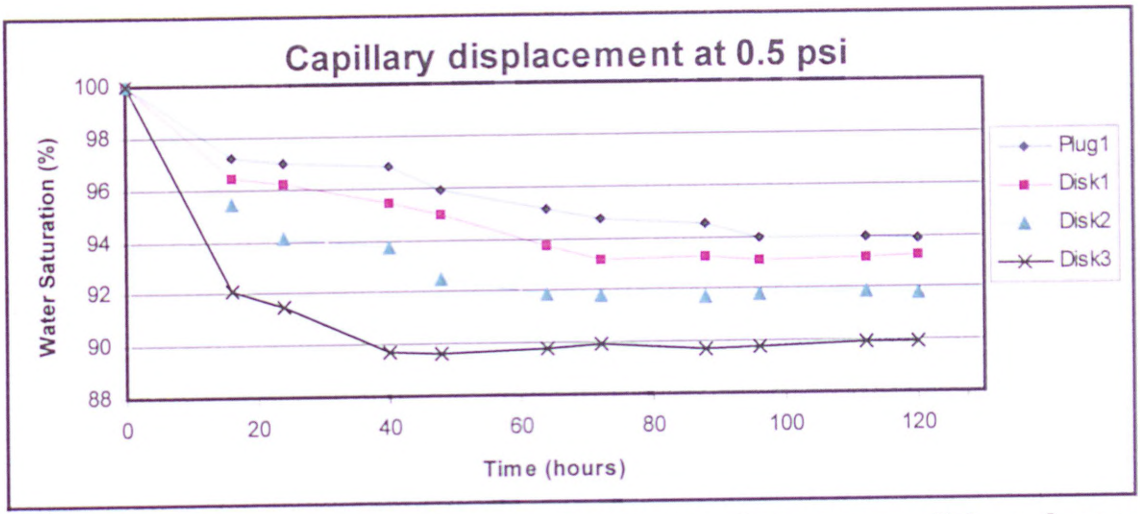

Figure (7.17-a) Comparison of capillary displacement between core disks and core plug at 0.5psi pressure.

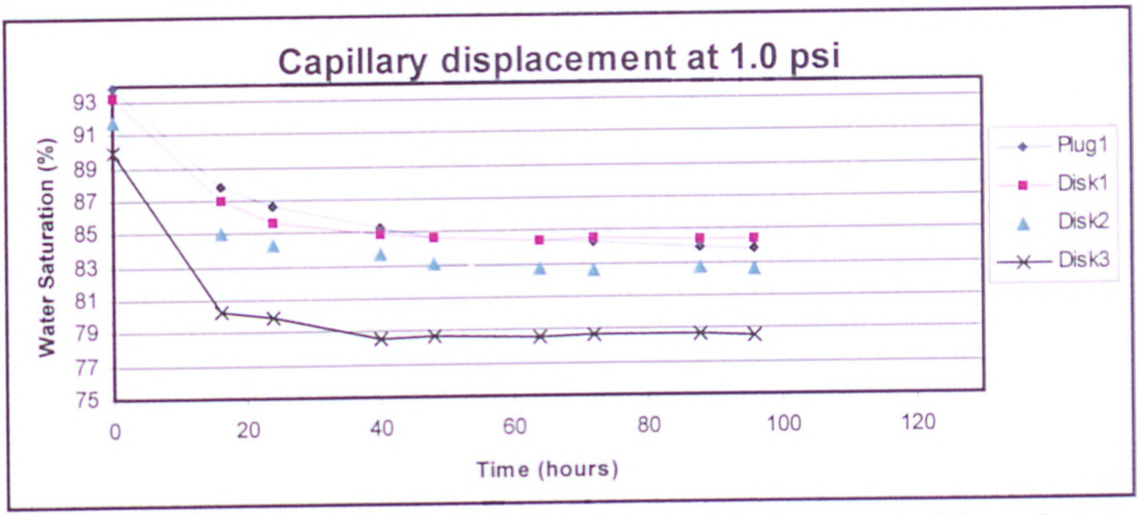

Figure (7.17-b) Comparison of capillary displacement between core disks and core plug at 1.0psi pressure.

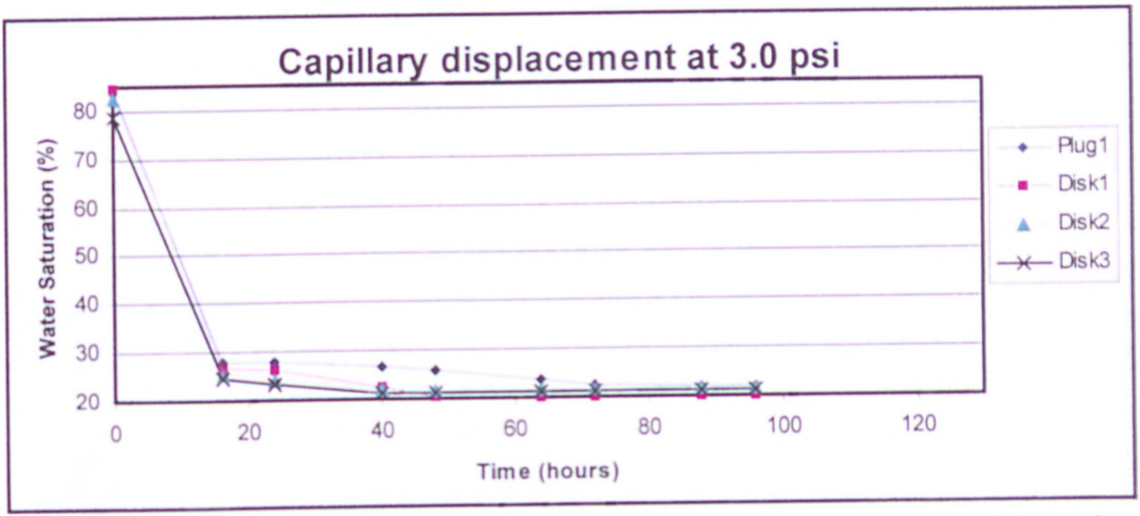

Figure (7.17-c.1) Comparison of capillary displacement between core disks and core plug at 3.0psi pressure.

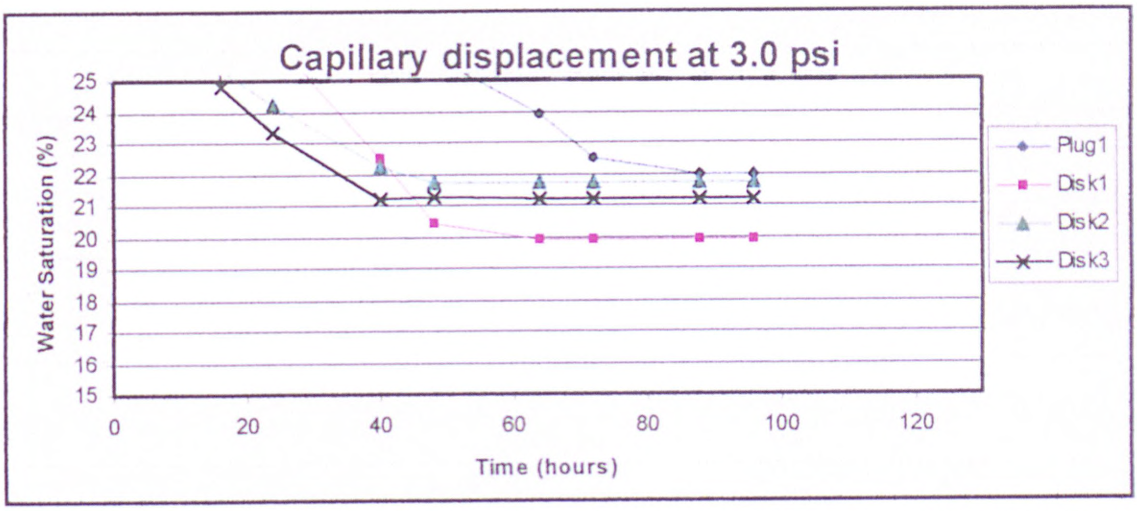

Figure (7.17-c.2) Comparison of capillary displacement between core disks and core plug at 3.0psi pressure (enlarging the equilibrium period of Figure 7.17-c.1).

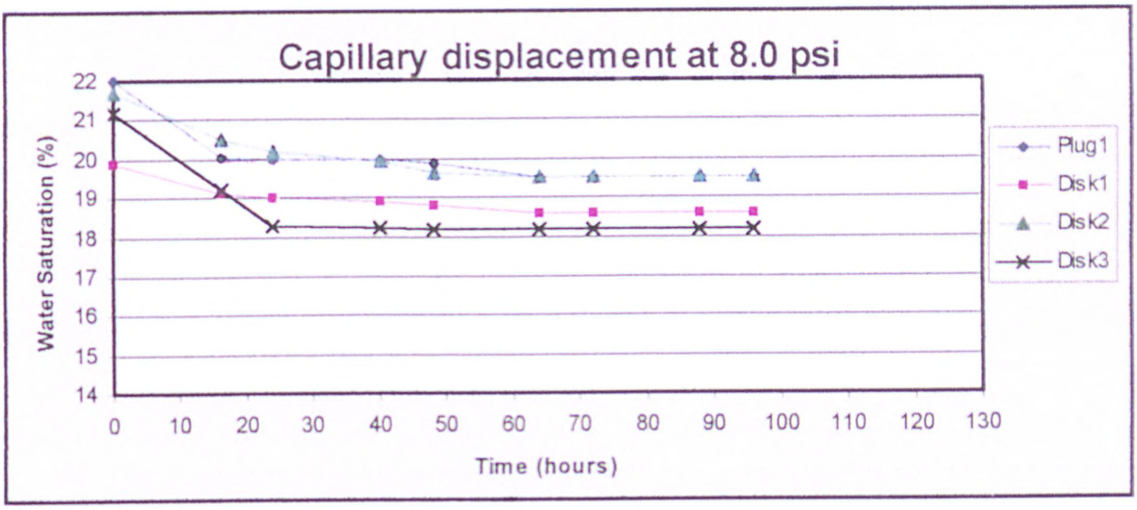

Figure (7.17-d) Comparison of capillary displacement between core disks and core plug at 8.0psi pressure.

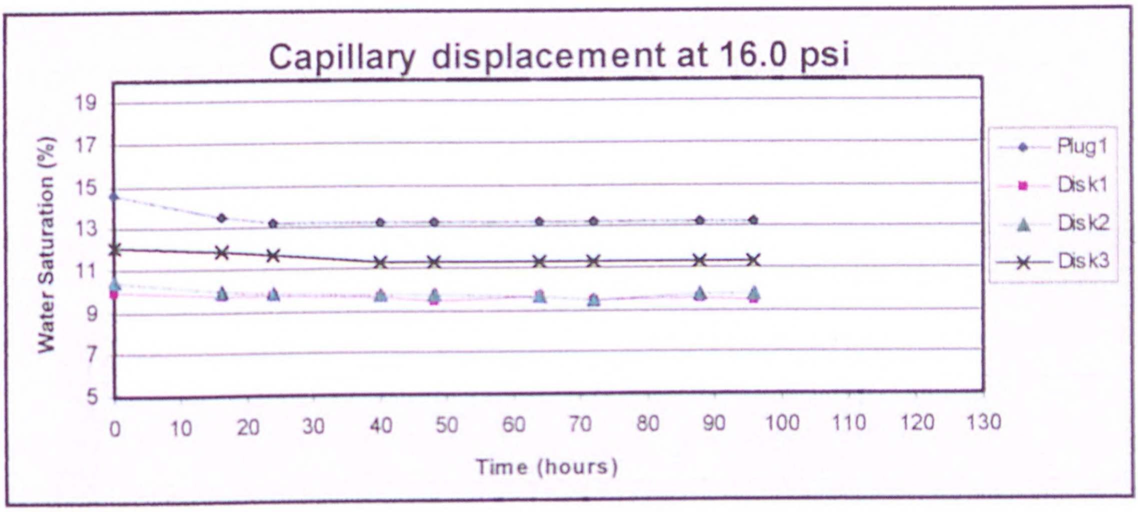

Figure (7.17-d) Comparison of capillary displacement between core disks and core plug at 16.0psi pressure.

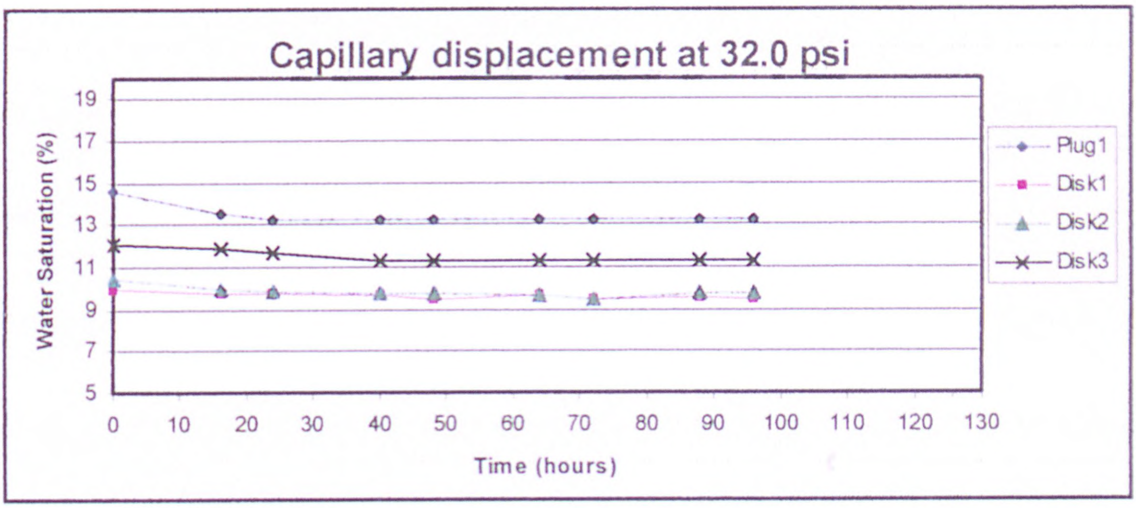

Figure (7.17-d) Comparison of capillary displacement between core disks and core plug at 32.0psi pressure.

CHAPTER 8

CONCLUSIONS AND SUGGESTIONS FOR FUTURE WORK

8.1 The use of CT Scanning in Core Sample Evaluation

Important results have been obtained while screening the sandstone rock samples by the CT scan method and the preliminary use of x-ray techniques in relative permeability measurements. These results, which were presented in Chapter 5, have led to the following conclusions:

- To obtain reliable and accurate results of scans of oil reservoir rock samples using a medical x-ray computed tomography unit, it is extremely important to re-calibrate the CT scanner using a special fused quartz (CT measurement = 1500 HU) as the main reference point. The fused quartz CT number should fall within the geological region of interest replacing the traditional use of water (CT measurement = 0.0 HU). This minimizes, the errors in x-ray attenuation coefficient measurements. Thus the accuracy and reproducibility of the data is ensured. It must be emphasized that the use of any CT scanner calibrated for medical purposes (using water as the main reference point), could lead to significant errors. Therefore, it is essential that any medical CT scanner is re-calibrated before it is used for rock imaging.

- To obtain a reliable relationship between CT measured attenuation coefficients and bulk plug porosities, it is important to work with homogeneous and pure materials. This allows the plug to be characterized by a single CT number, representative of the bulk measurement volume such that no impurities will distort the derived rock grain x-ray attenuation coefficient.

- Porosities measured using the CT scanning technique showed an out standing agreement with subsequent conventional porosity measurements (helium and liquid porosities). This demonstrates the validity and reliability of the CT scanning method for the porosity measurements.

- Porosity measurements obtained, using the single-scan technique, showed good agreement with the multiple-scan method. These measurements can be obtained more quickly and cheaply than using the dual-scan technique, but it is very desirable to use the subtracting CT method, i.e. dual-scanning (scanning the sample dry and 100% saturated with brine) whenever possible (i.e. when time and/or cost are not critical). This eliminates the requirement to estimate the grain x-ray attenuation coefficient of the rock.

- CT imaging can be extended to make non-destructive measurements of porosity for small sub-volumes within the rock. Precise measurements of porosity heterogeneity within any sample can be obtained using any CT method. This makes CT scanning a very powerful tool to assess the degree of homogeneity quantitatively and to assist in sample selection.

- CT examination of whole core provides a highly desirable means whereby a limited number of plugs can be targeted for removal. These plugs represent the core characteristics and avoid any man-made intrusions due to mud invasion, mechanical damage while drilling, sectioning or while handling the core.

- The newly developed CT single-scan porosity measurement is based on the direct relationship between x-ray attenuation and rock porosity and has formed the basis of the use of CT as a means for logging the porosity of whole core. Porosity logs of sandstone whole cores showed good agreement with helium porosities for core plugs which were removed from the scanned zones. This technique has the important advantage that it can be performed on sleeved core samples, which makes it extremely convenient for poorly consolidated formations.

- This study showed very interesting results in that samples from the upper and lower carboniferous St Bees, lower Penrith redstone and Clashach, were all found to be of comparable homogeneity to Berea Sandstone.

- Qualitative description for rock homogeneity must be always associated with a sub-volume unit, such as in the newly introduced heterogeneity scale. However, it was found that rock homogeneity is not an absolute property and porosity variation is dependent on the reference sub-volume size. For most homogeneous samples the porosity can vary significantly at smaller unit volumes.

- Nevertheless, the x-ray computed tomography technique superior for generating 3-D measurements both for the static and steady conditions. Using the existing technique in high rate unsteady state displacements is a serious mistake.

- Use of the 1-D x-ray method for measuring average fluid saturations, in unsteady state tests is not valid unless the tests are carried out at extremely low displacing rates.

8.2 Relative Permeability/Capillary Pressure Correlations

Investigation of the relative permeability/capillary pressure relationship involved extensive use of core analysis to obtain different rock properties such as porosity, permeability, wettability, relative permeability and capillary pressure. The results obtained, presented in chapters 5 and 6, led to the following conclusions;.

- The wettability has a great influence on relative permeability measurements, accordingly, it is vital to restore the original wettability of samples before relative permeability measurements are carried out. Since most of the mathematical models for deriving the relative permeability from the capillary pressure data rely on the identification of the wetting and the non-wetting phases, it is crucial that the wettability of the sample is determined. Using random samples with no wettability assessment will lead to misuse of the existing models especially for intermediate and oil wet reservoir rocks, and lead to serious errors in intermediate and oil wet reservoir samples. It can not be assumed that water is the wetting phase in all cases.

- The unsteady state laboratory tests most closely represent the reservoir flooding mechanism, and can be conducted in a much shorter time than steady state tests, but it is impossible to obtain detailed relative permeability data in favourable displacement conditions; data will be restricted to the two end point relative permeabilities (k_o at S_{wi} and k_w at S_{or}). Using a very high viscosity oil gives a reasonable range of relative permeability data. However, use of a high oil/water viscosity ratio leads to viscous fingering, which invalidates the data obtained. It is impossible to obtain a full curve experimentally using this technique, and any full relative permeability curve derived relies on questionable extrapolation. In conclusion, these tests should be carried out at reservoir waterflood rates and matched viscosity ratios, but the capillary end effect in low rate/viscosity ratio core floods will also invalidate the classical theory. Unfortunately, the limitations of capillarity and viscous fingering and very limited relative permeability data over a narrow range of water saturations cannot all be overcome simultaneously. This makes the interpretation of the unsteady state floods extremely difficult.

- Although the steady state method is time consuming and very expensive to run, its main advantage is that it produces the most reliable data and it is possible to define relative permeability across a broad saturation range even for systems with favourable mobility ratios, which cannot be done using the unsteady state method. Consequently, the experimentally measured steady state relative permeability data has been selected for comparison with data derived using the proposed mathematical models.

- The results obtained show that the use of existing mathematical models for deriving relative permeability data from capillary pressure curves for water wet reservoir rock samples leads to significant errors. Although Burdine's model exhibited "numerically" a reasonable agreement with the experimental data, the use of this model in its existing form certainly led to serious errors. The model, like others, continues to generate oil relative permeabilities for oil saturations below the residual value, which conflicts with the physical reality. This is a serious misrepresentation, as models definitely produce incorrect oil relative permeability values at water saturations ≥ (1.0 $-S_{or}$). Using these false relative permeabilities in classical reservoir engineering calculations will incorrectly predict that the reservoir will produce far more oil than is physically possible. Consequently, the predicted oil recovery will be higher than real recoverable oil. The model also ignores the effect of other rock properties including wettability variations and is assumed to be valid for any wettability, including intermediate wettability. Neglecting the effect of wettability variations on relative permeability is considered to be a major shortcoming in the previously available mathematical models.

- The newly developed model for deriving relative permeability data from capillary pressure curves showed outstanding results for water wet reservoir rock samples. The model has been developed to be representative, efficient and flexible in handling the practical applications of relative permeability data to oil reservoirs. Considering rock properties such as porosity and wettability and allowing for the residual oil saturation minimized errors, giving the new model superiority over previously proposed models. Although the new model was developed using air-brine capillary pressure data, the results obtained showed that relative permeability curves can be reliably generated from capillary pressure data obtained by the centrifuge or mercury injection methods. This makes the technique more versatile and widely applicable in practice.

- The new experimental approach for air-brine capillary pressure measurements using thin large diameter whole core disks definitely reduces the time required to attain capillary equilibrium, especially at high fluid saturations. As a result, the time to obtain the complete capillary pressure curve is remarkably reduced. The new approach overcomes a serious weakness of the air-brine technique. Additionally, the new approach may permit the practical use of water-oil capillary pressure measurements, previously seen as impractically slow. If this technique proves to be successful in water/oil systems it will be an important breakthrough in core analysis

- Omitting the inflow end effect and the depth of mud invasion (in formation damage assessment) when measuring water and oil permeabilities using Darcy's law leads to serious errors. The suggested new method will eliminate the dependence of measured permeabilities on the core plug length, and determine the permeability variations within the tested samples.

8.3 Suggestions for Future Work

1. X-ray computed tomography has the ability to study end effects in core sample flooding, by monitoring fluid saturations along and across the sample. Similar work was carried out by Morgan[180] using the ordinary 1-D x-ray technique. The CT scanner has been shown to be more accurate in fluid saturation measurements as the whole cross section can be easily included and it has the ability to display these results from any plane within the sample. Therefore it is recommended that this advanced technique is used to investigate this interesting phenomena including the effect of using mixing heads.

2. This technique could be employed easily and efficiently in air-brine capillary pressure measurements using the porous plate diaphragm. Conventional saturation measurement requires pressure depletion, opening the diaphragm to unload the sample(s) for weighing and saturation calculation therefrom. Then the sample(s) must be loaded again for the next pressure stage. This routine must be repeated for every pressure stage. Utilizing The CT scanner has the following advantages;

   a) Saturation can be measured and monitored continuously without interrupting the capillary displacement;
   b) All measurements are carried out (for different pressure stages) without unloading the sample(s), unless changing the porous plate itself;
   c) It eliminates handling errors, such as sample drying etc;

d) It is extremely convenient for poorly consolidated samples;

e) Saves time and work;

f) Measurements can be taken at precisely determined time.

3. After the required modification to eliminate errors in CT scanning is completed as presented in Chapter 5, this technique is strongly recommended for use as follows:-

- Studying the gravity effect in relative permeability measurements in general and in air-brine test in particular.

- Examining the technique for micro modeling and to compare the results against data obtained by simultaneous relative permeability measurements.

- Adapting the CT scan technique for unsteady state displacements will be a big break through in core analysis. This challenge has still to be met.

4. The mathematical models reviewed, including the newly presented one, must be applied to the derivation of relative permeabilities for intermediate and oil wet samples.
5. It is recommended that the new experimental approach for the porous plate capillary pressure measurements using thin large diameter whole core disks to be tried on an oil/water system.
6. A multi pressure sensor core holder is recommended to study the evidence for the effect of the inflow end and the mud invasion on using Darcy's law for permeability measurements.

REFERENCES

1 API RP 27: "Recommended Practice for Determining Permeability of Porous Media," Third Edition, September 1952, Reissued August 1956.

2 Kozeny, J.: "Uber Kpillare Leitung des Wassersim Boden," Sitzungsber. Akad. Wiss. Wien. Math. Naturwiss. KL., Abt. 2A, Vol. 136, p. 217,1927.

3 Carman, P. C.: "The Determination of the Specific Surface of Powders," Journal of the Society of chemical industry, Vol. 57, 1938.

4 Purcell, W. R.: "Capillary Pressures - their Measurement Using Mercury and the Calculation of Permeability therefrom," Trans., AIME, Vol. 186, p.39, 1949.

5 Gates, J. I. and Leitz, W. J.: "Relative Permeabilities of California Cores by the Capillary Method," paper presented at the API meeting, Los Angeles, California, p.286, May 11 1950.

6 Wyllie, M. R. and Gardner, G. H.F.: "The Generalized Kozeny-Carman Equation. Its Application to Multiphase Flow in Porous Media. Part 1. Review of Existing Theories," World Oil, p.121, March 1958.

7 Al-hussainy, R. and Hamphreys, N.: "Reservoir Management: Principles and Practices," JPT, p. 1129 – 1135, December 1996.

8 Stiles, J.: "Using Special Core Analysis in Reservoir Engineering- Wettability, Relative Permeability & Residual Oil Saturation," Aberdeen, June 1995.

9 Mcphee, C.: "Application to Petrophysics and Reservoir Engineering," Edinburgh, February 1999.

10 Thomas, G. W.: "Applied Reservoir Simulation," INTERA, Aberdeen, 1994.

11 Keelan, D. K.: "Core Analysis for Aid in Reservoir Description," SPE, November 1982.

12 Zhou, Xian-min, Torsaeter, O., Xie, X. and Morrow, N. R.: "The Effect of Crude-Oil Aging Time and Temperature on the Rate of water Imbibition and Long-term Recovery by Imbibition," SPE No. 26674, 1995.

13 Jadhunandan, P. P. and Morrow, N. R.: "Effect of Wettability on Crude-Oil/Brine/Rock System," SPE, p. 40, February 1995.

14 Osoba, J. S.: "Relative Permeability - what it is and how to put it to use in the field," The Oil and Gas Journal, p.326, 1953.

15 Dake, L. P.: "Fundamentals of Reservoir Engineering," Elsevier Scientific Publishing Company, 1978.

16 Hawkins, J. T.: "Comparison of Three Methods of Relative Permeability Measurement," SCA Conference Paper No. 8804, 1998.

17 Heaviside, J., Black, C. J. J. and Berry, J. F.: "Fundamentals of Relative Permeability and Theoretical Considerations," SPE No. 12173, October 1983.

18 Honarpour, M. and Mohamood, S. M.: "Relative Permeability Measurements: An Overview," JPT, p.963, August 1983.

19 19Buckley, S. I. and Leverett, M. G.: "Mechanism of Fluid Displacement in Sands," Trans., AIME, Vol. 195, p.91, 1952.

20 Welge, H. J.: "A Simplified Method for Computing Recovery by Gas or Water Drive," Trans., AIME, Vol. 91, p.91, 1952.

21 Johnson, E. F., Bossler, D. P. and Naumann, V. O.: "Calculation of Relative Permeability from Displacement Experiments," Trans., AIME, Vol. 216, p.370, 1959.

22 Jones, S. C. and Roszelle W. O.: "Graphical Techniques for Determining Relative Permeability from Displacement experiments," JPT, p.370, May 1978.

23 Saraf, D. N. and MaCaffery, F. G.: "Two and Three Phase 3 Relative Permeabilities: a Review," Petroleum Recovery Institute Report 81-8, Calgary Canada.

24 Honarpour, M., Koederitz, L. and Harvy, A.: "Relative Permeability of Petroleum Reservoirs," CRC Press, Inc. 1987.

25 Richardson, J. G., Kerver, J. K., Hafford, J. A. and Osoba, J. S.: "Laboratory Determination of Relative Permeability," Trans., AIME, Vol. 19, p.187, 1952.

26 Slobod, R. L., Chambers, A., Aime, M., and Prehn, W. L.: "Use of Centrifuge For Determining Connate Water, Residual Oil, And Capillary Pressure Curves of Small Core Samples," Trans., AIME, Vol. 192, p 41, 1952.

27 Nordtvedt, J. E., Watson, A. T., Mejia, G. and Yang, P.: "Estimation of Capillary Pressure and Relative Permeability Functions From Centrifuge Experiments," SPE No. 20805, 1990.

28 O'Meare Jr., D. J. and Lease, W. O.: "Multiphased Relative Permeability Measurements Using an Automated Centrifuge," SPE No. 12128, 1983.

29 Craig, F. F.: "The Reservoir Engineering Aspects of water flooding," SPE Monograph Vol. 3, 1971.

30 Schneider F. N.: "Three Procedures Enhance Relative Permeability Data," Oil and Gas Journal, May 1987.

31 Grupping, I. F.: "Petrophysical Evaluation Course," Aberdeen University 96/97

32 Archer, J. S. and Wall, C. G.: "Petroleum Engineering - Principles and Practice," Graham and Trotman, London, 1986.

33 Hearn C. L.: "Simulation of Stratified Waterflooding by Pseudo Relative Permeability Curves," JPT, p. 805, July 1971.

34 Pickell, J. J., Swanson, B. F. and Hickman, W. B.: "Application of Air-Mercury and Oil-Air Capillary Pressure Data in the Study of Pore Structure and Fluid Distribution," SPE No. 1227, 1966.

35 Koederitz, L., Harvey A. H. and Honarpour, M.: "Introduction to Petroleum Reservoir Analysis," Gulf Publishing Company, 1989.

36 Dullien F. A. L.: "Porous Media: Fluid Transport and Pore Structure," Academic Press., Second Edition, 1992.

37 Welge, H. J. and Bruce, W. A.: "The restored state Method For Determination of Oil in Place and Connate Water," Drilling and production practices, API, 1947.

38 Sondena, E., Bratteli, F., Normann H. P. and Kolltveit, K.: "The Effect of Reservoir Conditions on Saturation Exponent and Capillary Pressure Curves for Water-Wet Samples," Department of Physics, U. of Bergen, Norway and GECO Petroleum Lab.

39 Hassler, G. L. and Brunner, E.: "Measurements of Capillary Pressure in small Core Samples," Trans., AIME, Los Angeles Meeting, October 1944.

40 O'Meare Jr., D. J. and Crump, J. G.: "Measuring Capillary Pressure and Relative Permeability in a Single Centrifuge Experiment," SPE No. 14419, 1985.

41 Burdine, N. T., Gournay, L. S. and Reichertz, P. P.: "Pore Size Distribution of Petroleum Reservoir Rocks," Trans., AIME, Vol. 189, p.195, 1950.

42 Ritter, H. L. and Drake, L. C.: "Pore-Size Distribution in Porous Materials, Pressure Porosimeter and Determination of Complete Macropore-Size Distributions," IND. ENG. CHEM., Vol. 17, p.782, 1945.

43 Amyx, J. W., Bass, D. M. and Whitting, R. L.: "Petroleum Reservoir Engineering Physical Properties," McGraw-Hill, 1960.

44 Anderson, W. G.: "Wettability Literature Survey - Part 1: Rock/Oil/Brine Interactions and the Effects of Core Handling on Wettability," JPT, p.1125, October 1986.

45 Anderson, W. G.: "Wettability Literature Survey - Part 2: Wettability Measurement," JPT, p.1246, November 1986.

46 Anderson, W. G.: "Wettability Literature Survey - Part 3: The Effects of Wettability on the Electrical Properties of Porous Media," JPT, p.1371, December 1986.

47 Anderson, W. G.: "Wettability Literature Survey - Part 4: Effects of Wettability on Capillary Pressure," JPT, p.1283, October 1987.

48 Anderson, W. G.: "Wettability Literature Survey - Part 5: The Effects of Wettability on Relative Permeability," JPT, p.1453, November 1987.

49 Anderson, W. G.: "Wettability Literature Survey - Part 6: The Effects of Wettability on Waterflooding," JPT, p.1605, December 1987.

50 Morrow, M. R.: "Wettability and Its Effect on Oil Recovery," JPT, p.1476, December 1990.

51 Wagner, O. R. and Leach R. O.: "Improving Oil Displacement Efficiency by Wettability Adjustment," Trans., AIME, Vol. 216, p. 65, 1959.

52 Brown, C. E. and Neustadter E. L.: "The Wettability of Oil/Water/Silica System with Reference to Oil Recovery," JCP, p. 100, July-September 1980.

53 Nutting, P. G.: "Some Physical and Chemical Properties of Reservoir Rocks Bearing on the Accumulation and Discharge of Oil," Problems of Petroleum Geology, Wrather, W. E.and Lahee, F. H. (eds) AAPG, TUISA, p.825, 1934.

54 Chilingar, G. V. and Yen T. F.: "Some Notes on Wettability and Relative Permeabilities of Carbonate Reservoir Rocks, II," Energy Sources, Vol. 7, No. 1, p. 67-75, 1983.

55 Brown, R. J. S. and Fatt, I.: "Measurements of Fractional Wettability of Oil Field Rocks by the Nuclear Magnetic Relaxation Method," Trans., AIME, Vol. 207, p.262, 1956.

56 Fatt, I. and Klikoff, W. A.: "Effect of Fractional Wettability on Multiphase Flow Through Porous Media," Trans., AIME, Vol. 216, p. 624-32, 1959.

57 Gimatudinov, S. K.: "The Nature of the Surface of Minerals of Oil-Bearing Rocks," Izv. Vyssh. Ucheb. Zavedenii, Neft i Gaz 1963, Vol. 6, No. 7, p. 37-42.

58 Holbrook, O. C. and Bernard, G. C.: "Determination of Wettability by Dye Adsorption," Trans., AIME, Vol. 213, p. 261-64, 1958.

59 Iwankow, E. N.: "A Correlation of Interstitial Water Saturation and Heterogeneous Wettability," Producers Monthly, Vol. 24, No. 12, p. 18-26, October 1960.

60 Salathlie, R. A.: "Oil Recovery by Surface Film Drainage in Mixed-Wettability Rocks," JPT, Trans., AIME, Vol. 255, p.1216, October 1973.

61 Alba, P.: "Discussion on Effect of Fractional Wettability on Multiphase Flow Through Porous Media," Trans., AIME, Vol. 216, p. 426-32, 1958.

62 Moore, J.: "Laboratory Determined Electric Logging Parameters of the Bradford Third Sand," Producers Monthly, Vol. 22, No. 3, p. 30-39, March 1958.

63 Schmind, C.: "The Wettability of Petroleum Rocks and Results of Experiments to Study the Effects of Variations in Wettability of Core Samples," Erdoel und Kohle-Erdgas-Petrochemie, Vol. 17, No. 8, p. 605-09, 1964. English translation available from the John Crerar Library. Translation No. TT-65-12404.

64 Slobod, R. L. and Blum, H. A: "Method for Determining Wettability of Reservoir Rocks," Trans., AIME, Vol. 195, p. 1, 1952.

65 Neumann, A. W. and Good, R. J.: "Techniques of Measuring Contact Angles," Surface and Colloid Science, R. J. Good and R. R. Stromberg (eds.), Plenum Press, New York City, Vol. 11, p. 31-91, 1979.

66 Amott, E: "Observations Relating to the Wettability of Porous Rock," Trans., AIME, Vol. 216, p.156, 1959.

67 Cuiec, L. E. *et al.*: "Determination of the Wettability of Porous Rock," Rev. Inst. Franc. Du Petrole, Vol. 33, No. 5, p. 705-28, September-October 1978. English translation available from John Crerar Library, translation No. 81-13920-081.

68 Donaldson, E. C., Thomas, R. D., and Lorenz, P. B.: "Wettability Determination and Its Effect on Recovery Efficiency," SPEJ, p. 13-20, March 1969.

69 Hjelmeland, O. and Torsaeter, O.: "Wettability, the Key to Proper Laboratory Waterflooding Experiments," Intl. Energy Agency Workshop on Enhanced Oil Recovery, Bartlesville Energy Technology Centre, April 1980, CONF-8004140, U.S. DOE, p. 1-24, February 1981.

70 Ionescue, E. and Maini, B. B.: "A Review of Laboratory Techniques for Measuring Wettability of Petroleum Reservoir Rocks," Petroleum Recovery Inst., report 1983-3, Calgary, October 1983.

71 Marsden, S. S.: "Wettability-Its Measurement and Application to Waterflooding," J. Jap. Assoc. Pet. Tech., Vol. 30, No. 1, p. 1-10, January 1965.

72 Marsden, S. S.: "Wettability: The Elusive Key to Waterflooding," Petroleum Engineer, Vol. 37, No. 4, p. 82-87, April 1965.

73 Raza, S. H., Treiber, L. E., and Archer, D. L.: "Wettability of Reservoir Rocks and Its Evaluation," Producers Monthly, Vol. 32, No. 4, p. 2-7, April 1968.

74 Donaldson, E. C.: "Oil-Water-Rock Wettability Measurement," Proc. American Chemical Soc., Div. of Petroleum Chemistry, Vol. 26, No. 1, p. 110-22, (March 29-April 3, 1981).

75 Morrow, N. R. and Mungan, N.: "Wettability and Capillarity in Porous Media," report RR-7, Petroleum Recovery Research Inst., Calgary, January 1971.

76 Morrow, N. R.: "Capillary Pressure Correlations for Uniformly Wetted Porous Media," J. Cdn. Pet. Tech., Vol. 15, No. 4, p. 49-69, October-December 1976.

77 Morrow, N. R.: "The Effects of Surface Roughness on Contact Angle with Special Reference to Petroleum Recovery," J. Cdn. Pet. Tech., Vol. 14, No. 4, p. 42-53, October-December 1975.

78 Calhoun, J. C., Lewis, M., and Newman, R. C.: "Experiments on the Capillary Properties of Porous Solids," Trans., AIME, Vol. 186, p. 189-96, 1949.

79 Rapoport, L. A. and Leas, W. J.: "Properties of Linear Waterfloods," Trans., AIME, Vol. 189, p.139, 1953.

80 Leverett, M. C. and Lewis, W. B.: "Steady Flow of Gas-Oil-Water Mixtures Through Unconsolidated Sands," Trans., AIME, Vol.142, p. 107, 1941.

81 Sandberg, C. R. and Gournay, L. S.: "The Effect of Fluid-Flow Rate and Viscosity on Laboratory Determinations of Oil-Water Relative Permeabilities," Trans., AIME, Vol. 213, p.36, 1958.

82 Richardson, J. G.: "Calculation of Waterflood Recovery from Steady-State Relative Permeability Data," Trans., AIME, Vol. 210, p. 373, 1957.

83 Saraf, D. N. and Fatt, I.: "Three-Phase Relative Permeability Measurement Using a N.M.R. Technique for Estimating Fluid Saturation," Soc. Pet. Eng. J., Vol. 9, p. 235, 1967.

84 Craig, F. F., Jr.: "Errors in Calculation of Gas Injection Performance from Laboratory Data," JPT, Vol. 8, p. 23, 1952.

85 Geffen, T. M., Parrish, D. R., Haynes, G. W., and Morse, R. A.: "Efficiency of Gas Displacement from Porous Media by Liquid Flooding," Trans., AIME, Vol. 195, p. 29, 1952.

86 McCaffery, F. G.: "The Effect of Wettability on Relative Permeability and Imbibition in Porous Media," Ph.D. thesis, U. of Calgary, Alberta, Canada, 1973.

87 Yuster, S. T.: "Theoretical Consideration of Multiphase Flow in Idealized Capillary System," Proceedings of the Third World Petroleum Congress, Hague, Netherlands, Vol. 2, p. 437, 1951.

88 Morrse, R. A., Terwilliger, P. K., and Yuster, S. T.: "Relative Permeability Measurements on Small Core Samples," Oil Gas J., Vol. 46, p. 109, 1947.

89 Perkins, F. M., Jr.: "An Investigation of the Role of Capillary Forces in Laboratory Waterfloods," J PT, Vol. 11, p. 49, 1957.

90 Lefebvre du Prey, E. J.: "Factors Affecting Liquid-Liquid Relative Permeabilities of a Consolidated Porous Medium," Soc. Pet. Eng. J., Vol. 2, p. 39, 1973.

91 Odeh, A. S.: "Effect of Viscosity Ratio on Relative Permeability," Trans., AIME, Vol. 216, p. 346, 1959.

92 Wilson, J. W.: "Determination of Relative Permeability under Simulated Reservoir Conditions," AIChEJ, Vol. 2 part 1, p. 4, 1956.

93 Muskat, M., Wyckoff, R. D., Botset, H. G., and Meres, M. W.: "Flow of Gas-Liquid Mixture Through Sands," Trans., AIME, Vol. 123, p. 69, 1937.

94 Krutter, H. and Day, R. J.: "Air-drive Experiments on Long Horizontal Consolidated Cores," J PT, Vol. 12, p. 1, 1943.

95 Downie, J. and Crane, F. E.: "Effect of Viscosity on Relative Permeability," Soc. Pet. Eng. J., Vol. 6, p. 59, 1961.

96 Labastie A.,Guy, M., Delclaud, J. P. and Iffy Rene.: "Effect of Flow Rate and Wettability on Water-Oil Relative Permeabilities and Capillary Pressure," SPE No. 9236, 1980.

97 Levine, J. S.: "Displacement Experiments in a Consolidated Porous System", Trans., AIME, Vol. 201, p. 57, 1954.

98 Salter, S. J. and Mohanty, K. K.: "Multiphase Flow in Porous Media: I. Macroscopic Observations and Modeling," SPE No. 11017, 1982.

99 Pathak, P., Davis, H. T., and Scriven, L. E.: "Dependence of Residual Nonwetting Liquid on Pore Topology," SPE No. 11016, 26-29 September 1982.

100 Rathmell, J. J., Braun, P. H. and Perkins, T. K.: "Reservoir Waterflood Residual Oil Saturation from Laboratory Tests," JPT, February 1973.

101 LI, Y., and Wardlaw, N. C.: "Mechanisms of Nonwetting Phase Trapping during Imbibition at Slow Rates," Journal of Colloid Interface Science, Vol. 109, No. 2, February 1986.

102 McDougall, R. S. and Sorbie, S. K.: "The Impact of Wettability on Waterflooding: Pore Scale Simulation," SPE J. Reservoir Engineering, Vol. 10, No. 3, p. 208, August 1995.

103 Leverett, M. C.: "Flow of Oil - Water Mixtures Through Unconsolidated Sands," Trans., AIME, Vol. 132, 149, 1939.

104 Morrow, N. R.: "The Retention of Connate Water in Hydrocarbon Reservoirs," J. Cdn. Pet. Tech., Vol. 10, No. 1, p. 38-55, January-March 1971.

105 Purcell, W. R.: "Interpretation of Capillary Pressure Data," Trans., AIME Vol. 189, p. 369-71, 1950.

106 Kinney, P. T. and Nielsen, R. F.: "Wettability in Oil Recovery," World, Vol. 132, No. 4, p. 145-54, Oil March 1951.

107 Van Brakel, J. and Heertjes, P. M.: "Capillary Rise in Porous Media," Nature, Vol. 254, p. 585-86, April 17, 1975.

108 De Witt, L. A. and Scholten, J. J. F.: "Studies on Pore Structure of Adsorbents and Catalysts: III. Comparison of Pore Size Distributions Determined in Chrysostile and Zirconia Samples by Mercury Porosimetry and Nitrogen Capillary Condensation," J. Catalysis, Vol. 36, p. 36-47, 1975.

109 Morrow, N. R. and McCaffery, F. G.: "Displacement Studies in Uniformly Wetted Porous Media," Wetting, Spreading, and Adhesion, G. F. Padday (ed.), Academic Press, New York City 1978.

110 McCaffery, F. G.: "The Effect of Wettability on Relative Permeability and Imbibition in Porous Media," Ph.D. thesis, U. of Calgary 1973.

111 Brown, R. J. S. and Fatt, I.: "Measurements of Fractional Wettability of Oilfield Rocks by the Nuclear Magnetic Relaxation Method," Trans., AIME, Vol. 207, p. 262-64, 1956.

112 Owens, W. W. and Archer, D. L.: "The Effect of Rock Wettability on Oil-Water Relative Permeability Relationships," SPE AIME, p.873, July 1971.

113 Heiba, A. A., Davis, H. T. and Scriven, L. E.: "Effect of Wettability on Two-Phase Relative Permeabilities and Capillary Pressure," SPE No. 12172, 1983.

114 Jerauld, G. R. and Rathmell, J. J.: "Wettability and Relative Permeability of Prudhoe Bay: A case Study in Mixed-Wet Reservoirs," SPE No. 28576, February 1997.

115 Tamai, Y. and Aratani, K.: "Experimental Study of the Relation Between Contact Angle and Surface Roughness," J. Phys. Chem., Vol. 76, No. 22, p. 3267-71, 1972.

116 Morrow, N. R.: "Physics and Thermodynamics of Capillary Action in Porous Media," Ind. Eng. Chem., Vol. 62, No. 6, p. 32-56, June 1970.

117 Kyte, J. R. and Rapoport, L. A.: "Linear Waterflood Behavior and End Effects in Water-Wet Porous Media," Trans., AIME, Vol. 213, p. 423, 1958.

118 Civan, F. and Donaldson, E .C.: "Relative Permeability from Unsteady-State Displacements with Capillary Pressure Included," SPE No. 16200, June 1989.

119 Fulcer, Jr. and Ertekin,: "The Effect of the Capillary Number and Its Constituents on Two-Phase Relative Permeability Curves," SPE No. 12170, 1983.

120 Hetherington and George, Jr.: "Relative Permeabilities and Capillary Pressure in the Burgan and Wara Sands," Middle East Regional Meeting 81, March 1961.

121 Geffen, T. M., Owens, W. W., Parrish, D. R., and Morse, R. A.: "Experimental Investigation of Factors Affecting Laboratory Relative Permeability Measurements," Trans., AIME, Vol. 192, p. 99, 1951.

122 Osoba, J. S., Richardson, J. G., Kerver, J. K., Hafford, J. A., and Blair, P. M.: "Laboratory Measurements of Relative Permeability," Trans., AIME, Vol. 192, p. 47,1951.

123 Josendal, V. A., Sandford, B. B., and Wilson, J. W.: "Improved Multiphase Flow Studies Employing Radioactive Tracers," Trans., AIME, Vol. 195, p. 65, 1952.

124 Wyckoff, R. D. and Botset, H. G.: "Flow of Gas Liquid Mixtures Through Sands," Physics, Vol. 7, p. 325, 1936.

125 Stewart, C. R., Craig, F. F. Jr. and Morse, R. A.: "Determination of Limestone Performance Characteristics by Model Flow Tests," Trans., AIME, Vol. 198, p. 93, 1953.

126 Dunlap, E. N.: "Influence of Connate Water on Permeability of Sands to Oil," Trans., AIME, Vol. 127, p.215, 1938.

127 Miller, M. A. and Ramey, H. J. Jr.: "Effect of Temperature on Oil-Water Relative Permeabilities of Unconsolidated and Consolidated Sands," SPE No. 12116, 1983.

128 Sufi, A. S., Ramey, H. J., Jr and Brigham, W. E.: "Temperature Effects on Relative Permeabilities of Oil-Water Systems," SPE No. 11701, 1982.

129 Sufi, A. S., Ramey, H. J. Jr. and Brigham, W. E.: " Temperature Effects on Oil-Water Relative Permeabilities for Unconsolidated Sands," U. S. Department of Energy, Technical Report, 12056-35, 1982.

130 Weinbrandt, R. M., Ramey, H. J. Jr. and Casse, F. J.: "The Effect of Temperature on Relative and Absolute Permeability of Sandstone," Soc. Pet. Eng. J., Vol. 3, p. 13, 1971.

131 Muskat, M.: "Physical Principles of Oil Production," McGraw-Hill New York, 1949.

132 Thomas, R. D. and Ward, D. C.: "Effect of Overburden Pressure and Water Saturation on Gas Permeability of Tight Sandstone Cores," JPT, Vol. 2, p. 120, 1972.

133 Fatt, I. and Barrett, R. E.: "Effect of Overburden Pressure on Relative Permeability," Trans., AIME, Vol. 198, p. 325, 1953.

134 Sutera, S. P. and Shalk R.: "The History of Poiseuille Law," Annual review of Fluid Mechanics, Vol. 25, 1993.

135 Wyllie, M. R. and Gardner, G. H. F.: "The Generalized Kozeny-Carman Equation. Its application to Multiphase Flow in Porous Media. Part 2. A Novel Approach to Problems of Fluid Flow," Worlds Oil, p.210, April 1958.

136 Wall, G. C.: "Permeability: Pore Size Distribution Correlations," Journal of the institute of Petroleum, Vol. 51, No. 498, June 1965.

137 Reed, S. J.: "Liquid Permeability of Packed Particles: Why Perpetuate the Carmen-Kozeny Model?," J. Amer. Ceramic Society, November 1992.

138 Swanson, B. F.: "A Simple Correlation Between Permeabilities and Mercury Capillary Pressures," JPT, p. 2498, 1981.

139 Burdine, N. I.: "Relative Permeability Calculations from Pore Size Distribution Data," Trans., AIME, Vol. 198, p.71, 1953.

140 Rapoport, L. A. and Leas, W. J.: "Relative Permeability to Liquid in Liquid-Gas System," Trans., AIME, Vol. 192, p.83, 1951.

141 Wyllie, M. R. J. and Sprangler, M. B.: "Application of Electrical Resistivity Measurements to Problems of Fluid Flow in Porous Media," Bull. AAPC, Vol. 36 p.359, 1952.

142 Timmerman, E. H. Ed: "Practical Reservoir Engineering," Penwell Publ., p.10, 1982.

143 Fatt, I. and Dykstra, H.: "Relative Permeability Studies," Trans., AIME, Vol. 192, p.249, 1951.

144 Corey, A. T.: "The Interrelation Between Gas and Oil Relative Permeabilities," Trans., AIME, Vol. 207, p. 358, 1956.

145 Torcaso, M. A. and Wyllie, M. R. J.: "A Comparison of Calculated k_{rg}/k_{rw} ratio with Field Data," JPT, Vol. 6, p. 57, 1958.

146 Frick, T., Ed.: "Petroleum Production Handbook," Vol. 2, Soc. of Pet. Eng. of AIME, Dallas, Tx., p. 25, 1962.

147 Pirson, S. J., Ed.: "Oil Reservoir Engineering," McGraw Hill, New York, 1958.

148 Chardaire, C., Chavent, G., Jaffre, J., Liu, J. and Bourbiaux, B.: "Simultaneous Estimation of Relative Permeabilities and Capillary Pressure," SPE No. 19680, 1989.

149 Shouxiang, Ma., Jiang, Ming-Xuan and Morrow, N. R.: "Correlation of Capillary Pressure Relationships and Calculations of Permeability," SPE No. 22685, October 1991.

150 Savioli, G. B., Bidner, M. S., and Grattoni, C. A.: "The Influence of Capillary Pressure when Determining Relative Permeability From Unsteady-State Corefloods," SPE No. 23698, 1992.

151 Thompson, A. H., Katz, A. J. and Rasckhe, R. A.: "Estimation of Absolute Permeability From Capillary Pressure Measurements," SPE No. 16794, September 1987.

152 Chavent, G., Cohen, G. and Espy, M.: "Determination of Relative Permeabilities and Capillary Pressures by an Automatic Adjustment Method," SPE No. 9237, 1980.

153 Jennings Jr., J. W., McGregor, D. S., and Morse, R. A.: "Simultaneous Determination of Capillary pressure and Relative Permeability by Automatic History Matching" SPE No. 14418, 1988.

154 Choho, T., Pelce, V., Fasanino, G., and Picard, M.: "A New Method for Capillary Pressure and Relative Permeability Curve Matching for Gas/water Flow" SPE No. 19812, 1989.

155 Chardair, C., Chavent, G., Jaffre, J. and Liu, J.: "Multiscale Representation for Simultaneous Estimation of Relative Permeabilities and Capillary Pressure," SPE No. 20501, 1990.

156 Ohen, H. A., Amaefule, J. O., Hyman, L. A., Daneshjou, D. and Schraufnagel, R. A.: "A Systems Response Model for Simultaneous Determination of Capillary Pressure and Relative Permeability Characteristics of Coalbed Methane," SPE No. 22912, 1991.

157 Selly, R. C.: "Elements of Petroleum Geology," Freeman and Company, 1985.

158 Dare. K. K.: "A Critical Review of Core Analysis Techniques," 22nd Annual Tech. Meeting of the Pet. Soc. of CIM, Banff, Alberta, June 1971.

159 Robertson Research International Limited: "Core Analysis Training- Test Method," Doc. No. C.A.T. 3:5FR, 1994.

160 Hounsfield, G. N.: "A Method of and Apparatus for Examination of a Body by Radiation Such as X-or Gamma-Radiation," British Patent No. 1, London, Vol. 283, p. 915, 1972.

161 Huppler, J. D.: "Numerical Investigation of the Effects of Core Heterogeneities on Water Relative Permeability," SPE No. 2874, 1970.

162 Withjack, E. M.: "Computed Tomography for Rock - Property Determination and Fluid-Flow Visualization," SPE No. 16951, 1987.

163 Vinegar, H. J.: " X-ray CT and NMR Imaging of Rocks," JPT, p. 257-59, March 1986.

164 Vinegar, H. J., Wellington, S. L.: "Tomographic Imaging of Three Phase Flow Experiments," Rev. Sci. Inst., Vol. 58(1), p. 96-107, Jan 1987.

165 Hove, A. O., Ringen, J. K., and Read, P. A.: "Visualization of Laboratory Corefloods with the Aid of Computerized Tomography of X-rays," SPE Res. Eng., p. 148-54, May 1987.

166 Hunt, P. K., Engler, P., and Bajsarowicz, C.: "Computed Tomography as a Core Analysis Tool: Applications and Artifact Reduction Techniques," SPE No. 16952, 1987.

167 Coles, M. E., Muegge, E. L., and Mark, B. F.: "Use of Attenuation Standards for CAT Scanning Applications Within Oil and Gas Production Research," Society of Core Analysts Conference Paper 9223, 1992.

168 Wellington, S. L. and Vinegar, H. J.: "X-ray Computerised Tomography," JPT, p.885, August 1987.

169 Ringen, J. K. and Hove, A.: "The Use of X-ray Tomography in Core Analysis," North Sea Oil and Gas Reservoirs. The Norwegian Institute of Technology, Graham and Trotman, p.209, 1987.

170 Martin, J. B.: "Effects of Heterogeneity and Wetting on Relative Permeability Using Pore Level Modeling," SPE No. 36762, March 1997.

171 Charles, G. D.: "X-ray Absorption Methods, Chapter 42 :-Absorptionetry with Monochromatic X-rays," 1950.

172 Semat, H., and Albright, J. R.: "Introduction Atomic & Nuclear Physics," Chapman and Hall, 1971.

173 Harold E. J., and Cunningham, J. R.: "The Physics of Radiology," Fourth Edition, 1983.

174 Brooks, R. A. and Dichiro, G.: "Principles of Computer-Assisted Tomography in Radiographic and Radioisotopic Imaging," Phys. Med. Biol., Vol. 21, p.689, 1976.

175 Barrett, H. H. and Swindell, W.: "Radiological Imaging," Academic Press, New York City, 1981.

176 Evans,: " The Atomic Nucleus," McGraw-Hill Book Co, New York City, 1955.

177 Caolle, J. M. and Salmon, G.: "Computerized Tomography," Springer-Verlag, 1980.

178 Ter-Pogossian, M., Phelps, M. M. and Bornwell, G. L. (eds.): "Reconstruction Tomography in Diagnostic Radiology and Nuclear Medicine," University Park Press, Baltimore, 1981.

179 Heaviside, J. and Salt, H. J.: "A Systematic Approach: The Key to Successful Core Analysis," SPE No. 18385, 1988.

180 Morgan, F., McDowell, J. M. and Dotty, E. C.: "Improvements in the X-ray Saturation Technique of Studying Fluid Flow," Trans., AIME, p.183, 1950.

181 Bashir, A. A., and Mason, W. E.: "Core Sample Evaluation using X-ray Computed Tomography," The Robert Gordon University Conference, 1995.

182 Bashir A. A., Mackenzie, I. and Mason, W.E.: "X-ray Computed Tomography as a Powerful Tool in Core Evaluation," The Mediterranean Petroleum Conference, 1993.

183 Kyte, J. R.: "Linear Waterflood Behavior and End Effects in Water-Wet Porous Media," SPE, Vol. 213, p. 423-26, July 15 1957.

184 Richardson, J. G., Holstein, E. D., Rathmell, J. J. and Warner Jr., H. R.: "Validation of As-Received Oil-Based-Core Water Saturations From Prudhoe Bay," SPE No. 28592, Reservoir Engineering, February 1997.

185 Baldwin, B. A., and Yamanashi W. S.: "Persistence of Nonuniform Brine Saturation Distribution in SCA Electrical Resistivity Study Core Plugs after Desaturation by Centrifuging," The Log Analyst, January-February 1998.

186 Sprunt, E. S.: "CT Imaging of Electrical Resistivity Measurements: Nonuniform Water Saturation Can Be a Problem," Academic Press, Chapter 15, p. 371, 1992.

187 Baldwin, B. A., and Yamanashi, W. S.: "NMR Imaging of Fluid Saturation Distributions in Cores," SCA, No. 8714, Texas, 1987.

188 Melrose, C.: "Scaling Procedures for Capillary Pressure Data at Low Wetting-Phase Saturations," SPE No. 19594, Stanford U., p. 241-50, October 1989.

189 Archer, J. S.: "Use of a Reservoir Simulator To Interpret Laboratory Waterflood Data," SPE No. 3551, p. 343-47, December 1971.

190 Brown, H. W.: "Capillary Pressure Investigations," Trans., AIME, Vol. 192, p. 67, 1951.

191 Archer, J. S. and Wong, S. W.: "Use of a Reservoir Simulator to Interpret Laboratory Waterflood Data," SPEJ, August 1978.

APPENDIX I

BASIC ROCK PROPERTIES AND RELTIVE PERMEABILITY DATA

Core Sample No	Length (cm)	Diameter (cm)	Grain Density (gm/cc)	Porosity (%)	Permeability (mD)
S2	6.9	3.738	2.62	17.4	577
S5	7.57	3.67	2.63	30.9	2500
S8	7.35	3.77	2.63	20.3	183
S15	5.03	3.76	2.62	13.8	125

Table A.1 Selected samples routine data.

Core Sample No	Length (inch)	Diameter (inch)	Grain Density (gm/cc)	Porosity (%)
Disk 1	1	5	2.64	17.9
Disk 2	0.3	5	2.64	17.7
Disk 3	0.12	5	2.64	18.08
Clachach 1	2.5	1.5	2.635	17.3

Table A.2 Sandstone disks and samples routine data.

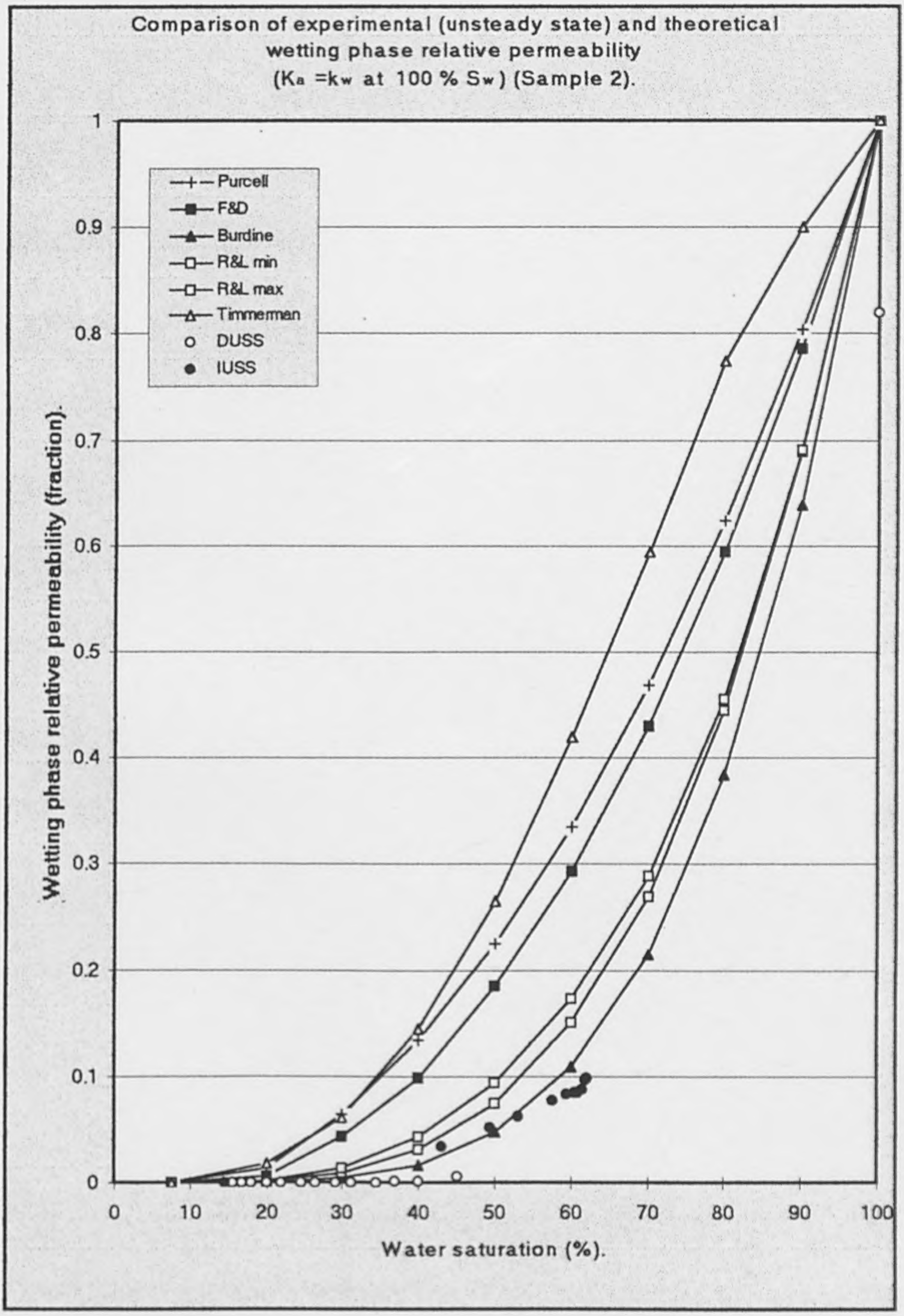

Figure (A.1) Comparison of experimental (unsteady state) and theoretical wetting phase relative permeability ($K_a = k_w$ at 100% S_w) for Sample 2.

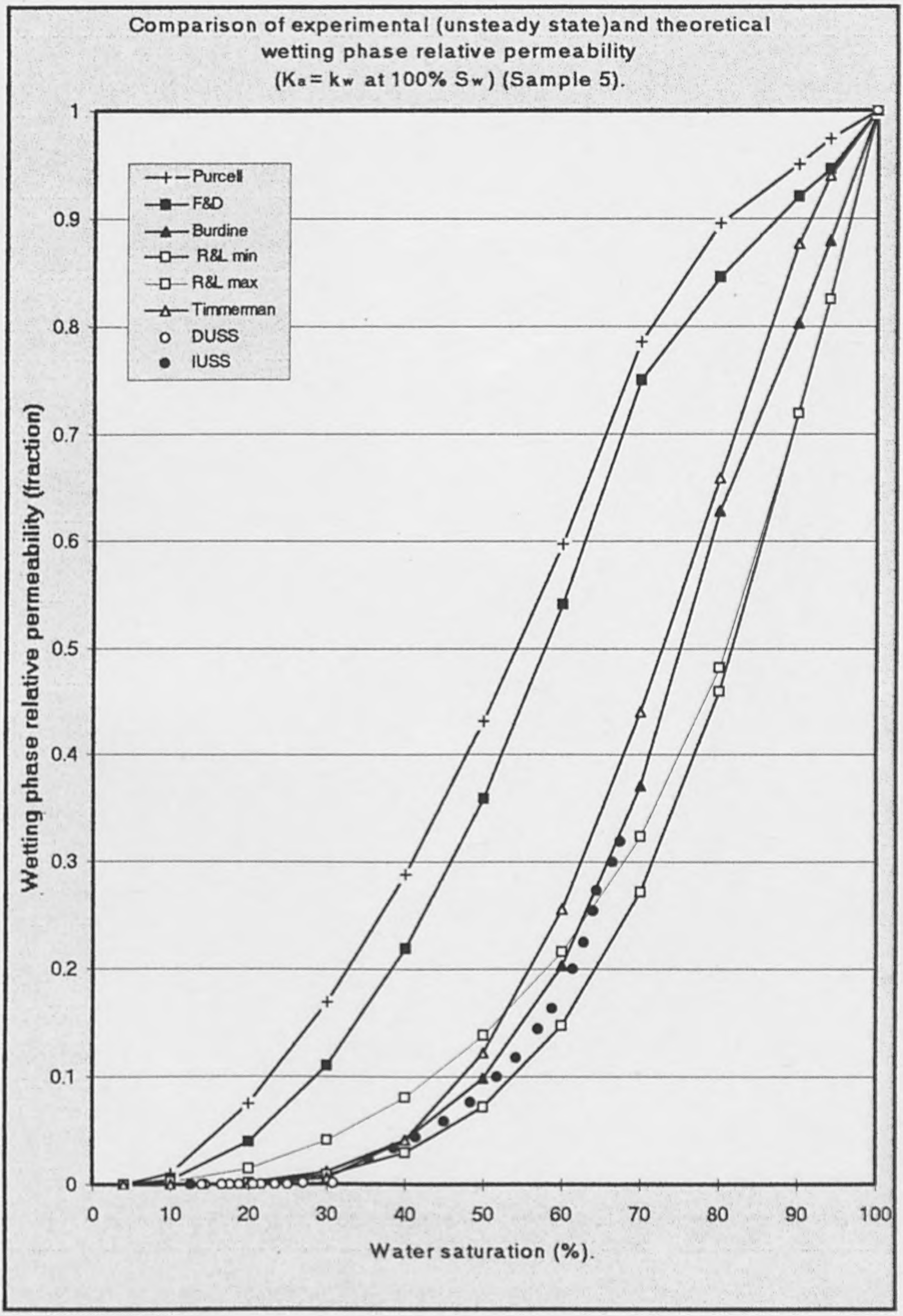

Figure (A.2) Comparison of experimental (unsteady state) and theoretical wetting phase relative permeability (K_a=k_w at 100% S_w) for Sample 5.

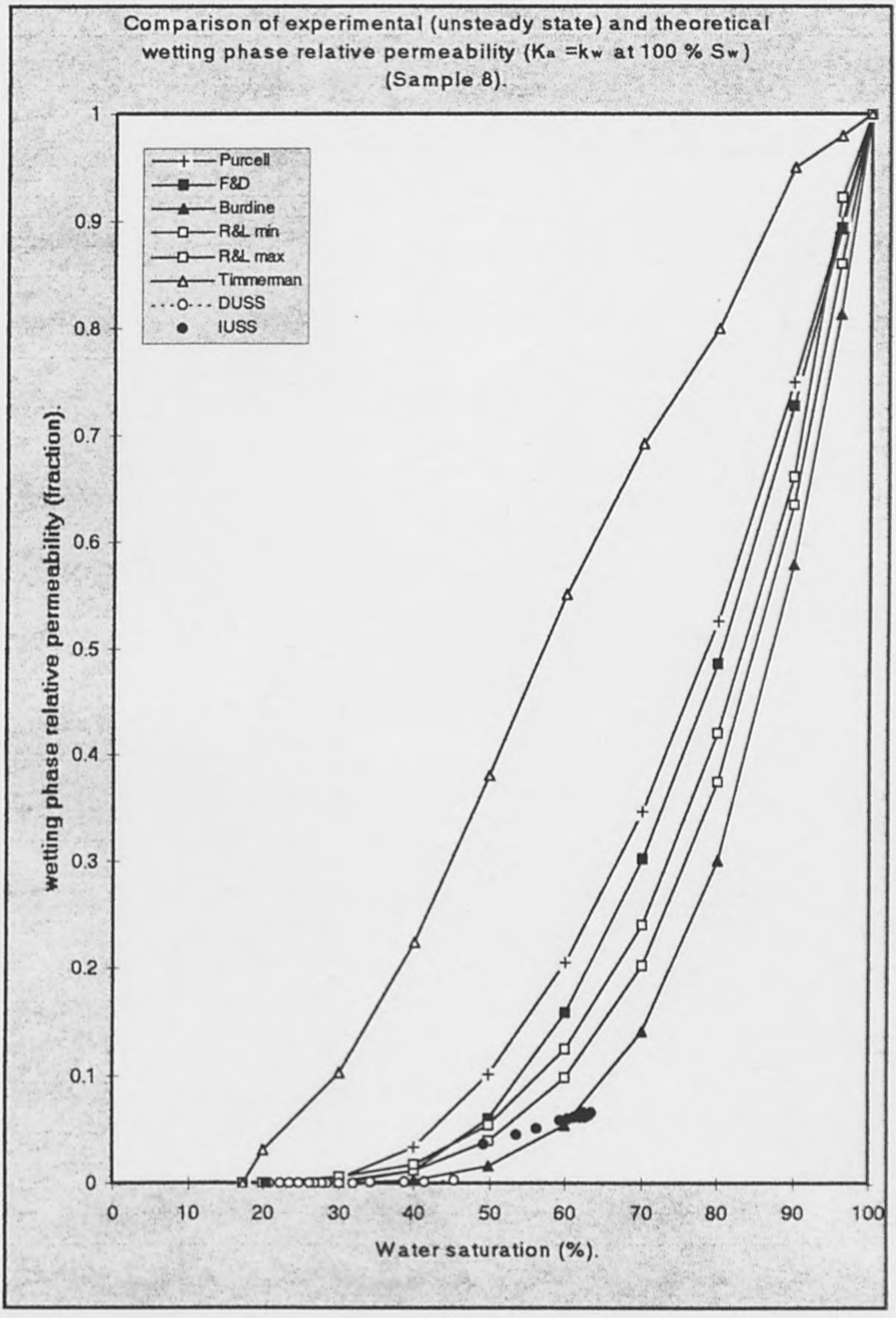

Figure (A.3) Comparison of experimental (unsteady state) and theoretical wetting phase relative permeability ($K_a = k_w$ at 100% S_w) for Sample 8.

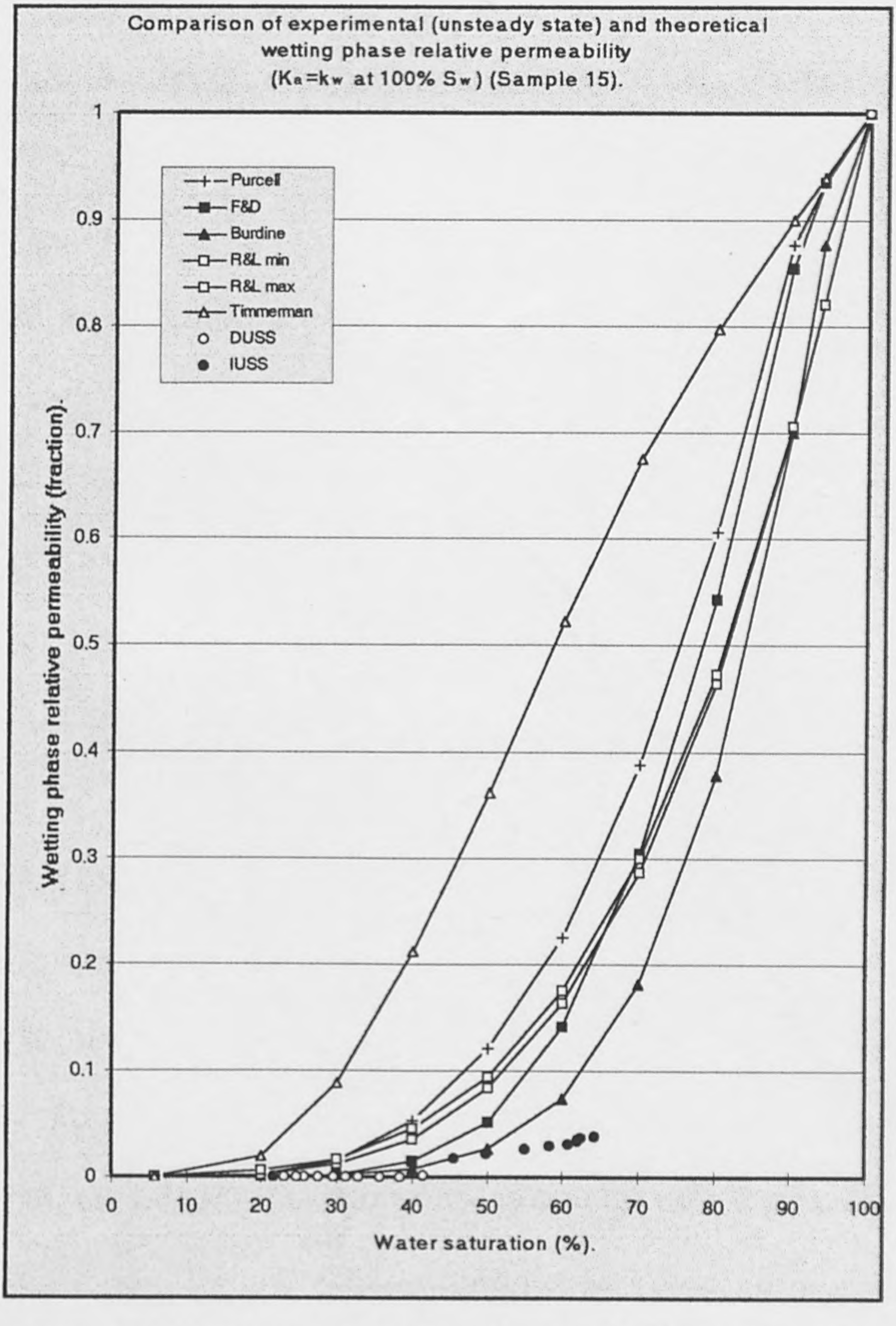

Figure (A.4) Comparison of experimental (unsteady state) and theoretical wetting phase relative permeability ($K_a = k_w$ at 100% S_w) for Sample 15.

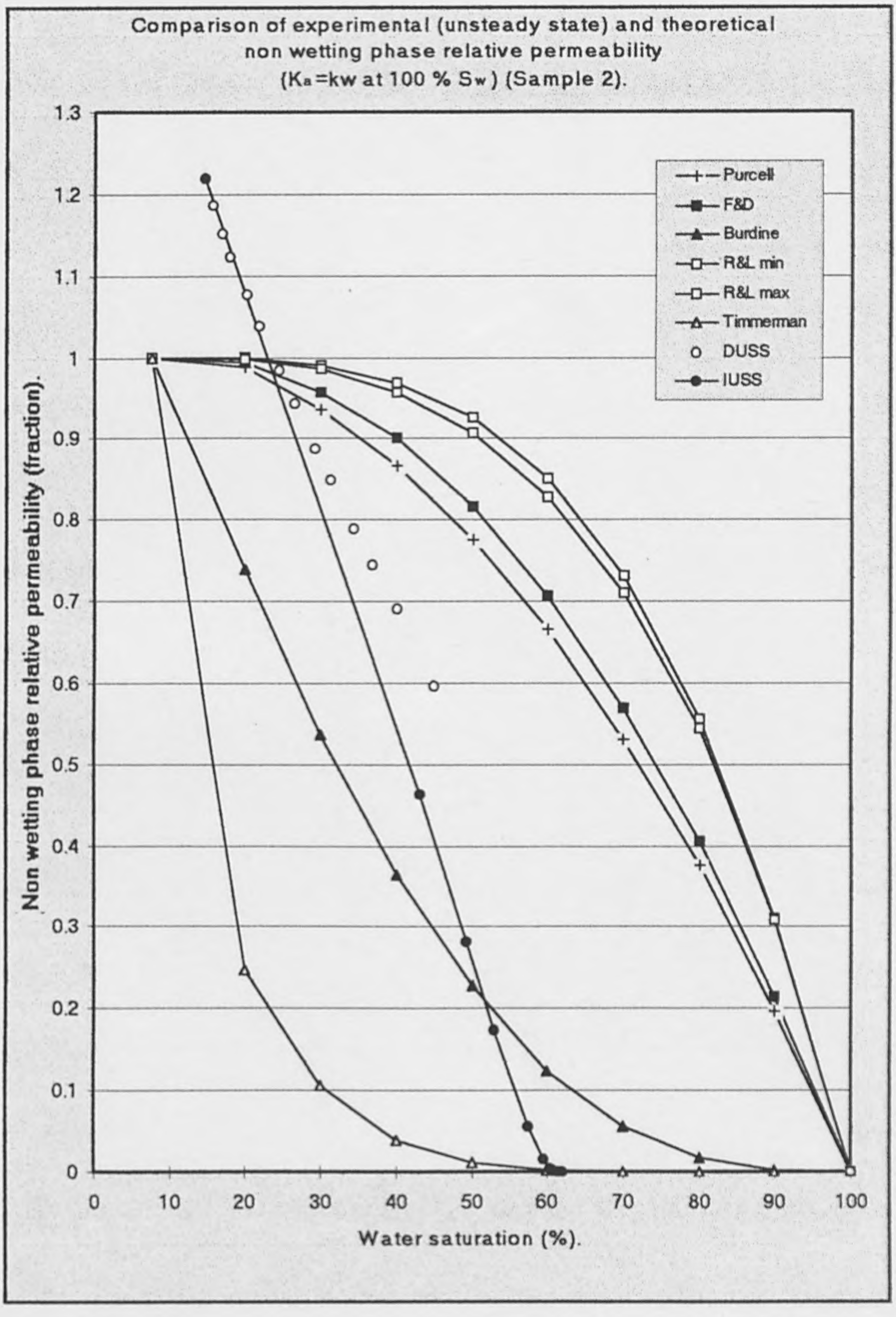

Figure (A.5) Comparison of experimental (unsteady state) and theoretical non wetting phase relative permeability (K_a= k_w at 100% S_w) for Sample 2.

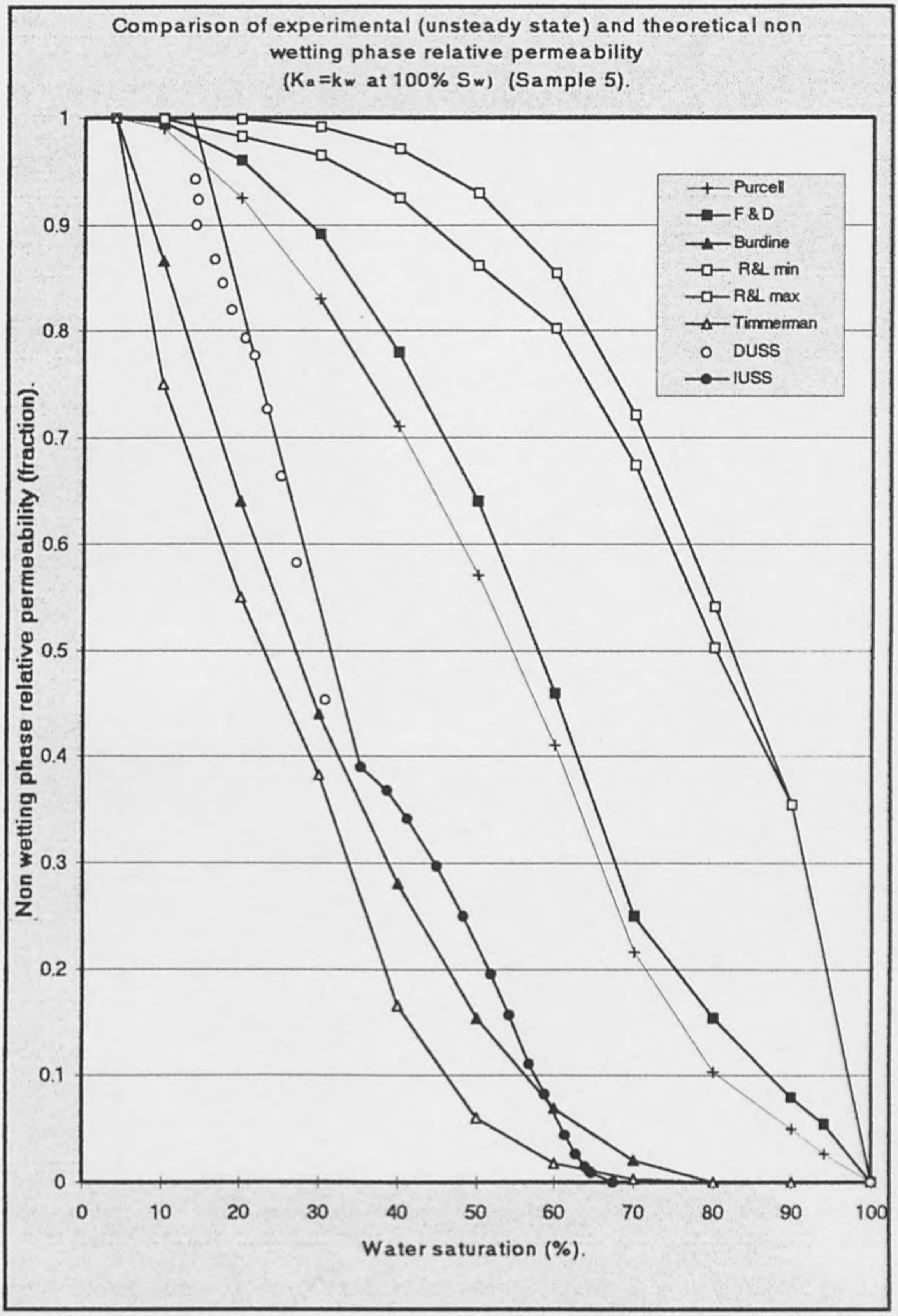

Figure (A.6) Comparison of experimental (unsteady state) and theoretical non wetting phase relative permeability ($K_a = k_w$ at 100% S_w) for Sample 5.

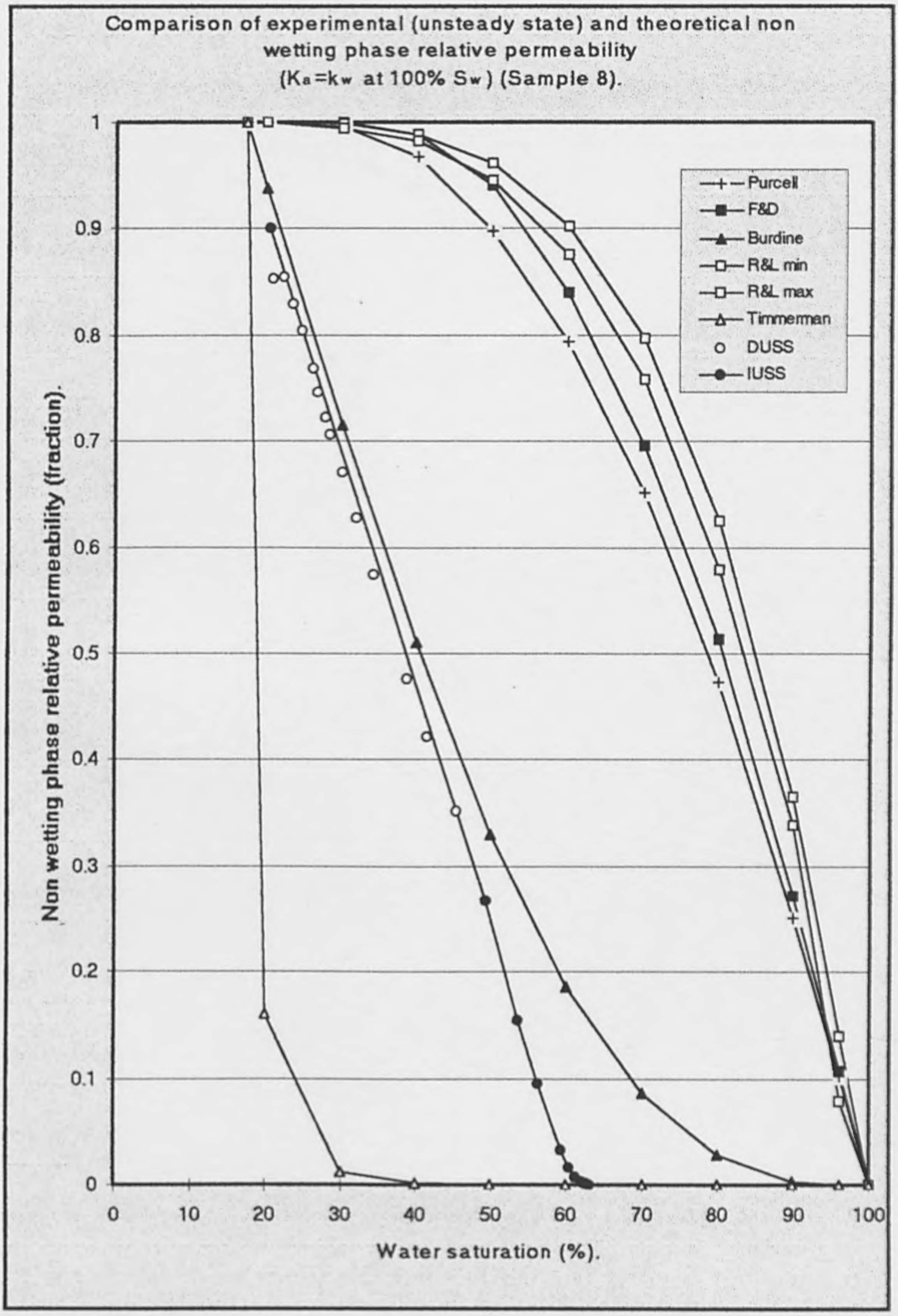

Figure (A.7) Comparison of experimental (unsteady state) and theoretical non wetting phase relative permeability ($K_a = k_w$ at 100% S_w) for Sample 8.

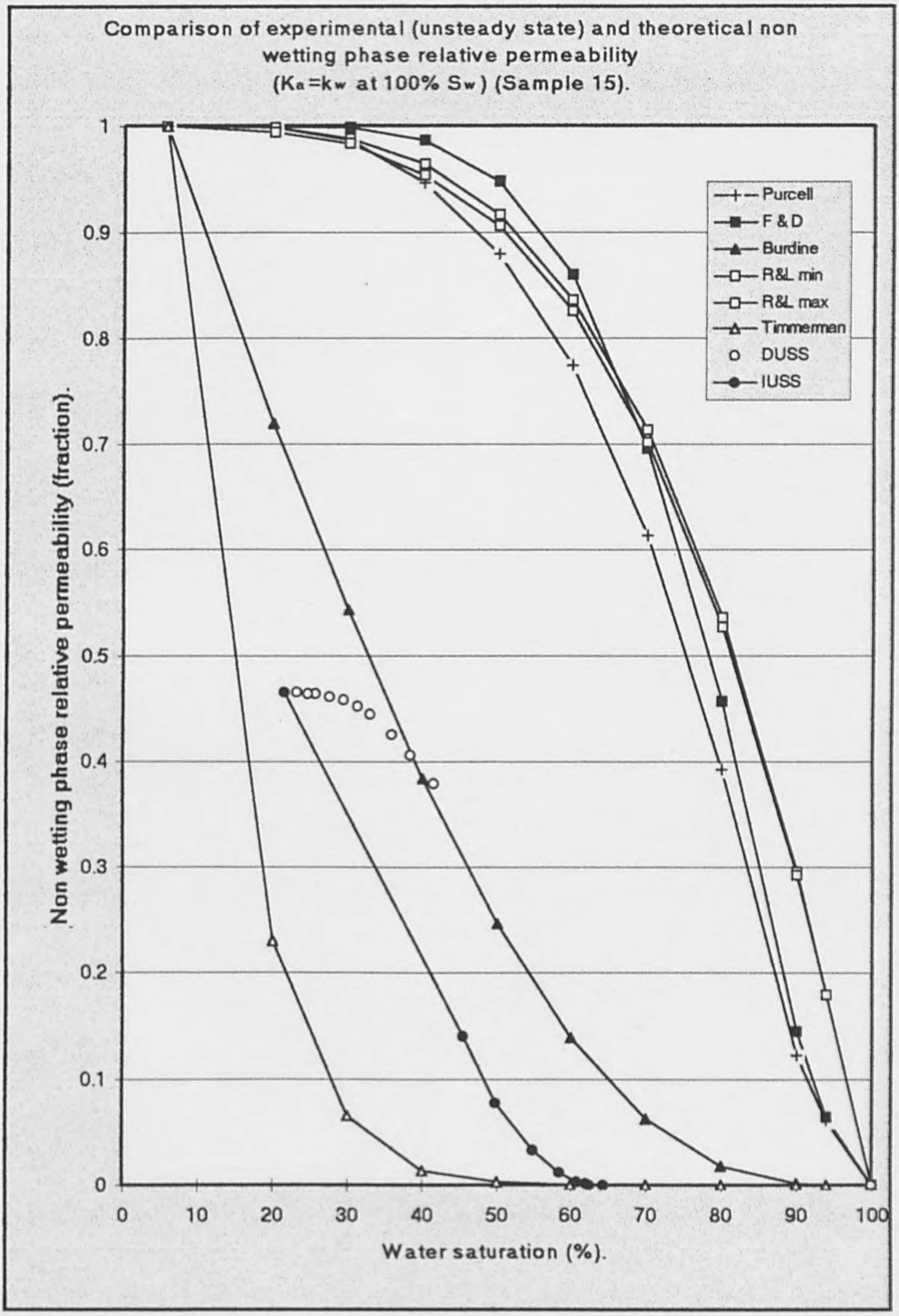

Figure (A.8) Comparison of experimental (unsteady state) and theoretical non wetting phase relative permeability (K_a= k_w at 100% S_w) for Sample 15.

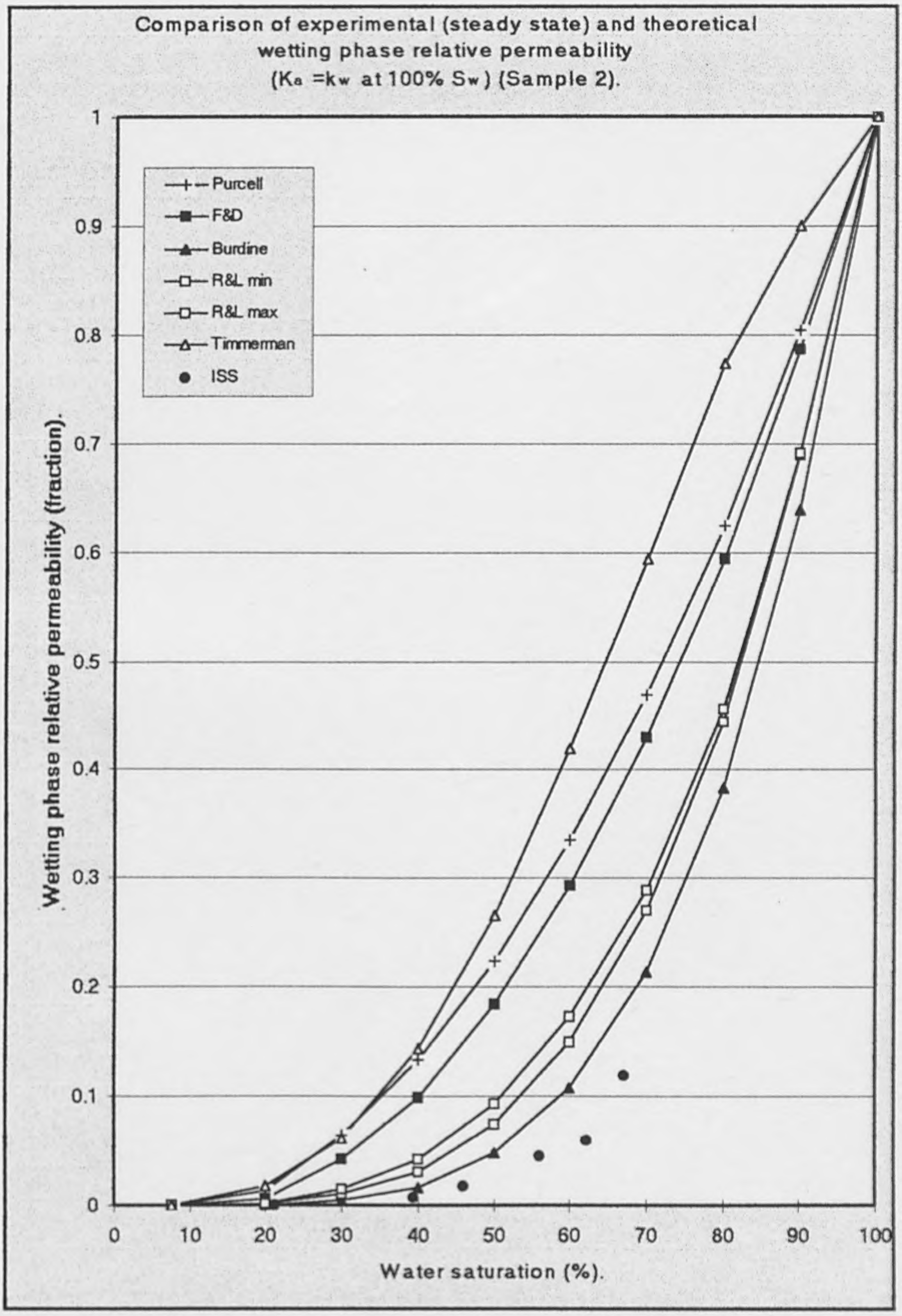

Figure (A.9) Comparison of experimental (steady state) and theoretical wetting phase relative permeability (K_a= k_w at 100% S_w) for Sample 2.

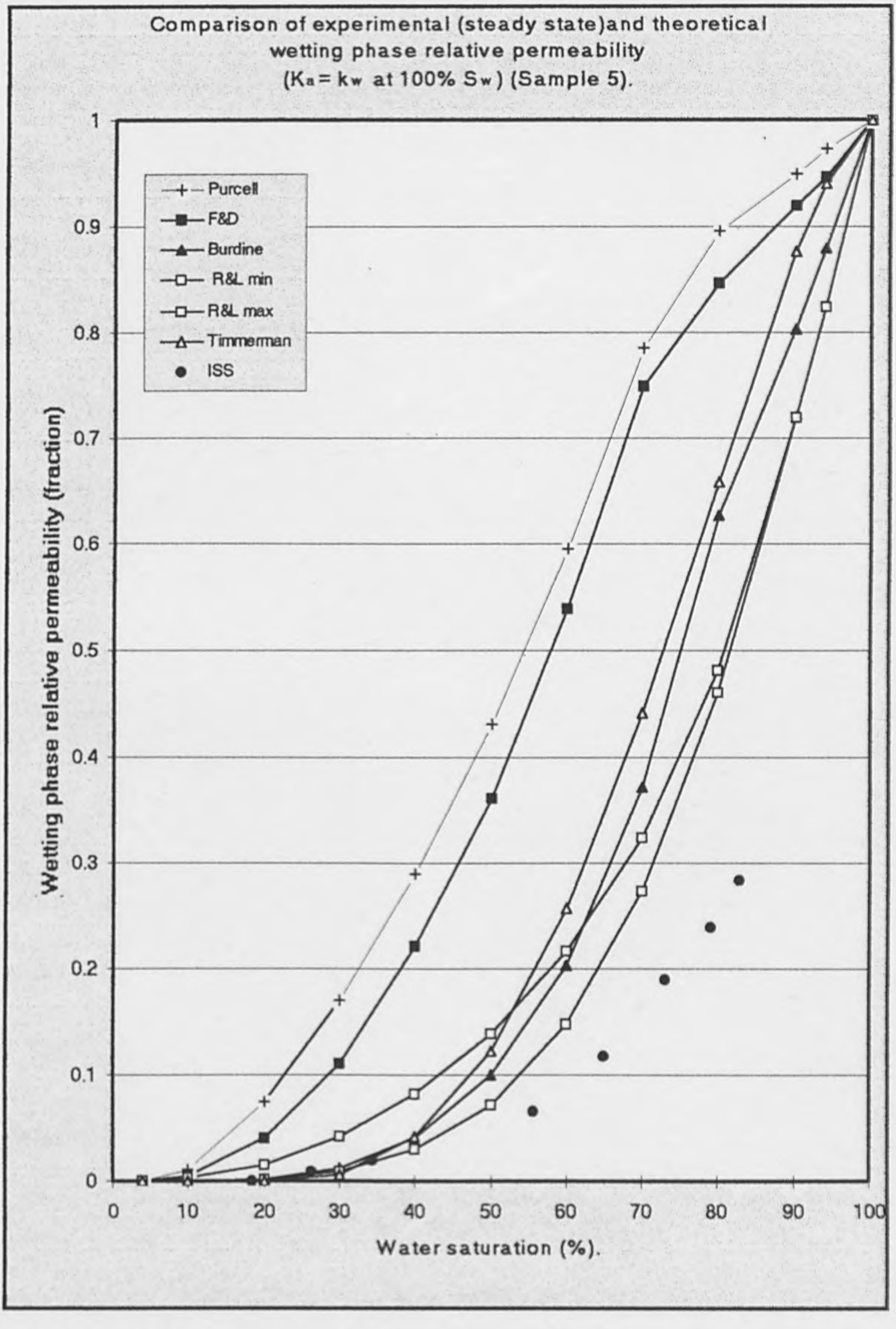

Figure (A.10) Comparison of experimental (steady state) and theoretical wetting phase relative permeability (K_a= k_w at 100% S_w) for Sample 5.

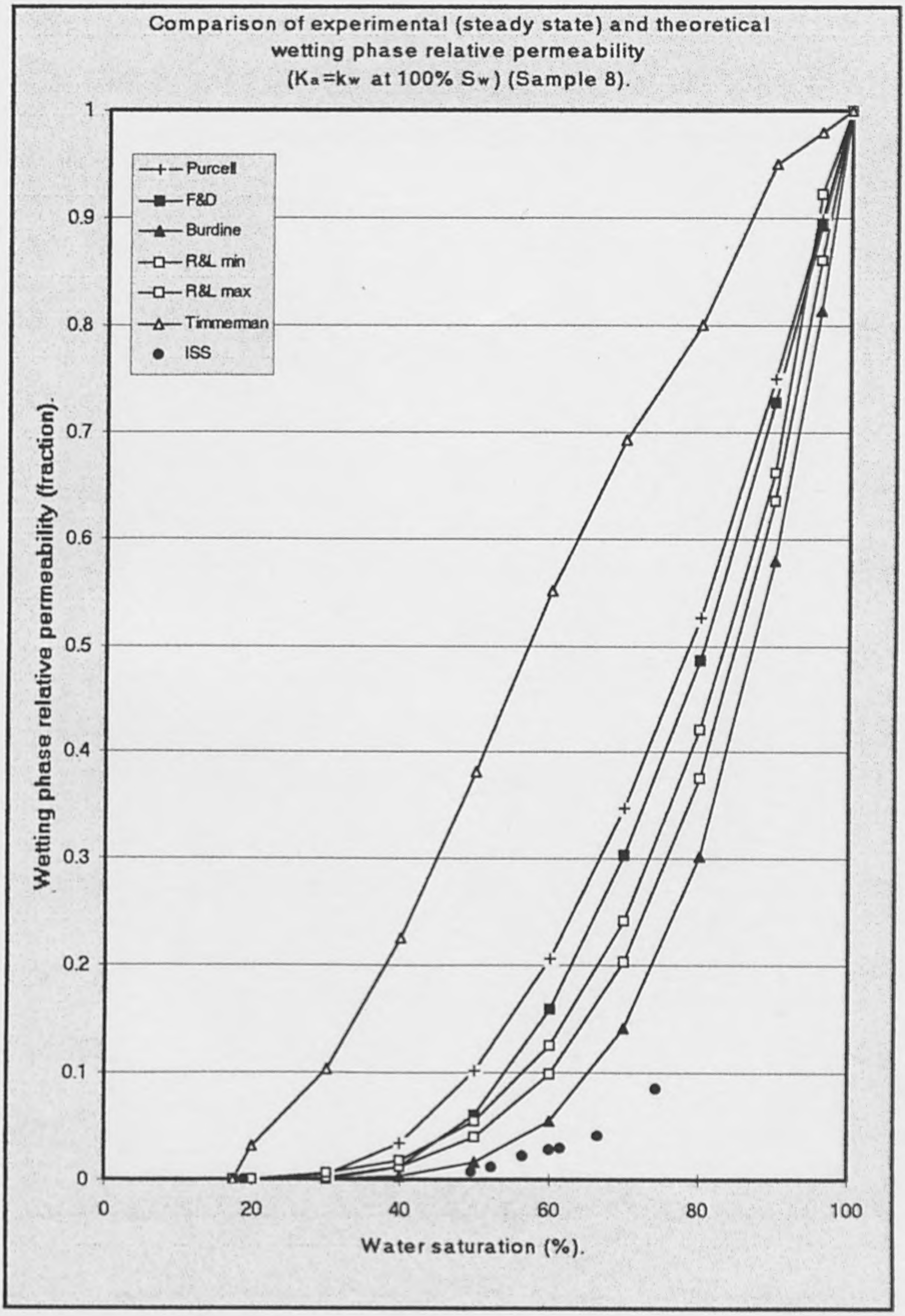

Figure (A.11) Comparison of experimental (steady state) and theoretical wetting phase relative permeability ($K_a = k_w$ at 100% S_w) for Sample 8.

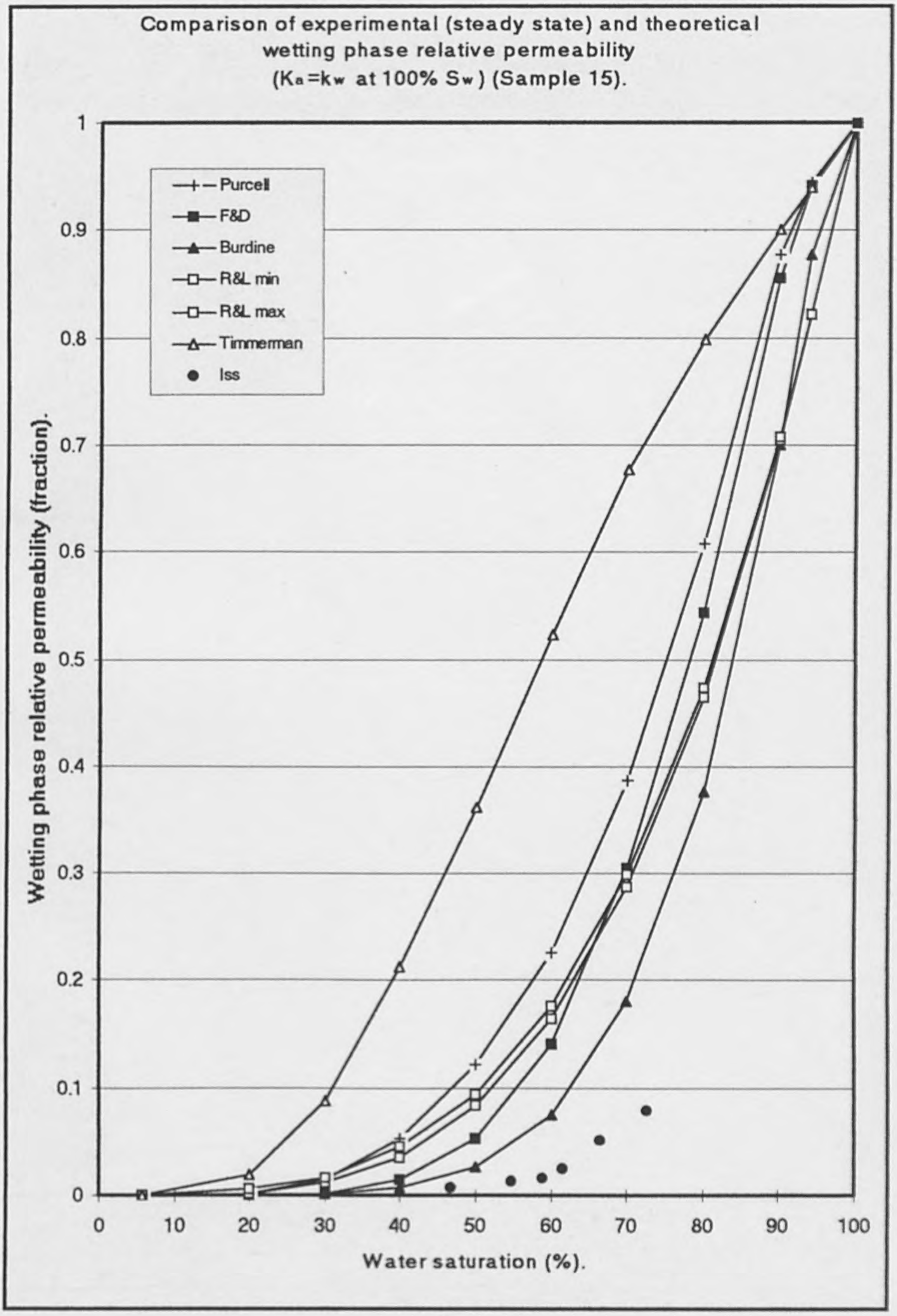

Figure (A.12) Comparison of experimental (steady state) and theoretical wetting phase relative permeability ($K_a= k_w$ at 100% S_w) for Sample 15.

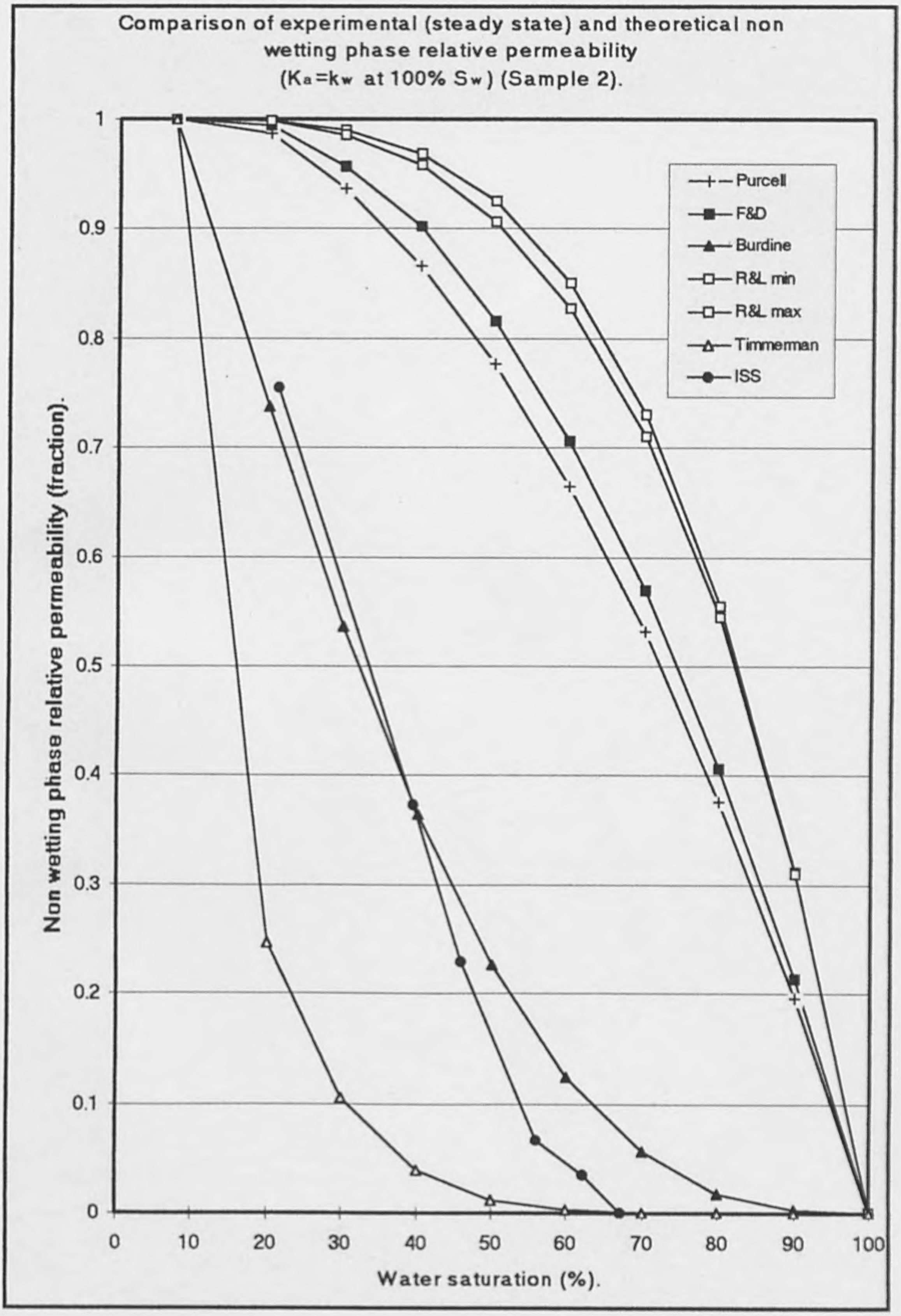

Figure (A.13) Comparison of experimental (steady state) and theoretical non wetting phase relative permeability ($K_a = k_w$ at 100% S_w) for Sample 2.

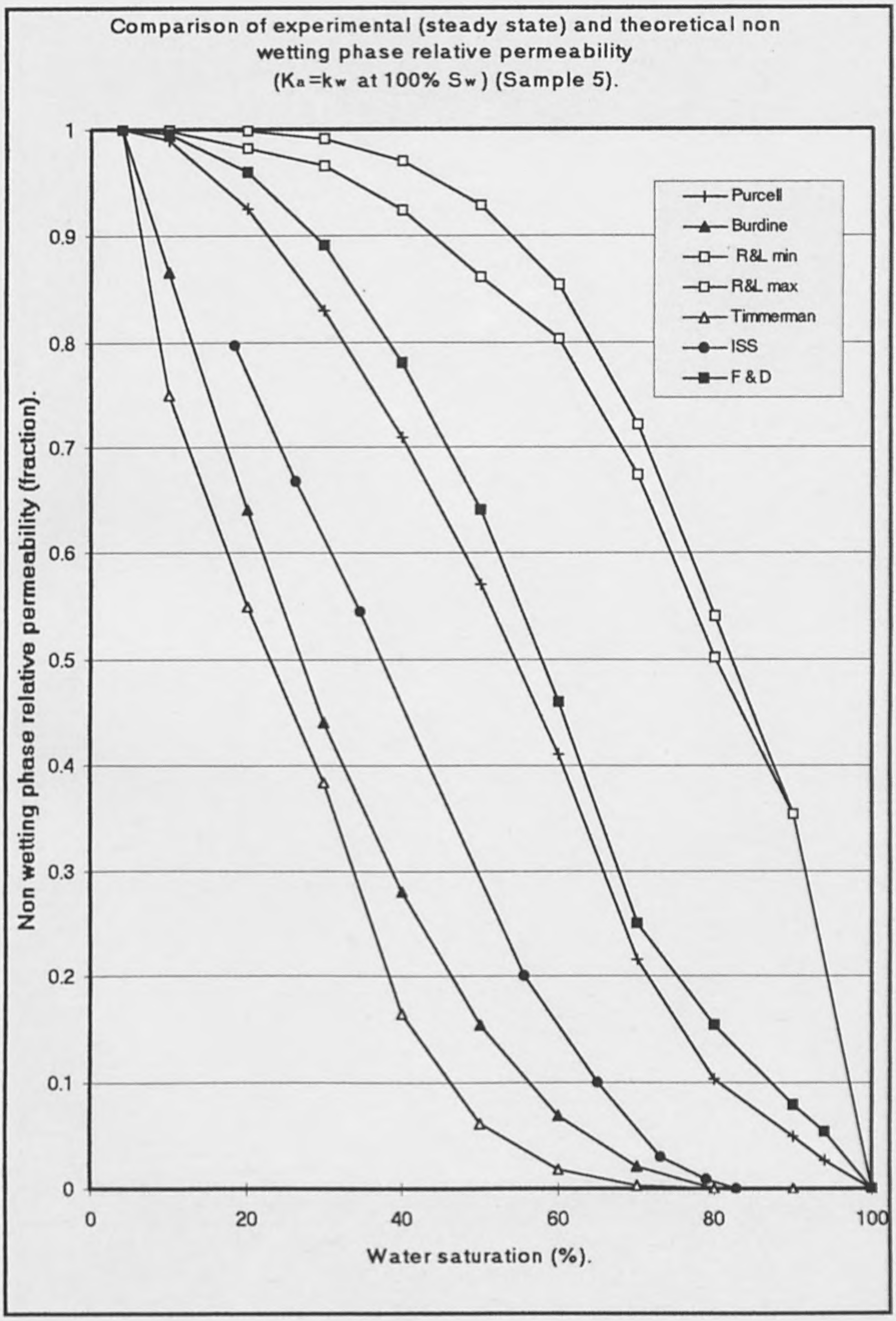

Figure (A.14) Comparison of experimental (steady state) and theoretical non wetting phase relative permeability (K_a=k_w at 100% S_w) for Sample 5.

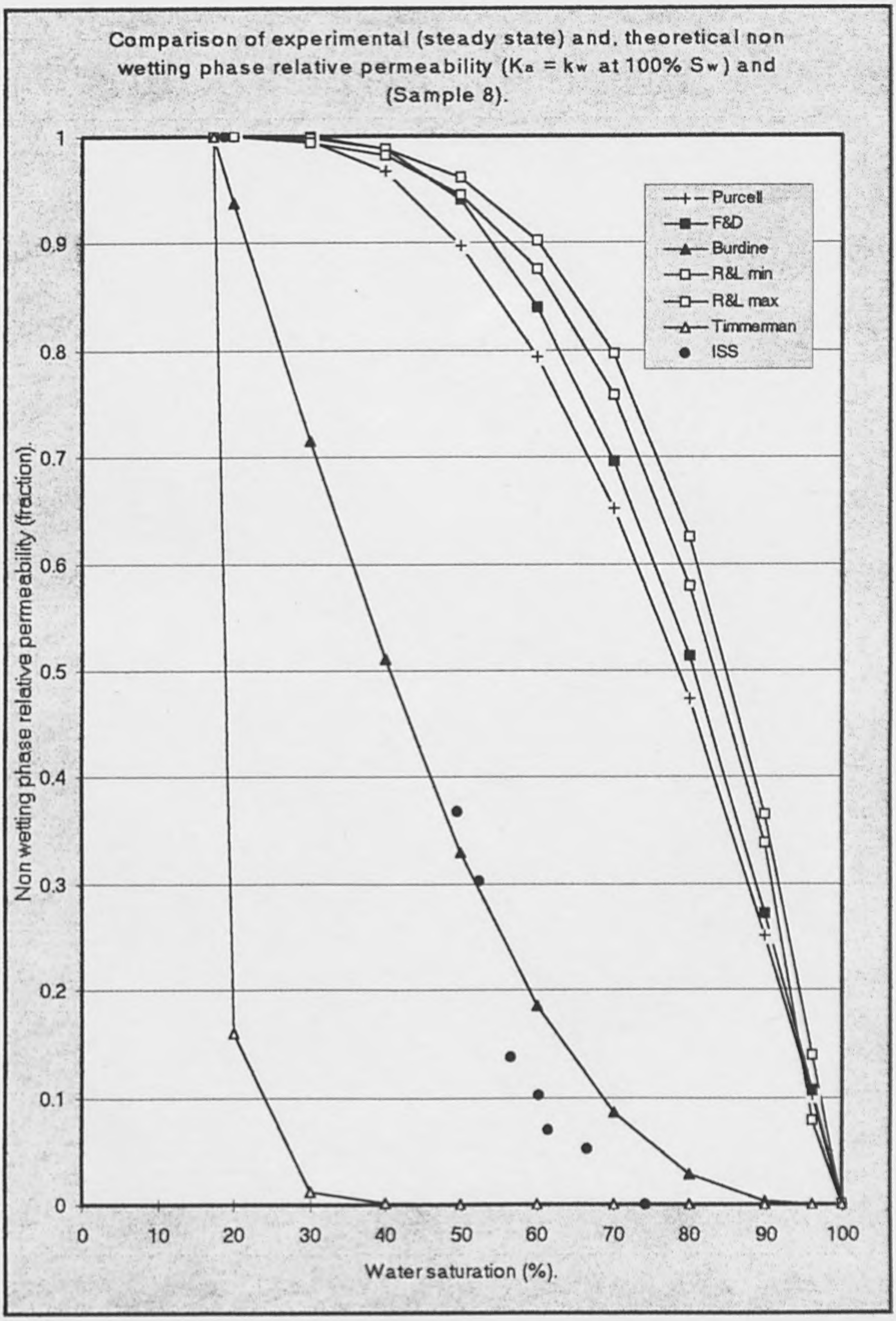

Figure (A.15) Comparison of experimental (steady state) and theoretical non wetting phase relative permeability ($K_a= k_w$ at 100% S_w) for Sample 8.

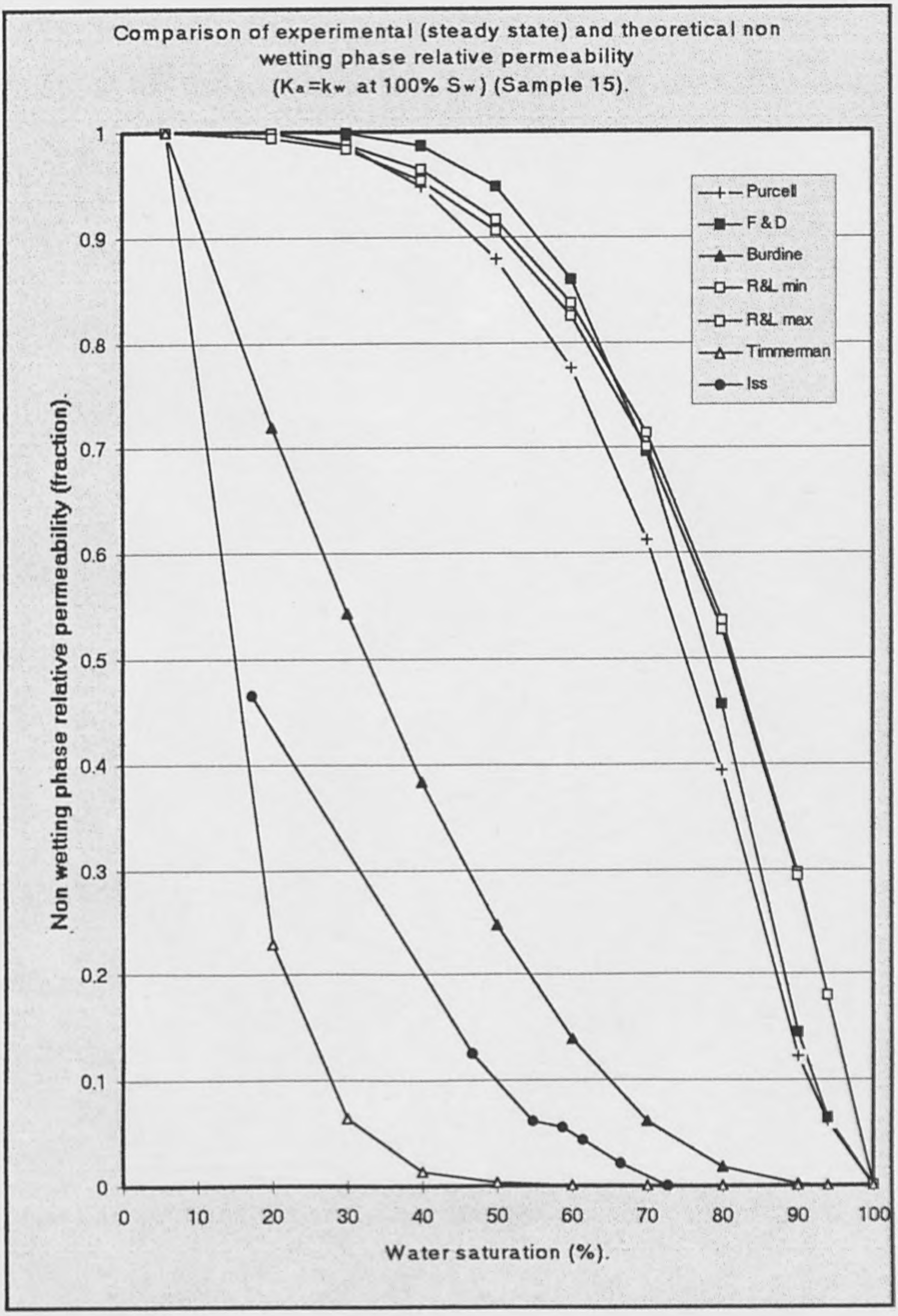

Figure (A.16) Comparison of experimental (steady state) and theoretical non wetting phase relative permeability ($K_a = k_w$ at 100% S_w) for Sample 15.